

DISSERTATION

REGIONAL-SCALE GROUNDWATER FLOW AND SALT TRANSPORT MODELS FOR
EXPLORING AGRO-ENVIRONMENTAL REMEDIATION STRATEGIES IN AN
IRRIGATED RIVER VALLEY

Submitted by

Eric D. Morway

Department of Civil and Environmental Engineering

In partial fulfillment of the requirements

For the Degree of Doctor of Philosophy

Colorado State University

Fort Collins, Colorado

Spring 2014

Doctoral Committee:

Timothy K. Gates

John W. Labadie
Domenico A. Baù
Michael J. Ronayne

ABSTRACT

REGIONAL-SCALE GROUNDWATER FLOW AND SALT TRANSPORT MODELS FOR EXPLORING AGRO-ENVIRONMENTAL REMEDIATION STRATEGIES IN AN IRRIGATED RIVER VALLEY

Irrigated lands in Colorado's Lower Arkansas River Valley (LARV), like many such lands worldwide, face an uncertain future as pressures on the region's limited water resources continue to increase. Irrigated agriculture is the largest consumer of water in the basin and therefore is targeted by urban interests for its senior water rights. Waterlogging and salinization, prevalent throughout the LARV, have diminished crop yields. Evapotranspiration from fallow and naturally-vegetated lands adjacent to cultivated fields and underlain by shallow water tables, resulting from inefficient irrigation practices, sustains non-beneficial consumptive use, a significant source of water loss from the region. Further, groundwater gradients resulting from the shallow (high) water tables drive saline groundwater back to the stream network, thereby degrading river water quality. A business-as-usual approach fails to recover lost crop production and the rural commerce it supports, does not curtail non-beneficial water use, and ensures continued degradation of river water quality.

Waterlogging and the salinization of cultivated fields, as well as non-beneficial consumptive use and degraded river water quality, are rooted in intense and inefficient irrigation, leaky canals, and failed drainage infrastructure. Past research has identified solutions to these age-old problems: basin-wide water management analyses for selecting sound water conservation initiatives; improved irrigation efficiency that reduces wasteful tail-water, deep percolation and delivery losses; and new or rehabilitated sub-surface drainage facilities are all

effective options. Accurately predicting the most effective intervention, or combination of interventions, is difficult in extensive and spatiotemporally variable areas like the LARV.

This work describes 1) the study locations, 2) data-collection efforts for system characterization and for support of model development, 3) development, calibration, and testing, of groundwater flow and salt transport models and 4) application of the models for describing baseline conditions and for exploring the trade-offs of potential solution strategies for two distinct regions in the LARV [referred to as the Upstream Study Region (USR) and the Downstream Study Region (DSR)]. An unprecedented database yields nine extensive target data sets used for calibration and testing of MODFLOW-UZF groundwater flow models and UZF-MT3DMS salt transport models and supports examination of alternative water management strategies.

Data indicate high soil water salinity that is exacerbated by shallow saline groundwater tables in the regions. Extensive soil water salinity surveys reveal average electrical conductivity of soil saturated extract, \overline{EC}_e , throughout the LARV that are near or exceeding crop salt tolerance thresholds in the 3–5 dS m⁻¹ range. Soil water extracted from cultivated field soil samples averaged 4.1 and 6.2 dS m⁻¹ between the USR and DSR, respectively. Of the more than 122,000 locations surveyed for soil water salinity in the LARV over a 7-year survey period, 42% exceeded the estimated crop salt tolerance threshold for the recorded crop type. These conditions correspond to estimated average crop yield reductions of 6% in the USR and 17% in the DSR.

Model simulation of baseline conditions indicates considerable temporal variation in the average water table depth. In the USR, the water table depth was less than 2 m across 50% of the cultivated area in 1999, but fell to a 6% fraction during the dry conditions of 2002. Roughly

17% of cultivated lands hosted a water table depth less than 2 m in the DSR from 2002 to 2007. Data reveal a significant relationship between decreasing depth to the water table and increasing soil water salinity.

Simulated output from model runs of several alternative management interventions (reduced irrigation applications, reduced canal seepage, lease-fallowing of cultivated land, and combinations thereof) is compared to baseline model results and relative improvements in water table depth and reduced non-beneficial consumptive use are quantified. Potential for lowering the water table by up to 1.1 and 0.7 m on average in the USR and DSR, respectively, is demonstrated. Further, predicted net annual water savings in non-beneficial consumptive use associated with the lowered water tables averaged $10.5 \cdot 10^6 \text{ m}^3$ (8,500 ac-ft) and $2.6 \cdot 10^6 \text{ m}^3$ (2,100 ac-ft) in the USR and DSR, respectively. Under each of the investigated scenarios, patterns of groundwater return flows to the river varied, highlighting the need to augment river flows to avoid violations to the interstate river compact that governs river operations in the LARV. In addition to simulating conditions resulting from altered groundwater flow, the calibrated baseline groundwater flow models provide the simulated subsurface flow required for salt transport simulations, whether for the non-reactive solute transport models described herein or for multi-species reactive transport models being developed in parallel research.

Baseline salinity conditions are quantified using the modified subsurface variably saturated solute transport code UZF-MT3DMS. The modified code was developed and verified with 1-, 2-, and 3-dimensional simulations under a variety of conditions, including steady, unsteady, nonreactive and reactive conditions. Under reactive conditions, nonlinear and nonequilibrium transport conditions were tested against analytical benchmarks, although they were not utilized in the LARV transport simulations. Among model grid cells with at least a

99% crop coverage, average simulated irrigation season dissolved salt concentrations in the upper layer containing the vadose zone for the USR and DSR are 3,040 and 5,750 mg L⁻¹ (corresponding to \overline{EC}_e of about 3.4 dS m⁻¹ and 6.3 dS m⁻¹), respectively, over their respective simulated periods. The average simulated groundwater return salt loads to the Arkansas River are 5,200 and 5,800 MT (metric tons) wk⁻¹, respectively. An evaluation of the baseline model output suggests that chemical reaction processes, such as precipitation and dissolution, should be incorporated into the salt transport models. By providing the simulations with a mechanism for adding and releasing salt to and from storage, model fits to observations of groundwater salt concentrations, soil water salt concentrations, and seasonal salt loading dynamics associated with groundwater return flows likely will be improved.

Without only a minimum level of intervention, the productivity of irrigated agriculture and the environmental quality of the stream-aquifer system in the LARV will remain at or below current sub-par levels. Due to the ever-increasing demand (and value) of water along Colorado's urbanized Front Range, the potential remains for permanent land dry-up as the water is reallocated to other uses. However, simulations of corrective actions that include mitigating inefficient application and delivery of irrigation water offer hope that the LARV's long and rich history of crop production will continue. Alternative management intervention scenarios highlight opportunity for lowering water tables for improving growing conditions, reducing non-beneficial consumptive use, and restoring river water quality.

ACKNOWLEDGEMENTS

The completion of this work would not be possible without the generous investment of time and energy of many individuals too numerous to name here. However, a sincere and special gratitude, the depth of which goes well beyond what is written, is reserved Dr. Timothy K. Gates. In addition to his patience and steady optimism, I would like to thank him for his wise council that extends far beyond the engineering research. Indeed, the friendship that has formed over the past decade is among my most treasured. As well, I wish to acknowledge and thank Dr. John Labadie, Dr. Domenico Baù, and Dr. Michael Ronayne for always being generous with their time, and supportive of this work.

The completion of this work is due almost entirely to the encouragement and support of my wife, Christina. Without her, this work would have been set adrift long ago. Sadly, the Saturdays, evenings, and early mornings spent working on school are unrecoverable, yet I thank the crew—Leif, Asa, Fletcher and most recently, Clara—for always greeting me at the front door, after a long Saturday, with, “daddy’s home!” Their readiness to forgive a father who spent too much time at the office, working on this document, is remarkable.

Finally, and most importantly, it is to Jesus of Nazareth this work is commended. It is to Him that I am forever thankful for authoring my testimony, and for weaving Christina, my dear family, and close friends, into its pages. Without His grace, offer of forgiveness, and call to follow Him, I would still be hopelessly scrambling in the dark.

PREFACE

The research described herein takes its place among a number of parallel research efforts. At the heart of this study are two regional-scale groundwater flow and transport modeling applications. These studies attempt to build upon and enhance the previously published regional-scale models of the Lower Arkansas River Basin (LARV) by seizing upon new data, new findings from sister studies at the field- and basin-scale, new software developments, and more advanced model-calibration techniques, culminating in a set of findings that describe some previously unconsidered trade-offs associated with water management decisions.

As the demand for Colorado's finite water resources continues to climb, due in large part to its sprawling "front range," but also in part to now decades-old inter-state water delivery agreements, pressure on 'senior' water right holders to sell their water shares outright is at an all-time high. Compounding the already complex set of competing interests is the rather unfortunate "use it, or lose it" principle, which discourages water conservation. Considering that more efficient irrigation delivery and application methods or the adoption of less water intensive crops could create a water surplus, competing interests need only to invoke the "use it, or lose it" principle to quickly disincentivize water saving modernization.

These studies rest upon tremendous and diverse observation datasets, the likes of which were not encountered in the literature (described in Chapter 3 and in parts of Chapters 5 and 6). An unparalleled field-scale modeling effort in the LARV also informs many aspects of the regional-scale models. New software capabilities implemented in the popular solute transport modeling code MT3DMS for simulation of regional-scale salt transport processes are described in Chapter 4 and applied in Chapter 6. However, the enhanced software, referred to as UZF-MT3DMS, requires a groundwater flow solution. This is provided by the MODFLOW models

with the UZF package activated and described in detail in Chapter 5. Over-arching conclusions, informed by the preceding chapters, as well as suggestions for future research, are summarized in Chapter 7. Just as the studies preceding my own played important roles in guiding the model development and applications described in the chapters that follow, it is my sincere hope that this work takes its place in the long history of LARV research endeavors and helps advance ongoing research efforts, eventually leading to real on-the-ground enhancements to this beautiful and valued region of Colorado.

DEDICATION

*For my Savoir,
Whose demonstration of true perseverance on the cross kept me going.*

*For my wife Christina,
I am forever thankful for your steady encouragement, love, and support, upon which I have come
to rely. “A wife of noble character is her husband’s crown” - Proverbs 12:4*

*For my children, Leif, Asa, Fletcher, and Clara,
If I had my time over again, I would redirect the time invested in school into each of you.
Now, let’s go exploring...*

TABLE OF CONTENTS

ABSTRACT	ii
PREFACE	vii
LIST OF TABLES	xii
LIST OF FIGURES	xiv
1 INTRODUCTION	1
1.1 IRRIGATED AGRICULTURE FACING CHALLENGES OF GLOBAL PROPORTIONS.....	1
1.2 CHALLENGES CONFRONTING IRRIGATED AGRICULTURE IN COLORADO ..	2
1.3 OBJECTIVES	8
1.4 DESCRIPTION OF THE STUDY REGIONS	11
1.5 DISSERTATION STRUCTURE.....	21
2 LITERATURE PERTAINING TO GROUNDWATER MODELING IN THE LARV AND TO AUTOMATED PARAMETER ESTIMATION FOR MODEL CALIBRATION	23
2.1 LITERATURE REVIEW OVERVIEW	23
2.2 LOWER ARKANSAS RIVER VALLEY MODELING EFFORTS, PAST AND PRESENT	23
2.3 LITERATURE RELATED TO PROPOSED MODEL PARAMETER ESTIMATION METHODOLOGY	27
3 REGIONAL ASSESSMENT OF SOIL WATER SALINITY ACROSS AN INTENSIVELY IRRIGATED RIVER VALLEY	41
3.1 SUMMARY	41
3.2 INTRODUCTION	42
3.3 METHODS AND MATERIALS.....	45
3.4 RESULTS AND DISCUSSION	53
3.5 CONCLUSIONS.....	69
4 APPRAISING OPTIONS TO REDUCE SHALLOW GROUNDWATER TABLES AND ENHANCE FLOW CONDITIONS OVER REGIONAL SCALES IN AN IRRIGATED ALLUVIAL AQUIFER SYSTEM	72
4.1 SUMMARY	72

4.2 INTRODUCTION	73
4.3 STUDY AREA	78
4.4 MODEL CONSTRUCTION AND COMPOSITION	81
4.5 MODEL CALIBRATION PROCEDURE	93
4.6 SIMULATION OF BASELINE GROUNDWATER CONDITIONS	107
4.7 INVESTIGATION OF IMPROVEMENT ALTERNATIVES	114
4.8 DISCUSSION AND CONCLUSIONS	129
5 MODELING VARIABLY SATURATED SUBSURFACE SOLUTE TRANSPORT WITH MODFLOW-UZF AND MT3DMS.....	134
5.1 SUMMARY	134
5.2 INTRODUCTION	135
5.3 DESCRIPTION OF APPROACH AND IMPLEMENTATION.....	138
5.4 BENCHMARK PROBLEMS.....	141
5.5 CONCLUSIONS.....	164
6 SIMULATING SALT TRANSPORT IN THE LOWER ARKANSAS RIVER VALLEY WITH UZF-MT3DMS.....	167
6.1 INTRODUCTION	167
6.2 LITERATURE REVIEW ON SALT TRANSPORT UNDER IRRIGATED CONDITIONS.....	170
6.3 STUDY AREAS FOR SALT TRANSPORT MODELING.....	181
6.4 UZF-MT3DMS MODEL CONSTRUCTION AND COMPOSITION	183
6.5 AUTOMATED SALT TRANSPORT MODEL CALIBRATION PROCEDURES....	203
6.6 FINAL CALIBRATED PARAMETER VALUES	216
6.7 CALIBRATION AND TESTING PERFORMANCE MEASURES	222
6.8 SIMULATION OF BASELINE SALINITY CONDITIONS	233
6.9 CONCLUSIONS.....	237
7 BROAD CONCLUSIONS AND RECOMMENDATIONS	244
7.1 CONCLUSIONS.....	244
7.2 SUGGESTED SYSTEM MONITORING ENHANCEMENTS	257
7.3 SUGGESTED SYSTEM MODEL ENHANCEMENTS.....	259
REFERENCES	265

LIST OF TABLES

CHAPTER 4 Tables

Table 4-1. Range of parameter values employed in the models.....87

Table 4-2. Description of results for selected alternative management scenarios. Canal seepage reductions were achieved by adjusting model canal conductance values such that the simulated baseline total volume of seepage along all canals in the region was reduced by the amount indicated (i.e., 50%, 80%).....118

Table 4-3. Change in recharge to groundwater expressed as a percent reduction from the baseline condition for selected alternative management scenarios in the USR. Values in parentheses indicate the magnitude of the recharge offset due to induced seepage from canals that resulted from lower water tables under the specified intervention. To calculate the net percent reduction in recharge, subtract the induced seepage from earthen canals percentage from the larger percent reduction in recharge from irrigation.....119

Table 4-4. Change in total recharge expressed as a percent reduction from the baseline condition for selected alternative management scenarios in the DSR. Values in parentheses indicate the magnitude of the recharge offset due to greater induced seepage from canals that resulted from lower water tables under the specified intervention.....120

CHAPTER 5 Tables

Table 5-1. Flow and transport model input parameters including water content (θ), residual (θ_r) and saturated (θ_s) water content, infiltration rate (J), saturated hydraulic conductivity (K), Brooks-Corey epsilon (ϵ) (Niswonger et al., 2006), Brooks-Corey pore-size distribution index (λ), Brooks-Corey air-entry pressure (h_b) (Healy, 1987), concentration (C), longitudinal dispersivity (α_L), transverse dispersivity (α_T), bulk density (ρ_b), Freundlich equilibrium constant (K_f), Freundlich exponent (a), mass-distribution coefficient (K_d), first-order mass transfer rate (β).....142

Table 5-2. Quantitative assessment between UZF-MT3DMS simulated results and analytical benchmarks for the variable dispersivity, Nonlinear, and non-equilibrium transport problems, and to output from other models for the variable precipitation and evapotranspiration conditions, 2- and 3-dimensional transport problem was conducted using Equation 4-4. The order of results is in keeping with the order of simulations discussed in the Results and Discussion section....145

Table 5-3. Model runtimes for MODFLOW/MT3DMS and CATHY/TRAN3D are calculated as the sum of the flow and transport solutions. HYDRUS and SUTRA simultaneously solve flow and transport and are therefore reported as a single value.....166

CHAPTER 6 Tables

Table 6-1. Summary of the observed salt concentration variability (1 standard deviation) in each canal derived from comparisons to the continuous record from the nearest upstream river gage.....213

LIST OF FIGURES

CHAPTER 1 FIGURES

Figure 1-1. Regional scale modeling efforts have focused on the upstream and downstream study regions, shown in dark green within the broader context of the Lower Arkansas River Valley, shown in light green.....3

Figure 1-2. The roughly eight-fold increase in the concentration of total dissolved solids in the Arkansas River has persisted through time when considering data reported in Odell (1964).....6

Figure 1-3. Cross section of the geology below the alluvial aquifer (Darton, 1906).....14

Figure 1-4. Plots (A) – (D) depict average monthly flow rates that were normalized by dividing each month by the average monthly flow rate for the period of record, typically 1975 to present. Plot (E) shows the historical storage in Pueblo and John Martin Reservoirs extending back to 1978. Shaded regions highlight the USR and DSR study periods within the context of the full period of record.....17

Figure 1-5 Perspective plots of the upper most layer of the (A) Upstream and (B) Downstream computational grids with ground elevation plotted. There is 30x vertical magnification to show relief.....20

CHAPTER 3 FIGURES

Figure 3-1. Upstream and Downstream study regions in Colorado's Lower Arkansas River Valley showing the location of study fields.....43

Figure 3-2. Visual summary statistics of \overline{EC}_e for surveyed seasons during the study period for both the Upstream (blue) and Downstream (red) study regions.....55

Figure 3-3. Relative frequency and fitted probability distributions for \overline{EC}_e values over all surveys in the Upstream Study Region and Downstream Study Regions.....55

Figure 3-4. Mean \overline{EC}_e over all midseason surveys plotted for regular survey fields and detailed survey fields on contours of mean D_{wt} measured over all of the corresponding irrigation seasons.....57

Figure 3-5. Soil texture diagrams displaying average soil texture and corresponding average EC_e over all calibration site soil samples taken in regular surveys (A) in the Upstream Study Region, and (B) in the Downstream Study Region.59

Figure 3-6. Relationship between average EC_e at different depths below ground surface at calibration sites with (A) four-week average EC_{gw} and (B) four-week average D_{wt} . The 3 – 5 dS m^{-1} zone of crop yield threshold is indicated on both plots.62

Figure 3-7. Distributions of EC_e with depth below ground surface at calibration sites Upstream and Downstream. The 3 – 5 dS m^{-1} zone of crop yield threshold is indicated on both plots. Boxes show 25th, 50th, and 75th quartiles, whiskers extend to 1.5 times the interquartile range of the box, outliers omitted for cleanliness.....63

Figure 3-8. \overline{EC}_e versus four-week average D_{wt} for all surveyed fields (A) Upstream and (B) Downstream. The 3 – 5 dS m^{-1} zone of crop yield threshold is indicated on both plots.....64

Figure 3-9. Example time series plots of D_{wt} , EC_e distributions from regular surveys (whiskers indicate +/- 1 standard deviation), and average EC_e at calibration sites in (A) field 41 in the Upstream Study Region and (B) field 350A in the Downstream Study Region.....65

CHAPTER 4 FIGURES

Figure 4-1. The (A) USR and (B) DSR within Colorado’s LARV showing major features and land classifications. Identified wells correspond to the time series plots in Figure 4-5.....76

Figure 4-2. Observed (A) irrigation application depths and (B) tail-water runoff fraction in the LARV. Data collected between 2004 and 2007 were used to generate the probability distributions.....90

Figure 4-3. Final estimated \bar{K}_H for layer 1 of the (A) USR and (B) DSR and the final estimated \bar{S}_y for layer 1 of the (C) USR and (D) DSR.....100

Figure 4-4. Residuals of simulated groundwater hydraulic head for (A) the USR and (B) the DSR.....102

Figure 4-5. Model performance in predicted groundwater table (GWT) elevation in cells containing monitoring wells at four locations in the USR [wells 42, 67, 80, and 90 (Figure 4-1A)] and four locations in the DSR [wells 321, 344, 356, and 398 (Figure 4-1B)]. Grey bars shown on observations indicate the upper and lower limits of the 95% inter-percentile range (IR), accounting for spatial and temporal variability as discussed in Section 4.5.1.2.....103

Figure 4-6. Groundwater return flow time series for (A) the USR and (C) the DSR (including a plot of volume pumped from groundwater wells), along with residuals of simulated groundwater return flow for (B) the USR and (D) the DSR.....105

Figure 4-7. Contour plots of baseline model simulation results for average irrigation season recharge to groundwater over the simulated periods for the (A) USR and (B) DSR, average irrigation season D_{wt} for the (C) USR and (D) DSR, and average irrigation season groundwater upflux to ET (GWET) for the (E) USR and (F) DSR.....108

Figure 4-8. The impact of alternative management interventions on D_{wt} in (A) the USR and (B) the DSR.....110

Figure 4-9. The potential for recovering non-beneficial consumptive use in the USR under a variety of alternative management interventions shown as (A) annual and (B) cumulative savings.....112

Figure 4-10. The potential for recovering non-beneficial consumptive use in the DSR under a variety of alternative management interventions shown as (A) annual and (B) cumulative savings.....113

Figure 4-11. The effect of management intervention C3 (Table 4-1) on recharge to groundwater (A) in the USR, and (B) in the DSR; on D_{wt} (C) in the USR, and (D) in the DSR; and on groundwater upflux to ET (GWET) (E) in the USR, and (F) in the DSR obtained by differencing the average irrigation season conditions under the baseline conditions (Figure 4-6) and those of scenario C3.....122

Figure 4-12. Simulated reduction in groundwater return flows to the Arkansas River in the (A) USR and (B) DSR for selected alternative management scenarios.....128

CHAPTER 5 FIGURES

Figure 5-1. Comparison between UZF-MT3DMS and analytical benchmarks provided in Vanderborght et al. (2005). (A, C) Concentration profiles after 10 days for two dispersivities. (B, D) Concentration breakthrough curves at 2 m below ground surface. (A inset) Results provided for both the implicit finite difference method and Total Variation Diminishing (TVD) scheme for Peclet number > 2148

Figure 5-2. Magnitude and timing of precipitation and evapotranspiration stresses applied to the variable precipitation and evapotranspiration condition benchmark [taken from Vanderborght et al. (2005)].....149

Figure 5-3. Simulated solute fluxes moving past the extinction depth in a (A) silt and (B) sand profile. Simulated concentrations at three depths (25, 50 and 100 cm) in a (C) silt and (D) sand profile.....153

Figure 5-4. (A) Concentration-depth profile (using a transformed depth coordinate, η) for a nonlinearly sorbing solute, and (B) concentration ‘fronts’ moving through an unsaturated profile through time. The analytical benchmark of (A) published in Vanderborght et al. (2005).....154

Figure 5-5. (A) Dissolved and sorbed concentrations in a 10 cm profile at 200 hr after a ‘pulse’ injection of a nonequilibrium sorbing solute. (B) Breakthrough concentrations at 10 cm with time depicted as pore volumes. Under the flow conditions listed in Table 5-1, one pore volume

is equal to 10 hours. At 20 pore volumes flow was interrupted to allow the dissolved and sorbed concentration to equilibrate, after which flow was restarted. The published analytical benchmarks are from Vanderborght et al. (2005).....157

Figure 5-6. A 2-dimensional benchmark problem was established using results from the U.S. Geological Survey’s VS2DT model after 60 days. Comparisons in the unsaturated zone are very close with some differences appearing in the saturated zone and may be a result of slight differences in the location of the water table as mass begins to move laterally.....159

Figure 5-7. Perspective plot of 3-dimensional model showing location of cross section provided in Figure 5-8 (not to scale) and observation point of Figure 5-9.....160

Figure 5-8. Cross sections comparing simulated extents of select isoconcentration contours after 730 days. UZF-MT3DMS concentrations are depicted by the color-filled contours while HYDRUS, TRAN3D, and SUTRA contours are shown by the lines described in the legend...161

Figure 5-9. Concentration time series comparison for a point 3 m below the ground surface (Figure 5-7) were made between (A) three models that solve Richards equation using 0.5 m vertical discretization, and (B) two coarse UZF-MT3DMS vertical discretization schemes and two alternative vertical discretizations of HYDRUS.....162

CHAPTER 6 FIGURES

Figure 6-1. Map of (A) the USR and (B) the DSR showing surface water monitoring points (triangles) as well as groundwater monitoring well locations.....182

Figure 6-2. The numerical model vertical discretization with the ground surface, water table, unsaturated zone, root zone, and bedrock shown.....187

Figure 6-3. Frequency histograms of \overline{EC}_e in surveyed fields over the USR (solid) and DSR (cross-hatched) for each season surveyed were made.....190

Figure 6-4. Dashed lines show transect locations for calculated salt load totals presented in the river and canals. Transect locations correspond to four USGS gages continuously collecting (every 15 min) flow and EC observations: (1) the Arkansas River at Catlin Dam, (2) Las Animas, (3) Below John Martin Reservoir, and (4) Coolidge, KS. Note that the Purgatoire River enters John Martin Reservoir from the south from outside the irrigated area.....191

Figure 6-5. Total annual discharge as measured by the Cañon City gage on the Arkansas River. Blue bars highlight the water years coinciding with the study period.....192

Figure 6-6. Fitted linear relationships between EC and TDS for (A) groundwater in the USR (B) surface water in the USR (C) groundwater in the DSR and (D) surface water in the DSR.....194

Figure 6-7. Salt load in the river and canals across four transects in the LARV located near the two study regions. Estimated contribution of salt load entering the LARV from the Purgatoire River also is shown.....198

Figure 6-8. Schematics of surface water features for (A) the USR and (B) the DSR for use in calculating groundwater return loads. Surface water return flows originating from irrigation tail-water are further partitioned into surface water and groundwater returns to account for significant differences in their respective salt concentrations.....201

Figure 6-9. Estimated initial salt concentration arrays for layer 1 of the (A) USR and (B) DSR and for layer 2 of the (C) USR and (D) DSR. Pilot points coincide with CSU groundwater monitoring well locations and were supplemented by additional pilot points where their density was deemed sparse.....207

Figure 6-10. Command areas, or fields operated under specific canals, in the two model regions are highlighted. Yellow triangles depict the spacing of CSU surface water monitoring points along two canals within each region. Data collected at these locations guided adjustment of the salt concentration of applied water.....209

Figure 6-11. Time series plots comparing the continuously monitored EC at the gage located at Catlin Dam on the Arkansas River to the discrete measurements taken in the (A) Rocky Ford Canal and in the (C) Catlin Canal. To view the “SP” (surface point) locations, readers are referred to Figure 6-1A. The distribution of the residuals (difference between discrete measurements and simultaneous measurements at the continuously monitored gage location) calculated in (A) and (C) are shown in (B) and (D), respectively.....210

Figure 6-12. Time series plots comparing the continuously monitored EC at the gage on the Arkansas River located below John Martin Reservoir to the discrete measurements taken in the (A) Amity and in the (C) Buffalo Canals. To view the “SP” (surface point) locations, readers are referred to Figure 6 1B. The distribution of the residuals (difference between discrete measurements and simultaneous measurements at the continuously monitored gage location) calculated in (A) and (C) are shown in (B) and (D), respectively.....211

Figure 6-13. Estimated aquifer porosity values for layer 1 of (A) the USR and (B) the DSR and for layer 2 of (C) the USR and (D) the DSR. Blue corresponds to more porous areas.....214

Figure 6-14. Estimated dispersivity values for layer 1 of (A) the USR and (B) the DSR and for layer 2 of (C) the USR and (D) the DSR.....216

Figure 6-15. The distribution of the final estimated starting salt concentration arrays for both layers in (A) the USR and (B) the DSR.....217

Figure 6-16. The distribution of the final estimated porosity arrays for both layers in (A) the USR and (B) the DSR.....218

Figure 6-17. An adjustment factor, initially set equal to 1.0 over the modeled areas, was used to adjust the initial estimates of porosity values. The final estimated adjustment factor values ranged between approximately 0.75 and 1.25.....219

Figure 6-18. The distribution of the final estimated dispersivity arrays for both layers in (A) the USR and (B) the DSR.....221

Figure 6-19. Groundwater salt concentration residuals for (A) the calibration and (B) the testing periods for both the USR and DSR.....223

Figure 6-20. Model performance in predicted groundwater salt concentration in comparison to observed salt concentration in monitoring wells at four locations in the USR [wells 42, 67, 80, and 90 (Figure 4-1A)] and at four locations in the DSR [wells 321, 344, 356, and 398 (Figure 4-1B)]. The wells shown here correspond with those selected in Figure 4-5.....225

Figure 6-21. Groundwater return salt load to the Arkansas River in the (A) USR and (B) DSR.....227

Figure 6-22. Location and frequency of cells in the USR and DSR used for generating a simulated layer 1 salinity distribution for comparison to the observed soil water salinity distribution.....229

Figure 6-23. Comparison of frequency distributions and fitted cumulative distribution function (CDF) of observed soil water salinity and simulated layer 1 salinity expressed as EC (dS m⁻¹) in (A) the USR and (B) the DSR. CDFs of \overline{EC}_e are plotted to provide consistency with Figure 3-3, where observations of \overline{EC}_e first were reported and discussed.....230

Figure 6-24. Average irrigation season dissolved salt concentration in layer 1 over the course of the simulated period for (A) the USR and (B) the DSR.....231

Figure 6-25. Temporal variability of the average simulated layer 1 dissolved salt concentration (expressed as EC_e) among the most common crops planted in the USR and DSR study regions. The 3-5 dS m⁻¹ zone of crop-yield reduction threshold is highlighted by the horizontal grey bar. Because the salt tolerance for fruits and vegetables is lower, a 1-3 dS m⁻¹ zone is shown in the bottom plot.....234

Figure 6-26. Simulated $D_{wr}-\overline{EC}_e$ versus observed $D_{wr}-\overline{EC}_e$ relationships for (A) the USR and (B) the DSR. Simulated $D_{wr}-\overline{EC}_e$ pairs are derived from average irrigation season values and include only those values from cells with > 99% crop coverage. Simulated \overline{EC}_e values are back-calculated from the concentration values simulated by UZF-MT3DMS.....235

CHAPTER 7 FIGURES

Figure 7-1. An upward trend in the number of days each year above 32.2 °C (90 °F) (gray bars corresponding to the right y-axis). The first and last days of each growing season with a maximum temperature above 32.2 °C (90 °F) is trending earlier and later, respectively. Figure built with an R script first described in Pederson et al. (2010).....253

Figure 7-2. Mean daily flow rates for the Cañon City gage are calculated using the data collected before the study period began in the USR (blue line) and after the start of the study period (red line). Julian Day 1 in this plot corresponds to the start of the “water year,” or October 1st.....254

1 INTRODUCTION

1.1 IRRIGATED AGRICULTURE FACING CHALLENGES OF GLOBAL PROPORTIONS

Today, agricultural resources (including both irrigated and non-irrigated agriculture) feed an estimated 7.1 billion people. Considering that the global population is forecast to increase by 1.8 billion people to 8.9 billion by 2050 (United Nations, 2004), the pressure to produce more with less will intensify. In order to satisfy the increasing demand, Tilman et al. (2001) project trends over the last 35 years to estimate that nitrogen fertilizer application will need to increase 1.9 – 3.9-fold, phosphorus fertilizer application will need to increase 2.4-fold, and irrigation water usage will need to increase 1.9-fold by 2050. Assuming these resources are available, the authors go on to point out that the impacts these increases will have on the environment are significant. Impacts include degradation of surface water and groundwater supplies as well as salinization of soils. Foley et al. (2005) summarize the dilemma as follows: “in short, modern agricultural land-use practices may be trading short-term increases in food production for long-term losses in ecosystem services, including many that are important to agriculture.”

The demand for high quality irrigation water, an already over-taxed resource, has brought the issue of sustainability to the fore. Further, roughly half of the terrestrial ‘useable’ land is already in pastoral or intensive agricultural production, likely relegating the expansion of global food output to lands that are increasingly difficult to irrigate or to sustain (Tilman et al., 2002). Compounding the problem further is the fact that much of the land currently in production has diminished yields due to waterlogging and salinization.

1.2 CHALLENGES CONFRONTING IRRIGATED AGRICULTURE IN COLORADO

The worldwide challenges of salinization and waterlogging also confronts irrigated agriculture in Colorado. However, salt is not the only constituent of concern. Naturally occurring chemical pollutants, including selenium (Se), uranium (U), and iron (Fe), have received attention because they often exceed total maximum daily loading (TMDL) standards (Donnelly, 2005; Mueller Price and Gates, 2008; Bailey, 2012). Once dissolved from the marine sediments underlying alluvial aquifers as well as from exposed bedrock outcrops, groundwater gradients sustained by inefficient irrigation methods transport the salt and other pollutants back to the river which effectively acts as the system drain. Not only does this process degrade river water quality, but downstream diversions distribute the poorer quality irrigation water to the land surface, where it evapo-concentrates (Wallender and Tanji, 2012) and interferes with plant development (Silva et al., 2008). In addition, inefficient irrigation practices prevalent throughout Colorado's irrigated lands, including the Lower Arkansas River Valley (LARV) (Figure 1-1), contribute a significant amount of water to non-beneficial consumptive use each year. Finally, "institutionalized inefficiency", intimating that the "structural features of Colorado's water management system...inhibit constructive reform and perpetuate inefficiencies in water use (Peak, 1977)," limit the ability of researchers and river administrators from implementing water saving and water quality preserving measures. Because the Arkansas River Compact, a formal agreement between Colorado and Kansas that ensures flow delivery at the CO-KS stateline, stipulates that flows cannot be materially depleted, and because most water-saving interventions eventually result in reduced groundwater return flow back to the river, they are disqualified from consideration. To summarize, the challenges currently facing the LARV considered here include 1) waterlogging, 2) salinization, 3) diminished river water quality with respect to a suite of

dissolved ions [salt, or total dissolved solids (TDS) is considered in this work], 4) significant volumes of water loss to non-beneficial consumptive use, and 5) the legal framework governing river operation that imposes a restrictive set of rules limiting the ability to address challenges 1 through 4 (this challenge is discussed in Section 7.2, “Recommendations”). Explanations of each of these challenges are provided next.

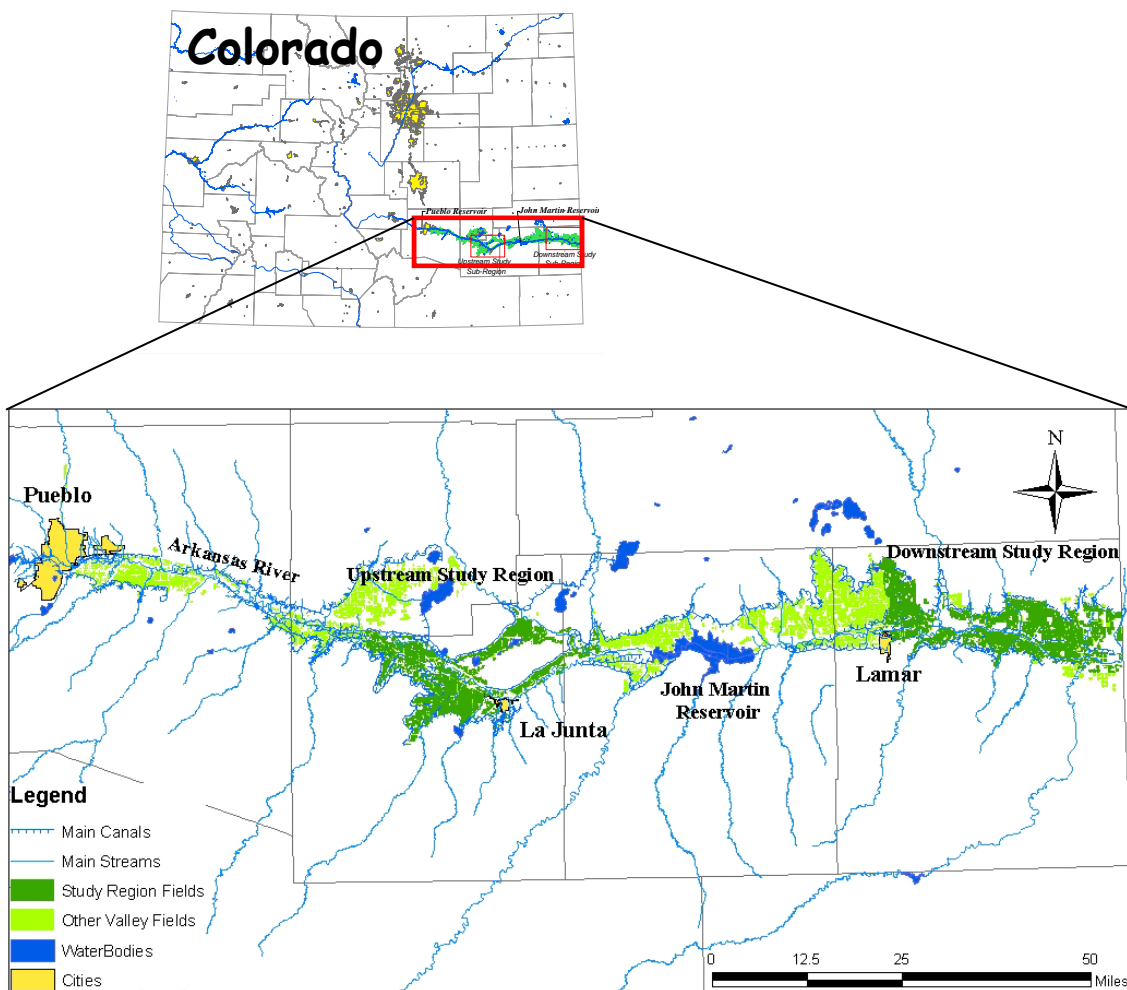


Figure 1-1. Regional scale modeling efforts have focused on the Upstream Study Region (USR) and Downstream Study Region (DSR), shown in dark green within the broader context of the Lower Arkansas River Valley, shown in light green.

1.2.1 Waterlogging and Salinization

Waterlogging is the process by which oxygen in the soil pores of the crop root zone is displaced by water thereby curtailing crop growth and yield (Wesseling, 1974; Evans and Fausey, 1999). Waterlogging often occurs in areas where the groundwater table is located at or near the land surface. Salinization inevitably accompanies waterlogging in arid and semi-arid environments and refers to the buildup of salts in the root zone due to the evaporative concentration of salts originally present in the water passing through the root zone, as well as from the dissolution of salts from native geologic and soil materials. Upflux from a high water table brings salinized groundwater back into the root zone. Evaporative concentration also contributes to the build-up of salts in the root zone. Salt accumulation in the soil water of the root zone depresses the osmotic potential that plants rely on to draw water from the soil pores. The higher the salt concentration becomes, the more energy a plant has to exert to draw water from the soil matrix. In addition to a higher expenditure of energy by the plant, certain salts also may have a toxic effect on plants at the cellular level, further stunting growth (Silva et al., 2008). If a threshold salinity value is crossed (depending on crop type) (Hanson et al., 1999) the stressed crop will begin to transpire less water and crop yield will be reduced (Fullen and Catt, 2004). In turn, the lowered ET will contribute to additional mounding of the water table, further compounding the problem. In summary, many of the rich soils of the LARV have reduced crop productivity as a direct result of shallow water tables and the salt build up that accompanies it. The rural commerce that depends on crop production also has suffered. For instance, in 2006 Houk et al. (2006) estimated that average annual agricultural production losses of approximately \$4.3 million occur in the USR alone.

In summary, a number of factors contribute to waterlogging and irrigation-induced salinization, including inadequate or poor drainage (Carpenter, 1983), seepage from conveyance

canals, excessive irrigation, and associated salt build up due to dissolution and evaporative concentration (Lal, 2004). The FAO (2009) currently estimates that between 20 and 30 million hectares of irrigated lands worldwide are seriously affected by salinity rooted in these sources. Therefore, the ratio of potential profit increases resulting from restored crop yields to capital expenditure addressing drainage, seepage, and inefficiency concerns on degraded lands will determine if such expenditure is prudent. The work presented herein does not factor in the value of improved infrastructure or crop yield, but focuses on developing data and models to help answer technical questions like, “how many centimeters will the saline water table be lowered if applied irrigation is reduced by 25%?”, among others.

1.2.2 Degradation of River Water Quality

Salt, as well as other dissolved constituents like selenium (Se), for example, return back to the river via surface and subsurface flows and have been at disturbingly high levels under the irrigation management practices in the LARV for a sustained period of time. Nearly 50 years ago Odell et al. (1964) documented an increase in TDS in the Arkansas River from 500 mg L⁻¹ near Pueblo to more than 4,000 mg L⁻¹ at the Colorado-Kansas state line. More recent measurements of electrical conductivity (EC), an indicator of TDS, over the last 10 years reveals that the same relationship persists today (Figure 1-2). A number of LARV studies describe in detail the recent status of river water quality degradation in the LARV (Donnelly, 2005; Mueller Price and Gates, 2008; Gates et al., 2009; Bailey, 2012).

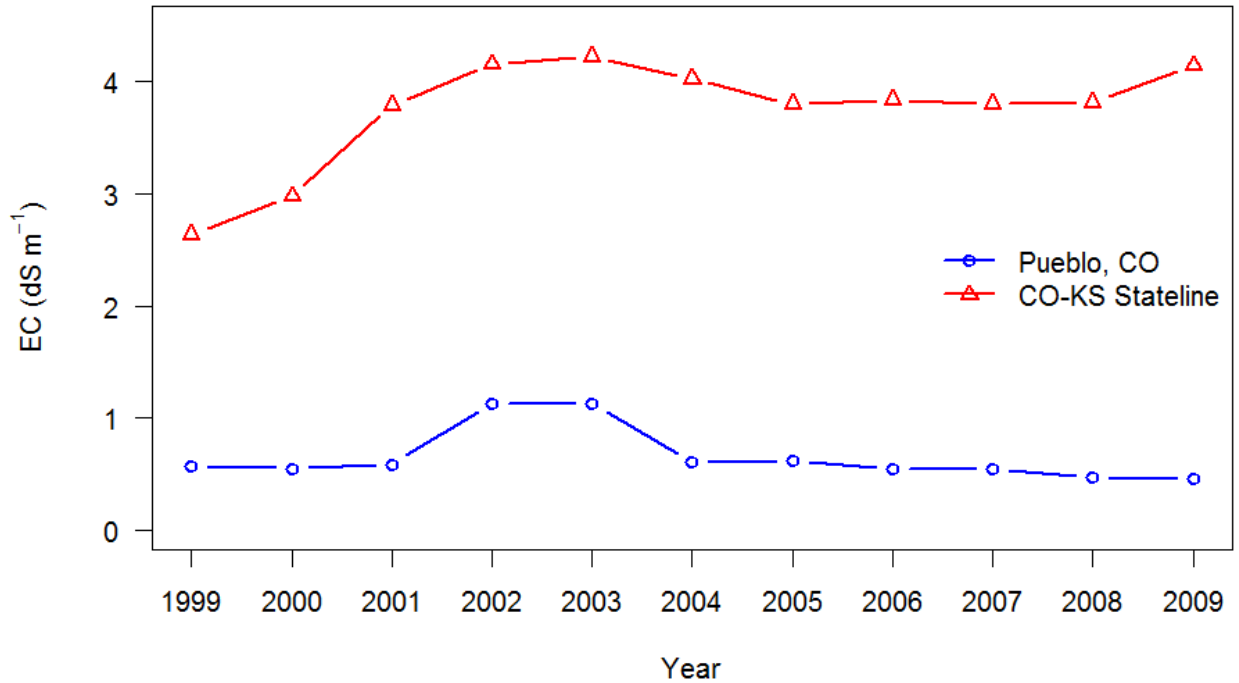


Figure 1-2. The roughly six-to-eight-fold increase in TDS (as indicated by EC) in the Arkansas River has persisted through time when considering data reported in Odell (1964). Measurements of EC are collected by two USGS stream gages. The first is located below the outlet of Pueblo Reservoir whereas the second gage is located in Coolidge, KS.

1.2.3 Non-beneficial Consumptive Use

Non-beneficial consumptive use refers to the component of water lost from the groundwater system to ET via upflux from shallow groundwater tables that does not contribute to crop water demand. Often, naturally-vegetated areas and fallowed lands border cultivated fields where excessive irrigation water is applied. Over-irrigation on the neighboring cropped fields sustains high water tables from which ET derived from the saturated zone occurs. Large tracts of naturally-vegetated and fallow land interspersed with the cultivated fields contributes to a significant volume of water lost to non-beneficial consumptive use in the LARV (Niemann et al., 2011).

1.2.4 A Restrictive Legal Framework For System-Wide Improvements

A number of potential alternative water management strategies exist for improving agricultural and environmental conditions in the LARV. Installing or rehabilitating existing subsurface drains is one way to reduce water table mounding and mitigate waterlogging and salinization. The use of artificial drainage, however, is not considered here since it would be applicable to a limited areal extent and the disposal of drainage water effluent may exacerbate surface water degradation. Drains accelerate the movement of infiltrated irrigation water back to surface water features (Tanji and Keyes, 2002) laden with salt and other dissolved constituents leached from the root zone.

Recharge reduction through improved irrigation efficiency is another way to reduce water table mounding, mitigate waterlogging, reduce upflux contributing to evapoconcentration of salts, reduce non-beneficial consumptive use occurring from adjacent lands, and reduce hydraulic gradients contributing to dissolution of salts and other pollutants from subsurface formations and driving poor quality groundwater back to the river. Sprinkler and drip irrigation systems that focus water delivery through the use of mobile or buried lines, respectively, apply a fraction of the water used in over-land or flood irrigation, the dominant form of irrigation in the LARV. Once the amount of water applied to irrigated fields is reduced, the deep percolation component of recharge to the shallow aquifer system and its removal helps facilitate water table subsidence.

Seepage from earthen delivery canals is detrimental to the health of the LARV in a number of ways. Like deep percolation leading to recharge, it is a significant source of both flow and salt to the shallow aquifer system contributing to waterlogging, upflux of saline groundwater to the crop root zone, non-beneficial consumptive use, and degradation of river water quality through increased mobilization of subsurface salts to the stream and drainage

network. Furthermore, seepage losses reduce the amount of water available during hot summer months when crop water demand is highest.

As was alluded to in Section 1.2, implementation of potential management alternatives is restricted by both intrastate and interstate water right agreements. Because the solution strategies listed above alter the magnitude and pattern of groundwater return flow to the river, water that can subsequently be used to satisfy water rights among downstream diversions, they materially deplete in usable quantity (Colorado Revised Statutes, 1949) Arkansas River flow and are therefore precluded from consideration without augmentation.

1.3 OBJECTIVES

The general methods for solving the irrigation-induced problems described in the preceding sections are well known. Sound regional water management, enhanced on-farm water application efficiency, improvements in water conveyance efficiency (e.g. lining or sealing earthen canals), and provision of sub-surface drainage facilities are all possible means by which remediation can be achieved (Umali, 1993). Often, however, it is difficult or impossible to accurately predict the effectiveness of a particular solution strategy, particularly when implemented over extensive and variable areas. In the LARV, like other areas suffering from irrigation-induced agroenvironmental problems, data are needed to accurately describe the baseline nature of the problems and models are needed that can be trusted to reasonably predict and describe solution strategies over regional scales

Thus, the first objective of this study is to firmly establish the nature, extent, and severity of soil water salt concentrations contributing to diminished crop yields in the LARV. Documentation of soil water salinity conditions using surveys conducted over the LARV, quantifies the central irrigation-induced threat that must be addressed through modeling

investigations. Moreover it establishes a baseline point-of-reference for comparing with future soil water salinity surveys should alternative water management interventions aimed at reducing soil water salinity and restoring crop yields be implemented. In other words, demonstrating a measurable reduction in soil water salt concentrations post-intervention is made possible by collecting a snapshot of pre-intervention conditions.

The second objective is to develop the calibrated regional-scale groundwater flow models necessary for evaluating baseline aquifer flow, water table, and soil water conditions in the LARV. Accomplishment of this objective is necessary before subsequent objectives, including the development of physically-based, distributed-parameter, regional-scale salt transport models for quantifying current salt concentrations in both the saturated and unsaturated zones can be pursued. The groundwater flow models are to be constructed using the unsaturated-zone flow (UZF1) package (Niswonger et al., 2006) coupled with MODFLOW-NWT (Niswonger et al., 2011), the most widely used groundwater modeling software in the world (Hill et al., 2010). The calibrated flow models developed herein play a supporting role for more detailed water quality models that include chemical reactions currently employed in the LARV by Colorado State University researchers (Bailey, 2012).

Upon accomplishment of objective two, objective three is to use the calibrated flow models to explore how well various alternative management strategies lower saline water tables and reduce non-beneficial consumptive use, and to what extent they alter groundwater return flows. Groundwater flow simulations, such as those described herein, are particularly well suited for providing a detailed description of the spatio-temporal groundwater and surface water exchanges. Because implementation of alternative water management scenarios in the LARV is contingent upon the preservation of historical groundwater return flows so as not to materially

deplete river flow, then historical groundwater return flow patterns (i.e., location and timing) need to be estimated. By knowing how current irrigation practices manifest as groundwater return flows, reservoir releases can be supplemented to satisfy interstate water agreements, described in more detail below. To summarize, the benefits of well-calibrated groundwater flow models are numerous: the severity and the spatial and temporal variability of current conditions can be characterized, the impact of alternate interventions on various water budget terms (e.g., non-beneficial consumptive use and crop ET) and water conservation can be explored, combinations of remedies can be investigated and ranked prior to investing capital in new or rehabilitated infrastructure, a foundation for solute transport modeling is provided (i.e., description of the groundwater flow field), and alterations to historical groundwater returns can be quantified. Several review papers highlight how previous computer models have addressed problems similar to those found in the LARV (Chang, 1992; Martin et al., 2005; Simunek and Bradford, 2008; Vrugt et al., 2008).

The fourth objective of the analysis aims to take full advantage of the surveyed soil water salt concentration dataset collected as part of the first objective. To accomplish this goal, modification of the popular MT3DMS (Mass Transport in 3 Dimensions Multiple Species) (Zheng and Wang, 1999a) model is necessary. MT3DMS, the most commonly used solute transport companion code that “piggy-backs” on MODFLOW’s flow solution, lacked functionality to seize upon the predicted unsaturated-zone flow terms. In order to take full advantage of the unsaturated-zone flow terms calculated by UZF1, MT3DMS is to be modified and tested against analytical solutions, as well as against results from other published codes, for predicting concentrations in the unsaturated zone. The modified code, referred to as UZF-MT3DMS, facilitates use of the soil water salinity survey results as a calibration dataset targeted

by the automated parameter estimation routines described later. Because UZF-MT3DMS relies on calculated fluid fluxes from a calibrated MODFLOW model, the Link Mass Transport (LMT6) package (Zheng et al., 2001) requires modification in order to complete the fourth objective. LMT6 organizes flow terms into a UZF-MT3DMS compatible format.

The fifth and final objective is to apply the UZF-MT3DMS code (objective four) to the USR and DSR. Both of the developed UZF-MT3DMS models rely on the calibrated groundwater flow models developed as part of objective two and are calibrated in part by the soil water salinity surveys completed in fulfillment of objective one. The UZF-MT3DMS models simulate salt movement in the subsurface (saturated and unsaturated zones) as a conservative (i.e., non-reactive) constituent that can be adequately described by advection and dispersion processes. To the extent that the models are unable to satisfactorily match observations, future salt transport models should consider including chemical reactions through the use of the “reaction” package included with UZF-MT3DMS.

Before proceeding, a more complete description of the LARV is provided, followed by a clear layout of the dissertation chapters.

1.4 DESCRIPTION OF THE STUDY REGIONS

An area representative of Valley conditions upstream of John Martin Reservoir, referred to as the Upstream Study Region (USR) (Figure 1-1) was the first area of concentration. This region extends about 62 km along the river between Manzanola, Colorado and Adobe Creek located just west of the city Las Animas and is discussed in detail by Gates et al. (2002) and Burkhalter and Gates (2005). In 2002, a second area, referred to as the Downstream Study Region (DSR) (Figure 1-1), was added downstream of John Martin reservoir between Lamar, Colorado and the Colorado-Kansas border.

Surface irrigation in the valley started in the 1870's with the construction of what is now called the Rocky Ford Canal and continues today (Sherow, 1990). By the middle 1880's, flows in the Arkansas River were fully appropriated for average water years (Abbott, 1985). Today, the appropriated water rights in the LARV exceed the average annual river flow, as is the case in most western United States river basins (Bittinger and Stringham, 1963). Because the LARV is located in a semi-arid environment, it suffers from the same mal-effects of waterlogging and salinization as many of the world's most productive irrigated regions (Ghassemi et al., 1995; Mudgway et al., 1997).

Irrigation in the LARV is dominated by flood and furrow methods. To a lesser extent, sprinkler and drip irrigation technologies are employed in pockets throughout found throughout the LARV (Gates et al., 2006; Gates et al., 2012). A variety of crops, including alfalfa, corn, sorghum, wheat, vegetables, melons, and legumes, have historically been grown in the LARV during the study period. LARV soils span a wide range of textures that are primarily loam or silty clay loam (Wittler, 2005).

The maximum temperatures recorded across the LARV during the study period were as follows. Near Pueblo (Vineland CoAgMet station), a maximum temperature of 39.9 °C (104 °F) was recorded on July 13th, 2003. Moving down valley, in the USR (Rocky Ford CoAgMet weather station), Las Animas (NCDC weather station), and DSR (Holly CoAgMet station) regions respectively, maximum temperatures of 40 °C (104 °F, recorded on 7/23/2005), 42 °C (108 °F, recorded on 6/1/2002) and 42 °C (108 °F, recorded on 7/3/2007), were recorded. The minimum temperatures recorded during the study period for the same stations were -39 °C (-38 °F, recorded on 12/1/2004), -26 °C (-15 °F, recorded on 12/24/2004, 12/8/2005, and 1/17/2007), and -27 °C (-17 °F, recorded on 12/8/2005). River elevations range between 1,643 m (5,390 ft)

which is where the river exits Pueblo Reservoir and 1,020 m (3,346 ft) at the Colorado-Kansas Stateline.

1.4.1 Geology of the Study Areas

The following overview of the geology of the LARV is synthesized from Darton (1906), Voegeli (1965), Weist (1965), Konikow and Bredehoeft (1974a), and Person and Konikow (1986). Many previous studies performed in the LARV provide rich hydrogeologic datasets with which to build and support the groundwater models presented herein.

The LARV can be described as a broad, shallow valley that is underlain by a series of sedimentary formations (Figure 1-3) of the late Cambrian to Tertiary age (Darton, 1906). A relatively uniform “Dakota” sandstone layer underlies the valley. Whereas this formation occurs at considerable depth below the USR, it rises to just below the alluvial aquifer (or ground surface in some spots) in the vicinity of John Martin Reservoir before declining again below the DSR. The Dakota formation is overlain by a series of marine sediments deposited in the last marine invasion, which is believed to have occurred during the Cretaceous Period. The layers above the Dakota Sandstone are lumped into three groups: 1) the Benton group, 2) the Niobrara formation, and 3) the Pierre shale. Within the Benton group are two shales, the Graneros and Carlisle, which sandwich the Greenhorn limestone layer. Members of this group are exposed south of the Arkansas River between La Junta and Las Animas, Colorado. The Benton group is succeeded by the Niobrara which is comprised of limestones lower down in the formation and limey shales higher up in the formation. Although much of the Niobrara is exposed west of Pueblo, it does underlie the alluvial aquifer between Manzanola and Swink, CO. If the Niobrara was deposited in Bent or Prowers County, subsequent erosion has removed it. The Pierre shale group, which

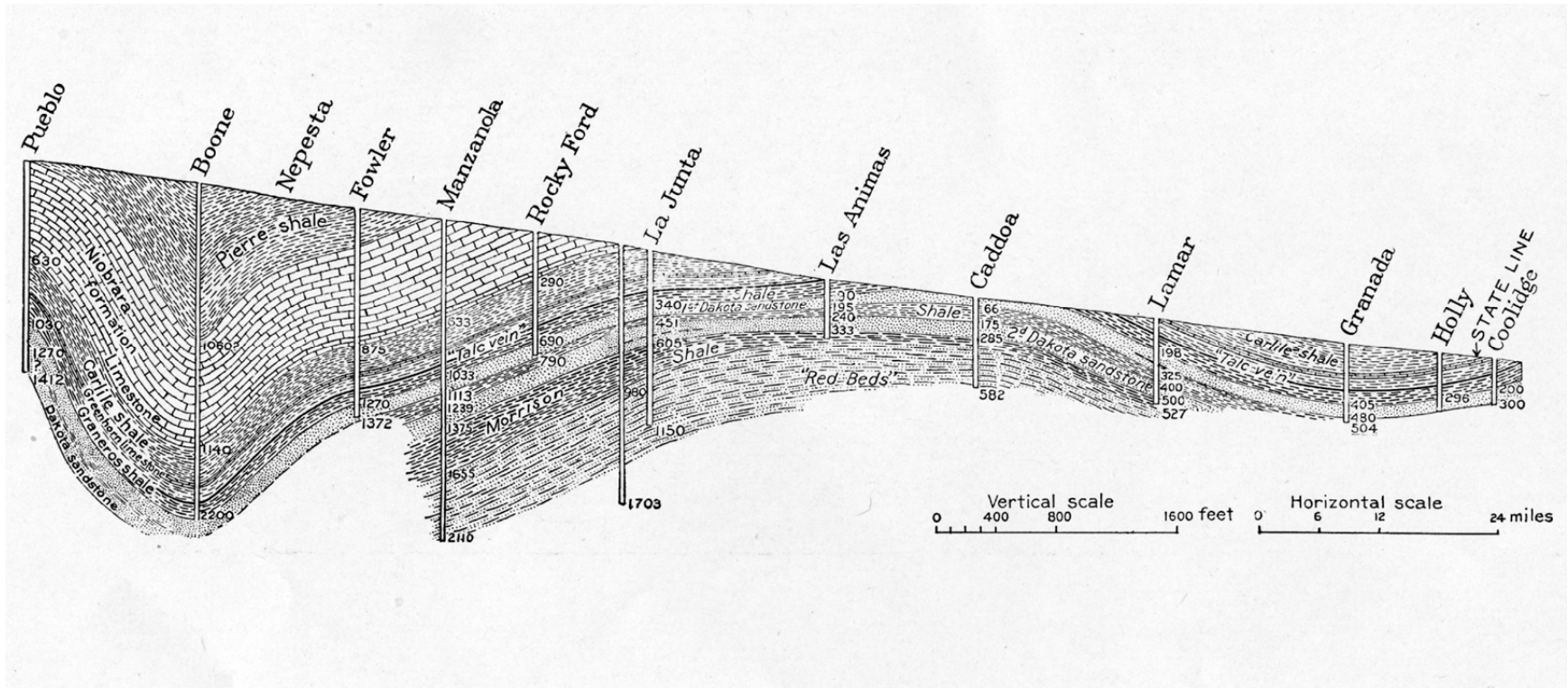


Figure 1-3. Cross section of the geology below the alluvial aquifer (Darton, 1906)

overlies the Niobrara, is a thick mass of cemented clay. Whereas the Pierre is thick near the Front Range, it thins in eastern Colorado where erosive processes of earlier Tertiary times have reduced it. The Pierre shale formation contacts the alluvial aquifer between Pueblo and Manzanola, CO, and is over 3,000 ft thick at its thickest point. This formation often has been found to contain numerous deposits of marine shells (Darton, 1906).

The valley fill material comes primarily from erosion and deposition during Pleistocene times (Weist, 1965). Alluvial grain size ranges from coarse gravel containing cobbles to clay (Major et al., 1970). Some faults have been found in the deeper formations of the valley, but do not require representation in the groundwater models of the alluvium (Voegeli, 1965; Weist, 1965).

Groundwater movement between the deeper formations does occur due to differences in hydraulic head, but is generally negligible due to the presence of shales. Where the shallow alluvial aquifers cut across the Dakota Sandstone, groundwater will move from one unit to the other. For example, in an area east of Lamar, CO, lower piezometric heads in the Dakota Sandstone lead to recharge from the alluvium (Voegeli, 1965). The affect that such a transfer has on the overall mass balance of the alluvial aquifer is uncertain. For this study, it is considered negligible compared to the other relatively high rates of recharge and discharge of groundwater in the alluvial aquifer.

1.4.2 Hydrology of the Study Regions

Traversing a circuitous 311 km (193 mi) across the high plains of Southeastern Colorado (Figure 1-1), the Arkansas River supplies the majority of the water used for irrigation in the LARV. Runoff entering the LARV from the Upper Arkansas River Valley (UARV), itself flanked by some of the highest peaks in the conterminous United States [numerous peaks exceed 4,250 m (14,000 ft)], is driven primarily by snowmelt. Managed releases from Pueblo Reservoir

(located at the outlet of the UARV) and John Martin Reservoir (located midway along the LARV) feed an extensive network of irrigation diversions that in turn support an estimated 109,000 ha (270,000 ac) of irrigated land.

Runoff from the UARV is supplemented in the LARV by tributary streams originating in the desert flanks of the valleys by modest precipitation associated with semi-arid regions. Near Pueblo reservoir, the LARV receives on average 28 cm (11 in) of precipitation each year. Moving eastward, precipitation increases slightly to 29 cm (11.5 in) in the La Junta area and to 38 cm (15 in) in Lamar. These updated estimates of precipitation correspond closely with earlier estimates of 30.5 cm (12 in) in Otero County by Weist (1965) and 38 cm (15 in) by in Otero and Prowers County by Voegeli (1965).

Groundwater return flow associated with over-irrigation supports downstream diversions as well. Because the Arkansas River is in good hydraulic connection with the alluvial aquifer, high water tables sustained by high recharge rates contribute water back to the river. Figure 1-4 shows normalized hydrographs of the average monthly flow rates measured at selected stream gages in the Arkansas River and tributaries in the USR and DSR of the LARV. Normalized monthly flow rates were computed by dividing that month's average streamflow rate by the average streamflow rate over 1975 – 2012 for that month. Figure 1-4A provides a sense of the spatial and temporal variability in the USR during the study period. In 1999, for example, streamflows were well above average (> 3) in the spring and early summer, but tapered off significantly ($< \sim 0.5$) in the later months of 1999. Normalized flow rates from all eight gages (Figure 1-4A–D) are telling of the extremely dry conditions in 2002 and 2003. In the years that follow, 2007 is the only year with consistently average (~ 1) or above average mean monthly

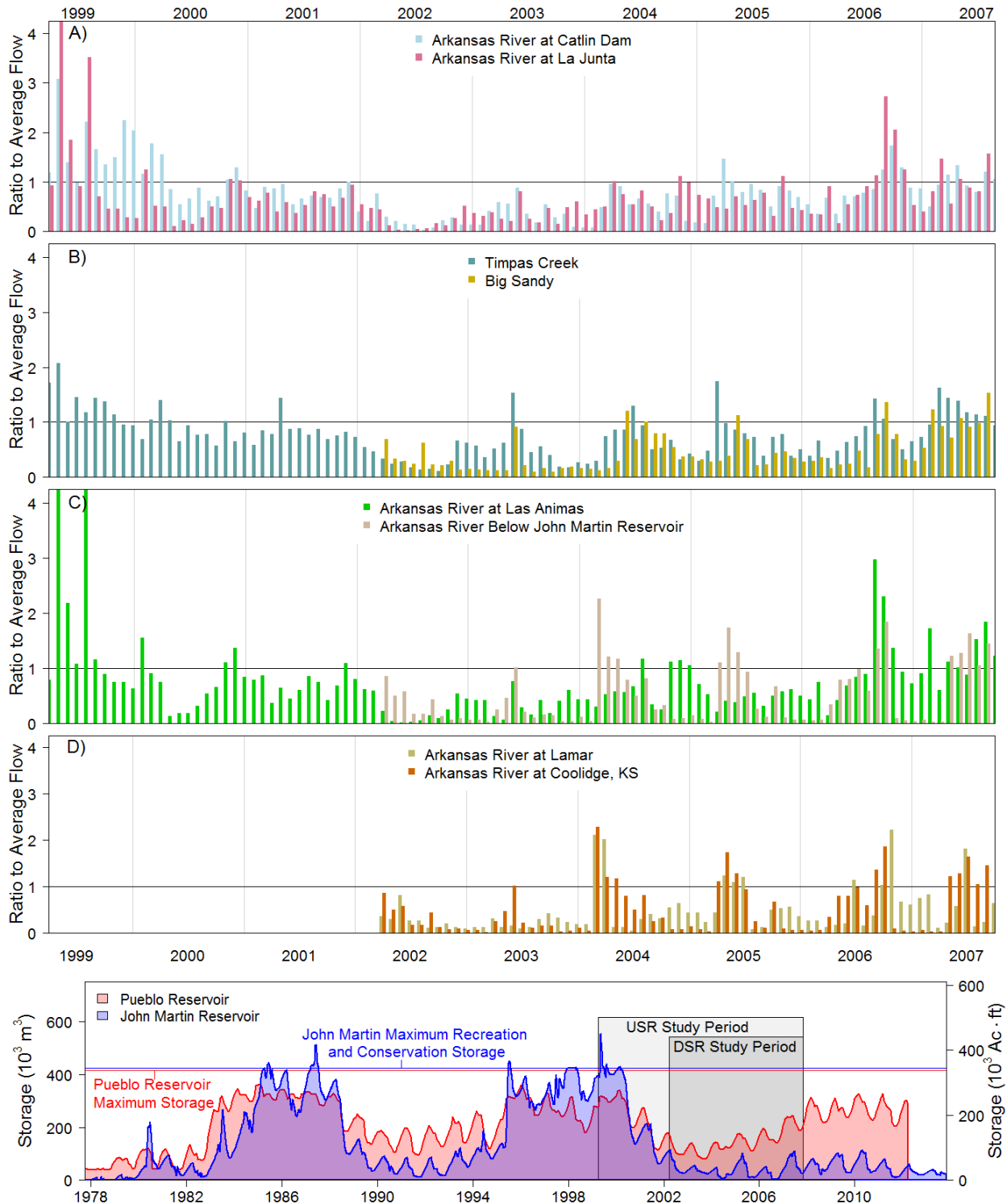


Figure 1-4. Plots (A) – (D) depict average monthly flow rates that were normalized by dividing each average monthly flow rate by the average monthly flow rate for the period of record, typically 1975 to present. Plot (E) shows the historical storage in Pueblo and John Martin Reservoirs extending back to 1978. Shaded regions highlight the USR and DSR study periods within the context of the full period of record.

flow rates. Further analysis is required to determine whether the above average (> 1) monthly flow rates inside the DSR (Figure 1-4D) are sustained by releases from John Martin reservoir. This would make sense, since the observed low normalized flows (< 1) that occur until the following year's runoff period are likely the result of depleted reservoir releases from storage. Storage time series in Pueblo and John Martin Reservoirs are shown in Figure 1-4E. Annual oscillations and multi-year trends in storage are observed for both reservoirs. In Pueblo Reservoir, a long-term cycle of approximately 10-12 years reveals that its stored volume, especially during dry periods (2002-2003), is not as susceptible to rapid drawdowns from operating capacity, as is seen in the John Martin Reservoir storage history (1988 and 2000). John Martin Reservoir, on the other hand, operates at or near "recreation and conservation" capacity from 1985 to 1988, and from 1995 to 2000. Starting in 2002 and extending through the end of the DSR study period, however, John Martin Reservoir has been drained to near its dead storage level by the end of each irrigation season. Conversely, Pueblo Reservoir storage experiences initial drawdown during the early years of the USR study period but shows a long-term rebound starting in 2004 that continues into 2012.

1.4.3 Previous CSU Work in the LARV Study Regions

Starting in 1998, researchers at Colorado State University (CSU) have made waterlogging, non-beneficial consumption, and degradation of water quality resulting from irrigation a focal point of efforts to revitalize agriculture in the LARV and to improve the environmental health of the river. Early efforts mapped the areal extent and severity of waterlogging and salinization in the LARV, salt loading in the Arkansas River, and non-beneficial consumptive use from non-cultivated lands. Upon documenting the most problematic areas through field data collection efforts, the focus shifted toward modeling the region with

finite difference computational groundwater flow and salt transport models. The calibrated computer models were used to investigate the impact of different management practices and improved infrastructure on reducing waterlogging and soil salinization, conserving water, and lowering salt and pollutant loads to the river in the USR (Gates et al., 2002; Houk, 2003; Burkhalter and Gates, 2005; Burkhalter and Gates, 2006). Further research activities have included developing a related spatial decision support system at the basin scale in order to improve water quantity and quality in the Arkansas River (Triana et al., 2009a; Triana et al., 2009b), mapping the extent and severity of dissolved selenium (Donnelly, 2005; Gates et al., 2009), quantifying and assessing uncertainty of non-point source salinity back to the Arkansas River (Mueller Price and Gates, 2008), developing techniques to utilize remote sensing technology to estimate salinity and ET (Elhaddad, 2007; Eldeiry and Garcia, 2008), monitoring canal seepage reduction before and after the application of linear anionic polyacrylamide in order to mitigate waterlogging and increase efficiency (Susfalk et al., 2008), evaluating non-beneficial consumptive use of groundwater from saline high water tables underlying uncultivated land (Hallberg et al., 2008), calibrating EM-38 electromagnetic induction meter (Geonics Ltd.) readings to Valley specific soil conditions for rapid reconnaissance of in situ salinity conditions (Wittler et al., 2006), designing the rehabilitation and installation of subsurface drains to lower the water table and increase salt leaching (Rotter, 2006), and studying field scale irrigation alternatives to model potential improvements (Gillham, 2004) needed to bring about basin-wide water management improvement. More recently, data have been gathered and analyzed and models have been developed and calibrated for describing and simulating nitrate and selenium transport in the subsurface unsaturated and saturated zones (Bailey, 2012; Bailey et al., 2012; Bailey et al., 2013a; Bailey et al., 2013b).

Comprehensive data collection efforts in both study regions consist of routine monitoring of groundwater and surface water sites. In addition, field salinity surveys across the regions are documented through 2006 in both study regions. Results from field activities in the LARV related to the present modeling effort is described later, but also is found in Gates et al. (2006) in addition to sources already cited. The gathered field data serve two important roles. First, many of the values assigned to model grid cells (Figure 1-5) are based upon field observations. Second, model results are verified against field observations during the calibration process.

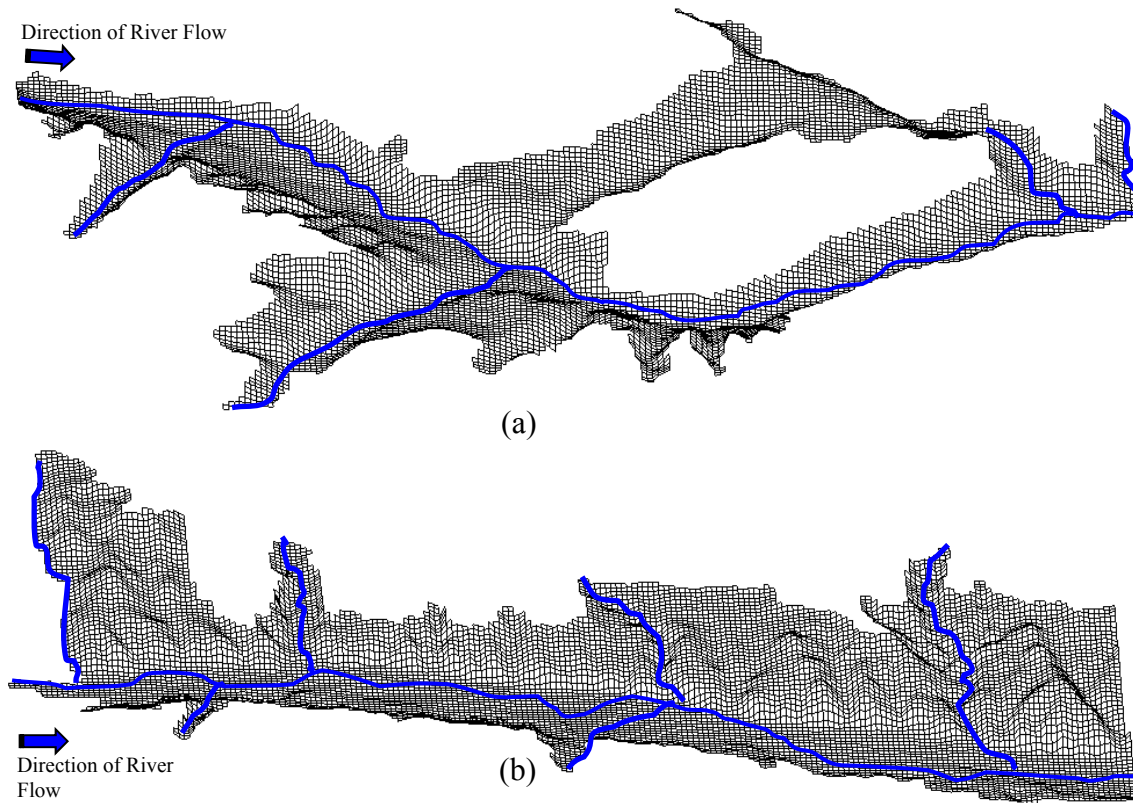


Figure 1-5. Perspective plots of the upper most layer of the (A) Upstream and (B) Downstream computational grids with ground elevation plotted. There is 30x vertical magnification to show relief.

1.5 DISSERTATION STRUCTURE

In Chapter 2, a literature review focused on past work in the LARV is presented (Section 2.1). Along with a presentation of peer-reviewed efforts related to automated model parameter estimation (Section 2.2) similar to what is pursued in Chapters 4 and 6. Chapters 3-6 each offer additional literature reviews pertinent to the topics they address. Finally, Chapters 3-5 are published in peer-reviewed journals, the citation information for which can be found in the footnote at the beginning of each chapter.

Chapter 3 focuses on the first objective. A detailed description of the soil water salinity survey approach is presented and results are compiled and discussed. Chapter 4 details the development of two regional-scale flow models developed for the USR and DSR. The developed models are calibrated by a diverse set of observations and therefore are well-suited for exploring the effects of alternative water management interventions. Much of Chapter 4 is devoted to a discussion of the predicted impact of the alternative management interventions on the problems of waterlogging, non-beneficial consumptive use, and alterations to historical groundwater return flow patterns. Next, Chapter 5 details the modifications made to the MT3DMS source code to incorporate solute transport in the unsaturated zone and presents seven test cases verifying the accuracy of the enhanced code and in so doing addresses the fourth objective listed above.

The culmination of the objectives addressed in the previous three chapters is found in Chapter 6. Armed with results from the detailed soil water salinity surveys in the LARV (Chapter 3), a well-calibrated flow model providing the fluid fluxes required by a salt transport simulation (Chapter 4), and a verified code capable of simulating values commensurate with the

findings from the surveys (Chapter 5), Chapter 6 presents two salt transport simulations that bring the body of work presented herein, together.

Each chapter restates its particular objective(s) after reviewing pertinent literature and follows with the familiar methodology-results-discussion-conclusions format. The final chapter of this dissertation (Chapter 7) discusses how each objective of the dissertation was met, concludes with over-arching findings, and offers direction for future research.

2 LITERATURE PERTAINING TO GROUNDWATER MODELING IN THE LARV AND TO AUTOMATED PARAMETER ESTIMATION FOR MODEL CALIBRATION

2.1 LITERATURE REVIEW OVERVIEW

Sections 3.2, 4.2, 5.2, and 6.2 present and discuss literature pertinent to the material presented in their respective chapters. Presented next, however, are two sections of literature review that discuss the long history of groundwater flow and salt transport modeling in the LARV (Section 2.2) and automated model parameter estimation techniques (Section 2.3). Material reviewed in Section 2.3 guided selection of the automated parameter estimation methodology pursued in Chapters 4 and 6.

2.2 LOWER ARKANSAS RIVER VALLEY MODELING EFFORTS, PAST AND PRESENT

The worldwide annual economic loss associated with waterlogging and salinization has been estimated at \$11 billion (Ghassemi et al., 1995) of which the LARV has a share. Modernization or rehabilitation of infrastructure coupled with sound water management may help reduce the economic losses associated with these problems (Lal and Shukla, 2004; Wallender and Tanji, 2012). Through the use of properly constructed and calibrated computer models engineers are able to equip decision makers to identify those infrastructure improvements and management strategies that bring about meaningful economic and environmental enhancement.

Early computer modeling efforts in the LARV began with the work of Moore and Wood (1967) on an analog model used to evaluate the effects of groundwater pumping in the Arkansas River. Among the reported results, they found that a net loss of flow in the Arkansas River

between the Fort Lyon Canal headgate and a point near the Otero-Bent county line increased from 7 cfs in May, a period before groundwater pumping increases in support of irrigation, to 37 cfs in July, the middle of the irrigation season. Thus, the impact of groundwater pumping on river flow was clearly demonstrated. Longenbaugh (1967) developed a transient digital model corresponding to a region of the LARV similar to that modeled by Moore and Wood (1967), and found similar swings in net river depletion between May [0.14 cms (5 cfs)] and July [0.48 cms (17 cfs)]. Predicted net accretions in the river flow during the winter of 1963-64 were approximately 0.17 cms (6 cfs) and match well the observed values for the region extending between the Fort Lyon Canal headgate and the city of Las Animas

Recognizing the buildup of salts in the LARV, a flow and transport model developed by Konikow and Bredehoeft (1974b) was used to predict salt accumulation in the alluvium over a 5-year period. Predictions from their model were revisited by Person and Konikow (1986) using 1982 data. Because the 1974 model was based on a single year's data collection effort, its predictions were significantly different than present day (at the time) observations, thus requiring a re-calibration of the model. Goff et al. (1998) simulated the effects on groundwater salinity and return flows to the Arkansas River under different management schemes using the model modified by Person and Konikow (1986).

Another groundwater model developed for the LARV is discussed in Cole et al. (1994). In this work, a MODFLOW model spanning from Pueblo to the Colorado-Kansas state line with 1.6 km (1 mile) (east-west) x 0.8 km (0.5 mile) (north-south) grid cells served as the modeling platform. The model period spanned 46 years with monthly stress periods and 5-day time steps. After an initial 8-year period used to calibrate the model with observations of the groundwater table elevation, the following 11 year time span was used to test model results, also performed

with observations of the groundwater table elevation. The model was used to investigate spatial and temporal variations in canal seepage losses; recharge from applied irrigation water; pumping from irrigation, municipal and industrial wells; addition of subsurface drainage; aquifer-stream interaction; consumptive use by woody and herbaceous phreatophytes; crop sub-irrigation; and recharge/discharge interactions between the valley-fill aquifer and adjacent lands. Four conclusions were reached:

- 1) The groundwater/surface water system is highly non-linear. Therefore, simplifying assumptions concerning linearization are to be avoided to maintain model integrity.
- 2) Nearly all of the groundwater recharge/discharge mechanisms are strongly time dependent. Care must be taken in assembling model input data to ensure model reliability.
- 3) Groundwater pumping has had an effect on stream flows. As expected, groundwater abstractions have reduced the availability of surface water at downstream diversion locations.
- 4) Model results have been checked and tested.

In 2002, concern over the high water table under the Bessemer Canal in Pueblo County initiated a groundwater modeling research effort specific to this portion of the LARV. A transient groundwater model was used to explore the effects of reduced recharge from overirrigation, lining various lengths of the Bessemer Canal, installing subsurface drainage, and increasing groundwater extraction through pumping (Brendle, 2002). Model results under each of the alternatives were effective in lowering the groundwater table, though to varying amount.

The predicted groundwater table fell by 0.9 m (3.0 ft) in a scenario that simulated 25% reduction in recharge to the irrigated lands. Installation of subsurface drainage at 3 m (10.0 ft) resulted in a simulated increase to the groundwater table depth of 1.2 m (6.8 ft) in the vicinity of the drains. Finally, an intervention that included complete sealing of the Bessemer Canal resulted in a predicted increase in the groundwater table depth of 1.5 m (5.0 ft) over the entire modeled area.

At approximately the same time, Gates et al. (2002) published steady-state results from the three dimensional model discussed above. Burkhalter (2005) and Burkhalter and Gates (2005; 2006) move from the problem identification found in Gates et al. (2002) to a systematic and comparative assessment of alternative solutions intended to mitigate waterlogging, salinization, salt loading, and non-beneficial consumptive use in the USR of the LARV. Results from different management alternatives, including reduced canal seepage, reduced recharge from over-irrigation (improved water management), improved subsurface drainage facilities, and combinations of these are provided. Researchers found potential for dramatic improvements in crop productivity in the LARV. An alternative management intervention that included a combination of reduced recharge (50%), reduced seepage (90%), and installation of subsurface drainage spaced at 50 m in fields with groundwater table depths of 2 m or less, relative crop yield increases of 5.5, 5.8, and 9.6% during each of the 3 simulated years, respectively, are predicted.

The model developed and reported by Burkhalter (2005) and Burkhalter and Gates (2005, 2006) to simulate conditions in the LARV and explore potential solution alternatives is not without limitations, however. Many of the simplifying assumptions inherent to the model are inappropriate under the range of conditions that exist during the extended period to be modeled in the proposed research. The original USR model simulated conditions in the aquifer between

April 1999 and October 2001, a period of relatively wet conditions. An important assumption was made possible by the wet conditions. There was always enough irrigation water to satisfy potential ET demands such that no deficit irrigation took place. That is, each irrigation event was assumed to completely fill the soil profile (Burkhalter, 2005). The new approach adopted for the dry conditions of 2002 and 2003 is described in Chapter 4, where details of the conceptual model are provided. To summarize, the major limitations of previous modeling studies that are addressed by the models described in Chapter 4 include simulation of unsaturated-zone flow (i.e., partitioning of infiltration to ET, deep percolation, and unsaturated-zone storage changes), a more diverse calibration dataset for constraining model calibration, use of automated model parameter calibration techniques for selection of “optimal” parameter values, doubling of the modeled areas within the LARV, lengthening of the USR simulated period with increased temporal resolution as compared to studies by Konikow and Bredehoeft (1974a, 1974b), a more diverse set of hydrologic conditions (i.e., wet, average, and dry) is included, and a diverse set of more spatially resolved datasets help guide the specified boundary conditions (e.g., precipitation, potential ET, land-use and crop-planting history, stratigraphy logs, pumping records, diversion records).

2.3 LITERATURE RELATED TO PROPOSED MODEL PARAMETER ESTIMATION

METHODOLOGY

The title of the 2006 Darcy lectures series poignantly asked, "All models are wrong: How do we know which are useful (Poeter, 2007)?" Referring to all models as ‘wrong,’ some of which are ‘useful,’ draws upon the idea that a numerical model cannot be formally proven, but rather only corroborated. Through extensive testing of a model’s ability to simulate or predict the real-world setting it is developed for, a sense of its usefulness (or alternatively, “wrongness”)

is gleaned. Several methods are available to help address a model's usefulness, an increasingly common concern among decision makers. Because the models described in the preceding have been developed using sparse (relative to their domain of application) and uncertain information (e.g. hydraulic conductivity, specific yield, etc.) due to the expensive and limited nature of data acquisition, their use for evaluation and decision making should be tentative until some notion of associated confidence can be attributed.

After calibration of the models using automated parameter estimation, evaluation alternative management scenarios can proceed. Generating the input files associated with the alternative management interventions and subsequent comparison to baseline conditions poses a significant challenge, but in light of the research objectives and the potential for capital investment in rehabilitated (i.e., lining of irrigation canals) or new (i.e., sprinkler and drip irrigation) infrastructure based on model results increases the stakes of the final analysis.

2.3.1 General Description of Model Parameter Estimation

Parameter estimation procedures attempt to estimate parameter values representative of aquifer properties in a mathematical model of a physical system by comparing model predictions of state variables to observations of the physical system state. Parameter values are systematically adjusted until some defined measure of the closest possible match between model output and observations is found (Tiedeman and Hill, 2007). Previous versions of the LARV models were calibrated using trial-and-error methods described in ASTM standards (1996). However, due to the availability of more sophisticated calibration techniques (i.e., automated parameter estimation software, such as PEST) and rich observation datasets (i.e., constraining information), trial-and-error techniques are increasingly obsolete. In fact, Carrera et al. (2005) argue that automated calibration, the process by which groundwater model parameters are systematically adjusted using mathematically driven algorithms, should be standard practice. Far

from being standard practice, Carrera et al. (2005) found that parameter estimation procedures were performed in only about 5% of the peer-reviewed journal articles pertaining to groundwater models as of the year 2005.

There are numerous advantages of automated parameter estimation techniques. In addition to expediting the calibration process, additional benefits include (Poeter and Hill, 1997):

- 1) Clues to the conceptual model's validity can be detected when estimated parameters are outside expected ranges; thereby, time can more appropriately be spent adjusting the conceptual model rather than parameter values,
- 2) Whereas human modelers are engaged in a never ending process to find "better" model fits, the automated parameter estimation technique efficiently finds the "best" fit for the given conceptual model, and perhaps most importantly,
- 3) Estimates of confidence intervals for model predictions (i.e. model reliability) using estimated parameter values are calculated.

Kitanidis (1996) argues that the challenge of parameter estimation is not only to reproduce observations of the modeled physical system, but also to ensure that the selected approach is capable of yielding reliable estimates of the predicted model output where observations are lacking. Clearly, there are many good and necessary reasons for adopting parameter estimation techniques in the analysis. Despite all of the available technology, however, it is important to adhere to sound reasoning regarding model formulation, to harbor an appropriate skepticism with respect to model results, and to proceed with the analysis once

satisfied that model assumptions are not violated. It is vital to keep in mind that model formulation may change drastically as new information becomes available (Bredehoeft, 2005).

The number of field observations upon which the developed and modified models of the LARV regions are supported is tremendous. In fact, none of the reviewed literature describes a data collection effort similar to the one found in Gates et al. (2002), Burkhalter and Gates (2005), and Gates et al. (2006). The observation database consists of 10 years of ground and surface water monitoring for water table depth and groundwater salinity and 7 years of soil water salinity monitoring. There are 100 and 118 groundwater sampling sites in the USR and DSR study areas, respectively. There are 164 and 100 surface water sampling sites in USR and DSR regions, respectively. Fourteen pump tests have been performed by the USGS inside the USR whereas only four were found to have been performed inside the DSR (Wilson, 1965). Results from the pump tests are used to verify the hydraulic conductivity field produced by the kriging procedure discussed in more detail below. Seepage measurements taken in canals from both study regions, including the Catlin, Fort Lyon, and Rocky Ford Highline canals in the USR and the Amity, Buffalo, and Lamar canals in the DSR serve as observations to check canal seepage predicted in the MODFLOW models. Results from numerous field-scale irrigation studies (Gates et al., 2012) are used to verify deep percolation fluxes calculated by the UZF1 package. Estimates of actual ET obtained from satellite imagery processed by the RESET model (Elhaddad and Garcia, 2008) constrained total ET simulated by the USR and DSR models. Finally, studies of non-beneficial consumptive use from shallow groundwater tables underlying naturally-vegetated and fallow lands (Niemann et al., 2011) guided manual adjustment of parameters related controlling its simulated equivalent.

Due to the computational enormity of the inverse problem in groundwater hydrology, parameters classically have been posed in two ways. In the first approach, unknown parameters are grouped in a zonation/parameterization framework. For example, a hydraulic conductivity field is free to have any number of areal zones (generally limited by computing facilities) and each finite-difference cell or finite-element node within a particular zone is assigned the same parameter value (Hsieh et al., 2007). Alternatively, a cell (or node) value can be calculated based upon the average parameter value for the particular zone. In this way, neighboring cells within the same zone can take on different values, but vary based on an established relationship to the zone's parameter value.

The second approach to the inverse problem is described in Kitanidis and Vomvoris (1983). Rather than representing model parameters within discontinuous zones, representations are estimated through kriging techniques. This is most commonly referred to as the geostatistical approach. Kriging is a powerful tool capable of accounting for variability at various scales. Generally, point measurements of the unknown parameter are used to describe the statistical structure of the spatially-varying parameter field. Equipped with that information, a parameter value is estimated for any point of interest within in the model domain, typically at the center of a finite-difference cell or at a node location within a finite-element mesh.

Regardless of which methodology is chosen, an appropriate level of model complexity, or in this case parameterization, should be sought. Ford (2006) calls for developing computer models that are “just barely good enough.” Here, Ford is not suggesting a posture of complacency or even laziness; rather, he is suggesting that all too often modelers succumb to the temptation to select the most sophisticated models available, anticipating increased benefit and insight. However, additional insight does not necessarily accompany a more complex model.

For example, the models described herein could be supplemented with several more MODFLOW packages, including the multi-node well (MNW) package (allows screened intervals in pumping wells to be specified), the reservoir (RES) package (adjusts leakage from a reservoir to an underlying groundwater system as the reservoir area expands and contracts in response to reservoir stage), and the streamflow-routing (SFR) package (routes return flow to the surface water system from the groundwater system through a specified stream network) among others. First, the cost of collecting information to support these and other packages needs to be considered. Second, the additional insight from these packages may not significantly contribute to the overall research objectives.

2.3.2 Previous Work in Model Parameter Estimation

Every model parameter value is uncertain. However, computational and financial resources often limit which parameters ultimately are allowed to vary in a more formal parameter estimation investigation. Thus, familiarity with the modeled field site and a survey of the literature may expedite the parameter estimation analysis by focusing on those parameters to which model predictions have been reported to be sensitive. A preliminary model sensitivity analysis likely will indicate which parameters can safely be neglected from further analysis due to insensitivity. It also may indicate problems with the selected conceptual model, scale of the computation model, or need for more field data.

2.3.2.1 Previous Work Focusing on Estimation of Hydraulic Conductivity as a Parameter

Our limited knowledge of physical systems, especially in the area of groundwater hydrology, has spawned a wide array of research pertaining to the key parameter of hydraulic conductivity. Hydraulic conductivity's substantial affect on model results is well-documented and is among the parameters that will be evaluated in the proposed research using parameter estimation techniques. The true hydraulic conductivity field is only one realization from the

probability distribution representing the background uncertainty about the suite of all possible hydraulic conductivity fields. Compounding the problem further is the fact that we only have sparse data from which to characterize the spatial variability of the true hydraulic conductivity field.

Work related to describing the uncertainty inherent in the hydraulic conductivity field of a groundwater model abounds. Freeze et al. (1990) frames the problem well:

Not only do we have uncertainty as to the parameter values needed for our design calculations, we even have uncertainty about the very geometry of the system we are trying to analyze. The uncertainties of lithology, stratigraphy, and structure introduce a level of complexity to geotechnical and hydrogeological analysis that is completely unknown in other engineering disciplines.

In addition to our uncertain knowledge of aquifer geometry and how to represent it in a numerical model, Garabedian (1986) and Carrera and Neuman (1986) have observed that model stability may hinge upon proper zonation of the hydraulic conductivity (or transmissivity, which is hydraulic conductivity multiplied by the saturated thickness) field.

Multiple approaches to estimating hydraulic conductivity have been suggested and reviewed (Gorelick, 1983; Keidser and Rosbjerg, 1991; Zimmerman et al., 1998; Carrera et al., 2005). Among them are fast Fourier transform, fractal simulation, linearized cokriging, linearized semianalytical cokriging, maximum likelihood, pilot point method, sequential self-calibration, pure zoning, and a combination of zoning and kriging. Zimmerman et al. (1998) conclude, based on tests using synthetic models with a specified “true” hydraulic conductivity, that parameter estimation techniques capable of identifying accurate spatial parameter relationships (i.e. the final estimated hydraulic conductivity field preserves the original parameter spatial relationships) is more important than accurate parameter values. Because

parameter structures are “at least as uncertain as the parameter values” (Zheng and Wang, 1996) and are likely to be a problem associated with the LARV models, structure of the hydraulic conductivity field requires attention.

Scheibe and Chien (2003) discuss a field-scale groundwater flow and solute transport model developed for a research site in Oyster, Virginia. After a bromide injection at the study site, breakthrough curves were sampled at numerous down-gradient monitoring wells. Six models ranging in complexity from simple (a homogenous deterministic representation of hydraulic conductivity) to complex (stochastic representation of hydraulic conductivity) were developed to see how well they could predict the observed breakthrough curves. Field observations of hydraulic conductivity, collected through falling-head permeameter measurements, borehole flowmeter measurements (Molz et al., 1994), and slug and pumping tests, were used to condition the data. Important conclusions drawn from the work include 1) complex representations of hydraulic conductivity do not necessarily improve transport predictions and 2) conditioning hydraulic conductivity to local point data provided little benefit to predicting breakthrough curves. This seems to suggest that if complex representations of hydraulic conductivity at the field-scale do little to improve model fit to observations, then only a modest degree of complexity should be necessary at the regional-scale.

Ronayne et al. (2008) describe a parameter estimation approach that simulates geologically plausible realizations of the aquifer structure found at the Lawrence Livermore National Laboratory (LLNL) site in California. Located in an alluvial fan, the hydraulic conductivity field exhibits a complex structure of highly permeable channels (referred to as “facies”) embedded in low-permeability flood plain deposits. Realizations of the horizontal hydraulic conductivity are evaluated on how closely the simulated response to a pumping well

matches observations from monitoring wells during an actual aquifer pump test. The degree of connectedness among the facies was found to dominate the flow pattern. Among the unique aspects of this work is the striking resolution of the groundwater model (7.3 million computation grid cells). Also of particular note is the process model run time of 50 to 60 minutes, very similar to that of the models presented herein.

Tsai et al. (2003a) and Tsai et al. (2003b) attempted to solve the parameter structure problem using Voronoi tessellation (Theissen polygons) to delineate zones of varying hydraulic conductivity. Their method couples Voronoi tessellation with genetic algorithm technology and searches for the optimal Theissen polygon scheme. While the research demonstrates that this coupling accurately predicts distributed parameter structure, its adoption is curtailed because no general package is provided. Also, the synthetic problem explored by the authors is relatively simple compared to the models developed for the LARV. Finally, no mention of computer processing run time is made.

In related work, Tung and Tan (2005) also used Voronoi diagrams to describe the zonation pattern of the hydraulic conductivity field. Rather than use genetic algorithms to optimize the zonation pattern as well as the parameter value of each zone, simulated annealing was employed. The methodology relies on the simulated placement of arbitrarily chosen generator points, similar to pilot points, to identify zones. The number of optimal zones is increased incrementally from two to some number n until three criteria are satisfied. When residual error between simulated and observed values is minimized, parameter uncertainty is constrained as suggested by Yeh and Yoon (1981), and when structural error based on a given number of zones is minimized, the optimization procedure stops. The procedure is performed on a relatively simple, albeit real-world, problem with the model consisting of 223 active cells in a

confined aquifer, as compared to the 15,000+ cells in each of the LARV models described herein.

Zheng and Wang (1999b) introduced Simulated Annealing (SA) and Tabu Search (TS) as two combinatorial optimization models capable of finding the best hydraulic conductivity structure for groundwater models. Although this method would further enhance currently adopted parameter estimation techniques, it is explored only for one dimensional models. Using these techniques in two and three dimensional models remains uninvestigated.

Many others have employed heuristic algorithms to the optimal parameter estimation problem (Zheng and Wang, 1996; Zheng and Wang, 1999b; Tsai and Yeh, 2004; Tung and Chou, 2004; Wu et al., 2008). A common thread in the literature suggests that the methodology is limited to numerically small (in terms of the number of active cells) problems and/or to steady state solutions. However, the work performed by Lin and Yeh (2008) coupled a heuristic approach to MODFLOW with a computationally large (100 x 100 cells) grid.

Fienen et al. (2008) point out that once zone boundaries are located, they act as constraints to the final solution for hydraulic conductivity values. Through hydraulic tomography, which seeks to synthesize information gleaned from sequentially pumping (or injecting) water into a well and simultaneously measuring responses at other wells (Yeh and Liu, 2000), an interactive inversion scheme using Bayesian geostatistical inverse theory allows zone boundaries to vary. The methodology makes use of prior information when available. As with other previously reviewed research, the models explored are relatively simple. Three models, each one two-dimensional, steady-state, and synthetic, with a relatively small number of active MODFLOW cells, were explored but are remarkably different from the research described in this

dissertation. The technique is demonstrated to be powerful, in that results from the method closely matched the ‘true’ synthetic field.

2.3.2.2 Previous Work on Estimation of Canal Seepage

In a case study that consisted of two infiltration experiments from an unlined canal located in southern France, Dages et al. (2008) show that the SWMS_3D code, which simulates the full 3-dimensional Richards equation, satisfactorily simulates groundwater recharge that results from surface-feature seepage losses. An important result from the research helps to sustain the simplified approach utilized by the general head boundary (GHB) package in MODFLOW which simulates seepage from earthen canals in the models developed herein. The authors noted that representing the variability of the soil properties underlying the canal with “greater detail did not necessarily improve water flow simulation” (Dages et al., 2008). In fact, three different realizations of soil hydraulic properties with varying complexity satisfactorily reproduced observations from flow experiments.

This issue is commonly referred to as “non-uniqueness” and often plagues automated parameter estimation algorithms. To overcome it, final estimated parameter values should be checked for reasonableness. In addition, automated parameter estimation software such as PEST (Doherty, 2002) offer options for supplying parameters search algorithms with “preferred values,” a form of regularization (Doherty, 2003). In situations where a non-unique solution exist, the algorithm prefers solution closer to the preferred solution over and against other possible solutions.

2.3.2.3 Previous Work on Estimation of Groundwater Recharge

Several papers devoted to the estimation of the groundwater recharge boundary condition are discussed in Fazal et al. (2005). Many of the groundwater modeling applications reviewed estimate recharge rates in order to determine the sustainability of pumped groundwater for

municipal supply, for example. If this approach is adopted, then sufficient knowledge of the other parameters in the groundwater model is necessary. Sanford (2002) addresses some of the complicating factors that affect estimation of recharge in models of regional-scale aquifer systems, including lithology, climate, and topology.

Weir (1989) warns that small errors in water table gradients or in the hydraulic conductivity field lead to appreciable errors in the estimation of recharge. Although a relatively rich dataset of hydraulic head observations has been built for LARV study region, it is not nearly dense enough, in space or time, to support estimation of recharge in this manner. Furthermore, observation of the hydraulic conductivity field is even sparser than the hydraulic gradients.

Parkhurst et al. (1996) used travel velocities of environmental tracers coupled with hydraulic head observations to guide estimation of recharge and hydraulic conductivity. Both parameters were adjusted until simulated values of groundwater travel times and hydraulic head were reached. Sanford (2002) noted that it is important to have independent estimates of effective porosity in order for this approach to work.

Bekesi and McConchie (1999) generate recharge realizations for a regional-scale groundwater model in New Zealand. The study site receives anywhere from 0.9 m to over 4 m of annual rainfall. Whereas the LARV lacks this level of precipitation, it is subject to heavy irrigation making the findings pertaining to recharge in the New Zealand study intriguing for the present study. Three hundred stochastic recharge datasets for a 28-year period with daily time steps were generated based on observations of rainfall and soil characteristics for the area. Although a numerical groundwater model was not subsequently utilized to evaluate what affect spatially uncertain recharge had on groundwater levels, calibration and testing of the recharge model was achieved using an analytical approach that relates recharge to groundwater levels.

Groundwater levels derived from this analytical approach, which used recharge as an input, were then compared to hydraulic head observations obtained from bores located throughout the study area. The condition of the mean recharge rate derived from all three hundred realizations was the only one used for comparison to the observed hydraulic heads. Simulated hydraulic head for this condition compared fairly well to observed values.

2.3.2.4 Previous Work on Estimation of Solute Transport Parameters

Perhaps one of the most studied aquifer systems in the United States is that of the Death Valley Regional Flow System on the California-Nevada border. The site was used historically to study underground nuclear detonations. More recently, Yucca Mountain, located within the boundaries of the Death Valley regional-scale model, has been identified as a potential storage site for nuclear waste. Motivation for an intense study to characterize the aquifer (D'Agnese et al., 1997; LeCain et al., 1998; D'Agnese et al., 1999; D'Agnese et al., 2002; Faunt et al., 2004) stems from the proximity of municipalities that extract groundwater for domestic supply. Clearly, radioactive contamination of the aquifer has potentially catastrophic consequences. The advective transport (ADV) module of MODFLOW-2000 was selected to model transport processes. Results from a parameter estimation analysis determined that 2 of the 9 hydraulic conductivity zones used were very important to predicting the movement of solutes due to advective transport. Other estimated parameters, including recharge, aquifer storage coefficients, That is, a 1-percent increase in the standard deviation of the parameter values could affect travel distance by as much as 0.5 and 0.7 percent in a north-south and east-west directions, respectively. At the regional-scale this represents significant distances. This work highlights the importance of an accurate flow field when detailed description of solute transport is necessary.

Whatever the selected methodology, it is important not to view any model as immutable and to keep in mind that a good calibration does not ensure a correct conceptual model

(Bredehoeft, 2005). Bredehoeft (2005) reviewed fourteen different published models and found that in nearly every model reviewed some deficiency exists. In some cases, predictions varied widely when multiple groups of analysts worked on the same problem. Other models suffered from new, “surprise” information that rendered previous conceptual models invalid. In other cases, post audits of model predictions showed them to be incorrect and, in the absence of additional data, modelers were left to wonder why.

3 REGIONAL ASSESSMENT OF SOIL WATER SALINITY ACROSS AN INTENSIVELY IRRIGATED RIVER VALLEY¹

3.1 SUMMARY

Extensive field investigations allowed depiction of soil water salinity within two large representative regions of a river valley that has been irrigated for more than 120 years. The nature and severity of the salinity problem is captured by hundreds of field surveys, encompassing tens of thousands of measurements and spanning 9 years. Soil water extract salinity, averaged over all surveys and all measured locations, is 4.1 dS m⁻¹ in the Upstream Study Region and 6.2 dS m⁻¹ in the Downstream Study Region. Variability over the measurements is substantial, with a coefficient of variation of approximately 0.51 Upstream and 0.39 Downstream. Relationships to soil and groundwater conditions also were explored, providing field-based insights into major contributing factors and into the value of measuring those factors as part of a salinity reconnaissance. A broad survey, like that described herein, affords a sense of the magnitude of economic loss, in terms of crop-yield reduction, that is exacted by irrigation-induced salinity. Evaluation of the measurements in relation to an estimated average threshold for crop-yield reduction indicates that approximately 42% of the more than 122,000 locations surveyed over both regions had EC_e values exceeding the corresponding threshold. Average yield reductions due to soil water salinity are approximately 6% over surveyed locations Upstream and 17% over locations Downstream. Moreover, survey results

¹ As published in the Journal of Irrigation and Drainage Engineering, Eric D. Morway, Timothy K. Gates, 2012, Vol. 128, No. 5, 393–405.

point toward general targets for irrigation and drainage planning and form a basis for the development of more detailed solutions using computational modeling.

3.2 INTRODUCTION

Irrigated agriculture forms a very important niche in world agriculture: it produces approximately one-third of the available food supply while taking up only approximately 18% of available cropland (Acquaah, 2005). The future of this critical enterprise is jeopardized by irrigation-induced salinization and waterlogging, rooted in poor drainage, seepage from conveyance canals, and excessive irrigation (Lal, 2004). Ghassemi (1995) estimated that up to 27% of the irrigated land in the United States was impacted by salinization, suggestive of a decline of crop yields and the rural commerce that depends on irrigation productivity. Postel (1999) corroborated this trend, estimating that worldwide, an additional 2 million ha of land are adversely impacted by salinization each year.

The Lower Arkansas River Valley (LARV) in Colorado (Figure 3-1) is typical of expansive long-irrigated stream-aquifer systems that are affected by soil and water salinity. The introduction of irrigation to the fertile alluvial soils in the LARV in the 1870s spurred the growth of a widespread agriculturally based economy with important benefits not only locally but also to the state of Colorado (Sherow, 1990). There are a total of approximately 109,000 ha (270,000 acres) of irrigated land across approximately 14,000 fields in the LARV. Water is provided to these fields by 25 main canals that divert flow from the river in accordance with Colorado water law and from approximately 2,400 wells that pump from the alluvial groundwater. The vast majority of fields are surface irrigated with less than approximately 10% irrigated with sprinklers (typically, center-pivot sprinklers) or drip lines.

In response to excessive irrigation, seepage from earthen canals, and inefficient drainage systems, groundwater tables in the LARV have risen in elevation, creating a number of challenging problems. High water tables have produced large hydraulic gradients that drive

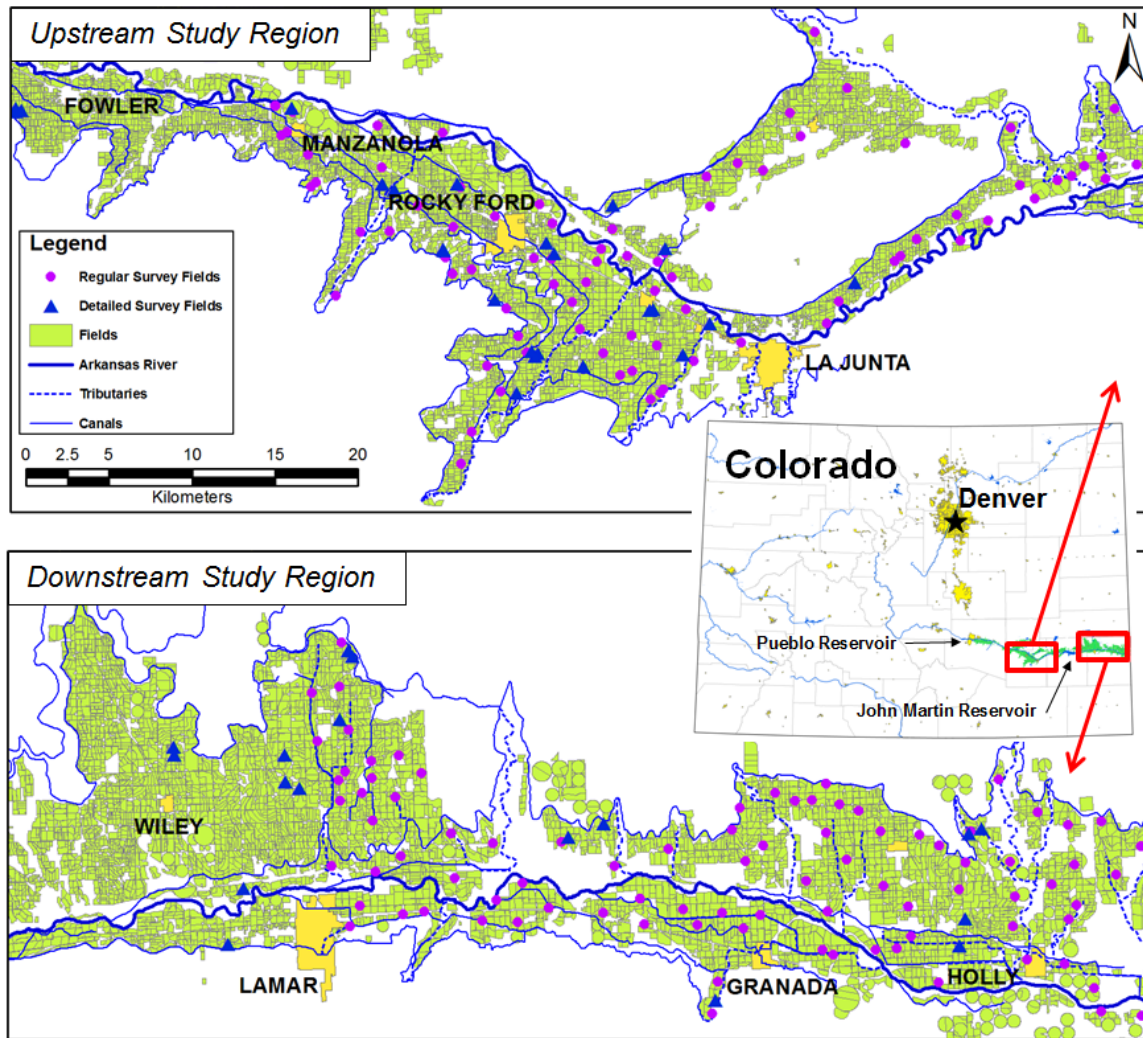


Figure 3-1. Upstream and Downstream study regions in Colorado's Lower Arkansas River Valley showing the location of study fields

subsurface flows back to tributaries, open drains, and the river. In some locations, these return flows dissolve salts and minerals (such as selenium and uranium) from the Arkansas Valley's marine shale outcrops and bedrock and from shale-derived soils, further increasing solute loads as the water moves through the underlying aquifer and makes its way back to streams (Mueller Price and Gates, 2008; Gates et al., 2009). High groundwater tables also extend out under

uncultivated and fallow land where substantial amounts of water are non-beneficially consumed (Niemann et al., 2011), and groundwater solute concentrations rise due to evaporative upflux from the shallow water table. Finally, upflux from saline high water tables under cropped fields, coupled with evaporative concentration, has salinized and waterlogged much of the rich soil of the river valley (Gates et al., 2006), causing reductions in crop yield (Burkhalter and Gates, 2005).

Much work has been done to survey and describe soil water salinity on irrigated lands around the world. Hendrickx et al. (1992) described four major methods available for conducting soil water salinity surveys: (1) qualitative visual assessment relating crop appearance to salinity levels, (2) retrieving soil samples from the field for laboratory analysis, (3) applying four-electrode sensors, and (4) applying electromagnetic (EM) induction sensors. Rhoades et al. (1999) described and compared the last three of these methods and their implementation. Corwin and Lesch (2003) listed a fifth and relatively recent method, remote sensing, which uses electromagnetic spectra measured with satellites or aircraft to estimate spatially variable soil water salinity levels over vast expanses (Bastiaanssen et al., 2000; Metternicht and Zinck, 2003; Elhaddad, 2007; Eldeiry and Garcia, 2008; Singh et al.). Wittler et al. (2006) and Cassel et al. (2008) reviewed and discussed past soil water salinity survey investigations, most of which have been conducted at the local scale ($\sim 10^2$ m²) or the field scale ($\sim 10^3$ – 10^4 m²).

In the LARV, considerable effort has been made to (1) estimate the extent and severity of waterlogging and salinization (Gates et al., 2006; Wittler et al., 2006), (2) gain a more complete understanding of the interdependent physical processes sustaining these problems (Susfalk et al., 2008; Shanafield et al., 2010; Niemann et al., 2011), (3) support the development of numerical models of the alluvial aquifer (Konikow and Bredehoeft, 1974a; Goff et al., 1998) with the final

goal of guiding best management practices (BMPs) (Burkhalter and Gates), and (4) post-audit the numerical simulations (Person and Konikow). A major component of these efforts, addressed in this study, is the collection and analysis of field data to characterize the nature and extent of soil water salinity over the valley. In contrast to past studies elsewhere, the focus is not solely on field-scale details of soil water salinity variability but on patterns that extend over the regional scale ($\sim 10^5$ – 10^6 m²) of a vast irrigated stream-aquifer system, the aim being to characterize the nature of widespread irrigation-induced salinization and to form a basis for strategic planning of extensive engineering and management schemes for salinity reduction. An unprecedented data set, spanning several years and tens of thousands of measurements over two representative study regions of the valley, is summarized. The data provide a unique depiction of the magnitude, severity, and variability of soil water salinity in an intensively irrigated river valley, typical of many in the western United States. Moreover, the relationship of soil water salinity to selected soil and groundwater properties, addressed in most previous studies by using controlled experiments or models of flow and salt transport, is examined broadly under actual field conditions. Not only are current system conditions described, but a platform is provided for calibration, testing, and application of regional-scale flow and salt transport models, which currently are under development.

3.3 METHODS AND MATERIALS

3.3.1 Study Sites and Approach

Starting in 1998, researchers at Colorado State University (CSU) have made understanding the degradation of water quality resulting from irrigation a focal point of efforts to revitalize agriculture in the LARV and to improve the environmental health of the river basin. As part of these efforts, both regular and detailed surveys have been conducted at the regional scale.

An area representative of valley conditions upstream of John Martin Reservoir, and referred to herein as the Upstream Study Region, was the first area of focus. This region covers approximately 50,600 ha (26,400 ha irrigated), extending approximately 78 km along the river between Manzanola, Colorado, and Adobe Creek located just west of the city of Las Animas (Figure 3-1). In 2002, a second regional-scale investigation was launched in an area of approximately 55,200 ha (33,000 ha irrigated) referred to as the Downstream Study Region (Figure 3-1), located downstream of John Martin reservoir and extending approximately 71 km between Lamar, Colorado, and the Colorado-Kansas state line. As part of broad studies of the irrigated stream-aquifer system within these regions, an effort was launched to characterize groundwater and soil conditions using groundwater monitoring wells distributed with an average density of approximately one well per 490 ha (one well per 270 irrigated ha) and estimating average soil water salinity over fields with an average size of 10 ha. This resulted in the installation of approximately 100 and 118 monitoring wells for regional-scale assessment of water table conditions in the Upstream and Downstream study regions, respectively. Approximately 80% of the fields that contained these monitoring wells also were selected for regular soil surveys. The sites of monitoring wells and surveyed fields initially were selected using a stratified random sampling method and were adjusted based on landowner permissions and preferences. To facilitate cost-effective and efficient assessment of valleywide conditions, only one groundwater monitoring well was installed in or beside fields that were associated only with the regular surveys. Also, though regular surveys for soil water salinity at the regional scale were conducted using multiple measurement locations within each field, the measurement locations were not geo-referenced with coordinates from the global positioning system (GPS). The regular surveys are described in more detail under the “Soil Water Salinity, Soil Texture,

and Soil Water Content Surveys” section below as well as in the studies by Gates et al. (2002), Burkhalter and Gates (2005), and Gates et al. (2006), along with other water- and irrigation-related studies conducted in the regions.

In addition to the regular surveys, detailed surveys also were conducted. These surveys “zoom in” to consider trends and variability in groundwater, crop, and soil conditions within the field units. In contrast to the regular surveys, detailed surveys were performed on fields which often contained multiple groundwater monitoring wells (in addition to the one installed for regional-scale assessment), and GPS readings were taken at each soil water salinity measurement location. Thus, in addition to providing more information descriptive of soil water salinity across the regional scale, detailed surveys reveal more information on spatial patterns within individual fields. Also, the location of fields for detailed surveys was more influenced by concerns related to grower cooperation than was the location of fields for regular surveys. Documentation of these detailed surveys can be found in the studies by Gillham (2004), Gates et al. (2006), Eldeiry (2006), Elhaddad (2007), and Gates et al. (2012).

Conjunctive soil water salinity and groundwater data were gathered in 835 regular surveys on a total of 83 fields over the period 1999–2005 in the Upstream Study Region and in 451 surveys on a total of 89 fields over 2002–2005 in the Downstream Study Region. Typically, measurements in groundwater monitoring wells associated with these fields were made weekly from mid-May to mid-August, bi weekly to monthly from mid-March to mid-May and from mid-August to mid-November, and monthly to bi-monthly during the off season (mid-November to mid-March). Regular surveys for soil water salinity typically were carried out early (15 March to 15 June) in the irrigation season and again at midseason (16 June to 15 September).

Approximately 193 detailed surveys on a total of 23 fields, studied over the period 1999–2008 in the Upstream Region, and 247 detailed surveys on a total of 25 fields, studied over 2001–2008 in the Downstream Region, are reported herein (fields were surveyed repeatedly over the course of the study). Most of the detailed survey fields were located within the Upstream and Downstream study regions, although a few lie just west of each of the regional-scale study areas. The detailed survey fields contained 1 to 18 monitoring wells, with an average of approximately six per field. Similar to the regular surveys, detailed soil water salinity surveys were conducted early and midway through the irrigation season and, in addition, were often monitored late in the season (16 September to 15 November).

3.3.2 Groundwater Monitoring

Monitoring wells were drilled to depths ranging between 3 and 18 m, cased with slotted 0.064 m (2.5 in.) diameter PVC and sealed with bentonite around the annulus at the soil surface. Measurements consisted of reading water table depth with manual tapes and floats or with electric tapes and reading the electrical conductivity (EC_{gw}), as specific conductance at 25°C, of the groundwater using conductivity probes. The probes were calibrated at least once daily using solutions of known conductance. Readings of electrical conductivity were taken with the probe just below the water table, near the bottom of the well, and midway along the water column in the well. These values were averaged to obtain the EC_{gw} values used in this study. Measured water table depth from ground surface, D_{wt} , in the regular surveys ranged from 0.01 to 13.5 m, averaging 2.9 m, in the Upstream Study Region. Values in the detailed surveys in the Upstream Region ranged from 0.04 to 9.0 m below ground surface, averaging 2.0 m. In the Downstream Study Region, values of D_{wt} measured in the regular survey fields ranged from 0.05 to 19.8 m below ground surface, averaging 3.8 m, and in the detailed surveys ranged from 0.03 to 10 m below ground surface, averaging 2.4 m.

3.3.3 Soil Water Salinity, Soil Texture, and Soil Water Content Surveys

Soil water salinity was represented in this study by the electrical conductivity of a soil paste extract (EC_e). Values of EC_e at locations in a field were estimated from measurements of apparent bulk soil conductivity taken with a Geonics EM-38 electromagnetic induction sensor (Rhoades et al., 1999). Wittler et al. (2006) described the analysis of soil samples gathered from fields within the LARV over 1999–2005 to develop and test calibration equations for use in regional-scale surveys to estimate EC_e from apparent bulk soil conductivity measured with an EM-38 used in the vertical orientation (EM_v). At each calibration site, readings of EM_v were taken with one or more EM-38 sensors. Horizontal orientation readings, EM_h , were collected but were not used during the analysis for reasons described by Wittler (Wittler, 2005) and Wittler et al. (2006). Soil augers were used to extract soil samples extending a few centimeters in length, beginning at the surface, and at approximate depths of 0.3, 0.6, 0.9, and 1.2 m from the surface near the left end, center, and right end of where the EM-38 readings were taken, yielding a total of 15 samples per calibration site for laboratory determination of EC_e (Wittler et al., 2006). Samples were gathered at 253 calibration sites in fields surveyed in the Upstream Study Region and at 161 sites in the Downstream Study Region. At approximately 10% of the sites, an additional sample was taken from the center hole at a depth of approximately 1.8 m. This collection of soil samples was assumed to represent the soil volume that contributed to the apparent bulk soil conductivity measured by the EM-38 at the site. Soil temperature was measured at every soil sampling depth in the center hole. Also, additional soil was gathered at every depth in the center hole for measuring the gravimetric soil water content. Soil texture for the samples from the center hole was determined using the hydrometer method and the USDA soil classification system (Gee and Bauder, 1986). In the present study, the EM_v data measured

in a field survey were first adjusted to a 25°C soil temperature standard by multiplying them by the following factor (Richards, 1954):

$$f_{tc} = 1.8509 - 0.0516951T + 0.000858442T^2 - 0.00000613535T^3 \quad (\text{Eq. 3-1})$$

where T (°C) = soil temperature averaged over measurements at 0.30-m increments between the ground surface and a depth of 1.2 m. A digital thermometer was used to measure T immediately upon bringing the soil sample to ground surface. Because of a marked increase in the soil water salinity between the two regions, two different calibration equations (Wittler et al., 2006) were developed for the fields located in the Upstream and Downstream study regions. The substantial increase in soil water salinity in the Downstream Study Region compared to the Upstream Study Region may be attributed, in part, to the increase in mean measured river EC used for irrigation from approximately 1.3 dS m⁻¹ Upstream to 3.0 dS m⁻¹ Downstream. It likely also is due to the higher mean measured EC_{gw}: approximately 3.1 dS m⁻¹ Upstream versus 4.7 dS m⁻¹ Downstream. The following calibration equation (Wittler et al., 2006) was used to estimate EC_e (dS m⁻¹) averaged over a depth of approximately 1.2 m from measurements of temperature-corrected EM_v measured in fields in the Upstream Study Region:

$$EC_e = 0.45 + 7.23EM_v^{1.78} + 19.54WC - 34.06EM_v(WC) \quad r^2 = 0.74 \quad (\text{Eq. 3-2})$$

where WC = average equivalent oven-dried gravimetric soil water content, estimated in the present study from soil samples taken between the ground surface and a depth of approximately 0.9 m in 0.3 m intervals from five locations within the field, typically near the center and within each quadrant of the surveyed field. Approximately 74% of the regular surveys and 70% of the detailed surveys conducted in the Upstream Study Region had accompanying WC data. Drawing from lessons learned in the early stage of the study in the Upstream Study Region, efforts in the Downstream Study Region, which began about 3 years after the data collection commenced in the Upstream Study Region, resulted in a more complete data collection, with 99% and 96% of

the regular and detailed surveys, respectively, having accompanying WC information. The calibration equation (Wittler et al., 2006) used for the fields in the Downstream Study Region was

$$EC_e = 2.33 + 7.16EM_v^{1.44} + 9.41WC - 23.18EM_v(WC) \quad r^2 = 0.54 \quad (\text{Eq. 3-3})$$

Estimates of EC_e using EM-38 sensors are unreliable for low soil water contents, i.e., for WC values less than approximately 0.07 for silt and loam soils (Rhoades et al., 1999). When qualitative measures conducted in the field were indicative of low soil water content, the field was not surveyed. Because collecting measurements of T and WC at every location where an EM-38 measurement is taken would be prohibitively time consuming for a regional-scale study, T was measured at one location in a surveyed field, typically the calibration site, or was estimated from data in a nearby field. When estimates of WC were unavailable, equations given in Figure 5(a) of Wittler (2006), which excluded WC as an explanatory variable, were utilized for the Upstream and Downstream Regions, respectively. Rocky soils, which could affect EM-38 readings, were not encountered in any of the surveyed fields.

For fields in the regular surveys, sites for EM_v measurements were determined by pacing off a rectangular grid pattern to obtain approximately 5–10 sites per hectare. If the field was unusually large (> 30 ha), it was not uncommon to survey only a portion of the field. When this occurred, an effort was made to cover the same portion of the field in subsequent surveys so as to maintain continuity in the dataset. A total of approximately 54,700 sites were measured in the regular surveys in the Upstream Study Region, and approximately 34,500 were measured in the Downstream Study Region. In the detailed surveys, sites for EM_v measurements were paced off with a density similar to or greater than that in the regular surveys, but GPS measurements also were recorded for each site. Approximately 16,600 sites were measured in the detailed surveys Upstream and approximately 18,000 sites Downstream.

3.3.4 Relative Crop Yield due to Soil Water Salinity

To estimate the impact of soil water salinity on crop yield in the two study regions, the relative yield (Y_r) function of Maas (1990) was applied to each measurement location within surveyed fields over the regions

$$Y_r = 100 - S_{YR}(EC_e - EC_{eT}) \quad (\text{Eq. 3-4})$$

where EC_{eT} = the threshold soil water salinity value (dS m^{-1}); and S_{YR} = rate of crop-yield reduction in percentage per dS m^{-1} increase in EC_e above EC_{eT} . Soil water salinity is only one of many factors (such as irrigation, fertilization, pesticide control, and cultivation practices) that influence crop yield. The value of Y_r in Equation 3-4 is an estimate of the crop yield under the given conditions of soil water salinity (as measured by EC_e) as a percentage of the estimated potential yield that would result if all factors (including soil water salinity) affecting crop yield were at ideal levels. The value of Y_r is useful for comparative purposes but suffers from the deficiency that it does not account for the interaction of soil water salinity with other yield-limiting factors. The description of such interactions is beyond the scope of the present study. Values of S_{YR} reported in the literature (Maas; Katerji et al., 2000 2000; Tanji and Kielen, 2002) for specific crops were used when records were available.

As recommended by Maas (1990) for cases (such as the LARV) where gypsum and calcite are the predominant salts (Cooper, 2006), EC_{eT} values were increased by 2 dS m^{-1} above the values provided in the studies by Maas (1990), Tanji and Kielen (2002), Katerji et al. (2000), and Kotuby-Amacher et al. (2000). The use of higher threshold values is supported by field studies in the LARV by Gates et al. (2012), who presented data that demonstrate reductions in crop evapotranspiration (ET) for corn, a major crop in the LARV, when soil water salinity levels reach values that are approximately 2 dS m^{-1} higher than the threshold EC_{eT} values reported by

Maas (1990). Assuming this drop in ET results in a corresponding drop in crop yield, Gates et al. (2012) also presented corroborating data showing reduction in biomass from crop cuttings with increasing EC_e for corn and alfalfa fields in the LARV. When data on planted crop type were not recorded (e.g., when differences between corn and sorghum were too subtle for the field technician to distinguish due to the early growth stage of crop, the crop had not yet sprouted, or records were omitted or lost), a value of 9.7%, the average of the values reported by Maas (1990) for corn and alfalfa, was used for S_{YR} because corn and alfalfa are the predominant crops in the LARV. Similarly, a value of 3.85 dS m^{-1} , the average for corn and alfalfa, was used in these cases.

3.3.5 Statistical Analysis

Statistical analysis of groundwater, soils, and relative crop-yield data was conducted using @RISK (version 4.5, 2005; Palisade Corporation, Ithaca, NY), SAS version 9.2 (SAS Institute Inc., Cary, NC), and R (R Development Core Team) software. This included calculation of summary statistics, fitting of probability distributions, correlation analysis, and nonlinear regression. The use of diverse software stems from the familiarity of the authors with tools available in the different software packages. The ease of analysis facilitated by a selected software package, and not any perceived shortcomings in other available software packages, led to its selection for a particular analysis.

3.4 RESULTS AND DISCUSSION

3.4.1 Severity and Variability of Soil Water Salinity

Regional-scale surveys are useful to indicate how acute the soil water salinity problem is broadly and to describe large-scale patterns of variability. The average values of electrical conductivity of an equivalent soil paste extract measured within fields, $\overline{EC_e}$ in regular and

detailed surveys are summarized in Figure 3-2 for the Upstream and Downstream study regions, respectively. Results suggest a serious salinity problem in the LARV, with the mean \overline{EC}_e computed over all fields within each survey within the irrigation season ranging from 3.4 to 4.6 dS m⁻¹ in the Upstream Study Region and from 4.5 to 8.0 dS m⁻¹ in the Downstream Study Region. These mean values are substantial compared to the estimated threshold values of approximately 3–5 dS m⁻¹ above which the yields of the predominant crops, alfalfa and corn, are reduced by soil water salinity (Maas, 1990; Gates et al., 2012).

Figure 3-2 depicts seasonal oscillations in the Downstream data, where a deeper average water table has been observed. This may be due to the flushing of salts from the upper soil zone in the early spring, when supply is high and ET demand is low, and the subsequent buildup of salts from evaporative concentration that may take place in the middle and later parts of the growing season. Frequency histograms of all \overline{EC}_e values estimated in surveys conducted over the years are shown in Figure 3-3 for the two study regions. The overall coefficients of variation (CV) for the fitted normal inverse Gaussian probability distributions were substantial, approximately 0.51 in the Upstream Study Region and 0.39 in the Downstream Study Region.

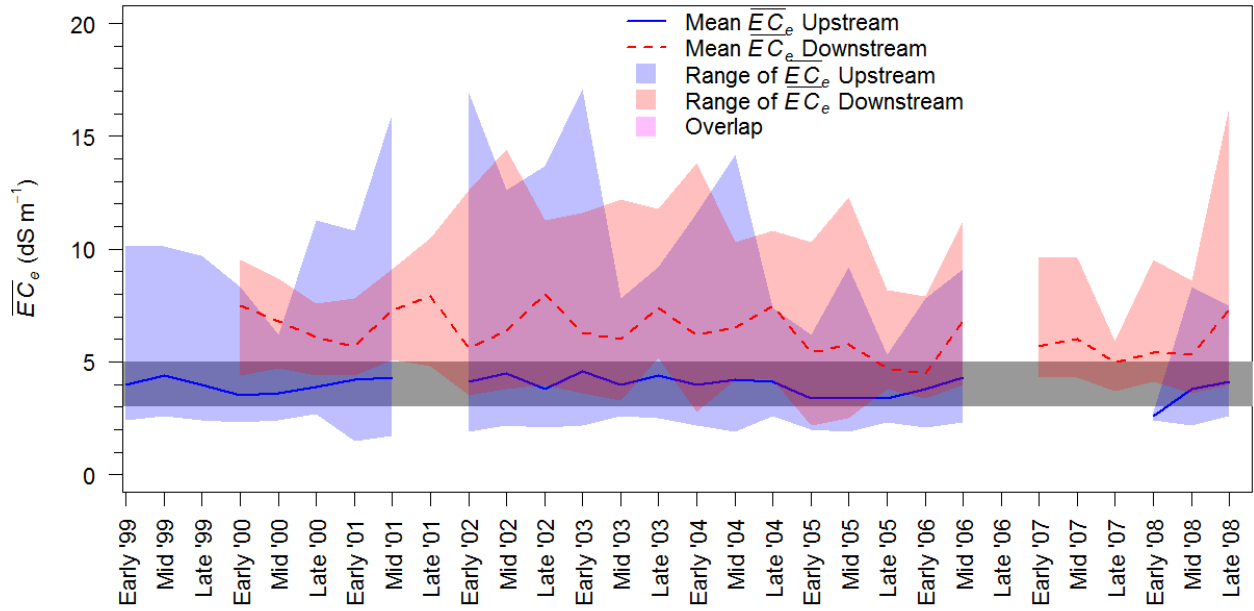


Figure 3-2. Visual summary statistics of \overline{EC}_e for surveyed seasons during the study period for both the Upstream (blue) and Downstream (red) study regions

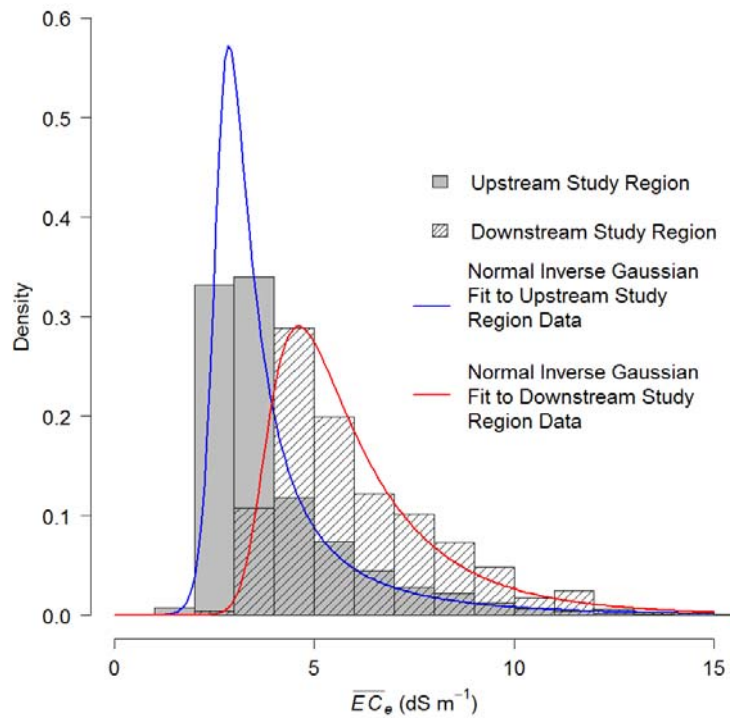


Figure 3-3. Relative frequency and fitted probability distributions for \overline{EC}_e values over all surveys in the Upstream Study Region and Downstream Study Regions.

The spatial CV values within the seasonal surveys, indicating relative variability over the surveyed region, varied from 0.26 to 0.68, averaging 0.46, in the Upstream Study Region. In the Downstream Study Region, spatial CV values for the seasonal surveys varied from 0.19 to 0.51, averaging 0.31. The considerable variability from field to field is depicted in Figure 3-4 by the overall mean \overline{EC}_e surveyed at midseason plotted on simulated contours of mean D_{wt} measured over all of the corresponding irrigation seasons. Generally, higher \overline{EC}_e values occurred in areas with shallower water tables. The relationship to D_{wt} is further explored later in the paper.

To more rigorously explore and better understand the sources of variability in the Upstream and Downstream datasets, a Generalized Linear Model (GLM) (McCullagh and Nelder, 1989) was fit to the log-transform of the data. The residuals between the log transformed values and the GLM were normally distributed, thereby justifying the use of the GLM to explore the significance of various effects (e.g., D_{wt} , EC_{gw} , etc.) on \overline{EC}_e . Effects were either fixed or random. Fixed effects in the GLM include region (i.e., Upstream or Downstream), year, and year by region. Random effects include field within location and year by field within location. Summarizing in statistical terms, the soil water salinity surveys were conducted as a completely randomized design with repeated measures. Using Tukey's adjustment (Milliken and Johnson) for multiple comparisons, the distribution of \overline{EC}_e values across a given region was found not to vary significantly from season to season. In each study region, the surveyed fields exhibited high correlation in \overline{EC}_e from one survey event to the next. Pearson correlation values were 0.82 and 0.79 in the Upstream and Downstream study regions, respectively. Correlations were calculated using all consecutive pairings of the regular survey data, or only those pairings that exist between one season to the next (e.g., early season 2002 to midseason 2002), as opposed to pairings

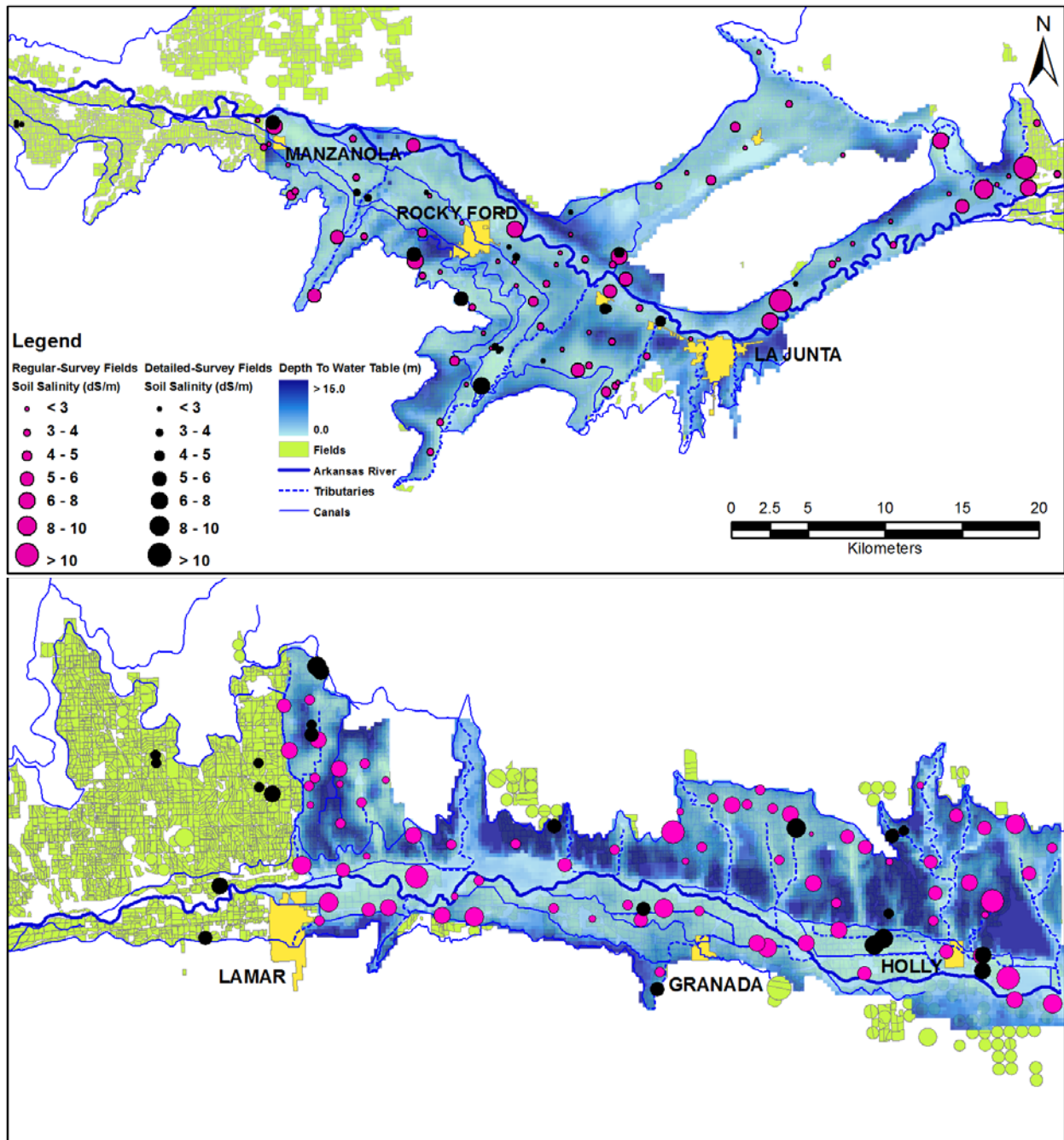


Figure 3-4. Mean \bar{EC}_e over all midseason surveys plotted for regular survey fields and detailed survey fields on contours of mean D_{wt} measured over all of the corresponding irrigation seasons.

using the next available survey (e.g., early season 2002 to early season 2003). This indicates that, as a group, the fields in either the Upstream or Downstream regions tended to collectively shift up or down or to remain roughly the same from one season to the next. A few fields were exceptions to this trend, which would be expected when substantial changes occurred in localized conditions, such as cropping patterns or irrigation water sources (from canal water to pumped groundwater).

Spatial patterns in EC_e at the field scale, including correlation, are not addressed in this paper; rather, only central tendency and degree of variability in EC_e within fields spanning the regions are explored. Analysis of the values of EC_e measured at points within individual fields over all (both regular and detailed) surveys indicates probability distributions that typically were skewed. Approximately 36% of surveyed fields had best-fit probability distributions that were inverse Gaussian, and 28% were loglogistic or lognormal. Spatial CV in EC_e within surveyed fields over the Upstream and Downstream Regions varied across all surveys from 0.01 to 1.20 in the Upstream Region and from 0.01 to 0.62 in the Downstream Region.

3.4.2 Impact of Soil Water Salinity on Crop Yield

Examination of the distribution over all point estimates of EC_e from all surveys in the Upstream Study Region reveals that 22% of the locations surveyed over the region suffer from values exceeding an estimated crop-yield threshold corresponding to the given crop. In the Downstream Study Region, approximately 70% of locations over the area exceed this threshold, indicating markedly greater salinity damage to crop productivity. Approximately 42% of the more than 122,000 locations surveyed over both regions had EC_e values exceeding the corresponding threshold.

Results revealed that the mean value of Y_r was 94% in the Upstream Study Region, indicating a mean yield reduction of approximately 6% due to excess soil water salinity. In the

Downstream Study Region, the mean value of Y_r was 83%, indicating a mean yield reduction of approximately 17%. Approximately 13% of the fields in the Upstream Region and 47% in the Downstream Region had estimated yield losses of 10% or greater due to soil water salinity. These estimates do not account for additional losses due to waterlogging or water stress, predicaments that also commonly accompany irrigated agriculture in semiarid environments.

3.4.3 Relationship of Soil Water Salinity to Soil Conditions

The average percentage of sand, silt, and clay over all calibration sites, with each site consisting of up to 15 or 16 samples, was calculated for each field in the regular surveys. The results are plotted in the soil texture diagrams of Figure 3-5 using the USDA soil classification system. In the Upstream Study Region, clay loam, sandy clay loam, and sandy loam were the

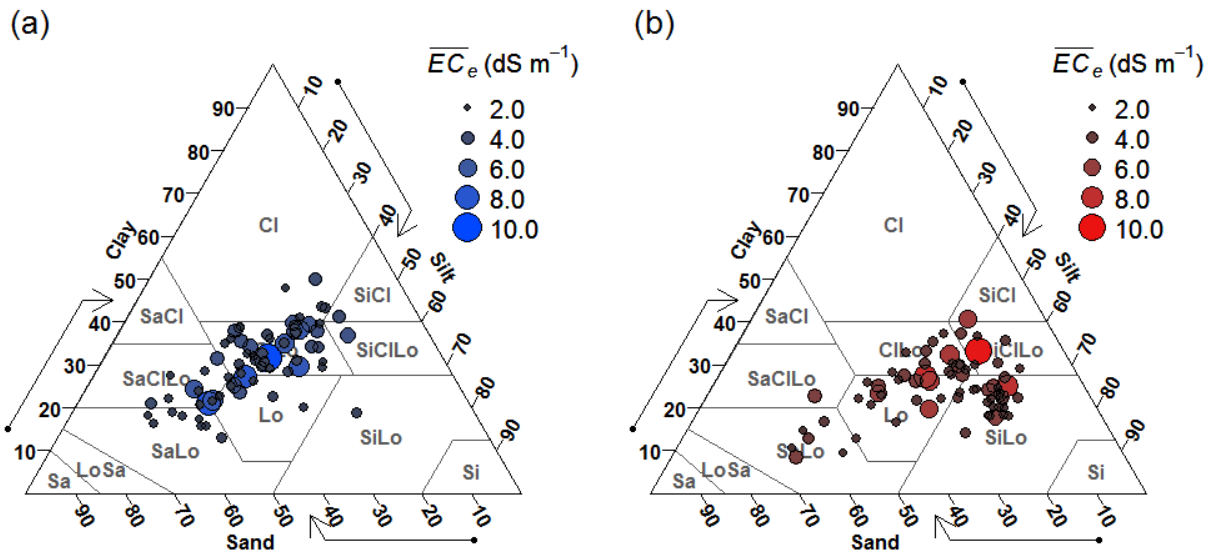


Figure 3-5. Soil texture diagrams displaying average soil texture and corresponding average EC_e over all calibration site soil samples taken in regular surveys (A) in the Upstream Study Region, and (B) in the Downstream Study Region.

three most commonly encountered soil types, whereas silty loam, loam, and clay loam were the most common Downstream. Ranges of the average percentages of sand in the surveyed fields

were 15–70% Upstream and 10–70% Downstream; the average percentages of silt were 15–60% Upstream and 20–65% Downstream; and the average percentages of clay were 15–50% Upstream and 10–40% Downstream.

To explore the general relationship of soil water salinity with soil texture on the surveyed fields, the values of EC_e estimated for soil samples gathered at all calibration sites over all regular surveys were averaged and plotted on the soil texture diagrams in Figure 3-5. No clear pattern can be detected in the data from the Upstream fields. However, in the Downstream Study Region, where sampled soils generally contained larger silt fractions, higher EC_e values were observed in fields with silt contents greater than approximately 40% and sand content less than approximately 35%. Because of the sheer number of factors that affect soil water salinity (e.g., irrigation water salinity, amount and frequency of irrigation, depth and salinity of groundwater, ET rates, proximity to seeping canals, etc.), it was not surprising that a more clear relationship between soil water salinity and soil texture did not emerge. These results from actual field conditions support results reported in the literature from controlled field experiments and from theory (Hoffman et al., 2007; Wallender and Tanji, 2012). That is, soil water salinity often was observed to be higher in silty and sandy loam soils in the presence of saline groundwater tables. A more rigorous analysis of the data would be needed to fully explore whether a cause and effect relationship is present provided the possibility of other driving forces.

Values of WC within the top 0.6–0.9 m averaged 0.16 with a CV of 0.27 over fields in the regular survey within the Upstream Study Region, with a corresponding average of 0.15 and a CV of 0.37 Downstream. Similarly, over fields in the detailed survey, WC averaged 0.13 with a CV of 0.31 Upstream and averaged 0.14 with a CV of 0.29 Downstream. Values of WC generally were greater at depths exceeding 0.9 m. Surveys were only conducted when the WC

was found to be sufficiently high to limit the error that occurs when estimating EC_e from EM-38 readings taken under dry conditions.

3.4.4 Relationship of Soil Water Salinity to Groundwater Conditions

Values of EC_{gw} measured in regular survey fields were averaged over the 4-week period preceding the date when calibration site soil samples were taken. These data were then pooled, categorized, and plotted in Figure 3-6A in relation to corresponding average EC_e values measured at calibration sites at various depths from ground surface. Values of EC_e for all soil samples taken at each depth for all fields that had an average EC_{gw} less than 1.5 dS m^{-1} were averaged and plotted in the $< 1.5 \text{ dS m}^{-1}$ position. Next, values for all soil samples taken at each depth for all fields with average EC_{gw} between 1.5 and 2.5 dS m^{-1} were averaged and plotted for the corresponding interval, and so forth. Figure 3-6B was developed in a similar fashion, relating average values of EC_e at different depths to 4-week average values of measured D_{wt} . Figure 3-6A and 3-6B indicate the manner in which EC_e tends to increase as EC_{gw} increases and as D_{wt} decreases across the regions.

The within-interval histograms also suggest trends in the soil water salinity profile with depth. These trends are illustrated more clearly in Figure 3-7, which presents the data in a more intuitive orientation. Distributions of average EC_e at varying depths (at soil surface and at 0.3, 0.6, 0.9, 1.2, and 1.8 m) of the calibration sites from the regular survey fields in the Upstream (Figure 3-7A) and Downstream (Figure 3-7B) Study Regions show a curved concentration

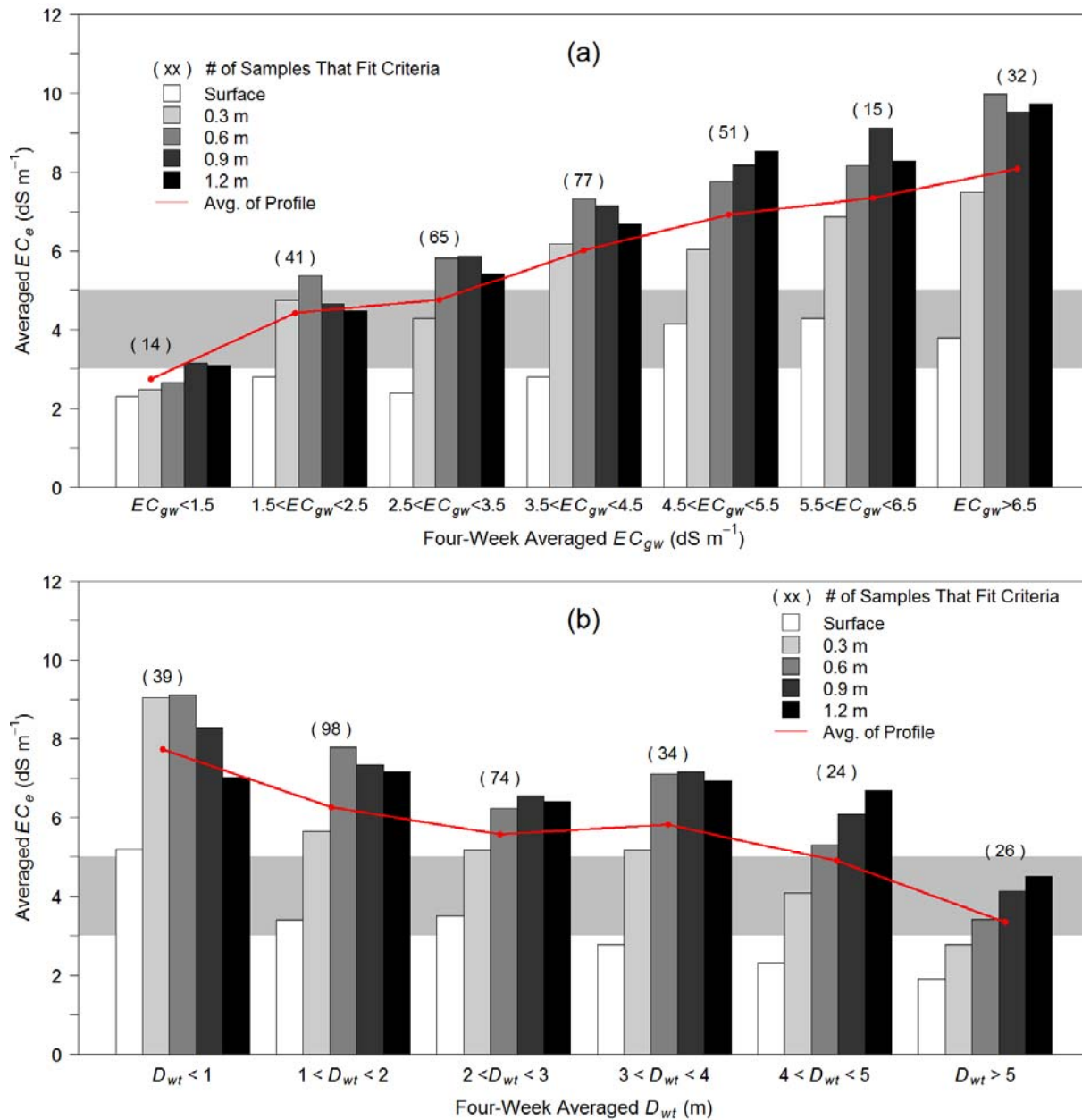


Figure 3-6. Relationship between average EC_e at different depths below ground surface at calibration sites with (A) four-week average EC_{gw} and (B) four-week average D_{wt} . The 3 – 5 $dS\ m^{-1}$ zone of crop yield threshold is indicated on both plots.

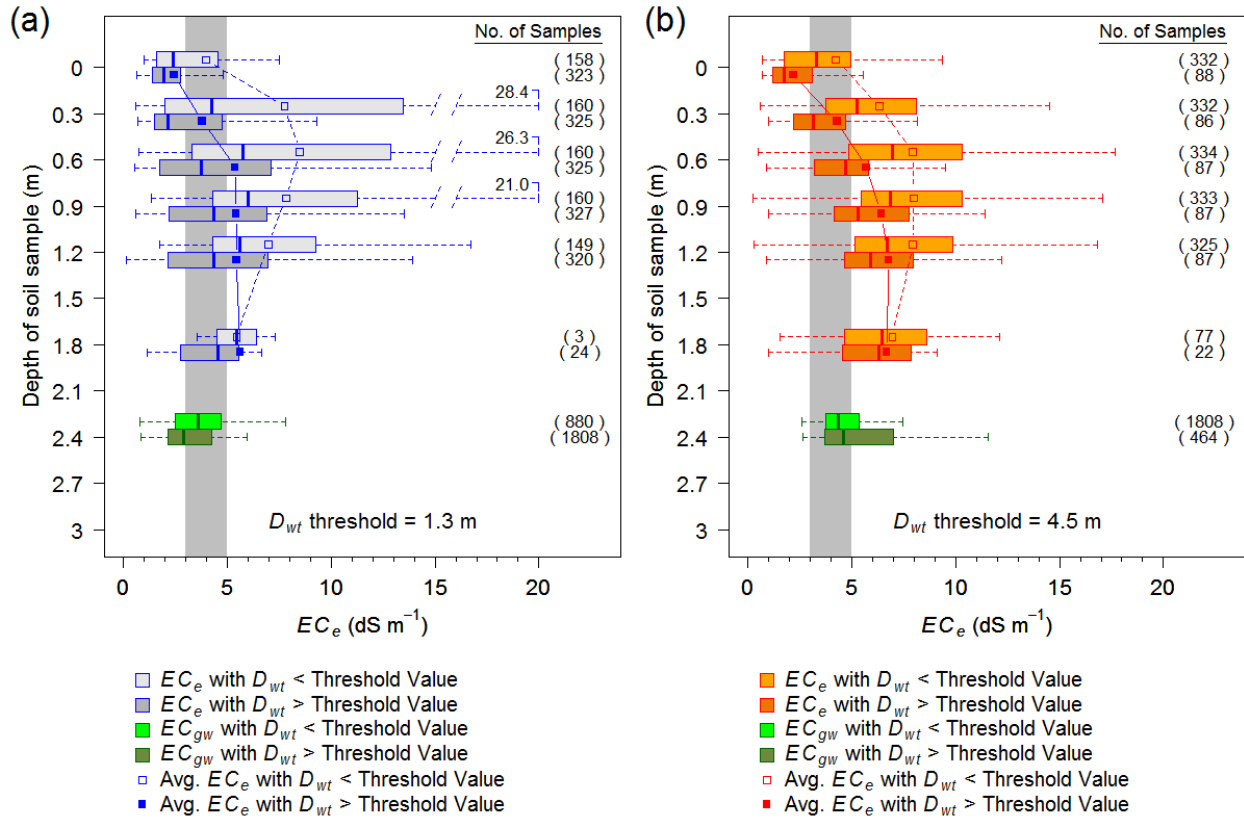


Figure 3-7. Distributions of EC_e with depth below ground surface at calibration sites Upstream and Downstream. The 3 – 5 $dS\ m^{-1}$ zone of crop yield threshold is indicated on both plots. Boxes show 25th, 50th, and 75th quartiles, whiskers extend to 1.5 times the interquartile range of the box, outliers omitted for cleanliness.

profile. Pairing the soil sample EC_e data with the previous 4-week average D_{wt} and subdividing the data based on their relationship to a threshold value reveals how the salinity profile in the soil is affected by the proximity of the water table to the root zone. Threshold values of 1.3 and 4.5 m for D_{wt} in the Upstream and Downstream regions, respectively, were derived from the nonlinear regression models fit to the data presented in Figure 3-8 (reported coefficient of determination values, r^2 , are statistically significant at significance level $\alpha = 0:05$). That is, EC_e values of 4 and 5 $dS\ m^{-1}$ for the Upstream and Downstream regions, corresponding to approximate crop-yield threshold values, would be expected when the D_{wt} is 1.3 and 4.5 m,

respectively (5 dS m⁻¹ was selected for the Downstream region because a smaller value would yield a much greater D_{wt} value for which data are sparse).

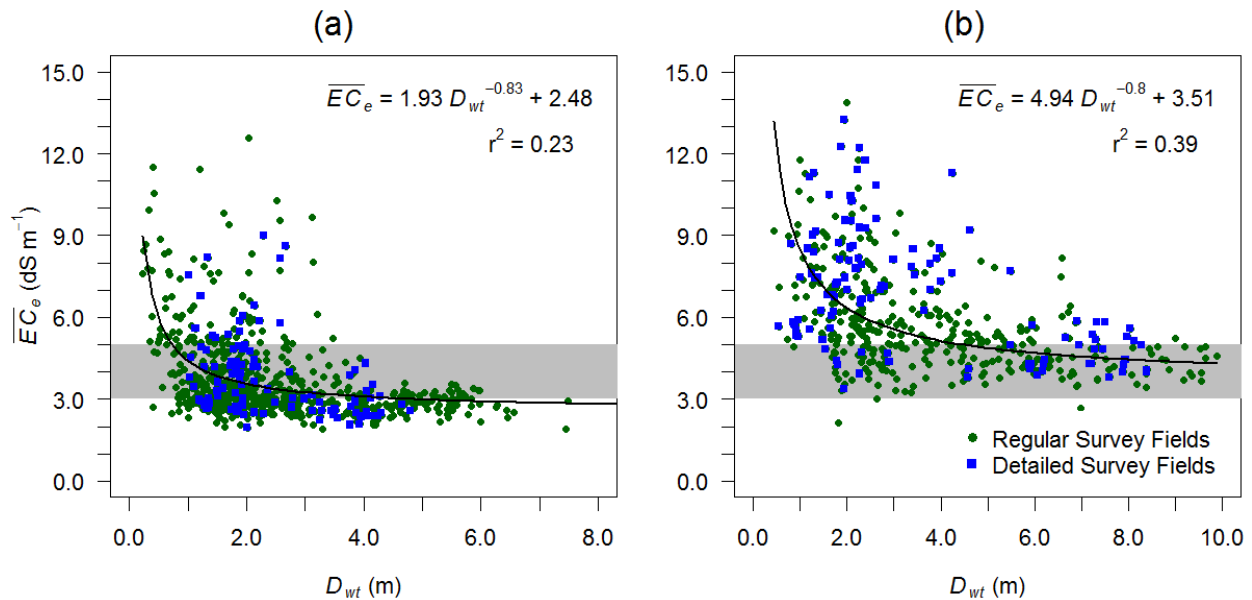


Figure 3-8. \overline{EC}_e versus four-week average D_{wt} for all surveyed fields (A) Upstream and (B) Downstream. The 3 – 5 dS m⁻¹ zone of crop yield threshold is indicated on both plots.

Differences in the salinity profile among samples with a D_{wt} greater than the threshold are evident and are suggestive of the potential for lowering EC_e levels in the crop root zone by controlling D_{wt} alone. These data provide field evidence that generally support the results presented by Hanson et al. (1999) and Xu et al. (2008), who used silt loam soil column experiments and a flow and salt transport model, respectively, to examine soil water salinity distributions in the unsaturated zone above water tables with D_{wt} values of 1.0, 1.5, 2.0, and 2.5 m. They reported a pattern of increasing EC_e with depth just below the ground surface, followed by a more gradual decline toward the water table, a result of the combined effects of evaporative

concentration of downward moving water with upflux from a saline shallow water table, similar to our field measurements at the calibration sites.

Exploration of data on the relation of EC_e to D_{wt} across a salinity-affected region can provide valuable guidelines for the planning of irrigation and drainage engineering interventions. For example, consider again Figure 3-8, which shows plots of EC_e versus 4-week averaged D_{wt} computed over all monitoring wells within each field. Though there is considerable scatter in the data (due to variation in irrigation practices, irrigation water salinity, soil types, EC_{gw} , crop ET, etc.), especially for shallower water tables, there is a statistically significant trend ($\alpha = 0.05$) of decreasing soil water salinity with increasing D_{wt} over these regions. The plots indicate that irrigation and drainage strategies in the Upstream Study Region should target D_{wt} values of approximately 1–4 m to avoid EC_e values that substantially impact crop yield. On the other hand, because of the markedly more saline conditions, a minimum target D_{wt} value of approximately 5 m would be needed in the Downstream Study Region to prevent EC_e values from exceeding the upper end of the estimated crop-yield threshold.

An additional sense of the relationship between EC_e and D_{wt} on a given field is gained by plotting time series data as shown in Figure 3-9. Whisker plots of EC_e values measured during regular surveys, plots of EC_e measured at calibration sites within the field, and plots of D_{wt} measured in the field monitoring well are presented for representative fields from the Upstream and Downstream Study Regions. Regardless of the numerous factors influencing EC_e measured in a field over time, the correspondence with D_{wt} is evident.

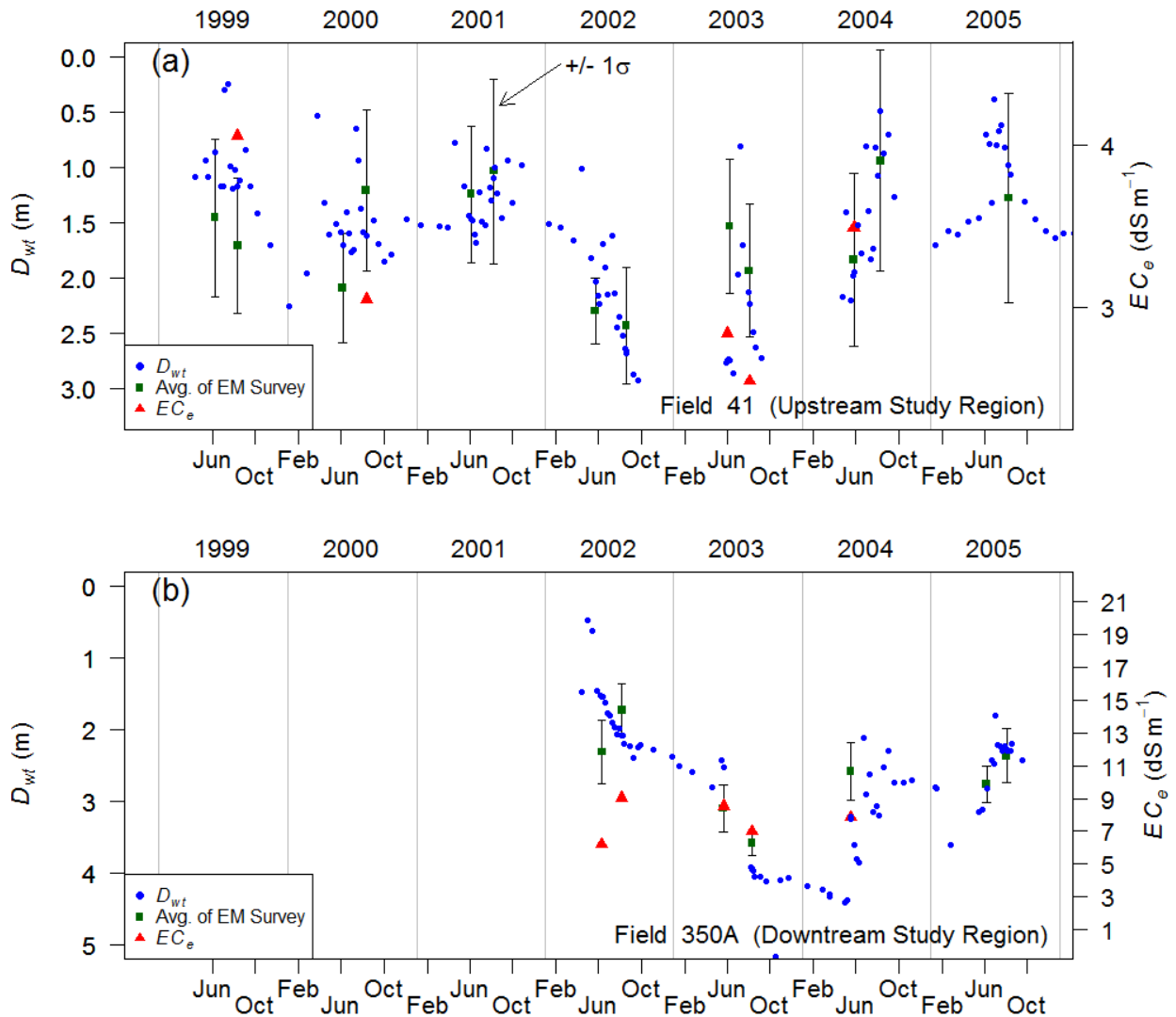


Figure 3-9. Example time series plots of D_{wt} , EC_e distributions from regular surveys (whiskers indicate ± 1 standard deviation), and average EC_e at calibration sites in (A) field 41 in the Upstream Study Region and (B) field 350A in the Downstream Study Region.

3.4.5 Use of Covariates with Regional Soil Water Salinity Survey Data

Data gathered in this study on D_{wt} , EC_{gw} , WC, and soil texture (per cent sand, silt, and clay) in conjunction with the regional soil water salinity surveys may be considered as covariates, or variables that contribute to an explanation of the variability in EC_e over the regions. To investigate the usefulness of the sampled covariates, comparisons were made

between the residual mean square (RMS) of \overline{EC}_e values with and without adjusting for the covariates (or combinations of the covariates). The RMS is the square root of the average of the squares of the difference between each observation and the mean of the observations (Milliken and Johnson, 2002). Benefits of such an analysis are twofold: 1) it may help guide other researchers in honing their data collection efforts (decreasing sample size for \overline{EC}_e , thereby saving time and money, while maintaining lower errors), and 2) it provides a relative rank of each covariate's ability to account for variation in observed \overline{EC}_e .

Covariates were not always sampled for while conducting a soil water salinity survey. For example, dry monitoring wells often precluded measurements of D_{wt} and EC_{gw} . Soil samples used to estimate WC were not collected during the first two years of surveying activity. Finally, soil texture samples were taken only from a subset of the surveyed fields due to time and fiscal constraints. Of the total number of field surveys conducted, 391 in the Upstream Study Region and 281 in the Downstream Study Region were complete with all covariates. This subset of the survey data were used in the analysis presented in this section.

Before proceeding with a regression analysis, a minor manipulation of the soil texture information was made. Because of the linear dependency that exists in the soil texture data [i.e., percent clay = 100 – (percent sand + percent silt)], a single variable estimated from the soil texture was sought for use in the regression. The Rosetta software (Schaap et al., 2001) was used to estimate residual volumetric water contents (θ_r) and saturated hydraulic conductivity (K_s) from percent sand, percent silt, and percent clay. This allowed \overline{EC}_e -covariate pairs to include individual soil texture constituents, as well as θ_r and/or K_s .

The RMS of the \overline{EC}_e values without covariates included in the analysis was 3.58e-2 (821 surveys) and 2.09e-2 (435 surveys) (the units are the same as the response variable, in this case

the \log_{10} of dS/m) in the Upstream and Downstream study regions, respectively. The RMS of \overline{EC}_e values in the reduced dataset in which all covariates were available, but not utilized, was $3.78e-2$ (391 surveys) and $2.15e-2$ (281 surveys) in the Upstream and Downstream Study Regions, respectively, and is referred to as the baseline scenario. Next, the covariates were used (one at a time or in combination) to adjust \overline{EC}_e values and the RMS was monitored to obtain a sense of each covariate's relative ability to account for the observed variance in \overline{EC}_e using the following equation:

$$\frac{RMS_1}{n_1} = \frac{RMS_2}{n_2} \quad (\text{Eq. 3-5})$$

where RMS_1 = residual mean square of the baseline scenario; RMS_2 = residual mean square adjusted for a specified covariate; n_1 = number of surveys used in the baseline scenario; and n_2 = equivalent number of surveys needed to achieve same RMS as baseline scenario.

Some covariates may not be of direct interest in some investigations. Nevertheless, in some cases, their inclusion in a study may help to reduce the number of field surveys for \overline{EC}_e while maintaining the same accuracy as a larger data collection effort and proving more cost-effective than gathering and evaluating additional \overline{EC}_e data.

Including D_{wt} as a covariate in the analysis, compared to including any other single covariate, consistently led to the largest reduction (approximately 20–25%) in the number of surveys needed to achieve the same RMS in both the Upstream and Downstream regions. Including measurements of D_{wt} , EC_{gw} , WC, and a parameter related to soil texture (percent sand, θ_r , etc.) together as covariates in the analysis led to an approximately one-third reduction in the number of surveys needed to maintain the same RMS as in the baseline scenario. Given the significant number of man-hours needed to perform field surveys, future studies that focus on the

characterization of soil water salinity may benefit from conducting fewer surveys, while collecting a few additional covariates, such as D_{wt} , and devoting the fiscal and time savings to other endeavors.

3.5 CONCLUSIONS

The soil salinization dilemma threatens long-term productivity over broad swaths of the world's vital irrigated lands. Efforts are needed to assess the extent and severity of the problem, not just at the individual field level but over regional scales, in support of the development of strategic measures for regional mitigation. This paper demonstrates the value of such surveys by reporting the use of regionally calibrated EM-38 sensors to assess soil water salinity, in association with key influencing factors, over large intensively irrigated areas of Colorado's LARV. Seasonal average values of EC_e in fields ranged from 3.4 to 4.6 $dS\ m^{-1}$ and from 4.5 to 8.0 $dS\ m^{-1}$ during the course of the study in the Upstream and Downstream study regions, respectively, with the crop-yield threshold being approached and exceeded in many fields. Average yield losses due to soil water salinity alone were estimated to be in the 6–17% range.

Spatial variability in EC_e within each of the regions was found sizeable, with spatial CV typically approximately 0.20–0.65 within a seasonal survey. Such data provide insight into the degree of ambiguity that can be expected in connection with efforts to assess salinity impacts over expansive irrigated regions that are affected by saline shallow groundwater underlying differing soil textures and irrigation practices. They underscore the caution that must be taken not to extrapolate a few field-scale evaluations for planning large-scale investments in engineering and management interventions.

Whereas spatial variability in EC_e was evident during each regional survey, results from a GLM demonstrated no statistically significant variability in the spatial statistics of EC_e over

time. Because of a wide range of hydrologic conditions over the study period (extremely wet in 1999 to severe drought in 2002 and 2003), this result was not expected. Drought effectively brought about conditions that would be similar to those expected to result from engineering interventions aimed at lowering the water table. In other words, the forced lack of irrigation water mimicked a reduced-irrigation or increased-drainage scenario intended to lessen waterlogging and salinization. This lack of response in observed regional statistics of soil water salinity levels may highlight the broad need to leach existing salts from the soil profile once the water table is depressed, which was not performed during the drought years. Furthermore, the accuracy of the EM-38 probe is more uncertain in dry settings, such as those experienced during the 2002 and 2003 surveys.

Relationships between EC_e and other covariates, including soil texture, D_{wt} , and EC_{gw} , were explored. Owing to the over 122,000 EM-38 survey points available from regular and detailed field surveys conducted over a 9-year period, the relationships are backed by a rich dataset. In the Downstream region, where the range of silt fractions were higher compared to the Upstream region, higher EC_e were detected. Soil samples from 295 calibration sites, in addition to the data from the regular and detailed surveys, generally support long-held views about the link between soil water salinity and D_{wt} that earlier have been deduced from theory and from local field experiments. When this information was plotted against estimated crop-yield threshold ranges for EC_e , the severity of the problem in the LARV was highlighted.

Regression relationships developed herein may provide valuable guidance on the EC_e - D_{wt} relationship in other similar settings with calcareous/gypsiferous soils. In particular, they suggest the need to control water tables for salinity management at depths in the 1.3–4.5 m range, somewhat greater than those that have been recommended in the literature. For example,

van Schilfgaarde (1984) reviewed studies which indicated recommended critical water table depths typically varying over the range 0.5–1.5 m. Similarly, Smedema et al. (2004) suggested a 1-m water table depth as an “indicative” drainage design criterion for salinity control in arid/semiarid zones. Numerical transport models to simulate conditions in the LARV are under development, focusing on groundwater salinity and salt return loads to the Arkansas River, as well as soil water salinity with associated impacts to crop productivity. The aim is to explore and recommend regional-scale interventions (such as improved irrigation efficiency, reduced canal seepage, artificial drainage, etc.) to successfully diminish these and related problems. Both the collected dataset and the analyses reported in this paper are being used to support and calibrate the salt transport model in both the saturated and unsaturated zones. Distributions of simulated EC_e values from computational cells spanning the root zone in cropped areas will be checked against the distributions described herein.

4 APPRAISING OPTIONS TO REDUCE SHALLOW GROUNDWATER TABLES AND ENHANCE FLOW CONDITIONS OVER REGIONAL SCALES IN AN IRRIGATED ALLUVIAL AQUIFER SYSTEM²

4.1 SUMMARY

Some of the world's key agricultural production systems face big challenges to both water quantity and quality due to shallow groundwater that results from long-term intensive irrigation, namely waterlogging and salinity, water losses, and environmental problems. This paper focuses on water quantity issues, presenting finite-difference groundwater models developed to describe shallow water table levels, non-beneficial groundwater consumptive use, and return flows to streams across two regions within an irrigated alluvial river valley in southeastern Colorado, USA. The models are calibrated and applied to simulate current baseline conditions in the alluvial aquifer system and to examine actions for potentially improving these conditions. The models provide a detailed description of regional-scale subsurface unsaturated and saturated flow processes, thereby enabling detailed spatiotemporal description of groundwater levels, recharge to infiltration ratios, partitioning of ET originating from the unsaturated and saturated zones, and groundwater flows, among other variables. Hybrid automated and manual calibration of the models is achieved using extensive observations of groundwater hydraulic head, groundwater return flow to streams, aquifer stratigraphy, canal seepage, total evapotranspiration, the portion of evapotranspiration supplied by upflux from the

² As published in the Journal of Hydrology, Eric D. Morway, Timothy K. Gates, Richard G. Niswonger, 2013, Vol. 495, 216-237.

shallow water table, and irrigation flows. Baseline results from the two regional-scale models are compared to model predictions under variations of four alternative management schemes: (1) reduced seepage from earthen canals, (2) reduced irrigation applications, (3) rotational lease fallowing (irrigation water leased to municipalities, resulting in temporary dry-up of fields), and (4) combinations of these. The potential for increasing the average water table depth by up to 1.1 and 0.7 m in the two respective modeled regions, thereby reducing the threat of waterlogging and lowering non-beneficial consumptive use from adjacent fallow and naturally-vegetated lands, is demonstrated for the alternative management intervention scenarios considered. Net annual average savings of up to about 9.9 million m³ (8,000 ac·ft) and 2.3 million m³ (1,900 ac·ft) of non-beneficial groundwater consumptive use is demonstrated for the study periods in each of the two respective study regions. Alternative water management interventions achieve varying degrees of benefits in each of the two regions, suggesting a need to adopt region-specific interventions and avoid a ‘one-size-fits-all’ approach. Impacts of the considered interventions on return flows to the river were predicted to be significant, highlighting the need for flow augmentation to comply with an interstate river compact and portending beneficial impacts on solute loading.

4.2 INTRODUCTION

Irrigated agricultural development in an alluvial river valley can often lead to shallow water tables due to excessive water application, seepage from earthen canals, and inadequate drainage systems, creating a number of challenging difficulties. Over time, these high water tables become salinized, contributing not only to waterlogging (inadequate soil pore aeration) but also to salinization of soils and diminishing crop yield. High water tables cause recharge from irrigation to seep back to streams, and these return flows can dissolve salts and other chemical

constituents as the water moves through the underlying aquifer, further increasing constituent loads. Also, as shallow groundwater flows laterally, it raises water tables beneath uncultivated and fallow land where substantial amounts of shallow groundwater may be non-beneficially consumed (herein, “non-beneficial consumptive use” signifies water evaporated and transpired without directly contributing to economic agricultural production). Groundwater solute concentrations increase beneath both cultivated and uncultivated land due in part to this evaporative upflux from shallow water tables (Ghassemi et al., 1995; Gates et al., 2006; Niemann et al., 2011; Morway and Gates, 2012).

Physically-based computational models often are used to investigate strategies for reducing waterlogging and salinization associated with shallow groundwater. For example, in northern India, Kumar and Singh (2003) employed a calibrated and tested model to investigate water-management scenarios aimed at reducing wide-spread waterlogging. Later, Singh et al. (2006) used a hydrological model to study the potential for waterlogging and salinity reduction through improved water management and reduction of canal seepage in India. In the Yaqui Valley of Mexico, Schoups et al. (2005a) used a hydrologic/agronomic model coupled with an optimization model to explore crop yield responses to increased reliance upon groundwater resources in a time of drought. In China’s Yellow River Basin, Xu et al. (2010) used a lumped-parameter model to investigate management and infrastructure rehabilitation alternatives for current irrigation practices to relieve water scarcity and to curb waterlogging and salinization in the upper part of the basin. A wide range of options were investigated: reduced canal seepage, rehabilitated control structures, improved water delivery scheduling, deficit irrigation, adjusted crop patterns, land leveling, and modernized irrigation methods (e.g., drip or sprinkler irrigation). Scenarios were simulated through adjustment of assorted empirical coefficients in the lumped-

parameter model and demonstrate the potential for lowering the water table by as much as 0.71 m using a combination of interventions. In the United States, a number of regional-scale waterlogging and salinity studies have been carried out in the San Joaquin Valley of California. Gates and Grismer (1989) and Gates et al. (1989) describe a groundwater flow and salt transport model that was used to help determine "economically optimal irrigation and drainage strategies for long-term regional management." Schoups et al. (2005b) present a regional-scale model that includes flow in both the saturated and unsaturated zones, as well as a reactive salt transport component, run over a 57-year period to simulate historic trends in salinity concentrations observed in both the shallow and deep aquifers.

The Lower Arkansas River Valley (LARV) in southeastern Colorado (Figure 4-1) has a long history of rich agricultural production but is vulnerable to a number of the irrigation-related problems typical of intensively irrigated valleys. As such, it has been the focus of several investigations over recent decades. Several models of the LARV were developed in the second half of the 20th century (Konikow and Bredehoeft, 1974a; Konikow and Bredehoeft, 1974b; Konikow and Person, 1985; Person and Konikow, 1986; Lefkoff and Gorelick, 1990; Goff et al., 1998; Brendle, 2002). Gates et al. (2002) published steady-state results from a three-dimensional model that was more expansive and more spatially and temporally resolved than the earlier models. Burkhalter and Gates (2005, 2006) used transient models to evaluate management scenarios intended to mitigate waterlogging, salinization, non-beneficial consumptive use, and salt loading to streams in a portion of the LARV. Simulated management options included reduced canal seepage, reduced recharge from over-irrigation (improved water management), improved drainage facilities, and combinations of these. Results suggested the potential for

dramatic improvements in crop productivity, water conservation, and improved water quality in the LARV.

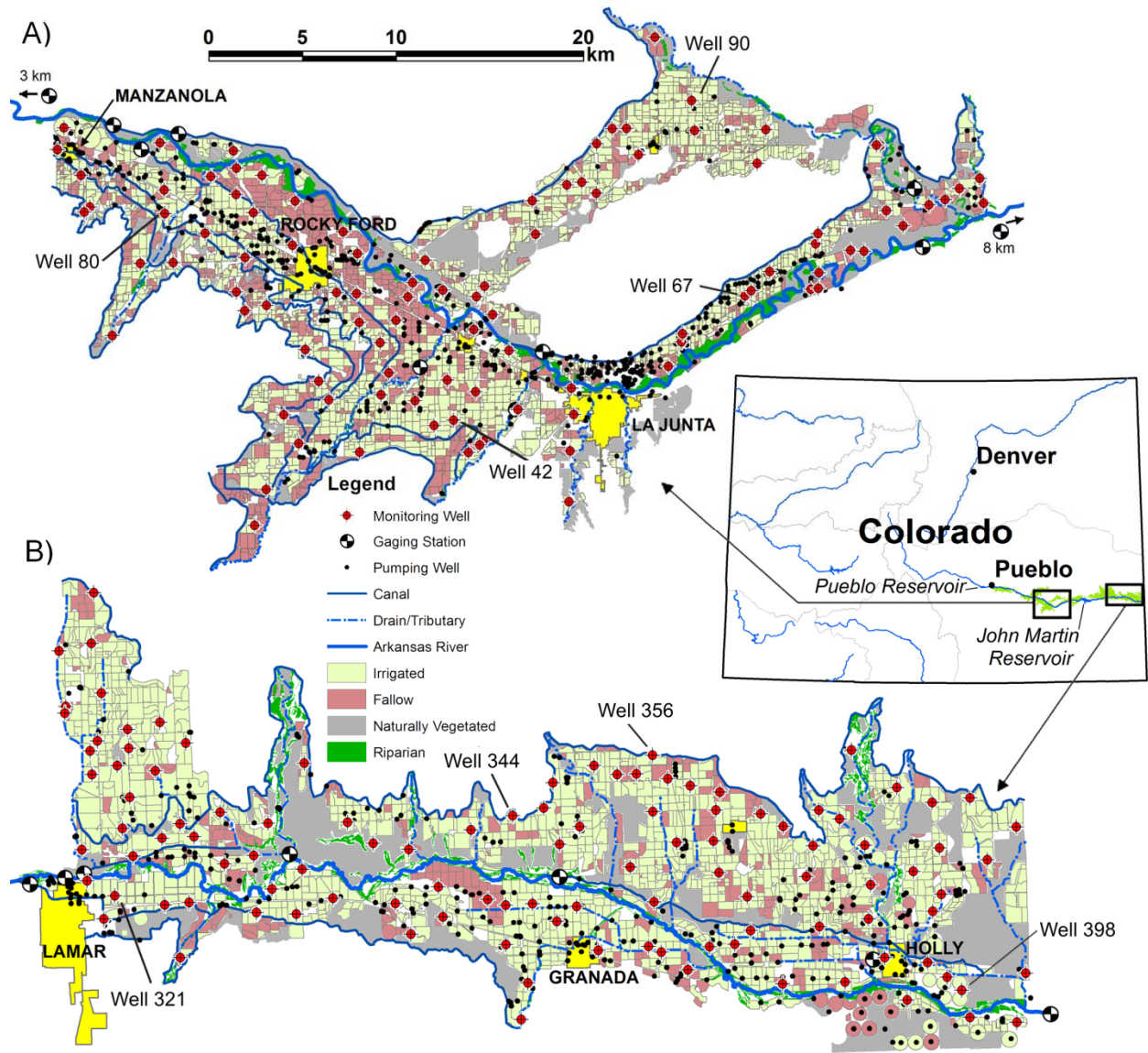


Figure 4-1. The (A) USR and (B) DSR within Colorado's LARV showing major features and land classifications. Identified wells correspond to the time series plots in Figure 4-5.

This paper provides a record of the calibration, testing, and application of regional-scale ($\sim 10^4 - 10^5$ ha) models of the irrigated alluvial aquifer system of the LARV with the aim of

discovering how to alter regional water tables and groundwater flow to establish conditions that enhance and sustain agricultural production, conserve water, and improve the riverine environment of the LARV. This effort builds upon the work of previous modeling studies of the LARV by developing detailed representation of hydrologic conditions and water-budget components over an expanded spatial and temporal extent, and by drawing upon substantially richer observation data sets for calibration. Though the potentially harmful effects of irrigated agricultural production on water supplies are related to both water quantity and water quality, a model that simulates only the flow of water, and not the transport of salts, can be very useful for better understanding existing groundwater table and flow conditions. Such conditions are of direct concern themselves, and include depth to the water table, upward flow lost to non-beneficial consumptive use, and the rate and timing of groundwater return flow to streams. Moreover, the accurate simulation of these groundwater table and flow conditions is a prerequisite for eventual solute transport modeling.

For model construction and calibration, a database is built from extensive field data gathered over 9 years from two regions, selected to be broadly representative of the entire LARV. To maximize the use of this unique dataset, the following major distinguishing features are implemented in the regional models described herein: (1) model calibration and testing are improved by using a diverse set of observations applied to both representative valley regions: groundwater hydraulic head, groundwater return flow, seepage from earthen canals, actual evapotranspiration (ET) within the soil zone, upflux to ET from the water table under naturally-vegetated and fallow land, and estimates of ratios of water table recharge to infiltrated irrigation water; (2) the modeled period is extended six years longer than in previous studies (Burkhalter and Gates, 2005; Burkhalter and Gates, 2006) and now includes wet, dry, and near-average

hydrological conditions; (3) unsaturated-zone flow processes are simulated over the regional scale using the unsaturated-zone flow (UZF1) package (Niswonger et al., 2006) developed for MODFLOW; (4) a water allocation algorithm is created that attempts to realistically recreate spatiotemporal irrigation patterns while honoring historical canal diversion records; (5) MODFLOW-NWT (Niswonger et al., 2011) is used for greater numerical stability during calibration (alleviating cell wetting and drying problems); (6) spatially-varying estimates of precipitation and potential ET rates are used in place of uniform estimates for each region; (7) highly resolved land-use and crop-planting classification are employed to more accurately account for actual ET; (8) an improved representation of the timing of seepage losses from earthen canals is used; and (9) hundreds of stratigraphic logs simultaneously guide and constrain spatially variable model parameters. This paper presents an approach for detailed simulation and evaluation of alternative management scenarios that are designed to conserve both water quantity and quality, but with consideration limited herein to water quantity-related issues. General results for this study may be evaluated for transferability to similar irrigated agricultural regions, and the approaches are presented as guidelines for studies of other such settings.

4.3 STUDY AREA

Situated on the High Plains (Figure 4-1) in semi-arid southeastern Colorado, the broad and thin alluvial aquifer of the LARV is underlain by a series of sedimentary formations of late Cambrian to Tertiary age (Darton, 1906). The lower formations, consisting of marine-derived shale, are relatively impermeable and serve as the lower boundary of the groundwater models (Moore and Wood, 1967; Person and Konikow, 1986). The Dakota sandstone formation underlies the alluvium in an area near the Colorado-Kansas border. Because of lower potentiometric heads in the sandstone as well as moderate porosity, recharge from the overlaying

alluvium may occur (Voegeli, 1965). However, relative to the much larger fluxes present in the shallow alluvium, this interaction is assumed negligible. The alluvium is in good hydraulic connection with the Arkansas River (Konikow and Bredehoeft, 1974a; Person and Konikow, 1986).

Because crop water requirements in the LARV are well in excess of the average annual precipitation of about 0.30 m, water requirements must be supplemented with locally pumped and diverted river water to achieve full crop production. Large-scale surface irrigation in the valley started in the 1870's and continues today (Sherow, 1990). Currently, the appropriated water rights in the LARV, including both native and trans-basin water, exceed the average annual river flow by as much as 40% in a low-flow year (Cain, 1985; Sutherland and Knapp, 1988). To help offset this imbalance, storage accounts in Pueblo and John Martin Reservoirs capture river flow during the winter months for later release during the irrigation season. There currently are a total of about 109,000 irrigated hectares (269,000 ac) in the LARV, distributed among about 14,000 fields. River water is delivered to fields by 25 major canals and about 2,400 pumping wells provide supplemental supplies from the alluvial groundwater. Flood-irrigation methods are predominant, with less than about 5% of fields irrigated with sprinklers or drip lines.

In recent years, there has been increased interest in transferring irrigation water rights to cities along Colorado's Front Range. To ward off the permanent purchase of irrigation water rights and the associated damage to the agricultural economy and rural communities, work is underway to develop a lease-fallowing program in the LARV. This program would allow municipal users to temporarily lease that portion of irrigation that is beneficially consumed on up to about one third of their historically-irrigated land. As a result, up to one third of the irrigated land could be dried up in any given year.

Some major constraints on operating the irrigation system in the LARV are Colorado water rights law and the Arkansas River Compact (with Kansas). The Arkansas River Compact prohibits changes to the system that would alter the return flow patterns (amount, spatial pattern, and timing) so as to cause the flow in the Arkansas River to be “materially depleted in usable quantity or availability for use to the water users in Colorado and Kansas” (Colorado Revised Statutes, 1949). Hence, reductions in excess surface or subsurface flows that result from any interventions, even if they facilitate temporary water transfers to municipalities and/or improve water quality problems, are prohibited unless properly augmented. Amending river flows with releases from reservoir storage such that depleted subsurface return flows are replaced may be one option for satisfying legal restrictions on river operation. If improved irrigation efficiency and lease-fallowing can indeed be achieved in conjunction with such offsetting measures, then it is believed that crop yields can be increased, river water quality can be improved, and permanent water transfers from agriculture can be reduced (Gates et al., 2006; Triana et al., 2009a; Triana et al., 2010).

For the present work, we apply regional-scale groundwater models to assess the potential effectiveness of management scenarios for improving groundwater conditions in the LARV. These models simulate the complex distribution of water in these broad agricultural settings, including the distribution of surface water, unsaturated and saturated groundwater flow, and ET fluxes constrained by detailed and heterogeneous sets of hydrologic observation data. Two study regions, together encompassing about 54% of the irrigated land in the LARV, were selected for analysis of the alluvial aquifer conditions (Figure 4-1). The Upstream Study Region (USR), representative of conditions upstream of John Martin Reservoir, is comprised of about 50,600 ha (26,400 ha of which are irrigated) extending about 78 km along the river from just west of

Manzanola eastward to Adobe Creek near Las Animas. Representing conditions downstream of John Martin Reservoir, the Downstream Study Region (DSR) covers a valley extent of about 55,200 ha (33,000 ha irrigated) stretching 71 km along the river from May Valley Drain near Lamar to the Colorado-Kansas border.

4.4 MODEL CONSTRUCTION AND COMPOSITION

4.4.1 Numerical Flow Models and Database

Two groundwater flow models are developed using the MODFLOW-NWT version of the groundwater flow model, MODFLOW (Harbaugh; Niswonger et al., 2011) Three dimensional models are used to simulate flows in the unconfined alluvial aquifers and irrigated soils of the USR and DSR for the periods 1999-2007 and 2002-2007, respectively. Readers are referred to Harbaugh (2005) and Niswonger et al. (2011) for details on the finite-difference formulation and the Newton solution method employed by MODFLOW-NWT.

Unsaturated-zone flow processes are simulated using the UZF1 package of MODFLOW (Niswonger et al., 2006). UZF1 uses the method of characteristics for solving a kinematic wave approximation for one-dimensional downward vertical flow in the unsaturated zone that is derived by neglecting the diffusive term in Richards equation. UZF1 also relies on the assumption of uniform hydraulic properties in the unsaturated zone for each vertical column of model cells. The unsaturated-zone flow equation solved by UZF1 that is coupled to the groundwater flow equation is:

$$\frac{\partial \theta}{\partial t} + \frac{\partial K(\theta)}{\partial z} + q_{ET} = 0 \quad (\text{Eq. 4-1})$$

where θ is volumetric water content in the unsaturated zone [L^3L^{-3}], $K(\theta)$ is the vertical hydraulic conductivity as a function of θ [LT^{-1}], and q_{ET} is the rate of ET removal from the unsaturated zone above the water table (expressed per unit depth [$LT^{-1}L^{-1}$]). The kinematic-wave

equation provides an efficient method for simulating unsaturated-zone flow, ET, and recharge over regional scales. If ET potential is not satisfied by unsaturated-zone water then MODFLOW-NWT also can simulate ET derived from groundwater upflux on the basis of a linear function of water table depth (Harbaugh, 2005). Additional detail of the approach used in UZF1 and its advantages are described in Niswonger et al. (2006) and Niswonger and Prudic (2004).

Two layers were used in each model to represent the alluvial aquifers in the LARV. The top layer is approximately 5 m thick in both models and encompasses the maximum extent of deeply-rooted crops (i.e. alfalfa). The extinction depth, or depth at which groundwater ET ceases (Harbaugh, 2005), does not fall below the top layer. The lower layer extends from the bottom of the upper layer down to the impervious shale. Shale formations, that can extend hundreds of meters below the alluvial aquifer, are not represented in the model. Grid cells have uniform areal dimensions of 250 m x 250 m in both horizontal directions, with a total of 15,600 and 18,600 active nodes in the USR and DSR models, respectively. A total of 447 weekly time steps are simulated in the USR and 291 weekly time steps in the DSR.

A number of model enhancements, as compared to previous modeling efforts in the LARV, are facilitated by a large and diverse number of field observations. The observation database includes 8.5 and 5.5 years of groundwater and surface water monitoring data in the USR and DSR, respectively. Included in the dataset are over 8,700 depth to groundwater measurements from approximately 100 monitoring wells in the USR and over 7,200 measurements from approximately 118 wells in the DSR. U.S. Geological Survey (USGS) stream gaging stations on the Arkansas River are located very near the beginning (upstream) and ending (downstream) boundaries of the models, enabling estimation of groundwater return flows

to the Arkansas River and its tributaries by water balance calculations. Surface water inflow across the model boundary is assumed negligible in most of the ungaged tributaries. Visual inspection of tributaries entering the modeled regions during routine data collection has verified this. Occasional intense rainfall events outside the modeled region contribute significant, but brief, surface water inflows to the modeled region through ungaged tributaries. These sporadic inflows likely contribute to some of the misfit between the simulated and ‘observed’ groundwater return flows. The elevations of surface waters are resolved by extensive differential global positioning system (DGPS) surveys conducted early in the study.

Continuous records of surface water diversions to canals and pumped volumes of groundwater obtained from the Colorado Division of Water Resources (CDWR) help constrain the various components of the water budget within the study regions. In addition, hundreds of observations of field-specific irrigation applications and associated water losses (Gates et al., 2012), along with estimates of total actual ET calculated by the RESET model (Elhaddad and Garcia, 2008) for cultivated and naturally-vegetated land (Niemann et al., 2011), further constrain the water budget within the study regions. A number of canal seepage observations derived from simultaneous inflow-outflow seepage measurements performed on the Catlin, Fort Lyon, and Rocky Ford Highline canals in the USR and on the Amity, Buffalo, and Lamar canals in the DSR have been used during model development {Susfalk et al, 2008; Shanafield et al, 2010; Martin 2013}.

4.4.2 Aquifer Properties

4.4.2.1 Hydraulic Conductivity and Stratigraphy

Hydraulic conductivity, was calibrated for the LARV in earlier efforts (Burkhalter and Gates 2005) by using manual trial-and-error techniques outlined in ASTM Standard D5981-96 (1996). In the present study, values of hydraulic conductivity (as well as river conductance

values for changing seepage) are varied through an automated calibration approach to achieve acceptable match between model-simulated values of hydraulic head (h) and groundwater return flow to the river (Q_{GW}), and values determined from field measurements.

Stratigraphy recorded in available driller's logs from across the LARV (Major et al., 1970) was categorized into four broad material classifications (gravel, sand, silt, or clay). The thickness of each stratigraphic layer within each of the two computational layers was calculated. Next, each of the material classifications is assigned through automated calibration a value of saturated horizontal hydraulic conductivity (K_H) from within the estimated range of values found in the literature (Freeze and Cherry, 1979; Domenico and Schwartz, 1998) for that material type. Finally, a composite depth-averaged value, \bar{K}_H , at each of the borehole locations is computed over the interval of stratigraphic layers within the two computation grid layers (Domenico and Schwartz, 1998):

$$\bar{K}_H = \frac{\sum (m_i K_{H_i})}{\sum m_i} \quad (\text{Eq. 4-2})$$

wherein K_{H_i} is the horizontal saturated hydraulic conductivity of stratigraphic layer i [LT^{-1}] and m_i is the corresponding thickness [L].

The values of K_H assigned to each of the four stratigraphic porous material groups initially are estimated using the automated calibration model UCODE. UCODE only estimated K_H values for each of the four texture categories and these values are used to estimate \bar{K}_H at each borehole location. \bar{K}_H values at borehole locations then are used to estimate values for all cells using ordinary kriging. This is similar to the pilot point approach described in Doherty (2003), but rather than granting each pilot point (borehole location) freedom to take on any \bar{K}_H value within a specified range, the stratigraphic record informs and constrains the value of each

pilot point. This approach results in a total of eight (four in each of the two layers) estimable parameters associated with hydraulic conductivity. This approach is limited, however, in its ability to fully specify the \bar{K}_H distribution over the modeled region. That is, the hydraulic conductivity assigned to a ‘sand’ stratigraphic layer would be the same throughout the model domain though the hydraulic conductivity of sand is likely variable across the model domain. The approach likely curtails UCODE’s ability to provide parameters that result in a good match to the measured data. Because of this limitation, a second attempt is made at automated parameter estimation (described in Section 4.5.1 below) using a uniformly distributed set of pilot points not constrained by stratigraphic considerations, but rather regularized (Doherty, 2003) by the hydraulic conductivities estimated by UCODE.

The flux between the stream and the aquifer is calculated using a standard leakance approach (e.g., Harbaugh, 2005). The hydraulic conductivity of the streambed material is assumed to be the same as that of the underlying aquifer material. The thickness of the streambed material is taken as the distance of flow between the elevation of the cell centroid and the elevation of the stream bottom. Analysis of aquifer pumping tests were reported by Wilson (1965) for 14 wells completed in the deeper alluvium inside the USR and for four wells in the DSR, yielding estimates of \bar{K}_H in the vicinity of the wells. Estimates of \bar{K}_H from the pumping tests are used to evaluate if \bar{K}_H values estimated by automated calibration are reasonable. Considering differences in scale and the large area over which simulated values are estimated, but where pumping tests were not made, there is good agreement (within an order of magnitude) between estimated values of \bar{K}_H used in MODFLOW and observed values of \bar{K}_H derived from pumping tests.

The saturated vertical hydraulic conductivity of the unsaturated zone, K_s , that is used in the Brooks-Corey equation (Brooks and Corey, 1966) is estimated by UCODE separate from the vertical hydraulic conductivity, \bar{K}_v , of the saturated zone. The ranges for the ratio of K_s to \bar{K}_H in layer 1 for both the USR and DSR are provided in Table 4-1, as is the ratio between \bar{K}_v and \bar{K}_H in the saturated zone.

4.4.2.2 Specific Yield

Depth-averaged specific yield values, \bar{S}_y , are estimated using a methodology similar to that discussed for hydraulic conductivity: final values are computed at borehole locations using estimates from UCODE, constrained by the porous material identified in stratigraphic layers, and are interpolated over the computational region using a kriging algorithm. Values of specific yield within any stratigraphic layer, S_{y_i} , are constrained to not exceed the values of saturated water content, θ_s (defined as THTS in UZF1), in each cell.

4.4.2.3 Unsaturated-Zone Soil Properties

The $K(\theta)$ term in Equation 4-1 is calculated using the Brooks-Corey equation

$$K(\theta) = K_s \left[\frac{\theta - \theta_r}{\theta_s - \theta_r} \right]^\varepsilon \quad (\text{Eq. 4-3})$$

where θ_r is the residual water content, and ε is the Brooks-Corey exponent. Initial estimates of θ_r are obtained in a fashion similar to hydraulic conductivity and specific yield; values are estimated at borehole locations using the stratigraphic information and interpolated to the MODFLOW grid, resulting in a spatially variable array of θ_s . A multiplier applied to the vertical

Table 4-1. Range of parameter values employed in the models.

Model Parameter	USR Range of Values	DSR Range of Values
Layer 1 \bar{K}_H	0.4 – 320 m/day	0.3 – 160 m/day
Layer 1 K_S / \bar{K}_H Ratio ^a	8.6e-6 – 1.1e-2	7.0e-5 – 2.9e-2
Layer 2 \bar{K}_H ^{b,c}	0.8 – 180 m/day	1.4 – 75 m/day
Layer 2 \bar{K}_V / \bar{K}_H Ratio	0.2	0.1
Layer 1 \bar{S}_y	0.10 – 0.32	0.01 – 0.33
Layer 2 \bar{S}_y	0.07 – 0.36	0.01 – 0.34
Layer 1 & 2 Specific Storage	1.7e-5	1.7e-5
Canal Conductance	3.9e-4 – 21 m ² d ⁻¹ m ⁻¹	1.7e-3 - 8.6 m ² d ⁻¹ m ⁻¹
Saturated K in UZF1	3.3e-3 – 0.15 m/day	1.1e-2 – 0.26 m/day
ϵ (Brooks-Corey exponent)	3.5	3.5
θ_s (UZF1)	0.18 - 0.43	0.18 – 0.39
Extinction Depth	1.2 – 4.5 m	1.3 – 4.5 m

^a K_S / \bar{K}_H ratios for layer 1 calculated as the ratio between VKS specified in UZF1 and K_b in the UPW package of MODFLOW-NWT

^b 14 observations of \bar{K}_H near pumping wells in the USR ranged between 13 – 620 m/day (Wilson, 1965)

^c 4 observations of \bar{K}_H near pumping wells in the DSR ranged between 78 – 372 m/day (Wilson, 1965)

hydraulic conductivity array is used to accelerate or slow the downward movement of percolating water applied at the ground surface, thereby affording more or less time for q_{ET} to be extracted from the unsaturated zone. Moreover, the simulated recharge to the groundwater table is correspondingly increased or decreased, depending on the manner in which the multiplier is manually adjusted.

4.4.3 Irrigation and Atmospheric Boundary Conditions

4.4.3.1 Evapotranspiration

The ASCE-PM methodology, well-established in numerous investigations (Allen et al., 1989; Ventura et al., 1999; Itenfisu et al., 2003) is adopted for calculating reference

evapotranspiration, ET_r , in the current study. Guidelines for calculating ET_r are provided in ASCE-EWRI (2005). Daily values of ET_r were calculated at CoAgMet weather stations (Colorado Climate Center, 2007) in the LARV and then interpolated using ordinary kriging to obtain spatially varying arrays over the modeled regions. Data collected at the CoAgMet sites include daily minimum temperature, mean temperature, maximum temperature, wind run, solar radiation, vapor pressure, maximum relative humidity, and minimum relative humidity (Ley et al., 2009). Remaining inputs required for calculating each field's daily potential ET include historical cropping patterns and corresponding values of crop coefficients, k_c (Allen et al., 1998). For each field located within both study regions, crop planting histories are obtained from the Farm Service Agency (FSA) in the appropriate county. Non-cultivated fields typically do not receive irrigation water, and include fields that are reportedly fallow or under the U.S. Department of Agriculture's conservation reserve program. Reduced values of potential ET are applied to fallow fields to simulated ET demand from volunteer crops or weeds. Estimates of daily potential ET are summed to obtain weekly potential ET values that honor both the stage-of-development and reported crop type for every field in the region. Weekly potential ET estimates for every field are converted to grid-based values, because grid cells do not correspond to field boundaries. Reductions in ET caused by salinity are not accounted for directly in the USR and DSR models. As discussed in Section 4.5.2 below, computed (simulated) values of the total ET (q_{ET} plus groundwater upflux to ET) were checked against values estimated using satellite imagery (Elhaddad and Garcia, 2008) as part of a final calibration process.

4.4.3.2 Irrigation Applications and Precipitation

Weekly infiltrated irrigation and precipitation depths are specified at the ground-surface boundary for use in calculating unsaturated-zone flows in UZF1 for irrigated fields in the region.

Methods are used to estimate when a given field would be irrigated and the associated amount of infiltrated irrigation.

A field receives irrigation water on a weekly, bi-weekly, or monthly (i.e., every four weeks) rotation schedule on the basis of crop type. A set of irrigation frequency codes further ensures that fields on the same schedule (e.g., monthly) received water in a staggered fashion in order to temporally distribute the demand for available water. Thus, ~25% of the fields with monthly irrigation frequencies receive water during the first simulated stress period (week 1), another ~25% receive water during the next stress period (week 2) and so on until the fifth week, at which point the pattern repeats. In MODFLOW, a stress period is an interval of time over which flow stresses acting on the modeled region are constant.

Several LARV farmers and extension agents were interviewed for information to guide in modeling irrigation schedules. For water-limiting situations, farmers were asked how they would choose to allocate irrigation water under the risk of losing the non-irrigated crop(s). This allowed priority ranking to be established in the following order: (1) onions, (2) peppers and tomatoes, (3) cantaloupe and melons, (4) pumpkins and squash, (5) alfalfa and corn, (6) barley, beans, and oats, (7) sorghum, (8) wheat, and finally (9) grass/pasture. Priority ranking codes in conjunction with irrigation frequency codes are used in the model to distribute the available irrigation water (a combination of diverted and pumped volumes) among the many cropped fields.

Water-balance data on hundreds of surface irrigation events over dozens of fields in the LARV were gathered by Colorado State University between 2004 and 2008 (Gates et al. 2012). These data included applied irrigation volume (expressed as average depth over each irrigated field), precipitation volume, volume of surface runoff at the end of the field (hereafter referred to

as tail-water runoff), infiltrated volume, volume of ET, and volume of deep percolation. Based upon data gathered over the period 2004–2007, applied irrigation depths are generated from a fitted log-normal probability distribution (Figure 4-2A) with the mean value adjusted to

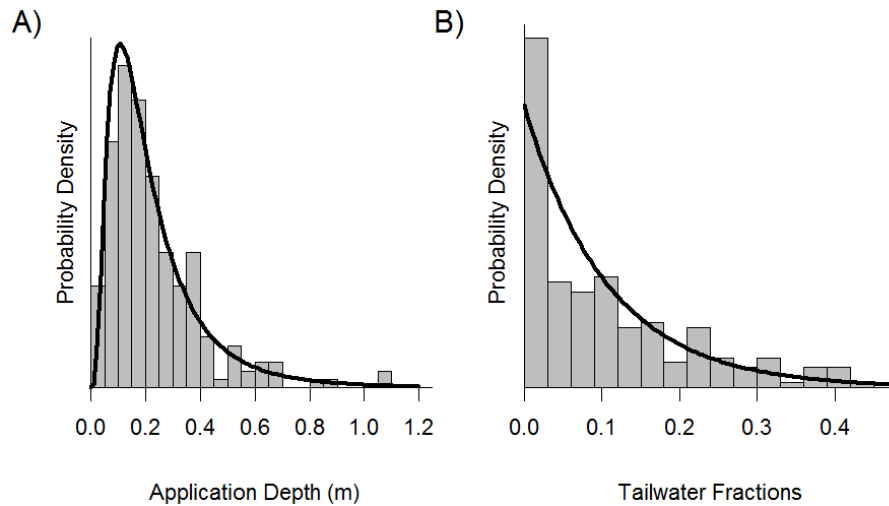


Figure 4-2. Observed (A) irrigation application depths and (B) tail-water runoff fraction in the LARV. Data collected between 2004 and 2007 were used to generate the probability distributions.

correspond to the crop type for each irrigated field. The distribution is log-normal with a mean and standard deviation of 0.25 and 0.18 m, respectively. Figure 4-2B shows the distribution of tail-water runoff fraction (TRF = ratio of tail-water runoff volume to applied irrigation volume) used in this study. The fitted distribution is exponential with a mean of 0.11. Data revealed that nearly all irrigation events with 0.025 m or more of tail-water runoff were derived from irrigation application depths exceeding 0.13 m. Therefore, the model accounts for tail-water runoff only if the applied amount exceeds 0.13 m.

For each field modeled to receive irrigation for a given week, random values of applied irrigation depth and TRF are generated from the distributions shown in Figure 4-2. Infiltrated irrigation depth for a field, is calculated as the difference between the generated applied depth

and the tail-water runoff depth (computed as the product of the generated values of applied depth and TRF). Most of the monitored fields used to estimate the distributions were planted with either alfalfa or corn. Log-normal distributions are generated for crops other than alfalfa or corn using lower mean values because they are irrigated more frequently. In these instances, the coefficient of variation ($CV = \text{ratio of standard deviation to mean}$) of the original distribution is used to calculate the standard deviation of the distribution with the altered mean.

Simulated weekly infiltrated irrigation depths across the region not only honor frequency distributions derived from field studies, but also are constrained to sum to the total weekly diverted flow volumes measured at the respective canal headgates by the CDWR plus the recorded volumes pumped from groundwater wells. Area-weighted adjustments are made to the measured flow diversions for cases where the canal command areas (collective set of fields serviced by a particular canal) lie partially outside the study regions. Interviews with ditch superintendents revealed that little, if any, water is run out the end of the canals as unused water.

Spatially varying rainfall data were obtained from the National Oceanic and Atmospheric Administration (NOAA) website (NOAA, 2008). NEXRAD Doppler radar records contain precipitation estimates on a 4.7 km square grid cell basis over variable time spans. Summing over a period corresponding to each model stress period generated a raster map used to estimate the precipitation on each cultivated field, fallow field, naturally-vegetated area, and riparian zone. Raster map precipitation estimates are compared against rain gage data collected by the National Weather Service and CoAgMet weather stations located in the LARV. Values > 0.70 were found for Pearson correlation (Helsel and Hirsch, 1992) between these two precipitation datasets. Considering the coarse spatial resolution of the Doppler radar data and the small spatial areas (on the order of 10^2 cm^2) measured for the weather station data, the correlation is

considered good. A final step partitions the precipitation into an estimated 70% effective (infiltrated) precipitation and 30% surface runoff and interception loss.

4.4.3.3 Well Pumping

The model is set up to account for the monthly pumping volume documented by CDWR in the historical records for all pumping wells (shown in Figure 4-1) including those used for municipal, industrial or commercial purposes. Every irrigation pumping well is assigned a number corresponding to the closest identified tract of irrigated land. Tracts are comprised of a group of fields belonging to (or managed by) a particular owner (or operator). By establishing this relationship, delivery of pumped water for irrigation is restricted to nearby fields. In general, pumping supplies roughly 5 percent of the total irrigation water.

4.4.3.4 Canal Seepage

Seepage from each of seven earthen canals in the USR and six in the DSR is simulated using the MODFLOW RIV package, with hydraulic heads specified along the canals based upon estimated data from the field. Weekly diverted flows to canals are reduced by an amount equivalent to the simulated canal seepage loss to ensure mass balance in the simulation. If the canal seepage losses associated with the total generated infiltrated irrigation for fields in a canal command area are found to differ by more than 1% from the total canal seepage simulated by the model, a new infiltrated irrigation pattern is generated using the updated seepage losses and the model is rerun, with the process repeated until convergence is achieved. Also, as explained further in Section 4.5.2 below, simulated canal seepage is compared to field data on canal seepage to perform manual adjustment of canal conductance values.

Groundwater inflows to the modeled region from the desert escarpment on the north and south sides of the LARV are assumed negligible relative to the large volumes of water seeping from the canals that typically form the boundaries along the escarpment. A no-flow boundary is

used where groundwater is assumed to flow essentially parallel to the boundary – for example, along the Colorado-Kansas state line that forms the eastern boundary of the DSR model and along the western boundary of the USR model. Tributaries to the Arkansas River form the eastern boundary of the USR and western boundary of the DSR and are represented by the RIV package. Groundwater exchange between the alluvium and the underlying thick sequence of shale is deemed negligible, an assumption adopted by previous studies (Konikow and Bredehoeft, 1974a; Person and Konikow, 1986).

4.4.3.5 Initial Values

Initial values of h are calculated by appending a steady-state stress period to the beginning of the simulation. The stresses specified in the steady-state simulation are calculated by averaging all stresses from the transient part of the simulation. This approach produces initial h values representing average conditions over the simulated period, which subsequently serve as the initial values for the transient simulation. In a similar fashion, the initial values of θ in the unsaturated zone for the transient period are determined during the steady-state stress period.

4.5 MODEL CALIBRATION PROCEDURE

4.5.1 Automated Calibration

The groundwater models for the two study regions are calibrated using a combination of automated and manual procedures (Carrera et al., 2005; Poeter et al., 2005; Tiedeman and Hill, 2007). The automated parameter estimation software codes UCODE (Poeter et al., 2005) and PEST (Doherty, 2002) are employed to minimize the residuals between selected simulated and observed variables. The need to keep the total number of estimated parameters (e.g., Section 4.4.2.1) to a minimum due to limited parallel processing resources and a familiarity with UCODE software initially motivated its selection for executing the automated parameter

estimation. Attempts to achieve better calibrated fits, with particular focus on simulated groundwater return flows, were made using a generously supplemented set of pilot points coupled with the regularization techniques available with the PEST suite of software (Doherty, 2002). Anticipated improvements in the objective function are achieved to a varied extent and are discussed in more detail in Section 4.5.1.4 below. The use of both UCODE and PEST in sequential fashion is not meant to imply superiority of one over the other.

Observations of h and groundwater return flows to the Arkansas River (estimated from mass balance calculations using measured and estimated flows in the stream and canal network) serve as the first two of a total of six variables for which the models of the study regions are calibrated to estimate selected parameter values. These two variables are the only ones used in the automated calibration procedures. The remaining four variables (listed and described in more detail in Section 4.5.2) were adjusted using manual calibration. The omission of some of the variables from automated calibration was driven by a desire to keep the search process efficient, to more directly control the influence that certain observation datasets might have on inordinately or inadequately adjusting the values of model parameters, and to avoid the introduction of significant non-linearity to the automated calibration procedures. Model calibration periods extend from the beginning of April, 1999 to the end of March, 2004 for the USR and from the beginning of April, 2002 to the end of March, 2006 for the DSR. The remainders of the simulation periods are reserved for model testing.

Both UCODE and PEST minimize the weighted sum of squared errors, commonly referred to as residuals, by adjusting parameter values for selected aquifer properties. The objective function minimized by UCODE that quantifies the simulated-observed misfit is defined as

$$S(\mathbf{b}) = \sum_{j=1}^{N_h} \omega_{h_j} [h_j - h'_j(\mathbf{b})]^2 + \sum_{k=1}^{N_Q} \omega_{Q_k} [Q_{GW_k} - Q'_{GW_k}(\mathbf{b})]^2 \quad (\text{Eq. 4-4})$$

where S is the value of the objective function, \mathbf{b} is a vector containing values of each of the parameters being estimated, N_h is the number of groundwater hydraulic head observations, N_Q is the number of groundwater return flow observations, h_j is the j th observed hydraulic head [L] being matched by the regression, $h'_j(\mathbf{b})$ is the simulated hydraulic head [L] that corresponds to the j th observed hydraulic head (a function of \mathbf{b}), Q_{GW_k} is the k th observed groundwater return flow [L^3T^{-1}] being matched by the regression, $Q'_{GW_k}(\mathbf{b})$ is the simulated groundwater flow [L^3T^{-1}] that corresponds to the k th observed return flow, ω_{h_j} is the weight for the j th hydraulic head observation, and ω_{Q_k} is the weight for the k th groundwater return flow observation. The weights in Equation 4-4 are equal to the inverse of the variance of the measurement (either h or Q_{GW}) resulting in a dimensionless residual (Hunt et al., 2006; Tiedeman and Hill, 2007). This approach allows for calibration targets with non-commensurate units (e.g. [L] for h compared to [L^3T^{-1}] for Q_{GW}) to be evaluated in a single objective function. Assignments of the weights proceeded based upon established guidelines (Hill, 1998), as described in more detail below. The parameters \mathbf{b} that are adjusted by the automated parameter estimation procedures include \bar{K}_H , and by extension the riverbed conductance as described in Section 4.4.2.1; saturated vertical hydraulic conductivity of the unsaturated zone, K_s ; and \bar{S}_y .

4.5.1.1 Measurement of Observed Hydraulic Head

Observations of shallow groundwater tables were collected routinely from approximately 100 and 118 monitoring wells distributed over the USR and DSR, respectively. Wells were cased with a 6.35 cm (2.5 in) screened PVC, with total depths ranging from 2.4 m (~8 ft) to 20 m

(~66 ft) below ground level and were sealed at the surface with bentonite clay to inhibit leakage of surface water around the well annulus. Measurements typically were taken weekly to bi-weekly during the irrigation season and monthly to bi-monthly during the off-season using a calibrated manual or electrical sounding tape. A total of 4,962 values of h_j were available for calibration in the USR and 5,528 values in the DSR. For testing, 3,742 values and 1,636 values were available for the USR and DSR, respectively.

4.5.1.2 Calculation of Weights for Groundwater Hydraulic Head Observations

Weights assigned to the observations h_j are based on numerous field-scale (~ 1 – 10 ha) studies performed in parallel with the regional-scale study. In regional-scale studies of the LARV, one monitoring well was installed in each monitored field and the water table depth was measured to estimate h_j within that field (Gates et al., 2012; Morway and Gates, 2012). In about two dozen intensively-monitored fields, however, numerous monitoring wells (up to 14 per field) were installed to gain insight into the spatial variability of h over the field scale. Using data from these intensively-monitored fields, nearly 7,000 residuals are computed by differencing each observed value of h within a given field for a particular sampling event from the average value of h computed for that field and sampling event. Pooling the residuals revealed that the spatial variability of h within a single field (average field size was roughly twice the model grid-cell size) for a given sampling event could be described by a standard deviation of approximately 0.51 m. Assessment of temporal variability associated with h observations was made by analyzing a number of time-series of h measured at one-hour intervals with pressure transducers and dataloggers. Each hourly observation of h in a given well was subtracted from the weekly average value of h , resulting in nearly 40,000 residuals with a standard deviation of about 0.12 m. The UCODE ‘standard deviation’ statistic (Poeter et al., 2005, pg. 83) then is used to

calculate a weight reflective of uncertainty in estimates of h_j , namely $\omega_{h_j} = \sqrt{0.51^2 + 0.12^2} = 0.53$ m (note that UCODE squares the supplied standard deviation, resulting in a variance as noted above). The same weight is applied to all head observations. PEST uses a slightly different expression for the weights. The weights in PEST are the square roots of the weights in Equation 4-4.

4.5.1.3 Measurement of Groundwater Return Flow

Records of gaged flows diverted from the river into canals were obtained from the Colorado Division of Water Resources. In both study regions, only two tributaries to the river were gaged, resulting in a need to estimate a number of other surface return flows which, in addition to ungaged tributary flows, included irrigation tail-water and precipitation-runoff for each week of the simulation. Storage changes in the river are estimated from measured stage changes and from surveyed cross-sections. Return flow residuals used to account for unmeasured inflows, including groundwater exchange with the mainstem Arkansas River, are calculated as

$$Q_{UR_k} = Q_{IR_k} - Q_{OR_k} + \sum_{l=1}^{N_T} Q_{T_{kl}} - \sum_{m=1}^{N_C} Q_{C_{km}} + \Delta S_{R_k} \quad (\text{Eq. 4-5})$$

where Q_{UR_k} is the total unaccounted-for return flow [L^3T^{-1}] to the river during the k th week and can be either a net gain (+) or loss (-); Q_{IR_k} and Q_{OR_k} are the k th flows [L^3T^{-1}] entering and exiting (as measured by gaging stations) at the upstream and downstream ends of the river reach, respectively; $Q_{T_{kl}}$ is the k th flow [L^3T^{-1}] measured in the l th gaged tributary along the river reach; N_T is the number of gaged tributaries along the river reach; $Q_{C_{km}}$ is the k th flow [L^3T^{-1}] measured in the m th gaged canal that diverts from the river along the reach; N_C is the number of gaged canals along the river reach; and ΔS_{R_k} is the k th rate of change in the volume of water

stored [L^3T^{-1}] in the Arkansas River associated with measured changes in river stage. Because Q_{UR_k} includes unmeasured tributary flow and other surface return flows, in addition to groundwater return flow to the river and tributaries, then $Q_{GW_k} \leq Q_{UR_k}$. Values of Q_{UR_k} computed with Equation 4-5 are reduced by estimates of unmeasured surface flows to obtain values of Q_{GW_k} for use in Equation 4-4 within UCODE and PEST.

4.5.1.4 Calculation of Weights for Groundwater Return Flow Observations

Groundwater return flow targets are weighted in Equation 4-4 using the procedure described in Poeter et al. (2005) and Hill and Tiedeman (2007). Gaged flow records (maintained by either the USGS or the CDWR) in the modeled regions typically were of ‘good’ or ‘fair’ quality (USGS, 2008) indicating that about 95-percent of measured daily flows were within ± 10 and ± 15 percent, respectively, of the true value. It was estimated that there was a 90-percent probability that the true value of ΔS_{R_k} was within $\pm 20\%$ of the value estimated using stage and river hydraulic geometry data. Following the steps outlined in Hill and Tiedeman (2007, pgs. 297-298), weekly calculated flow observations were weighted by first calculating a CV value for every week and then ensuring that the proper settings in UCODE were specified (Poeter et al., 2005, pg. 83). The resulting CV values used for calculating ω_{Q_k} assigned to the weekly groundwater return flow targets ranged between 0.06 and 57.80 [$L^3T^{-1}(L^3T^{-1})^{-1}$] with an average value of 0.88 in the USR, and between 0.05 and 6.09 [$L^3T^{-1}(L^3T^{-1})^{-1}$] with an average value of 0.20 in the DSR. This weighting scheme led to roughly a 75% contribution to the final objective function from comparison to h_j values and 25% contribution from comparison to Q_{GW_k} values in the USR and 80% contribution from comparison to h_j values and 20% contribution from comparison to Q_{GW_k} values in the DSR, respectively.

The parameters listed above are estimated by solving Equation 4-4 in UCODE, in conjunction with stratigraphic data as described in Section 4.4.2.1 above. In an effort to achieve a better match between values of $Q'_{GW_k}(\mathbf{b})$ and Q_{GW_k} , Equation 4-4 is re-solved to refine the calibration of \bar{K}_H values by using a gridded pilot-point approach in PEST that is independent of stratigraphic record observations. Initial values of \bar{K}_H in this technique are set to the final values that are determined by UCODE. Figure 4-3 shows the final estimated \bar{K}_H and \bar{S}_y arrays for layer 1 of the USR and DSR models. Additionally, Figure 4-3 highlights that the exploratory borehole locations used by UCODE (“+” symbols) to estimate the \bar{K}_H and \bar{S}_y arrays do not coincide with the alternative set of gridded pilot points used by PEST (green triangles) in the follow-up automated calibration run, as well as shows the location of the aquifer pumping tests conducted by the USGS (Wilson et al, 1965).

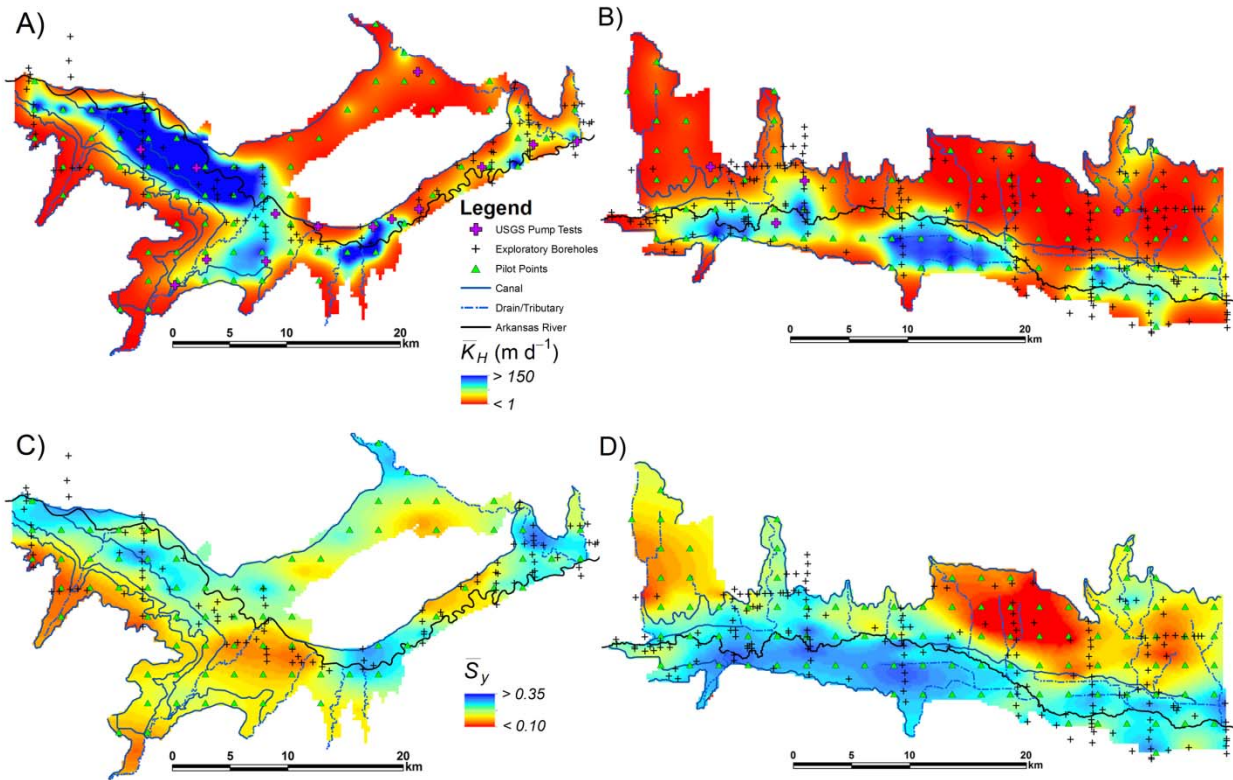


Figure 4-3. Final estimated \bar{K}_H for layer 1 of the (A) USR and (B) DSR and the final estimated \bar{S}_y for layer 1 of the (C) USR and (D) DSR.

The use of PEST results in a 2% lowering of the value of the objective function, S , below that obtained by UCODE in the USR and about a 25% reduction in the value in the DSR. The final \bar{K}_H values estimated by PEST are well-correlated with the UCODE results. In the USR, Pearson correlation values between the post-UCODE and post-PEST \bar{K}_H fields in layers 1 and 2 are 0.67 and 0.78, respectively. In the DSR, the correlations in layers 1 and 2 are 0.89 and 0.74, respectively. Considering that the PEST search algorithm explores the parameter space unconstrained by stratigraphic observations, yet finishes with a spatial pattern similar to

UCODE, suggests that the original approach to estimating \bar{K}_H values constrained by information from stratigraphic surveys works relatively well as compared to PEST.

4.5.2 Manual Calibration

Manual calibration is based upon the following observations: (1) measurements of canal seepage used to ensure that simulated values fall within the observed range (Susfalk et al., 2008; Shanafield et al., 2010; Martin, 2013), (2) total actual ET calculated by the RESET model using satellite imagery (Elhaddad and Garcia, 2008), (3) field estimates of groundwater ET (Niemann et al., 2011), and (4) estimates of recharge to infiltration ratios (Gates et al., 2012). Guided by these information categories (observation groups), manual adjustments are made to the values of canal conductance, potential ET, extinction depth, and a multiplier applied to the K_s array. Because fewer target values are available for the manual-calibration variables, parameter adjustment to match target values requires discriminating judgment about what is physically reasonable based upon experience with conditions in the LARV. In some instances, recommended values from the literature are used (e.g., Brooks-Corey ε). The approach for adjusting potential ET to achieve a close match between simulated and actual ET from satellite imagery assumes that the resulting simulated q_{ET} reflects the impact of current soil water salinity levels on potential ET. In both models, manual adjustment of potential ET was made by a maximum amount of 25%. Automated parameter estimation procedures were rerun after each round of manual adjustments to ensure that the “best” possible fit between simulated and observed h and Q_{GW_k} were maintained. The impact of manual adjustments on h and Q_{GW_k} typically were small, as were the subsequent updates to parameters subject to automated adjustment.

4.5.3 Calibration and Testing Performance Measures

For the calibration periods, values of root mean square error for groundwater head ($RMSE_h$) (Boyle et al., 2000) are 1.92 m and 1.71 m for the USR and DSR, respectively, and are 2.51 m and 1.72 m, respectively, during the testing period for measured water table depths that spanned between 0.01 m and 13.48 m for the USR and between 0.05 m and 19.82 m for the DSR. Given that the locations of the observed hydraulic head, h_j , are well-distributed over the modeled regions (Figure 4-1) and that the average of the residuals, $h'_j(\mathbf{b}) - h_j$, for the USR and DSR are -0.18 m and -0.41 m during the calibration period and -0.12 m and 0.03 m during the testing period (Figure 4-4), the model is considered to simulate well the groundwater hydraulic

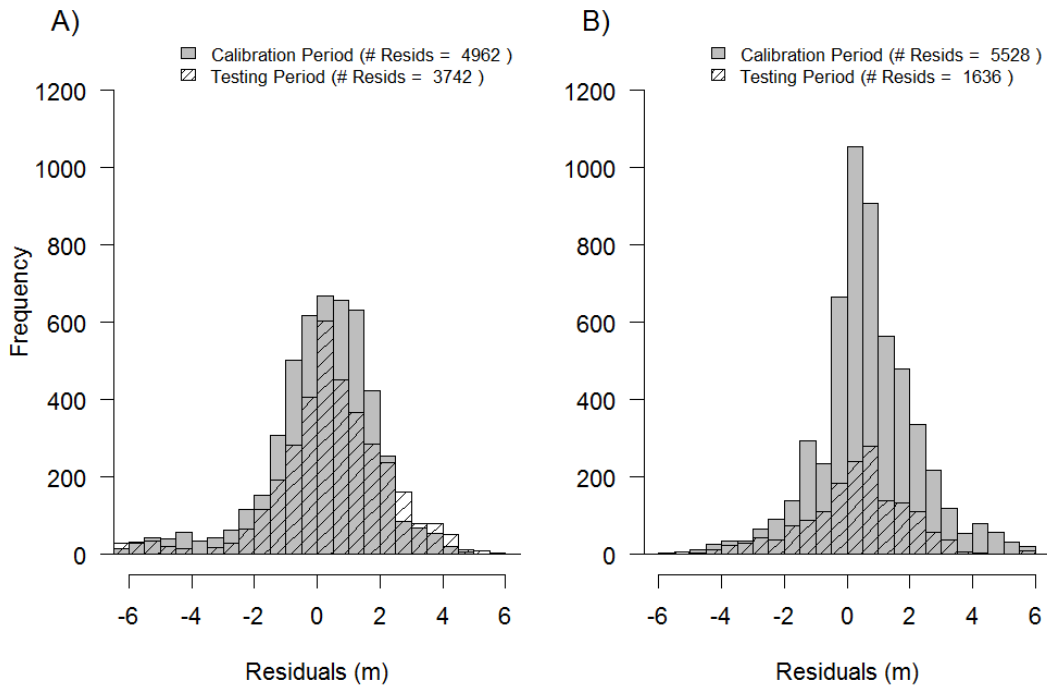


Figure 4-4. Residuals of simulated groundwater hydraulic head for (A) the USR and (B) the DSR.

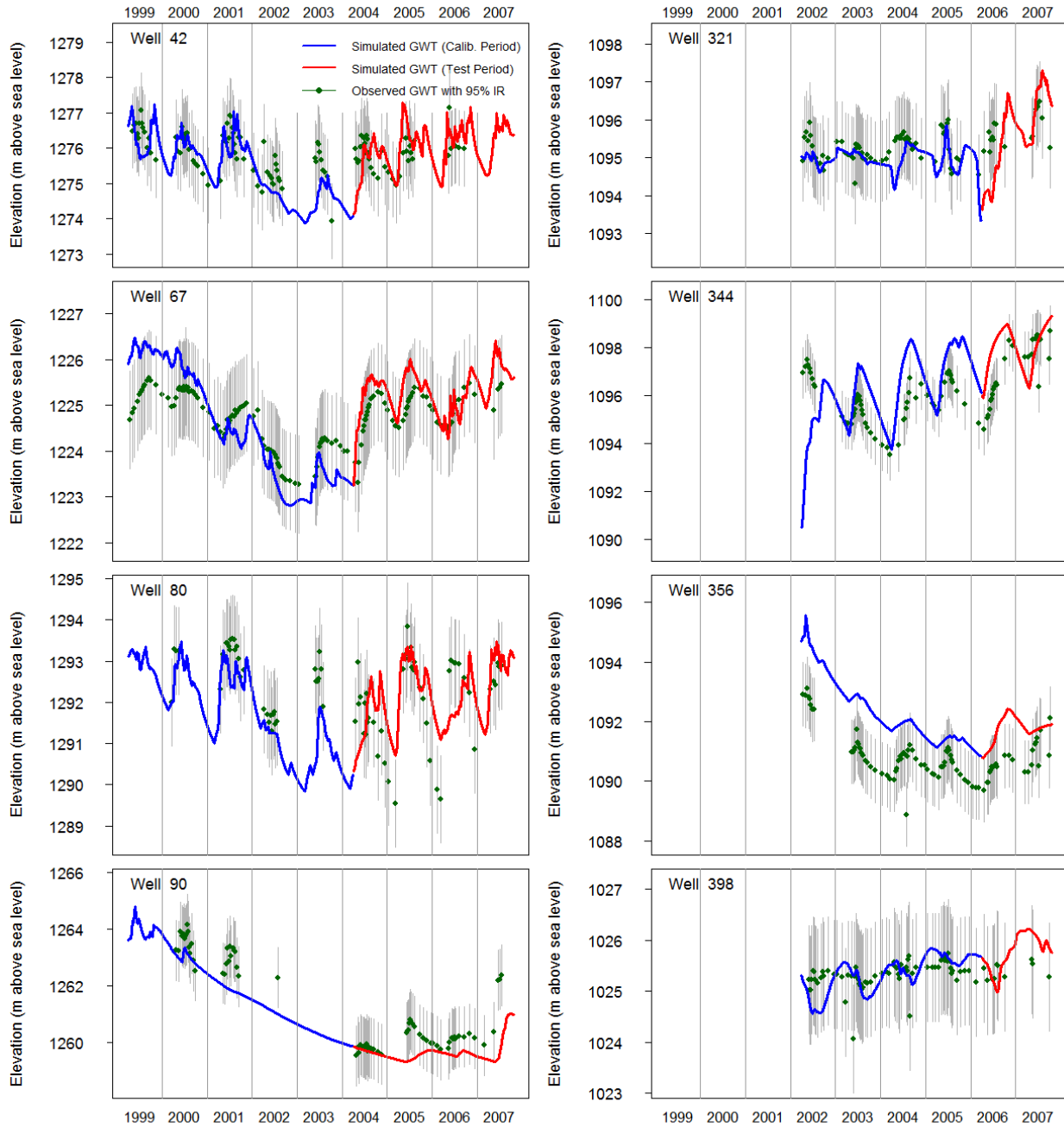


Figure 4-5. Model performance in predicted groundwater table (GWT) elevation in cells containing monitoring wells at four locations in the USR [wells 42, 67, 80, and 90 (Figure 4-1A)] and four locations in the DSR [wells 321, 344, 356, and 398 (Figure 4-1B)]. Grey bars shown on observations indicate the upper and lower limits of the 95% inter-percentile range (IR), accounting for spatial and temporal variability as discussed in Section 4.5.1.2.

head. Figure 4-5 demonstrates model performance by comparing simulated water table elevation to observed water table elevation at four locations spread throughout each of the two study

regions. Results indicate that the models of the USR and DSR generally capture multi-year and within-year trends in hydraulic head.

The root mean square error for groundwater return flow ($RMSE_Q$) values are $3.8e6$ and $8.7e5 \text{ m}^3 \text{ wk}^{-1}$ ($3,100$ and $700 \text{ ac}\cdot\text{ft wk}^{-1}$) for the USR and DSR, respectively, during the calibration period. For the testing period, $RMSE_Q$ values are $3.6e6$ and $1.1e6 \text{ m}^3 \text{ wk}^{-1}$ ($2,900$ and $900 \text{ ac}\cdot\text{ft wk}^{-1}$) in the USR and DSR, respectively. Weekly groundwater return flows over the total modeled period are estimated to range between $-24.7e6 \text{ m}^3 \text{ wk}^{-1}$ and $21.6e6 \text{ m}^3 \text{ wk}^{-1}$ ($-20,000 \text{ ac}\cdot\text{ft wk}^{-1}$ and $17,500 \text{ ac}\cdot\text{ft wk}^{-1}$) in the USR and between $-4.3e6 \text{ m}^3 \text{ wk}^{-1}$ and $3.2e6 \text{ m}^3 \text{ wk}^{-1}$ ($-3,500 \text{ ac}\cdot\text{ft wk}^{-1}$ and $2,600 \text{ ac}\cdot\text{ft wk}^{-1}$) in the DSR, where a negative groundwater return flow indicates a net loss of water from the river to the alluvial aquifer. Due to the relatively transmissive material located along the river, it is not unrealistic for pumping wells near the river to induce an overall net loss from the river during certain periods, which was one of the motivating factors in Kansas vs Colorado lawsuit (U.S. Supreme Court, 1995) regarding the Arkansas River Compact. Figure 4-6 shows the variability and estimated uncertainty in values of Q_{GW_k} along with model predictions of Q'_{GW_k} over the calibration and testing periods. Uncertainty is indicated by the central 95% inter-percentile range between the 2.5th percentile and 97.5th percentile estimates, derived from analysis of measurement error and spatial and temporal variability associated with the terms in Equation 4-5. Frequency histograms of the values of the residuals, $Q'_{GW_k}(\mathbf{b}) - Q_{GW_k}$, also are depicted (Figure 4-6B and Figure 4-6D). Average groundwater return flow residuals are $7.1e5$ and $-3.0e5 \text{ m}^3 \text{ wk}^{-1}$ (580 and $-240 \text{ ac}\cdot\text{ft wk}^{-1}$) for the USR and DSR, respectively, during the calibration period and are $-2.4e5$ and $-1.3e3 \text{ m}^3$

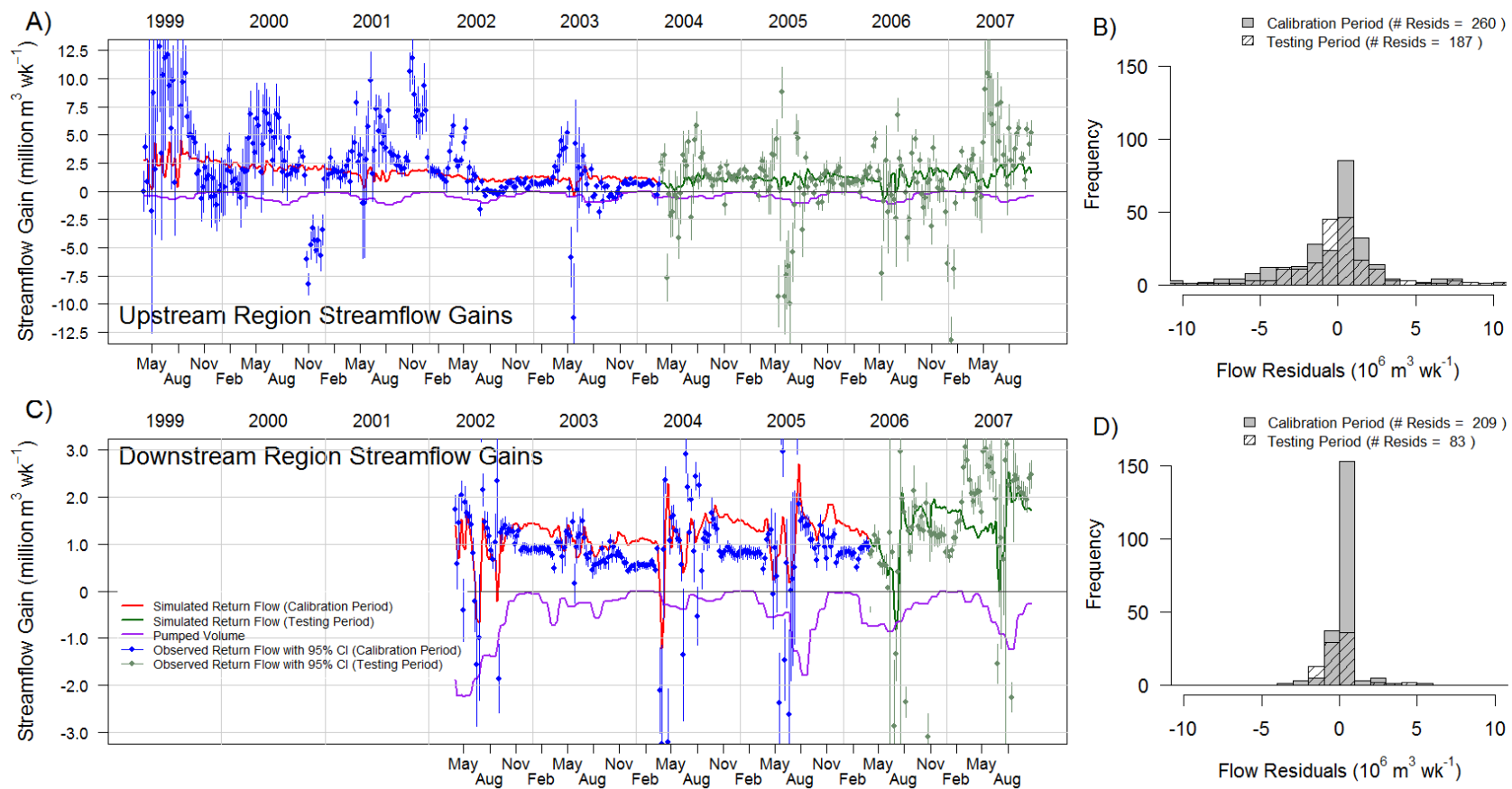


Figure 4-6. Groundwater return flow time series for (A) the USR and (C) the DSR (including a plot of volume pumped from groundwater wells), along with residuals of simulated groundwater return flow for (B) the USR and (D) the DSR.

wk^{-1} (-190 and -1 $\text{ac}\cdot\text{ft}\ \text{wk}^{-1}$) for the USR and DSR during the testing period. The average value of $\sum_{m=1}^{N_c} Q_{C_{k_m}}$ during the growing season over the modeled period is $2.1\text{e}6$ ($1,700\ \text{ac}\cdot\text{ft}\ \text{wk}^{-1}$) in the USR and $1.5\text{e}6\ \text{m}^3\ \text{wk}^{-1}$ ($1,200\ \text{ac}\cdot\text{ft}\ \text{wk}^{-1}$) in the DSR.

Large and fluctuating diverted flows to canals, errors in the historical cropping patterns that guided simulated values of irrigation application, significant variability in irrigation practices among neighboring farms in the LARV, and the wide range of irrigation return flow time lags (derived in part from the variability of the thickness and porous media types of the unsaturated and saturated zones), give cause to expect large variability in return flow. Moreover, in the USR, values of return flow to the river from tail-water runoff were estimated using field observations collected during 2004-2007, years which were markedly drier than the early years of the modeled period, 1999-2001. Because of significantly wetter hydrologic conditions in 1999-2001, the estimated return from tail-water runoff is likely under-predicted, suggesting that the degree of misfit indicated in Figure 4-6 may also be a result of errors in the observed values in addition to errors in the simulated values. Errors associated with the estimated tail-water runoff amounts are manifested not only in the magnitude of the return flows targeted by the automated calibration software, but also would interfere with the simulated values of recharge to the water table; that is, too much water would have been specified as infiltration in the UZF1 package, leading to an over-prediction of recharge. Finally, the reliability of the *observations* is compromised further if significant volumes of water flow into the study areas through ungaged tributaries during intense rain events surrounding the modeled regions or if a portion of water diverted into irrigation canals is eventually released into ungaged tributaries of the Arkansas

River. In such instances, much of the unaccounted-for flow, Q_{UR_k} , would be attributable to surface water return flow, not to groundwater, Q_{GW_k} .

4.6 SIMULATION OF BASELINE GROUNDWATER CONDITIONS

The calibrated groundwater models were applied first to simulate groundwater flow conditions in the alluvial aquifer system over the periods 1999–2007 in the USR and 2002–2007 in the DSR. These conditions establish a comparative baseline for use in evaluating the likely impact of alternative management scenarios in subsequent simulations.

4.6.1 Baseline Groundwater Recharge

Simulated irrigation-season recharge to groundwater under baseline conditions, averaged over all years in the simulation period, is illustrated in the contour plots of Figure 4-7A and Figure 4-7B for the USR and DSR, respectively. Average recharge rates range from near zero to approximately 10 mm/day in both regions. The average recharge rates over the simulation periods are 1.1 and 0.9 mm/day across the USR and DSR regions, respectively. On a year-to-year basis, the ratio of recharge to infiltrated water (irrigation and precipitation) during the irrigation season ranges from 0.30 to 0.54 in the USR and 0.31 to 0.42 in the DSR.

4.6.2 Baseline Water Table Depth and Associated Waterlogging

Researchers have noted that crop yields begin to decline due to waterlogging in silt loam and loamy sand soils when water tables are maintained at average D_{wt} values less than about 3 m. Kahlow and Azam (2002) estimate crop yield losses associated with increasing acuteness of waterlogging for wheat, sugarcane, and cotton using D_{wt} bins of < 1 m, 1 – 2 m, and 2 – 3 m. In a separate effort, Kahlow and Ashraf (2005) considered D_{wt} values ranging from 0.5 m to 3 m to evaluate the tradeoffs between diminished yields

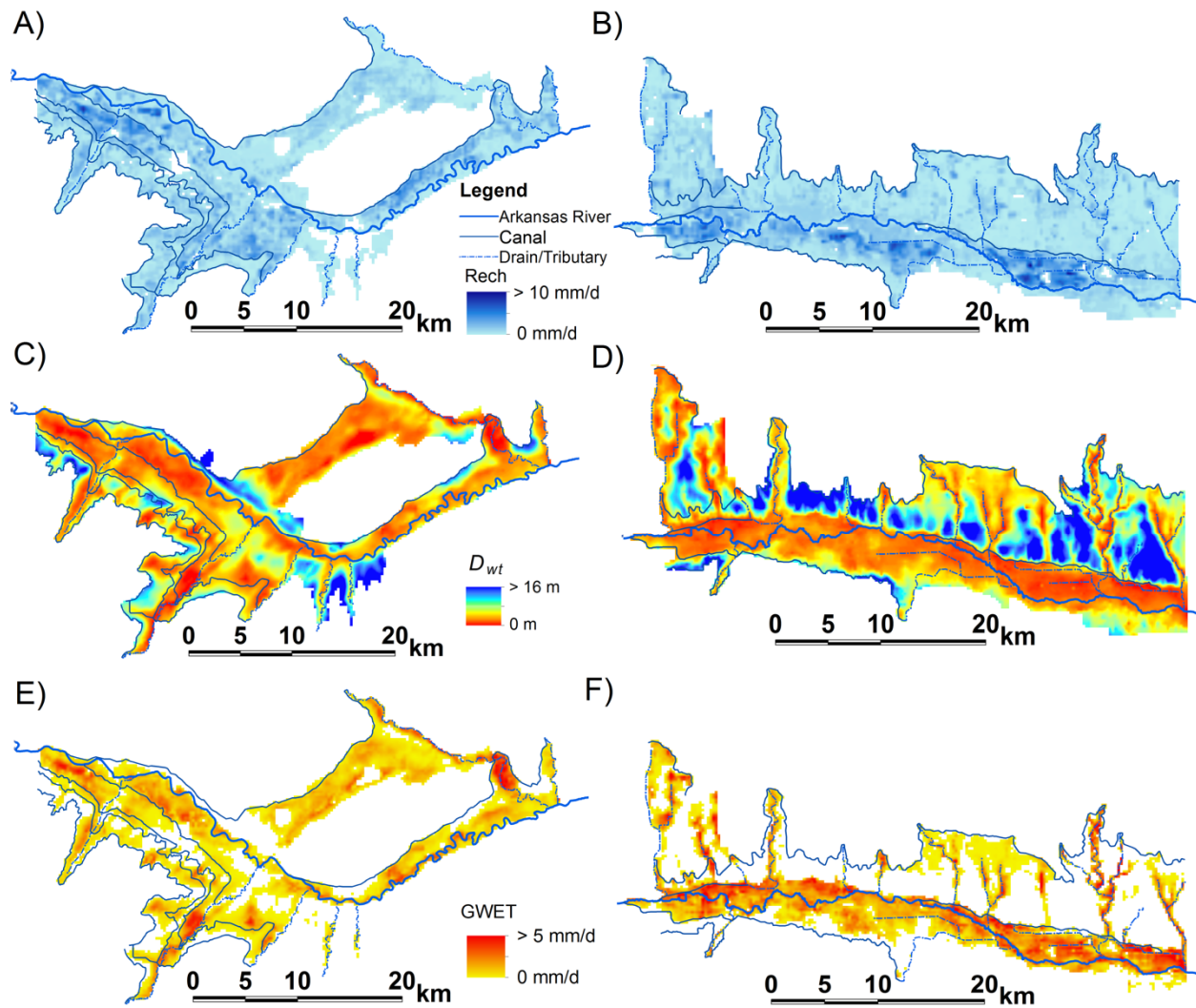


Figure 4-7. Contour plots of baseline model simulation results for average irrigation season recharge to groundwater over the simulated periods for the (A) USR and (B) DSR, average irrigation season D_{wt} for the (C) USR and (D) DSR, and average irrigation season groundwater upflux to ET (GWET) for the (E) USR and (F) DSR.

resulting from waterlogging and the benefits of upflux from the water table contributing to ET for a variety of crops. Nosetto et al. (2009) and Heuvelmans (2010) used similar threshold values of D_{wt} to assess the health of cultivated lands. Similar ‘binning’ is used herein to quantify the extent and severity of waterlogging present in the LARV.

The baseline value of D_{wt} (Figure 4-7C and Figure 4-7D) averaged over the irrigation seasons within the respective simulation periods varies substantially over the modeled regions, but tends to be smaller both in the low-lying lands adjacent to the tributaries and river and near the earthen canals where seepage occurs. A number of region-specific trends are evident in Figure 4-8 for baseline conditions (“Base”). For example, in the USR in 1999, more than half of the cultivated lands are subject to the threat of waterlogging ($D_{wt} < 2$ m). During the course of the next several years, the increasingly dry hydrologic conditions result in less irrigation and a consequent increase in D_{wt} . Over 2004–2007 conditions slowly return to higher water table elevations. A much different trend takes place in the DSR, where over 2002–2007 the areal extent of cultivated land with varying degrees of waterlogging (i.e. $D_{wt} < 1$ m, 1 m $< D_{wt} < 2$ m, etc.) remains relatively unchanged from year to year under the baseline conditions. Monitoring for D_{wt} in the DSR commenced in 2002 after the relatively wet period that extended from 1999–2001. Thus, the DSR simulation spans a relatively dry period that may have followed a substantial increase in D_{wt} . Furthermore, a deeper water table persists across the DSR compared to the USR, thereby tempering the response of D_{wt} to ambient hydrologic conditions. Even so, significant tracts of land in both regions maintain an average $D_{wt} < 2$ m. For example, in the USR, more than 50% of the total cultivated land has $D_{wt} < 2$ m in 1999, dropping to as little as 6% in 2002, but averaging 19% over the entire simulation period (Figure 4-8A). In the DSR, the average spatial extent of cultivated lands with a $D_{wt} < 2$ m during the course of the simulated period is about 17% (Figure 4-8B). Restricting the analysis to only the cropped portion of the cultivated lands (i.e. omitting fallow fields), it is found that 24% and 21% of the cropped area in the USR and DSR, respectively, have $D_{wt} < 2$ m. The annual value of D_{wt} averaged over the

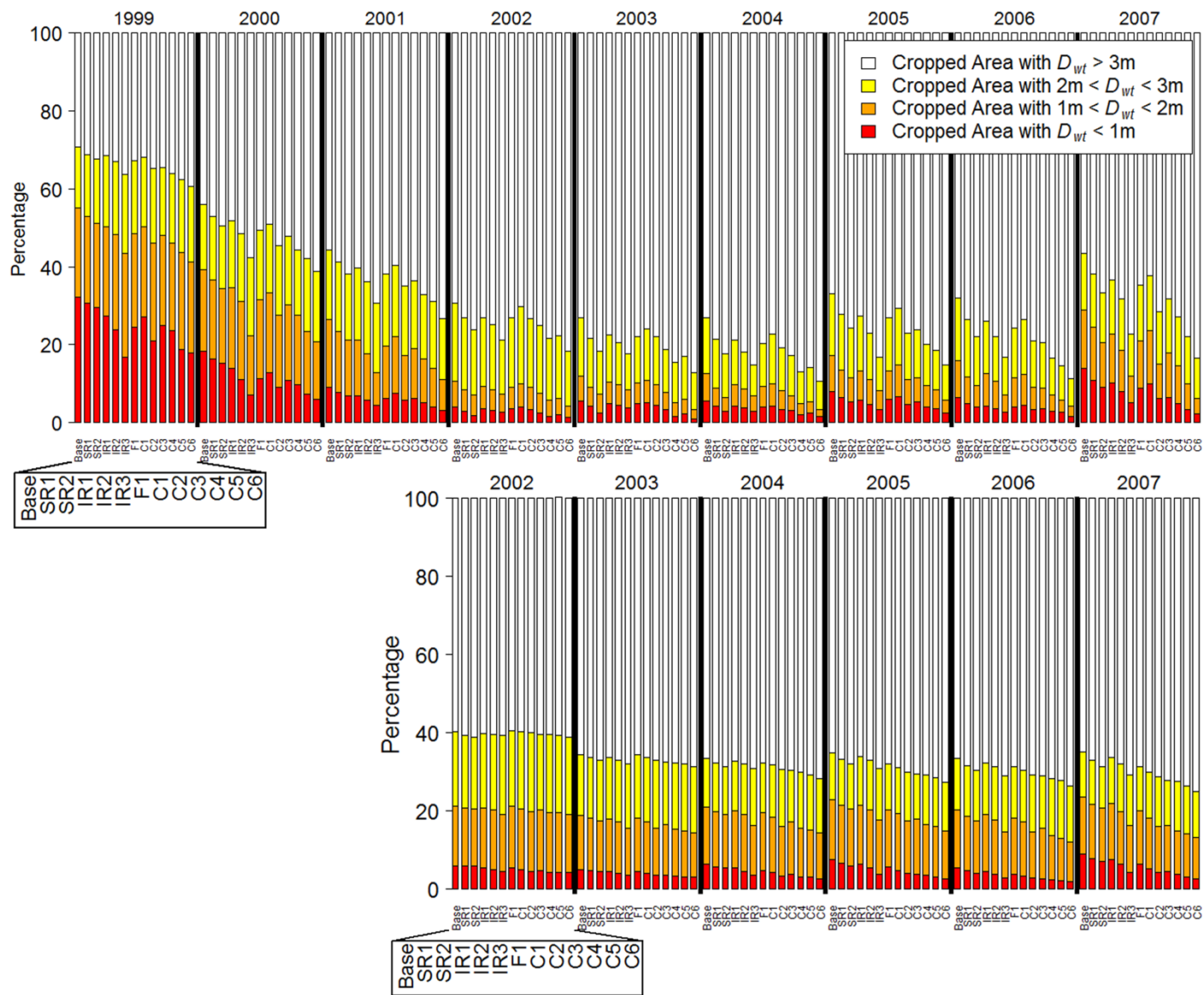


Figure 4-8. The impact of alternative management interventions on D_{wt} in (A) the USR and (B) the DSR.

entire USR varies between approximately 3 m and 5.9 m over the simulation period while in the DSR the annual mean D_{wt} varies between just under 6 m to slightly more than 7 m. Although the D_{wt} is on the average greater downstream, the spatial extent of land underlain by a very shallow water table, $D_{wt} < 1$ m, also is larger in the DSR. The prevalence of vicinities with acute waterlogging conditions ($D_{wt} < 1$ m) in the DSR as compared to the USR is likely responsible, at least in part, for the higher soil water salinity in the DSR that was reported by Morway and Gates (2012). The higher water tables further contribute to greater non-beneficial groundwater consumptive use losses in the DSR.

4.6.3 Baseline Groundwater Upflux and Non-beneficial Consumptive Use

The total volume of groundwater ET to non-beneficial consumption under fallow and naturally-vegetated land for the baseline conditions over the entire simulated period was 261e6 m³ (212,000 ac·ft) and 205e6 m³ (167,000 ac·ft) for the USR and DSR, respectively (Figure 4-7E, Figure 4-7F, Figure 4-9, and Figure 4-10). The percentage of total ET provided by groundwater under cropped land is 22% and 25% in the USR and DSR, respectively. This is lower than what is found under naturally-vegetated land, where the percentage of total ET provided by groundwater is 51% and 49% in the USR and DSR, respectively, due largely to the fact that groundwater, not irrigation water, is relied upon to meet ET requirements in naturally-vegetated areas.

The largest amounts of groundwater ET occurred under cropped lands (with the exception of 2002 and 2003 in the USR). However, total groundwater ET for the overlapping simulation period for the two models (i.e. 2002–2007) is greater in the DSR, despite a greater average D_{wt} . This is due in part to less irrigation in the DSR due to junior surface water rights,

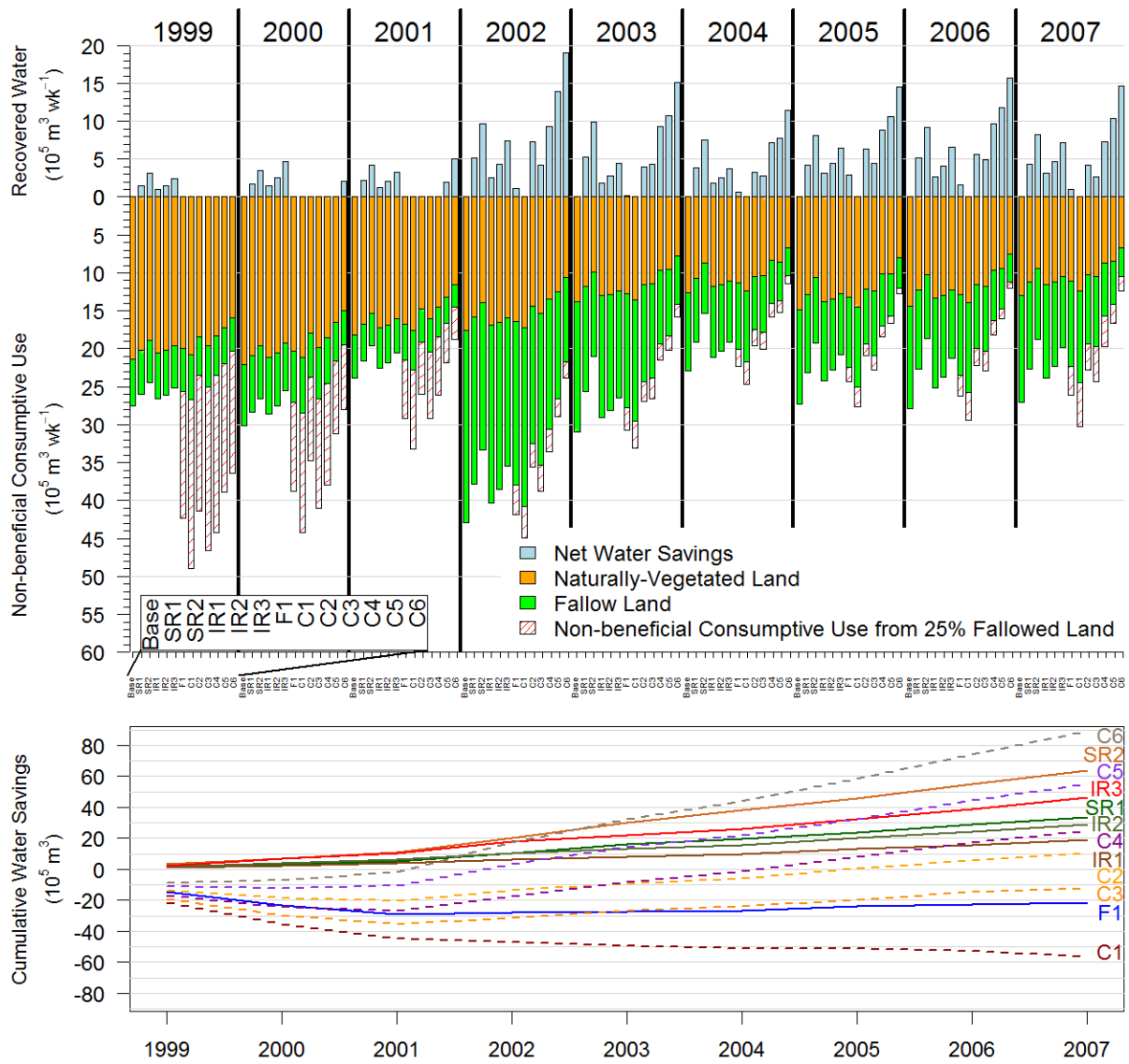


Figure 4-9. The potential for recovering non-beneficial consumptive use in the USR under a variety of alternative management interventions shown as (A) annual and (B) cumulative savings.

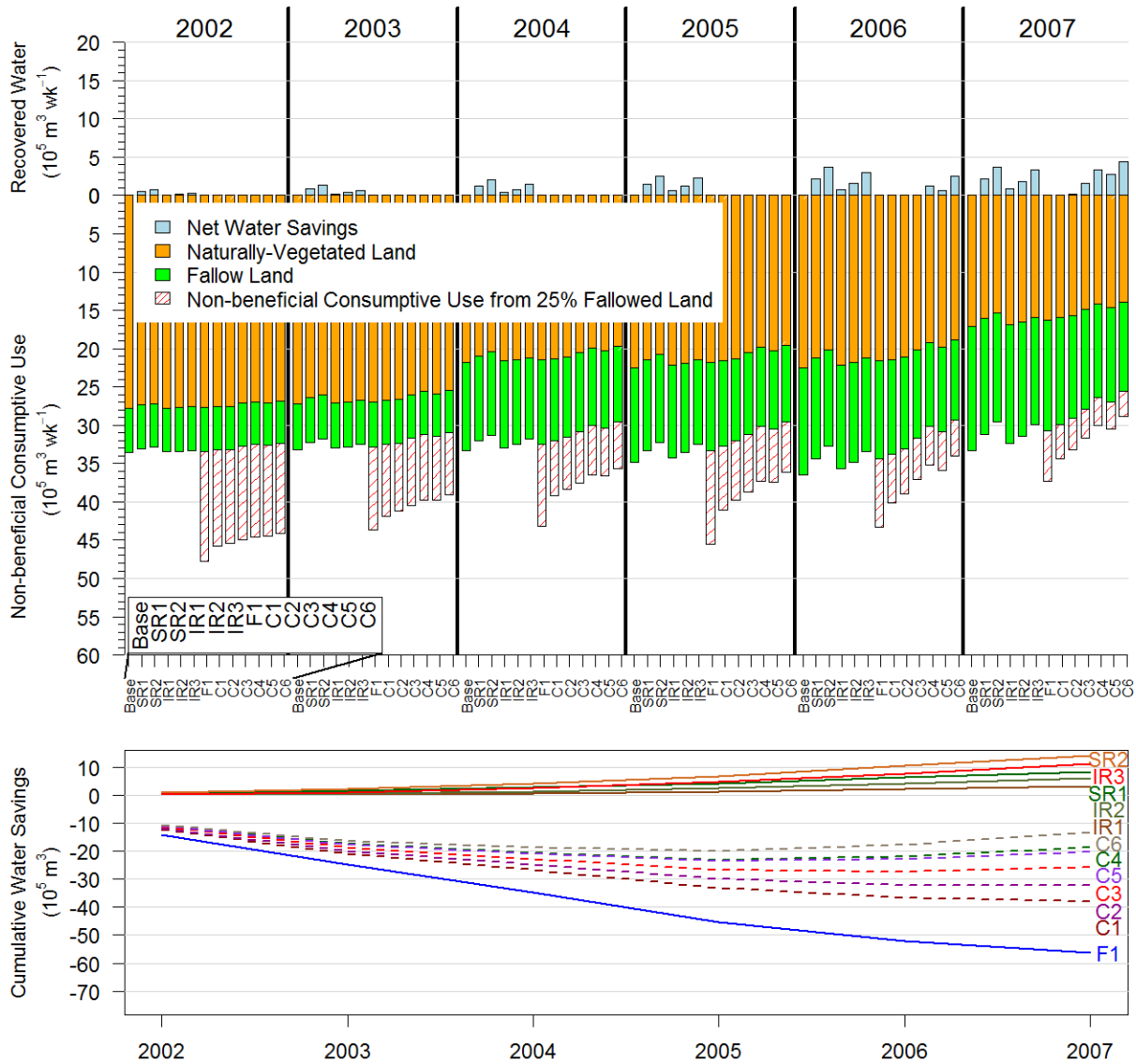


Figure 4-10. The potential for recovering non-beneficial consumptive use in the DSR under a variety of alternative management interventions shown as (A) annual and (B) cumulative savings.

leading to increased reliance on groundwater for growing crops. Also, although the average D_{wt} is greater in the DSR, the spatial extent of lands with $D_{wt} < 1$ m is greater, leading to the larger groundwater upflux to ET.

In an effort to estimate the total groundwater ET occurring over the entire LARV, simulated groundwater ET results from the two study areas are extrapolated to the remaining

fallow and naturally-vegetated lands of the entire LARV (using 2003 land survey data). The resulting estimate of $8 \times 10^8 \text{ m}^3$ (650,000 ac·ft) of water lost to non-beneficial consumptive use from the nearly 200,000-ha (500,000-ac) expanse of the LARV between 1 April, 1999 and 31 October, 2007 exceeds by about $6.2 \times 10^7 \text{ m}^3$ (50,000 ac·ft) the volume required to fill to capacity John Martin Reservoir, which is located between the two study regions,. Demonstrating the magnitude of the total non-beneficial groundwater consumptive use highlights the potential in considering the recovery of a portion of this non-beneficial loss through management interventions aimed at lowering the water table.

4.6.4 Baseline Groundwater Return Flow to the River

The average simulated groundwater return flow to the Arkansas River in the USR region is $1.3 \times 10^6 \text{ m}^3 \text{ wk}^{-1}$ (1,000 ac·ft wk^{-1}) over the entire simulation period (1999-2007). Considering only 2002-2007, the portion of the simulation period common to both study regions, the comparative average simulated groundwater return flows are $1.0 \times 10^6 \text{ m}^3 \text{ wk}^{-1}$ (850 ac·ft wk^{-1}) and $0.8 \times 10^6 \text{ m}^3 \text{ wk}^{-1}$ (620 ac·ft wk^{-1}) for the USR and DSR, respectively (Figure 4-6). These return flows represent 15% and 11%, respectively, of the total infiltrated irrigation and precipitation volume in the two regions over the same period. Variability of the weekly groundwater return flow over the full modeled periods is considerable: the CV expressed as a percentage is 47% in the USR and 60% in the DSR. Net groundwater return flows are occasionally negative, indicating a net loss of river water to the alluvial aquifer. However, this is predicted to happen only during the irrigation season when groundwater pumping in support of irrigation is highest.

4.7 INVESTIGATION OF IMPROVEMENT ALTERNATIVES

Shallow water tables that lead to waterlogging problems and water losses via non-beneficial upflux, along with competition from urban areas for limited irrigation water supplies,

can be addressed through a number of improvement strategies. These include improvements in water conveyance efficiency (e.g. lining or sealing earthen canals), enhanced irrigation application efficiency, and lease-fallowing arrangements, all of which are considered here for both the USR and the DSR. The calibrated models are used to estimate impacts of varying degrees and combinations of these alternatives on recharge to groundwater, D_{wt} , groundwater upflux to non-beneficial consumptive use, and return flows to the river.

4.7.1 Reduced Canal Seepage

Seepage from earthen irrigation canals in the LARV has been found to range between less than $0.01 \text{ m}^3 \text{ s}^{-1} \text{ km}^{-1}$ to $0.12 \text{ m}^3 \text{ s}^{-1} \text{ km}^{-1}$ (Susfalk et al, 2008; Martin, 2013) and provides a substantial source of recharge to shallow groundwater. Seepage reduction is possible through a suite of canal lining and sealing alternatives. Scenarios that investigated reduced canal seepage were created by lowering the conductance term associated with canal segments to reduce simulated seepage rates in comparison to baseline conditions. Simulated seepage reduction scenarios span from moderately aggressive (SR1) to very aggressive (SR2), where higher aggressiveness indicates a higher level of capital and labor investment necessary for implementation.

4.7.2 Reduced Irrigation

Application of irrigation water to fill the soil water deficit and to supply water for ET usually results in some deep percolation below the crop root zone, part of which recharges the underlying groundwater. In salinity-affected areas, like the LARV, a minimum amount of deep percolation is necessary to adequately leach the soil profile of excess salt. However, when deep percolation is excessive, substantial groundwater recharge can occur, contributing to a shallow water table. Deep percolation can be reduced by adopting improved surface irrigation methods (e.g. land leveling, adjusting applied flow rates using surge irrigation or altered irrigation sets,

reducing the length of the field along the irrigation stream) or by converting to sprinkler or drip irrigation methods. Thus, if the amount of water applied to irrigated fields is reduced, then the resulting groundwater recharge subsequently will be reduced, leading to a drop in harmfully high water tables.

Scenarios that reduce irrigation applications too much may also reduce leaching and thereby exacerbate salinization. They also could fail to meet the crop water requirement, resulting in diminished crop yields. Alternative management schemes ideally would find a balanced solution which provides reduced irrigation that maintains adequate leaching and provides enough water yet lowers the water table and reduces dissolved salts carried by groundwater upflux into the crop root zone. If struck, this balance would result in improved crop yields through increasing soil aeration and lowering the crop-stressing osmotic potential caused by high salt concentrations. The improved yields come at the expense of increased consumptive use. As this study does not include salt transport modeling, these competing factors are not considered.

Scenarios of reduced irrigation application were modeled by lowering applied amounts on cropped fields. Simulated scenarios span from moderately aggressive (IR1) to very aggressive (IR3). Irrigation application reductions in excess of 40% would fail to supply the crop with adequate water and therefore were omitted from the analysis. Irrigation reductions were made on fields receiving an allotment of canal water. Irrigation applications supplied by pumped groundwater were small relative to surface water irrigations and were not altered in the alternative management scenarios.

4.7.3 Lease Following

To help relieve the pressure placed on rural communities to sell their senior water rights to expanding urban markets, the Arkansas Valley Super Ditch was devised (McMahon and

Smith, 2011). Rather than a permanent transfer of water out of agriculture, farmers can temporarily lease their rights (typically in dry years) within the Super Ditch framework while retaining the water rights for future growing seasons. Implications for the model include converting some fraction of the cropped lands to fallow during each irrigation season.

A 25% lease-fallowing scenario was considered in the current effort. Under this scenario the total irrigated land area was reduced by 25% from baseline conditions in any given year. Implementation of the lease-fallowing scenario impacted two important model inputs: applied irrigation was removed from fallowed fields, and potential ET arrays were reformed to reflect the absence of a crop demand. Fields selected for rotational fallowing did not include those that received pumped groundwater during the simulated period. The fallowing algorithm followed a crop hierarchy that first randomly converted corn fields, then hayfields (grass), and finally alfalfa fields (in that order) to fallow. Small deviations from the specified crop hierarchy were allowed in order to achieve the 25% fallowed land area target.

4.7.4 Combination Scenarios

Combinations of improvement alternatives also were investigated. Scenarios C1 and C2 combine the lease fallowing option with two different levels of reduced irrigation applications. Scenarios C3-C6 go a step further by also considering varying levels of canal seepage reduction. The considered combination scenarios may achieve a level of benefit (as measured by D_{wt} and upflux to non-beneficial ET) not attainable through individual intervention alone. The considered combination scenarios span from moderately aggressive (C3) to very aggressive (C6).

Table 4-2. Description of results for selected alternative management scenarios. Canal seepage reductions were achieved by adjusting model canal conductance values such that the simulated baseline total volume of seepage along all canals in the region was reduced by the amount indicated (i.e., 50%, 80%).

Alternative Management Scenario Abbreviated Name	Alternative Management Scenario Description
Baseline	Calibrated baseline conditions, no simulated intervention
SR1	50% reduction in canal seepage
SR2	80% reduction in canal seepage
IR1	10% reduction in irrigation applications
IR2	20% reduction in irrigation applications
IR3	40% reduction in irrigation applications
F1	25% of baseline irrigated fields converted to fallow
C1	25% of baseline irrigated fields converted to fallow, 20% reduction in remaining irrigation applications
C2	25% of baseline irrigated fields converted to fallow, 40% reduction in remaining irrigation applications
C3	25% of baseline irrigated fields converted to fallow, 20% reduction in remaining irrigation applications, 50% reduction of canal seepage
C4	25% of baseline irrigated fields converted to fallow, 20% reduction in remaining irrigation applications, 80% reduction of canal seepage
C5	25% of baseline irrigated fields converted to fallow, 40% reduction in remaining irrigation applications, 50% reduction of canal seepage
C6	25% of baseline irrigated fields converted to fallow, 40% reduction in remaining irrigation applications, 80% reduction of canal seepage

4.7.5 Impacts on Groundwater Recharge

Several scenarios, listed in Table 4-2, are selected to exemplify the range of simulated results. The scenarios reduce predicted average recharge to the groundwater, as summarized in Table 4-3 and Table 4-4. The reported annual recharge reductions demonstrate considerable year-to-year variability for each proposed intervention. For example, the average reduction in

Table 4-3. Change in recharge to groundwater expressed as a percent reduction from the baseline condition for selected alternative management scenarios in the USR. Values in parentheses indicate the magnitude of the recharge offset due to induced seepage from canals that resulted from lower water tables under the specified intervention. To calculate the net percent reduction in recharge, subtract the induced seepage from earthen canals percentage from the larger percent reduction in recharge from irrigation.

Scenario	1999	2000	2001	2002	2003	2004	2005	2006	2007
SR1	4.4%	9.7%	14.9%	29.1%	20.0%	13.3%	11.8%	15.2%	9.0%
SR2	7.7%	17.4%	26.8%	51.6%	38.7%	25.8%	20.4%	27.2%	16.5%
IR1	12.7% (1.2%)	18.3% (1.9%)	20.1% (2.6%)	7.1% (3.1%)	13.6% (2.0%)	17.7% (1.9%)	16.4% (1.9%)	14.4% (3.0%)	14.8% (2.5%)
IR2	23.1% (2.0%)	31.6% (3.1%)	31.9% (4.2%)	11.1% (4.7%)	21.3% (3.0%)	28.9% (3.0%)	27.9% (3.1%)	24.2% (4.9%)	26.3% (4.1%)
IR3	42.9% (3.4%)	53.7% (4.7%)	49.0% (7.0%)	18.4% (7.7%)	33.8% (3.8%)	46.9% (4.8%)	47.2% (5.4%)	40.3% (8.0%)	47.5% (7.3%)
F1	29.2% (1.8%)	33.1% (3.1%)	30.9% (3.9%)	9.8% (3.7%)	17.8% (2.2%)	28.2% (2.6%)	21.2% (2.7%)	22.9% (4.5%)	24.2% (3.6%)
C1	37.9% (0.9%)	41.8% (1.7%)	39.2% (1.9%)	15.8% (2.0%)	25.8% (1.3%)	35.8% (1.5%)	32.6% (1.7%)	32.3% (2.5%)	34.7% (2.4%)
C2	52.6% (2.3%)	57.8% (3.8%)	51.6% (4.9%)	21.1% (4.5%)	36.2% (2.8%)	49.2% (3.3%)	48.4% (3.9%)	43.7% (5.8%)	51.0% (5.5%)
C3	43.0%	51.7%	53.6%	46.3%	46.5%	48.6%	44.1%	48.0%	44.8%
C4	46.8%	59.7%	65.3%	68.6%	65.0%	60.9%	53.3%	59.6%	52.9%
C5	58.4%	68.3%	66.6%	53.6%	58.4%	62.0%	60.2%	60.6%	62.5%
C6	62.8%	76.9%	78.5%	75.8%	76.3%	74.4%	70.7%	73.1%	71.5%

Table 4-4. Change in total recharge expressed as a percent reduction from the baseline condition for selected alternative management scenarios in the DSR. Values in parentheses indicate the magnitude of the recharge offset due to greater induced seepage from canals that resulted from lower water tables under the specified intervention.

Scenario	2002	2003	2004	2005	2006	2007
SR1	9.1%	12.1%	13.1%	11.3%	13.7%	12.1%
SR2	14.7%	20.1%	22.4%	19.6%	24.2%	21.6%
IR1	5.1% (0.1%)	8.6% (0.2%)	10.1% (0.2%)	9.7% (0.3%)	9.2% (0.4%)	10.7% (0.4%)
IR2	10.0% (0.2%)	17.0% (0.3%)	19.7% (0.3%)	19.5% (0.6%)	17.8% (0.8%)	20.9% (0.8%)
IR3	18.7% (0.4%)	31.5% (0.6%)	36.1% (0.6%)	37.2% (1.0%)	33.3% (1.4%)	39.1% (1.5%)
F1	18.4% (0.2%)	24.4% (0.2%)	28.0% (0.4%)	27.1% (0.9%)	25.8% (1.2%)	29.6% (1.4%)
C1	25.2% (0.3%)	34.3% (0.4%)	38.1% (0.4%)	37.6% (1.0%)	34.8% (1.3%)	39.9% (1.5%)
C2	31.4% (0.4%)	43.1% (0.6%)	47.5% (0.6%)	48.1% (1.2%)	43.7% (1.6%)	49.9% (1.8%)
C3	34.0%	46.0%	50.4%	48.8%	47.8%	51.8%
C4	39.4%	53.7%	58.9%	56.7%	57.7%	60.9%
C5	40.1%	54.7%	59.7%	59.2%	56.9%	61.8%
C6	45.6%	62.4%	68.3%	67.0%	66.6%	70.7%

recharge in the USR under the SR2 intervention ranged between 8% in 1999 to 52% in 2002, a 44 percentage point spread. In the DSR, the C6 intervention had the largest inter-annual range with 46% in 2002 and 71% in 2007, a 25 percentage point spread. In the USR, the minimum reduction in recharge occurred under the conditions that result from the SR1 intervention, namely 4% in 1999, whereas the maximum of 79% occurred under the C6 intervention in 2001. The minimum reduction in recharge in the DSR, that is 9% in 2002, also occurred under the SR1 intervention whereas a maximum reduction of 71% occurred in 2007 under the C6 scenario. Although reduction in irrigation applications reduces recharge, which can lower the water table and mitigate both waterlogging and non-beneficial consumptive use, it also could lead to an increase in root zone salinity if salt-leaching is not adequate. This tradeoff will need to be assessed further upon completion of a calibrated salt transport model.

The predicted changes in recharge display considerable spatial variability over the regions, as exemplified in the contour plots of percent change in average recharge over the irrigation seasons within the simulation periods, shown in Figure 4-11A and Figure 4-11B for scenario C3. In general, scenario C3 led to a widespread reduction in recharge in the both the USR and DSR, with a few locales of increased recharge. Some of the lease-fallowed fields in areas with increased recharge under the alternative management perhaps receive small allotments of irrigation water in the baseline simulation leading to little or no recharge for the baseline condition. Once fallowed, however, springtime precipitation on the same fields, now not affected by crop ET demand, likely results in greater amounts of recharge relative to the baseline amounts.

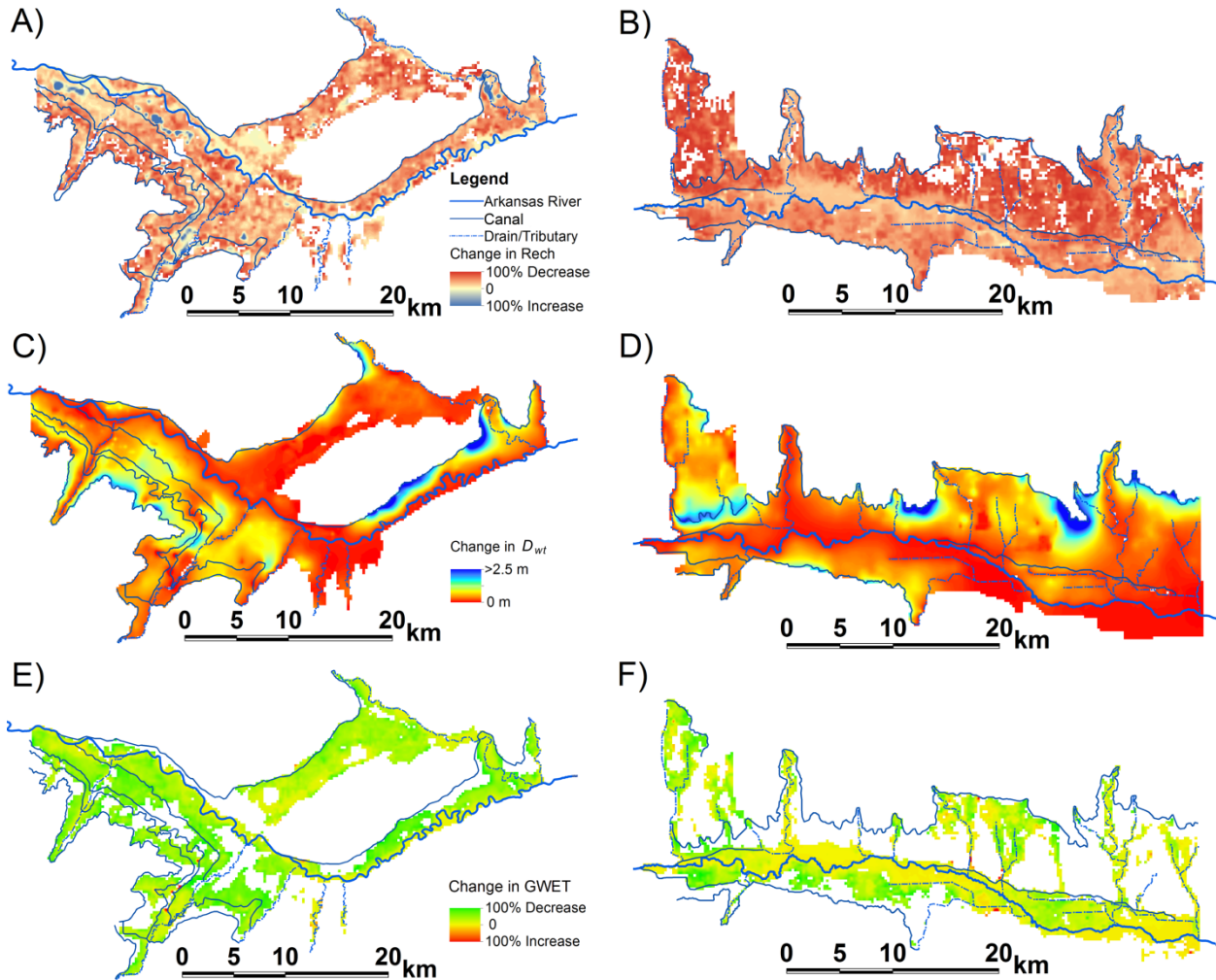


Figure 4-11. The effect of management intervention C3 (Table 4-1) on recharge to groundwater (A) in the USR, and (B) in the DSR; on D_{wt} (C) in the USR, and (D) in the DSR; and on groundwater upflux to ET (GWET) (E) in the USR, and (F) in the DSR obtained by differencing the average irrigation season conditions under the baseline conditions (Figure 4-6) and those of scenario C3.

Simulation results show that recharge reduction derived from lower irrigation applications was offset (albeit by relatively small amounts) by an increase in seepage from irrigation canals. That is, reduced irrigation applications led to reduced recharge, which in turn resulted in an increase in D_{wt} , a desirable effect. The deeper water table, however, increased the gradient between the stage in the canal and the local water table, thereby inducing additional

seepage adjacent to the canal. Therefore, if an intervention targeting reduced recharge through lowering irrigation application amounts and/or lease fallowing is not also accompanied by an intervention to reduce canal seepage, then the full benefit of the intervention will not be realized. Results for scenarios IR1, IR2, IR3, F1, C1, and C2 demonstrate this for both study regions (Table 4-3 and Table 4-4). The values in parentheses in these tables indicate the amount of increased recharge from canal seepage that would offset the reduced recharge for the combination scenarios where this situation occurred. Values in Table 4-3 and Table 4-4 without an accompanying value in parentheses reflect that seepage reduction measures were included in the scenario, thereby curtailing additional seepage that would result from a deeper water table in the vicinity of the canals.

The seepage reduction scenarios, SR1 and SR2, resulted in simulated recharge reduction not only adjacent to the canals but also under cropped areas. Lower water tables resulting from reduced seepage created a thicker unsaturated zone extending throughout the study regions, and in so doing extended the time required for downward flux to reach the water table, providing more opportunity for ET extraction from the unsaturated soil profile. The net effect was a simulated reduction in recharge of 10% in the USR and 6% in the DSR, resulting from irrigation deep percolation, despite the fact that the SR scenarios do not directly target reducing recharge under cropped land. The models do not apply the “saved” water (non-seeped canal water) to irrigated ground, assuming instead that it would remain in the river.

4.7.6 Impacts on D_{wt} and Waterlogging

All of the considered modeled scenarios resulted in deeper simulated D_{wt} over the USR and DSR, compared to the baseline, as indicated in Figure 4-8. The alternative management interventions had a greater effect on D_{wt} in the USR than in DSR. Due to the preponderance of senior water rights in the USR, more irrigation water is available than in the DSR. With more

water in the canals contributing to seepage as well as to greater irrigation applications, the scenarios implemented in the USR remove larger volumes of water from the simulation than do the same scenarios applied to the DSR, explaining in part the greater increase in D_{wt} in the USR. A longer historical simulation period would need to be run and analyzed to determine if a more significant increase in D_{wt} in the DSR takes longer to manifest.

In the scenarios that do not include conversion of 25% of cropped fields to fallow (i.e. SR1, SR2 and IR1-IR3), the cropped area with a simulated average $D_{wt} < 1$ m decreased by 19% – 50% [380 ha (940 ac) – 1,860 ha (4,600 ac)] for the range of management scenarios considered in the USR and by 9% – 41% [200 ha (490 ac) – 890 ha (2,190 ac)] in the DSR. The cropped area with $1 \text{ m} \leq D_{wt} \leq 2 \text{ m}$ decreased by 12% – 35% [280 ha (680 ac) – 800 ha (1,980)] for the range of management scenarios considered in the USR and by 2% – 13% [75 ha (190 ac) – 620 ha (1,530 ac)] in the DSR for this scenario. For the scenarios that simulated a 25% conversion of cropped fields to fallow (i.e. F1 and C1-C6), larger reductions in land area affected by waterlogging were achievable. The intervention with maximum effect on the water table was C6 in both study regions for each year of the respective simulation periods. The cropped area with a simulated average $D_{wt} < 1$ m was reduced by 70% [2,500 ha (6,180 ac)] in the USR and by 54% [1,410 ha (3,470 ac)] in the DSR. The spatial distribution of changes shown in the contour plots of Figure 4-11C and Figure 4-11D for scenario C3 reveal that the largest increases in D_{wt} occur in areas adjacent to the canals, reflecting the strong causal relationship between seepage and sustained shallow water tables. The simulated reductions in the water table were not large enough to reduce well yields or dry up pumping wells, likely due in part to the mandated limitations on pumping that take place in the LARV (U.S. Supreme Court, 1995).

4.7.7 Impacts on Groundwater Upflux and Non-beneficial Consumptive Use

The modeled scenarios resulted in predictions of significant change in groundwater upflux to ET from baseline conditions. An indication of the spatial variability of this change over the USR and DSR is shown in the contour plots of the percent change in groundwater ET averaged over the irrigation season for scenario C3 in Figure 4-11E and Figure 4-11F. Generally, groundwater ET decreased substantially over the modeled regions. For example, the percentage of total ET provided by groundwater under cropped land for scenario C3 dropped from 22% to 15% and from 25% to 20% in the USR and DSR, respectively. Scenario C6 produced the largest decline in the portion of total ET contributed by groundwater in both regions; a substantial drop to 9% in the USR was observed, whereas a comparatively small drop to 19% in the DSR was achieved. However, for some scenarios, including C3, there were some areas where groundwater ET was predicted to increase, likely due to increased extraction of groundwater to satisfy ET demand under cropped fields where large reductions in applied irrigation water were simulated.

Reducing the contribution of groundwater upflux to ET under cropped land can be beneficial if the underlying water table is saline. By limiting groundwater ET, the upward movement of salts into the root zone contributing to salinization is reduced. However, in areas where the contribution of salts from a saline water table is of less concern, reducing groundwater ET may hamper crop production due to the elimination of an important water supply resource, especially on cultivated lands that are under-irrigated.

Results displayed in Figure 4-9 and Figure 4-10 indicate the potential for recovering a portion of non-beneficial consumptive use in the USR and DSR, respectively. Figure 4-9A and Figure 4-10A show the estimated annual non-beneficial consumptive use on fallow and naturally-vegetated lands. Where the non-beneficial consumptive use decreased under an

alternative management scenario, the water recovered was calculated as the difference between the total volume as groundwater ET under the baseline condition and that under the respective scenarios. Plots of the cumulative sum of recovered water over the simulation periods are shown in Figure 4-9B and Figure 4-10B for the USR and DSR, respectively. In both regions, an immediate increase in the non-beneficial consumptive use from fallow lands occurred for the six combination scenarios (C1-C6) due to the 25% increase in fallow land area. This component of non-beneficial consumption decreased over the simulated period as D_{wf} increased due to the reduced recharge under these lands. Similarly, non-beneficial consumptive use was reduced with time under the extent of naturally-vegetated and original fallowed ground. However, despite the overall increase in D_{wf} under this newly-fallowed land and throughout the broader regions due to markedly lower recharge, results indicate that it would take several years before a net reduction in non-beneficial consumption (increase in recovered water) would take place. That is, the additional non-beneficial consumptive from the newly-fallowed ground initially outpaces the water savings from under naturally-vegetated and previously-fallowed ground. Results indicate that the full benefit of recovered water would not be realized until several years beyond the current simulated period for a number of the considered scenarios. As was described above, agricultural fields in production were chosen for lease-fallowing based on their reported crop type. The results here suggest that initial D_{wf} is an important consideration when selecting fields for dry up under leasing agreements. Social and economic factors, absent from the present analysis, would act to further refine the selection of fields as good candidates for lease-fallowing.

A between-region comparison of simulated groundwater ET under the baseline conditions shows roughly 20-25% greater non-beneficial consumption in the DSR (Figure 4-7E and Figure 4-7F). It would seem that larger volumes of water would be recoverable under

improved management scenarios if applied to the DSR; however, model results suggest otherwise. With the exception of scenarios C4, C5, and C6 in 2006 and 2007, the combination scenarios exacerbate non-beneficial consumptive use in the DSR (Figure 4-10B) while the other alternative management scenarios bring about relatively small water savings. Two possibilities may explain this unexpected result. First, the largest contribution of non-beneficial consumptive use occurs under naturally-vegetated lands (Figure 4-10A), large tracts of which lie along the Arkansas River and its tributaries (Figure 4-1B). These are the same areas that had a small response in D_{wt} under the alternative management scenarios (e.g. see Figure 4-9D for scenario C3). With only small increases in D_{wt} , the non-beneficial consumptive use in naturally-vegetated lands remains high. Second, fields were selected on a semi-random basis under the lease-fallowing option (see Section 4.7.3). A more discriminating approach for fallowing cropped lands that focuses on fields with larger D_{wt} may help depress non-beneficial consumptive use derived from the newly-fallowed fields, a large component of the total non-beneficial consumptive use occurring in scenarios that include the lease-fallow option. When contrasted with results from the USR (Figure 4-9B), where significantly larger water savings (through reduced non-beneficial consumptive use) were found, reasons for implementing alternative management scenarios for this purpose in the DSR remain lacking at this point in the analysis. A longer simulation period, especially that includes wetter conditions (i.e. with greater flow diversions to canals), may reveal greater potential for non-beneficial consumptive use savings in the DSR.

4.7.8 Impacts on Groundwater Return Flow to the River

Colorado water law and the Arkansas River Compact restrict the suite of possible alternative management scenarios available to decision makers through a requirement that patterns of groundwater return flow to the Arkansas River remain materially unaffected by any

proposed action. The considered interventions listed in Table 4-2 were predicted to alter the annual groundwater return flows substantially, with reductions ranging 10% – 43% in the USR and 4% – 29% in the DSR. Example time series of simulated reductions in groundwater return flows to the river, ΔQ_{GW} , are shown for scenarios S1, IR2, F1, and C3 in Figure 4-12. To implement management schemes that result in reduced groundwater return flows will require exploring ways to mimic baseline groundwater return flows by making up modeled flow deficits using reservoir storage and releases, thereby insuring that downstream water users receive their water entitlement. Implementation of the lease fallow scenarios, for example, would result in less consumptive use by crops (with the saved water being leased to Front Range municipalities)

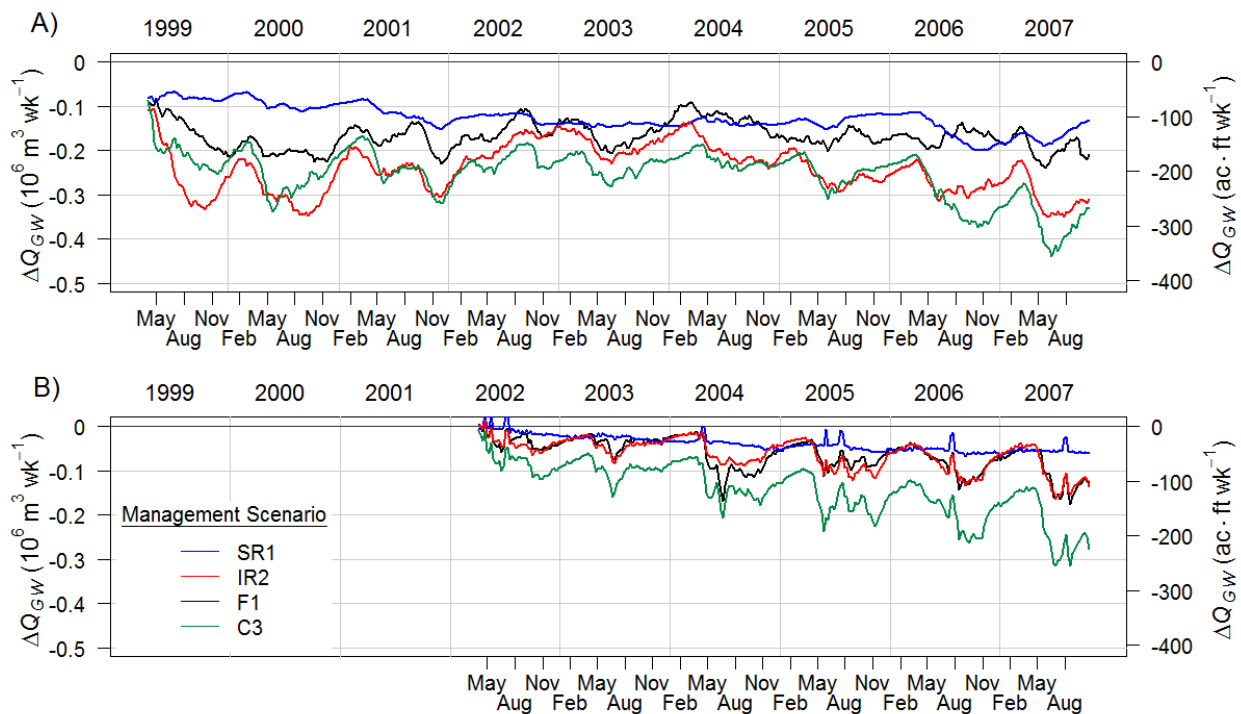


Figure 4-12. Simulated reduction in groundwater return flows to the Arkansas River in the (A) USR and (B) DSR for selected alternative management scenarios.

with the side-effects of reduced recharge and increased D_{wt} , with reduced waterlogging and groundwater ET, but also diminished groundwater return flows. Likely additional benefits, not considered in the present paper, would be reduced soil salinization and reduced loading of salts and other pollutants (e.g. selenium, nitrate, and uranium) to the river. In lease-fallowing or improved irrigation efficiency scenarios, water losses that previously were diverted as part of the gross irrigation application and returned to the river could be left in the river and stored in reservoirs. Augmenting river flow with appropriately-timed releases from these reservoirs to account for depleted return flows may allow satisfaction of two otherwise competing goals – improving quantity and quality characteristics of the irrigated soil-aquifer system and maintaining river flow patterns. In order to know how much to augment river flow in lease-fallowing scenarios, a longer period of simulation (> 20 years) will be needed to assess the change in groundwater return flows, especially in cases where the fallowed fields are located at larger distances from streams.

4.8 DISCUSSION AND CONCLUSIONS

Calibration and testing of groundwater models developed for two representative regions of a typical intensively-irrigated river valley, Colorado's LARV, are guided by observations of groundwater head, groundwater return flows, aquifer stratigraphy, seepage from earthen canals, and estimates of actual ET from satellite imagery. In addition, findings from parallel field-scale studies not only serve as calibration targets [e.g. upflux to ET from the water table, and recharge-to-infiltration ratios], but double as constraints on model inputs [e.g. irrigation application and tail-water runoff amounts]. Modeled periods encompass a range of hydrological extremes, from extensive flooding to severe drought. Regional-scale representation of unsaturated-zone flow processes is explicitly simulated with the UZF package developed for MODFLOW with

calibration encompassing a two-step automated procedure, guided by information on aquifer stratigraphy, and complemented with manual procedures. The amount of information from which the models are constructed and calibrated is unusual in its scope, yielding tools useful for examining, in a rich spatial and temporal setting, optional scenarios for improving groundwater level and flow conditions. These scenarios encompass ways to lower the water table, reduce non-beneficial groundwater consumptive use, and meet municipal water demands without permanent dry-up of productive irrigated land.

Analyses of the spatial and temporal results of the alternative management interventions demonstrate that significantly lowering the water table and reducing non-beneficial consumptive use is possible through management improvements involving reduced irrigation applications, reduced canal seepage, and lease-fallowing of irrigated land. However, considerable differences between the USR and DSR responses suggest that discretion in pinpointing areas to make capital and labor investments will likely lead to a focus on the USR. For example, the USR showed a greater propensity for responding to management intervention through larger increases in D_{wt} and more significant savings of non-beneficial consumptive use.

Model application also reveals that the choice of intervention within either region may not be as obvious as first thought. In general, increased levels of intervention are met with greater reductions in the mal-effects of over-application of irrigation water and inefficient infrastructure, though not always. Scenarios that include a lease-fallow option result in greater non-beneficial consumptive use losses over the near term by virtue of the expansion of the areal extent of fallow land in areas underlain by shallow water tables. With time, however, as the predicted regional water table depth increases, the water savings under naturally-vegetated and previously-fallowed land, achieved through lease-fallowing, outpaces any ancillary non-

beneficial consumptive use for most scenarios simulated in the USR. In the DSR, on the other hand, the simulated lease-fallowing scenarios only served to exacerbate the non-beneficial consumptive use. Modification of the considered lease-fallowing scenarios to find optimal intermittent lease-fallowing rotations (total number of fallowed fields, number of years a field remains fallowed) and to select fields that overlay areas of deeper groundwater is needed to help determine if a condition of net savings of non-beneficial consumption can be achieved after a reasonable period of time.

Collateral benefits are found to occur in the canal seepage reduction scenarios. Not only is recharge to the shallow alluvial aquifer reduced by curtailing seepage, but the resulting lower water table creates a thicker unsaturated zone leading to longer residence times and larger withdrawal of the draining irrigation water by ET. Thus, seepage reduction scenarios also reduce recharge occurring under crop lands. Conversely, the alternative management schemes that reduce irrigation application amounts without also including a canal seepage reduction option induce some additional seepage due to a larger hydraulic gradient created by the resulting deeper water table. The additional canal seepage offsets some of the recharge reduction aimed at alleviating the sustained high water tables.

Of the scenarios considered, the aggressive combination scenario C6 applied to the USR serves to demonstrate the largest potential for lowering the water table and for reducing groundwater non-beneficial consumptive use. Changes in groundwater return flows that would result under this and similar scenarios call for accompanying river management strategies to insure compliance with Colorado water law and the Arkansas River Compact to prevent injury to downstream water users. Although modeling provides indispensable insight into likely effects on groundwater conditions, before money and effort are invested toward infrastructure

rehabilitation and modernization, the social, legal, and economic trade-offs also need to be considered.

A sensitivity toward water politics in the basin seemingly has paralyzed system-wide change targeting basin-wide improvements in the past (Hukkinen, 1993). Moreover, Peak (1977) argued that a “fragmented set of rules, rights, special interests, and quasi-public administrative bodies” formed in Colorado’s past inhibit reform intended to meet emerging challenges facing the future administration of river water. The recent willingness to consider water banking and lease-fallowing arrangements signals a new flexibility. Nevertheless, while the technically-based options herein are backed by a detailed analysis and point to prospects for marked system improvement across regional scales, satisfying legal and policy constraints undoubtedly will prove more challenging than model development. Submitting the models to optimization algorithms that seek to maximize the benefits of improved water table and groundwater flow conditions and minimize the effect on return flow patterns may be an important avenue for future research in preparation for launching a pilot implementation project in the field.

Finally, the effects of these scenarios on the related issues of solute mobilization and transport currently are being investigated through the application of solute-transport models that include both the saturated and unsaturated zones of the subsurface system and are geared toward regional-scale analysis. These models consider soil water salinity effects on ET for a more complete evaluation of the impacts of alternative management scenarios on crop yields. Results discussed herein tell only half of the full story, which concerns not only groundwater table and flow but groundwater quality; the ability of the investigated scenarios to mitigate salt, selenium, and nitrate pollution in the stream-aquifer system tells the other half. A final analysis is

envisioned in which the results described herein, as well as those from the solute-transport models currently being developed, will provide water managers with a fuller description of the potential value and tradeoffs of the alternative management options.

5 MODELING VARIABLY SATURATED SUBSURFACE SOLUTE TRANSPORT WITH MODFLOW-UZF AND MT3DMS³

5.1 SUMMARY

The MT3DMS groundwater solute transport model was modified to simulate solute transport in the unsaturated zone by incorporating the Unsaturated-Zone Flow (UZF1) package developed for MODFLOW. The modified MT3DMS code uses a volume-averaged approach in which Lagrangian-based UZF1 fluid fluxes and storage changes are mapped onto a fixed grid. Referred to as UZF-MT3DMS, the linked model was tested against published benchmarks solved analytically as well as against other published codes, most frequently the U.S. Geological Survey's Variably-Saturated Two-Dimensional Flow and Transport Model. Results from a suite of test cases demonstrate that the modified code accurately simulates solute advection, dispersion, and reaction in the unsaturated zone. Two- and three-dimensional simulations also were investigated to ensure unsaturated-saturated zone interaction was simulated correctly. Because the unsaturated-zone flow solution is analytical, large-scale flow and transport investigations can be performed free from the computational and data burdens required by numerical solutions to Richards equation. Results demonstrate that significant simulation runtime savings can be achieved with UZF-MT3DMS, an important development when hundreds or thousands of model runs are required during parameter estimation and uncertainty analysis. Three-dimensional variably saturated flow and transport simulations revealed UZF-MT3DMS to have runtimes that are less than one tenth of the time required by models that rely on Richards

³ As published in *Groundwater*, Eric D. Morway, Richard G. Niswonger, Christian D. Langevin, Ryan T. Bailey, Richard W. Healy, 2012, Vol. 51, No. 2, 237-251.

equation. Given its accuracy and efficiency, and the wide-spread use of both MODFLOW and MT3DMS, the added capability of unsaturated-zone transport in this familiar modeling framework stands to benefit a broad user-ship.

5.2 INTRODUCTION

The suite of numerical codes from which practitioners, researchers, and managers can select to simulate water and solute transport in the unsaturated zone is diverse. Examples include VS2D (Lappala et al., 1987; Healy, 1990), STOMP (White et al., 1995), UNSATCHEM (Suarez and Simunek, 1997), RAFT (Chilakapati et al., 2000), TOUGHREACT (Xu et al., 2003), and HYDRUS (2D/3D) (Šimůnek et al., 2006), among others (Šimůnek and Bradford, 2008a). The diversity of codes stems from various nuanced approaches accounting for soil heterogeneity, nonlinear soil physical properties, non-uniform root activity, and rapidly changing boundary conditions in the near-surface (Van Dam and Feddes, 2000; Vanderborght et al., 2005). Unfortunately, the use of these models for watershed-scale modeling is often hampered by the numerical solution of Richards equation in the unsaturated zone. Richards equation is difficult to solve due to its parabolic form and the nonlinear relationships between soil water pressure head, hydraulic conductivity, and water content. Sharp wetting and/or drying fronts moving through the soil profile further compound the problem and require lengthy computational times (Ross, 1990; Van Dam and Feddes, 2000). At the watershed scale, additional concerns arise during the calibration process when distributed parameters used in Richards equation are perturbed to unrealistic values due to an insufficiently fine discretization scheme (Downer and Ogden, 2004). Furthermore, actual data characterizing the unsaturated zone over regional and basin scale extents that serves as input into Richards equation are rarely, if ever available (McGrath et al., 2008a; Niswonger and Prudic, 2009). Owing to these difficulties, numerous investigations have

sought a computationally efficient alternative for approximating Richards equation that provide reasonable representations of the timing of recharge and solute loading to aquifers and streams (Struthers et al., 2006; McGrath et al., 2008a; McGrath et al., 2008b 2011; Harman et al., 2011).

One such alternative, built for use with the widely used MODFLOW groundwater flow model (Harbaugh, 2005; Hill et al., 2010) is the Unsaturated-Zone Flow (UZF1) package (Niswonger et al., 2006). The UZF1 package was created to provide “an efficient means of simulating recharge” while at the same time accounting for evapotranspiration (ET), storage, and flow effects in the unsaturated zone (Niswonger and Prudic, 2004; Niswonger et al., 2006), thus providing a much-needed link between near surface hydrology and subsurface groundwater flow across watershed scales (Barlow and Harbaugh, 2006). UZF1 accomplishes this goal by using the method of characteristics to solve a kinematic wave equation for unsaturated flow that is derived by neglecting the diffusive term in Richards equation. UZF1 also relies on the assumption of uniform hydraulic properties in the unsaturated zone for each vertical column of model cells.

The value of tools like UZF1 has been a topic of some debate (Singh, 2002; Twarakavi et al., 2008; Niswonger and Prudic, 2009). Controversy typically centers on the tradeoffs between speedier but simplified approaches like UZF1 and more accurate but data and computationally intensive requirements of Richards equation based models. With regard to UZF1, errors associated with the kinematic wave approach (Smith and Hebbert, 1983; Struthers et al., 2006 2008; Twarakavi et al., 2008) are likely small relative to the errors resulting from scaling effects and a reduced set of parameters representative of a highly complex system (Doherty and Welter, 2010). However, the benefits of a faster model are realized during automated calibration and uncertainty analysis, which may require hundreds (or thousands) of model runs.

The purpose of this paper is to describe an approach for simulating solute transport in the subsurface using fluid fluxes from MODFLOW simulations that include UZF1 representation of the unsaturated zone. Our approach is implemented in the MT3DMS code, which is commonly used with MODFLOW. We describe modifications made to the MT3DMS source code followed by comparisons of simulated results to published benchmarks solved analytically and with other published codes. This work, referred to as UZF-MT3DMS hereafter, is meant to build on the computationally efficient flow solution across regional-scales for the unsaturated zone (UZF1) by modifying MT3DMS to solve solute transport in the unsaturated zone (Zheng, 2009).

Physically based, watershed-scale models that include the unsaturated zone (Corwin, 1996; Vanclooster et al., 2005) that are both robust and efficient can improve our understanding of both human impacts (Keating et al., 2005; Schoups et al., 2005b; Panday et al., 2009) and climate variability (Earman and Dettinger, 2011) on the *quality* of groundwater resources since unsaturated-zone transport affects the fate of contaminants as they are transmitted between land surface and the water table (Nielsen et al., 1986) as well as to streams (Kirchner et al., 2000). This new functionality will stand to benefit the large number of MODFLOW and MT3DMS users (Panday and Huyakorn, 2008; Hill et al., 2010) by providing the capabilities necessary for extending existing regional-scale MODFLOW-MT3DMS models to the unsaturated zone. Moreover, just as UZF1 is the basis for simulating unsaturated flow in GSFLOW (Markstrom et al., 2008), a tightly-coupled modeling platform for simulating groundwater and surface water interaction with PRMS (Leavesley et al., 1983) and MODFLOW, UZF-MT3DMS is a step toward adding solute transport to GSFLOW.

Comparisons presented herein highlight the performance of UZF-MT3DMS under steady, unsteady, non-reactive, and reactive conditions, with options for specifying either

nonlinear equilibrium sorption or non-equilibrium sorption conditions. In addition, UZF-MT3DMS was tested in 1, 2, and 3-dimensional simulations to ensure that source-code modifications aimed at facilitating transport in the unsaturated zone did not interfere with multi-dimensional calculations of the saturated zone. Finally, comparisons of the total simulation time between UZF-MT3DMS and three other models included in the 3-dimensional test scenario demonstrate the shorter simulation runtimes that can be achieved with UZF-MT3DMS.

5.3 DESCRIPTION OF APPROACH AND IMPLEMENTATION

To maintain consistency with the MT3DMS paradigm and develop a scheme that could be implemented in the current code structure, we focused on development of a simple volume-averaged approach in which UZF1 fluid fluxes and calculated storage changes are mapped onto a fixed grid. Vertical fluxes at grid cell boundaries are calculated by integrating the results from the UZF1 solution over each time step. These grid-based fluxes and storage changes are subsequently passed to MT3DMS. Although fluid fluxes simulated by UZF1 and mapped to the fixed grid only are in the vertical direction, dispersive solute transport is represented in 2- and 3-dimensions (e.g. Figure 5-6 and Figure 5-8). An important limitation with this approach, in addition to those limitations of the UZF1 package, is that the fixed grid used for solute transport must be fine enough to accurately represent concentration profiles.

Although this approach could be used for any Lagrangian-based unsaturated flow model, the UZF1 package for MODFLOW-2005 (Harbaugh, 2005) and MODFLOW-NWT (Niswonger et al., 2011) was used for the benchmark problems described here. The governing equation for unsaturated-zone flow solved by UZF1 is (See Eq. 3 in Niswonger et al., 2006):

$$\frac{\partial \theta}{\partial t} + \frac{\partial K(\theta)}{\partial z} + a = 0 \quad (\text{Eq. 5-1})$$

where θ is water content, $K(\theta)$ is hydraulic conductivity as a function of θ , t is time, z is elevation, and a is evapotranspiration (ET) rate per unit depth. Readers are referred to the UZF1 documentation and associated publications (Niswonger and Prudic, 2004; Niswonger et al., 2006) for details of the implementation of the method of characteristics to solve Equation 5-1. The Lagrangian formulation for solving unsaturated flow in UZF1 was mapped onto an Eulerian grid for the transport simulation calculated by MT3DMS. This transformation of coordinates is done by volume averaging water contained in the vertical interval spanned by each grid cell to estimate that cell's water content and by integrating vertical fluxes at cell boundaries. In cells containing the water table, water volumes from the saturated and unsaturated zones are computed and then averaged over the entire volume of the cell; in the standard MT3DMS version, the effective cell volume is only the saturated part, which means the effective cell volume can change with water table fluctuations. For a cell containing the water table, our approach redistributes the water in the unsaturated and saturated zones over the volume of the cell. Errors with this approximation can be minimized by enhancing vertical grid resolution near the water table.

The resulting grid-based water content and fluid fluxes are then passed to MT3DMS using a flow-transport link file (Zheng et al., 2001). MT3DMS is a separate program from MODFLOW; the flow-transport link file is created by MODFLOW, and used subsequently by MT3DMS. New arrays in the flow-transport link file include volumetric water content, θ ($L^3 L^{-3}$) in partially saturated cells (including cells that contain the water table); vertical volumetric flow rate, UZFLX ($L^3 T^{-1}$) between partially saturated cells (positive in the direction of increasing layer indexes); groundwater discharge at the surface, UZQOUT (when heads rise above ground surface elevation); volumetric ET rate from the unsaturated zone, UZ-ET ($L^3 T^{-1}$);

and the volumetric ET rate from the saturated zone, GW-ET ($L^3 T^{-1}$), when the water table elevation is above the extinction depth, where the extinction depth is defined as the depth over which root uptake is possible.

The ‘mixed form’ continuity equation for solute transport solved by MT3DMS is described in Huang et al. (1998) and is written

$$\begin{aligned} \frac{\partial M}{\partial t} = & \frac{\partial}{\partial x} \left(\theta D_x \frac{\partial C}{\partial x} \right) + \frac{\partial}{\partial y} \left(\theta D_y \frac{\partial C}{\partial y} \right) + \frac{\partial}{\partial z} \left(\theta D_z \frac{\partial C}{\partial z} \right) - \frac{\partial}{\partial x} (q_x C) - \frac{\partial}{\partial y} (q_y C) \\ & - \frac{\partial}{\partial z} (q_z C) + q_s C_s + \sum_{n=1}^N R_n \end{aligned} \quad (\text{Eq. 5-2})$$

Where M is the solute mass per unit volume of soil and includes both the aqueous and sorbed phases of solute, C is the dissolved concentration, θ is the water content, t is time, x , y , and z are the Cartesian coordinate directions, D_x , D_y , and D_z are the hydrodynamic dispersion coefficient values along the x , y , and z directions, respectively, q_x , q_y , and q_z are the volumetric flow rates per unit volume of aquifer in the x , y , and z directions, respectively, and q_x , and q_y are zero for cells above the water table, q_s is the fluid source or sink flux, C_s is the concentration of the source or sink flux, and $\sum R_n$ is the chemical sink/source term that describes the rate of change in solute mass for a modeled species due to N chemical reactions.

The solution of Equation 5-2 follows Zheng and Wang (1999a), except for the storage term (right-hand-side of Equation 5-2) that was modified to consider changes in water content with time. Thus, the storage term was approximated as Huang et al. (1998):

$$R \frac{\partial(\theta C)}{\partial t} = R_{i,j,k}^{n+1} \frac{\theta_{i,j,k}^{n+1} C_{i,j,k}^{n+1} - \theta_{i,j,k}^n C_{i,j,k}^n}{\Delta t} \quad (\text{Eq. 5-3})$$

where n is the old time level with known concentrations and $n+1$ is the new time level with unknown concentrations. Retardation (R) is updated using the concentration found at the last iteration.

MT3DMS has several approaches for simulating solute transport, but when unsaturated-zone transport is active, only the implicit finite difference algorithm and the total-variation-diminishing (TVD) solution techniques are supported. Solutions invoking the method of characteristics (MOC) or its variants are not yet supported when unsaturated-zone flow is simulated. A forth-coming paper by Bailey et al. (2013b) details modifications made to RT3D, a numerical code that originally solved the coupled partial differential equations describing reactive-flow and transport of either mobile and/or immobile species in the saturated zone, but now solves for multi-species reactive transport in variably-saturated systems and serves as a modeling platform for applications requiring simulation of between-species chemical reactions.

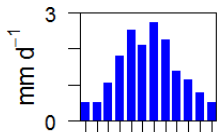
5.4 BENCHMARK PROBLEMS

In order to verify the accuracy of this new approach, simulated results were checked against analytical solutions as well as results from other numerical models. One-dimensional comparisons were tested against analytical solutions published in Vanderborght et al. (2005) as well as simulated results from VS2DT (Healy, 1990) for the following set of flow and transport conditions: 1) steady flow with three alternative dispersivities (α_L) (scenario 1), 2) unsteady flow with two alternative soil types (scenarios 2 and 3), 3) steady flow with nonlinear sorption (scenario 4), and 4) steady flow with nonequilibrium transport with flow interruption (scenario 5). Two and three dimensional simulations (scenarios 6 and 7, respectively) were tested against results from VS2DT, HYDRUS 3D (Šimůnek et al., 2008b), SUTRA (Voss, 1984; Voss and Provost, 2002), and the coupled flow and transport modeling system of CATHY/TRAN3D

Table 5-1. Flow and transport model input parameters including water content (θ), residual (θ_r) and saturated (θ_s) water content, infiltration rate (J), saturated hydraulic conductivity (K), Brooks-Corey epsilon (ϵ) (Niswonger et al., 2006), Brooks-Corey pore-size distribution index (λ), Brooks-Corey air-entry pressure (h_b) (Healy, 1987), concentration (C), longitudinal dispersivity (α_L), transverse dispersivity (α_T), bulk density (ρ_b), Freundlich equilibrium constant (K_f), Freundlich exponent (a), mass-distribution coefficient (K_d), first-order mass transfer rate (β).

Scenario	Dimensions	Flow Condition	Initial Conditions	Boundary Conditions	Model Parameters	Figure
1	1	Steady Flow	$\theta(z,t=0) = 0.378639$ $C(z,t=0) = 0$	$J = 5 \text{ cm d}^{-1}$ $C(z=0) = 100$ for $0 < t < 1 \text{ d}$ $C(z=0) = 0$ for $t > 1 \text{ d}$	$\alpha_L = 0.1, 1.0, 10.0 \text{ cm}$	5-1
2	1	Unsteady Flow	$\theta(z,t=0) = 0.231$ $C(z,t=0) = 100$ for $0 < z < 20$ $C(z,t=0) = 0$ otherwise	$J = \text{varies}$ (See Fig. 2) $ET = \text{varies}$ (See Fig. 2) $C(z=0) = 0$ for $t > 0$ Extinction Depth = 150 cm	†UZF1: $\epsilon = 4.0989$ ‡VS2D: $\lambda = 1.82, h_b = -75 \text{ cm}$ $K = 22.5 \text{ cm d}^{-1}$ $\theta_s = 0.485, \theta_r = 0.13$ $\alpha_L = 5.0$	5-3A, 5-3C
3	1	Unsteady Flow	$\theta(z,t=0) = 0.080$ $C(z,t=0) = 100$ for $0 < z < 20$ $C(z,t=0) = 0$ otherwise	$J = \text{varies}$ (See Fig. 2) $ET = \text{varies}$ (See Fig. 2) $C(z=0) = 0$ for $t > 0$ Extinction Depth = 150 cm	†UZF1: $\epsilon = 3.8734$ ‡VS2D: $\lambda = 1.82, h_b = -16 \text{ cm}$ $K = 4000 \text{ cm d}^{-1}$ $\theta_s = 0.351, \theta_r = 0.04$ $\alpha_L = 1.0$	5-3B, 5-3D
4	1	Steady Flow	$\theta(z,t=0) = 0.40$ $C(z,t=0) = 0$	$J = 2 \text{ cm d}^{-1}$ $C(z=0) = 10 \text{ mg mL}^{-1}$ for $t > 0$	Flow not simulated, J and θ preset $\alpha_L = 1.0$ $\rho_b = 1.0 \text{ mL}^{-1}, a = 2/3$ $\rho_b K_f = 1 \text{ mL}^a (\text{g mg}^{a-1})^{-1}$	5-4
5	1	Steady with flow interruption at 20 pore volumes (200 h)	$\theta(z,t=0) = 0.50$ $C(z,t=0) = 0$	$J = 0.5 \text{ cm h}^{-1}$ $C(z=0) = 100\,000 \text{ mg mL}^{-1}$ for $0 < t < 0.01 \text{ h}$ $C(z=0) = 0 \text{ mg mL}^{-1}$ for $t > 0.01 \text{ h}$	Flow not simulated, J and θ preset $\alpha_L = 1.0$ $\rho_b = 1.0 \text{ mL}^{-1}$ $\rho_b K_d = 10 \text{ mL g}^{-1}, \beta = 0.1 \text{ h}^{-1}$	5-5

Table 5-1. (Continued)

Scenario	Dimensions	Flow Condition	Initial Conditions	Boundary Conditions	Model Parameters	Figure
6	2	Steady Flow	$\theta(x,z,t=0) = 0.105$ $C(x,z,t=0) = 0$	$J = 10 \text{ cm d}^{-1}$ $C(3.75 < x < 6.25) = 1 \text{ mg mL}^{-1}$ for $t > 0$	†UZF1: $\varepsilon = 4.0$ ‡VS2D: $\lambda = 2.0, h_b = -5 \text{ cm}$ $K = 250 \text{ cm d}^{-1}$ $\theta_s = 0.45, \theta_r = 0.10$ $\alpha_L = 50 \text{ cm}, \alpha_T = 20 \text{ cm}$	5-6
7	3	Unsteady Flow	$\theta(x,y,z,t=0) = 0.22$ $C(x,y,z,t=0) = 0$	 <p>J: J M A D</p> $C(3000 < x < 5000,$ $2000 < y < 3100) = 1 \text{ mg mL}^{-1}$ for $t > 0, C(x, y) = 0$ otherwise Left side constant head = 42 m Right side constant head = 32 m	UZF1: $\varepsilon = 4.0$ $K = 50 \text{ m d}^{-1}$ $\theta_s = 0.45, \theta_r = 0.10$ $\alpha_L = 100 \text{ m}, \alpha_T = 40 \text{ m}$	5-7, 5-8, 5-9

† The Brooks-Corey exponent ε in UZF1 is used in the following equation $K(\theta) = K_s \left[\frac{(\theta - \theta_r)}{(\theta_s - \theta_r)} \right]^\varepsilon$ where K_s is the saturated hydraulic conductivity.

‡ The Brooks-Corey parameters h_b and λ in VS2DT are used in the following equation $K_r = (h/h_b)^{-2-3\lambda}$ where K_r is the relative hydraulic conductivity and h is the pressure-head used in Richards equation.

§ The parameters ρ_b and a are used to calculate retardation, R , for the Freundlich isotherm expressed in the following form $R = 1 + \frac{\rho_b}{\theta} a K_f C^{a-1}$

¶ The parameters K_d and β are used to calculate non-equilibrium sorption using the following equation $\rho_b \cdot \partial \bar{C} / \partial t = \beta (C - \bar{C} / K_d)$ where \bar{C} is the concentration of the sorbed phase. The mass transfer coefficient α , used in Equation 12 of Vanderborght et al. (2005) and equal to 0.01 h^{-1} in the original benchmark differs from β used in MT3DMS by a factor of $\rho_b K_d$ (Zheng and Wang, 1999a).

(Gambolati et al., 1994; Bixio et al., 2000; Camporese et al., 2010). Whereas scenarios 1, 4, and 5 were tested against analytical benchmarks, scenarios 2 and 3 were tested against simulated results from VS2DT, because no analytical benchmark exists for these scenarios. These simulations are summarized in Table 5-1.

Qualitative and quantitative measures of model performance are organized into graphical and tabular formats, respectively. Quantitative assessment of UZF-MT3DMS results to either analytical benchmarks or other model output was calculated using Equation 4-4 (Kutner et al., 2004, Eq. 2.72; Vanderborcht et al., 2005, Eq. 64):

$$R^2 = 1 - \frac{SSE}{SSTO} = 1 - \frac{\sum_{i=1}^N (p_i - m_i)^2}{\sum_{i=1}^N (m_i)^2 - \frac{\left(\sum_{i=1}^N m_i\right)^2}{N}} \quad (\text{Eq. 5-4})$$

where *SSE* is the sum of squared deviations between the model and the benchmark, *SSTO* is the total variation in the dataset (Kutner et al., 2004), and p_i and m_i are the UZF-MT3DMS and benchmark output vectors, respectively, at position or time i , depending on which simulated output is being checked (e.g. concentration at multiple locations of a profile for a particular time, mass flux at a particular location through time). In addition to new R^2 values calculated for the present work, R^2 values from Vanderborcht et al. (2005) have been added to Table 5-2 to facilitate comparison to the models evaluated in that effort. Values of R^2 greater than 0.9 indicate a “perfectly acceptable simulation,” whereas values of between 0.6 and 0.9 are deemed “satisfactory” (Chiew et al., 1993).

Table 5-2. Quantitative assessment between UZF-MT3DMS simulated results and analytical benchmarks for the variable dispersivity, Nonlinear, and non-equilibrium transport problems, and to output from other models for the variable precipitation and evapotranspiration conditions, 2- and 3-dimensional transport problem was conducted using Equation 4-4. The order of results is in keeping with the order of simulations discussed in the Results and Discussion section.

Simulation	R ²					
	From Vanderborght et al. (2005)					
	UZF-MT3DMS	HYDRUS	MACRO	SWAP	MARTHE	WAVE
Variable Dispersivity (scenario 1)						
Conc. Breakthrough @ 2 m						
$\alpha_L = 0.1$	0.996	0.820	0.980	-	0.970	0.640
$\alpha_L = 1.0$	0.999	0.950	0.998	0.999	0.997	0.780
$\alpha_L = 10$	0.999	0.994	0.999	0.999	0.998	0.790
Conc. Profiles @ 10 days						
$\alpha_L = 0.1$	0.996	0.940	0.996	-	0.990	0.770
$\alpha_L = 1.0$	0.999	0.970	0.998	0.999	0.999	0.810
$\alpha_L = 10$	0.999	0.984	0.998	0.998	0.999	0.680
Variable Weather Conditions (scenarios 2 and 3)	UZF-MT3DMS					
Conc. Breakthrough	Silt	Sand				
@ 25 cm Depth	0.997	0.999				
@ 50 cm Depth	0.970	0.997				
@ 100 cm Depth	0.954	0.996				
Mass Breakthrough						
@ 150 cm Depth	0.899	0.860				

Table 5-2. (Continued)

Simulation	R ²					
	UZF-MT3DMS	From Vanderborght et al. (2005)				
		HYDRUS	MACRO	SWAP	MARTHE	WAVE
Nonlinear equilibrium sorption (scenario 4)						
Transformed Coord. (η)						
@ 20 days	0.909	0.931	0.945	0.945	0.928	-
@ 40 days	0.921	0.981	0.991	0.982	0.975	-
@ 60 days	0.989	0.983	0.988	0.988	0.979	-
Non-equilibrium sorption (scenario 5)						
Conc. Breakthrough	0.9332	0.995	0.970	0.950	0.980	-
2-Dimensional Model (scenario 6)						
Conc. Profiles @ 60 days	0.9991					

Checks for mass balance errors were made apart from the UZF-MT3DMS code to ensure continuity was not violated. For the solver tolerances used in these tests, mass balance errors did not exceed 1%.

5.4.1 Scenario 1: Variations in Dispersivity

The first scenario focused on the dispersion component of the governing transport equation by considering three different dispersivities in a 1-dimensional steady flow regime. These simulations used a 200 cm column with 1 cm vertical discretization and flow and transport conditions described in scenario 1 of Table 5-1, all in accordance with the analytical benchmark originally described in Vanderborght et al. (2005). In the VS2D simulation, the bottom boundary was specified as a gravity drain which acts as a fixed flux boundary with the flux set equal to vertical hydraulic conductivity at the current pressure head. Because MODFLOW-UZF1 does not provide this type of boundary condition, the model domain was extended 10 cm below the upper 200 cm to facilitate gravity drainage.

Results from a transport scenario with three alternative dispersivities are shown in Figure 5-1. For the case where α_L equals 0.1 (Figure 5-1a and Figure 5-1b), a Peclet number ($\Delta x/\alpha_L$) greater than the recommended threshold of 2 (Zheng and Bennett, 2002) resulted in artificial oscillation. In an advection dominated scenario, options such as the TVD scheme in MT3DMS eliminate the artificial oscillation (subplot of Figure 5-1a) and more closely match the analytical solution. There is a small amount of over-prediction of concentration near the bottom of the profile in the UZF-MT3DMS simulation with α_L equal to 10 cm. This is likely a result of placing the bottom boundary of the model domain within α_L distance of the upper 200 cm of the domain, thereby allowing the boundary condition to slightly interfere with the simulated results

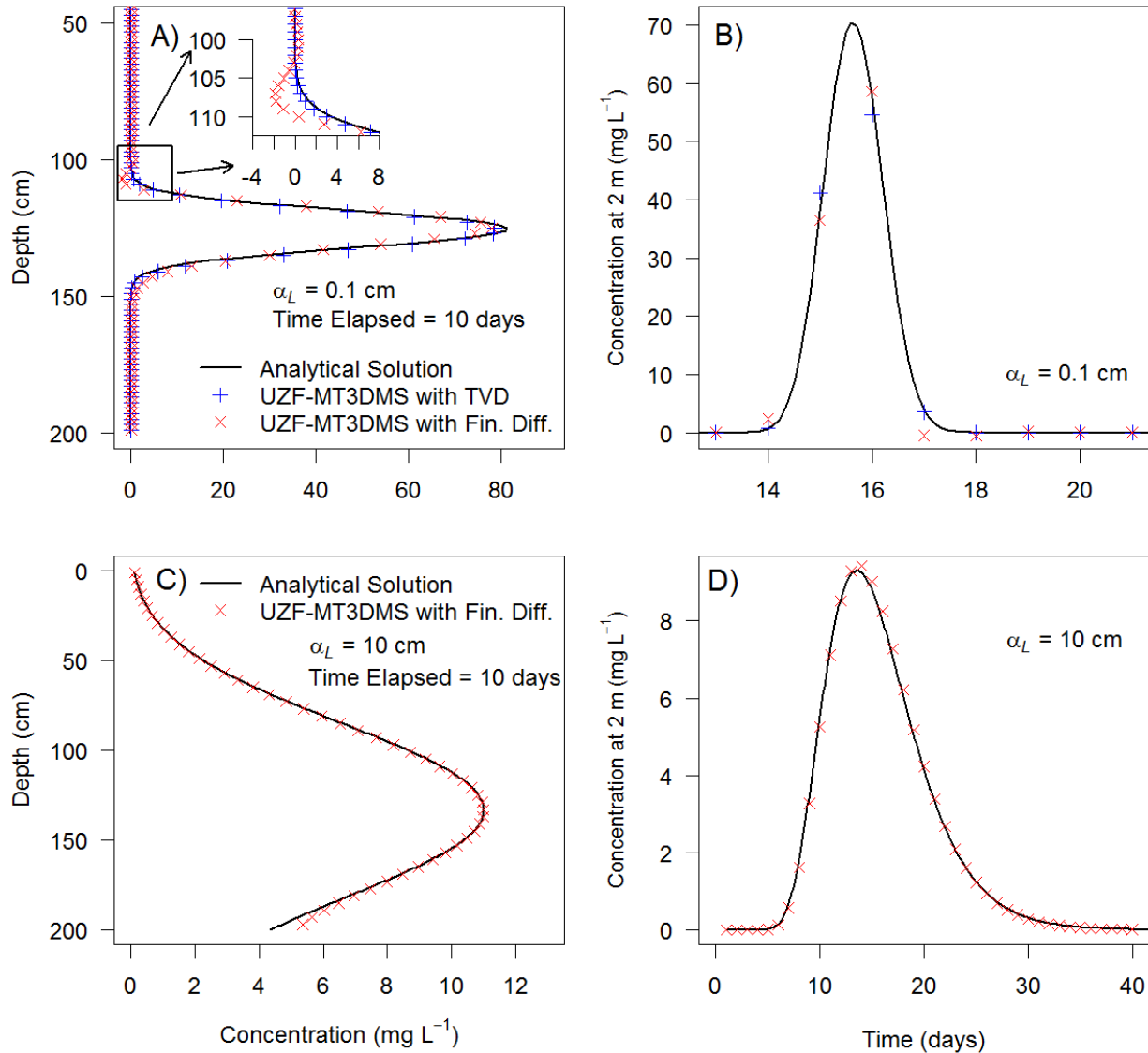


Figure 5-1. Comparison between UZF-MT3DMS and analytical benchmarks provided in Vanderborght et al. (2005). (A, C) Concentration profiles after 10 days for two dispersivities. (B, D) Concentration breakthrough curves at 2 m below ground surface. (A inset) Results provided for both the implicit finite difference method and Total Variation Diminishing (TVD) scheme for Peclet number > 2 .

of the upper 200 cm of the model domain. However, the effect of the bottom boundary condition on the breakthrough curve does not strongly affect the overall fit as indicated by the R^2 statistic (Table 5-2).

5.4.2 Scenarios 2 and 3: Variable Precipitation and Evapotranspiration Conditions

Scenarios 2 and 3 were designed to test model performance in a highly variable (depicted graphically in Figure 5-2) flow-regime for two different soil textures, silt and sand, respectively. To the best of our knowledge, the kinematic wave approach has not been tested using a realistic daily weather signal that also considers root uptake. Therefore, scenarios 2 and 3 are important tests highlighting the ability of UZF1 to convert infiltration to recharge while also simulating the effects of ET as a function of water content in the soil profile. Previous tests of the kinematic wave approach (Smith and Hebbert, 1983; Charbeneau, 1984; Struthers et al., 2006) consider only a simple infiltration boundary condition.

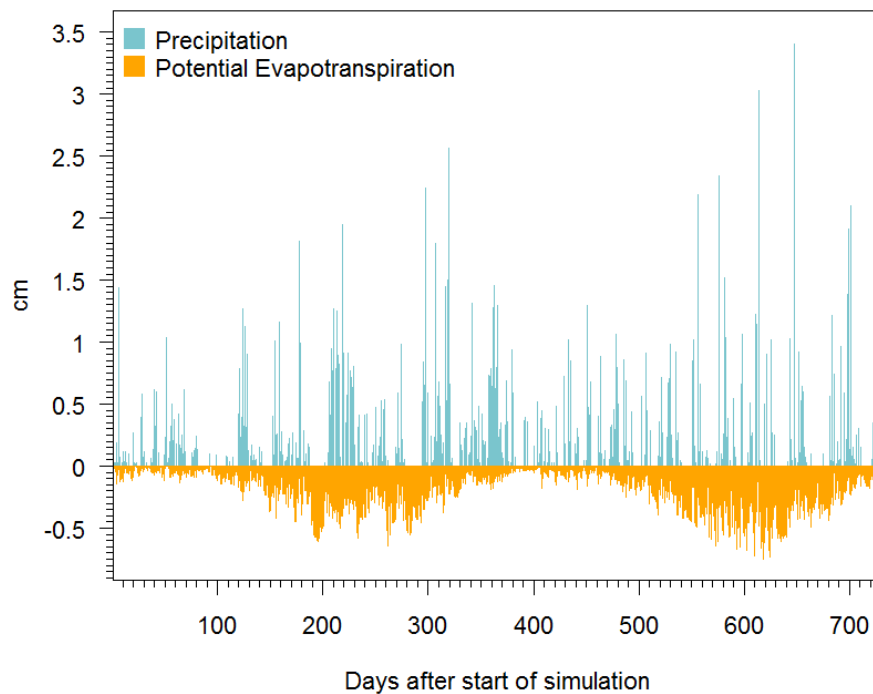


Figure 5-2. Magnitude and timing of precipitation and evapotranspiration stresses applied to the variable precipitation and evapotranspiration condition benchmark [taken from Vanderborght et al. (2005)].

An important change made to the variable precipitation and evapotranspiration benchmarks described in Vanderborght et al. (2005) was necessary because the original benchmark used an evaporation boundary condition at the soil surface. While in some settings an evaporation-only boundary condition may best approximate field conditions, the majority of applications that stand to benefit from UZF-MT3DMS capabilities more commonly require an ET boundary condition. That is, the effect of soil moisture uptake across a specified depth interval (extinction depth) on unsaturated-zone transport problems is an important characteristic to accurately represent; it may simultaneously signal the presence of solute loading while also affecting its timing. For example, in areas where enough soil moisture storage persists to sustain plant growth and therefore ET, then there is likely enough unsaturated-zone soil moisture to result in recharge and solute loading (Seyfried et al., 2005). However, longer residence time in the unsaturated zone will occur as a result of ET (Harman et al., 2011). Thus, the need to simulate soil moisture extraction over a specified range of the soil profile is a more appropriate test for the UZF-MT3DMS model. Because no analytical benchmark exists for this problem, UZF-MT3DMS was compared to solutions calculated by VS2DT (Healy, 1990) for silt and sand materials described in Brooks and Corey (1964). Therefore, R^2 values reported in Table 5-2 under the variable precipitation and evapotranspiration condition heading are between UZF-MT3DMS and VS2DT. An option was added to the UZF1 package to simulate capillary-pressure-dependent ET. This approach differs from the original ET formulation described in Niswonger et al. (2006) wherein ET is extracted over the extinction depth interval at a rate limited by the extinction water content or equal to the ET demand divided by the length of the interval, resulting in a demand per unit depth. The need for this option stemmed from the

comparison to VS2DT that also simulates ET in a capillary-pressure-dependent fashion (Lappala et al., 1987).

A noteworthy difference already touched upon between UZF1 and VS2DT that cannot be addressed through additional user options relates to the resolution of infiltrating fronts. Whereas VS2DT uses a finite difference formulation to solve Richards equation for routing flow through the unsaturated zone, the Lagrangian approach of UZF1 results in sharp wetting fronts. Because UZF1 does not simulate capillary-potential gradients, differences between the two solutions become more pronounced when model parameters reflect fine-grained sediment, hence the unsteady-flow benchmark includes simulations with both fine-grained and coarse-grained sediment.

Infiltration amounts were specified such that all of the water infiltrated through land surface, resulting in identical cumulative infiltration for the two models. Similarly, the cumulative ET volume for the sand material was equal between the two simulations, while the total ET over the simulated period was 2% lower in UZF1 for the silt material. The models simulate ET on the basis of the capillary pressure in the root zone and these results provide a rigorous comparison between UZF1 and VS2DT. The simulated ET is very similar between the two models for both the fine- and coarse-grained sediment ($R^2 = 0.94$ and 0.92 , respectively), indicating UZF1 partitions precipitation into ET and deep percolation similarly to the VS2DT numerical solution to Richards equation. Further analysis of the results revealed that the additional 2% of ET predicted by VS2DT was due to a small amount of upward movement of water into the root zone to satisfy ET demand, a process UZF1 does not simulate. The bottom boundary condition was the same as in scenario 1.

To better understand the differences in deep percolation (downward flux through the depth of 150 cm) for the silt simulation ($R^2 = 0.66$), a closer examination of simulated results was made. First, it was discovered that the flux residuals for deep percolation were smaller for the silt simulation relative to the sand simulation (L^2 -norm silt = 1.12 and L^2 -norm sand = 1.55, where the L^2 -norm is sometimes referred to as the Euclidean norm). This was because the magnitude of the ET was much greater for the silt simulation due to water being held up in the root zone, thereby reducing the magnitude of the deep percolation for the silt simulation. Thus, the relative errors for deep percolation were larger for the silt simulation, which results in a lower R^2 value relative to the sand simulation. Because the absolute amounts of water moving through the silt profile are very similar for both the UZF1 and VS2DT models, the concentrations and thus mass breakthrough values also will be similar, as depicted by the R^2 values for concentration breakthrough at 25, 50, and 100 cm equal to 0.99, 0.97, and 0.95, respectively, discussed in more detail below.

Simulated differences between UZF-MT3DMS and VS2DT for mass breakthrough (Figure 5-3a and Figure 5-3b) and concentration breakthrough (Figure 5-3c and Figure 5-3d) are provided at several depths for the silt (Figure 5-3a and Figure 5-3c) and sand (Figure 5-3b and Figure 5-3d) simulations, respectively. Greater differences are observed in the simulation for the silt sediment than for the sand, an expected result because UZF1 neglects the diffusive terms of Richards equation. The effect of this assumption is more conspicuous in the mass breakthrough associated with the silt simulation, although its effects also can be observed in the sand simulation. In the case of the silt simulation mass breakthrough, the highly variable infiltration rates are greatly attenuated in the subsurface due to diffusion associated with capillary pressure gradients that are simulated by VS2DT, whereas this variability is much less attenuated in the

UZF-MT3DMS simulation because capillary pressure gradients are neglected. Despite differences associated with diffusion in water, the timing of and magnitude of mass-arrival simulated by the two models is in close agreement. For the sand simulation, the air-entry pressure is much lower and results in a sharper wetting front as predicted by Richards equation, and the two solutions are in close agreement, which is confirmed by the R^2 statistic (Table 5-2).

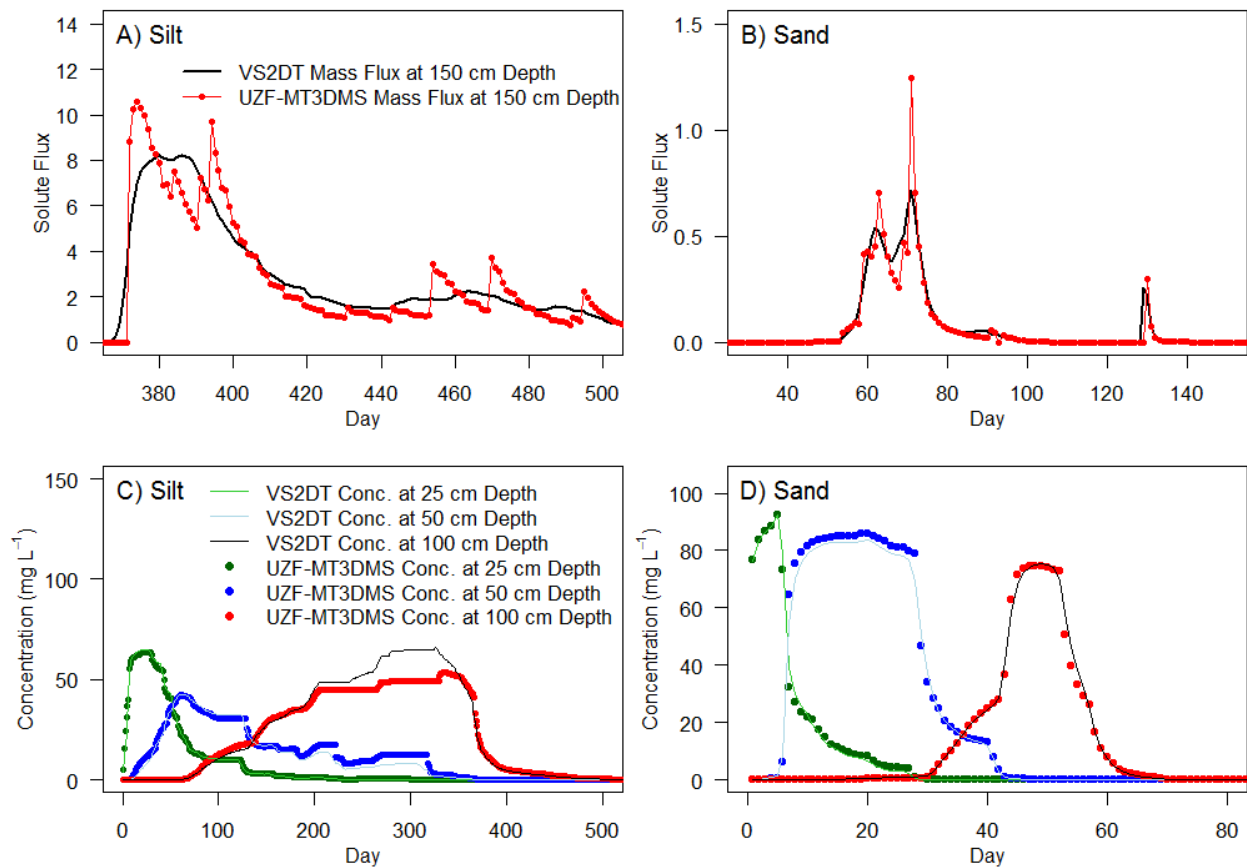


Figure 5-3. Simulated solute fluxes moving past the extinction depth in a (A) silt and (B) sand profile. Simulated concentrations at three depths (25, 50 and 100 cm) in a (C) silt and (D) sand profile.

Differences between UZF-MT3DMS and VS2DT are relatively small, with some exception for the 100 cm depth in the silt simulation (Table 5-2). A more in-depth examination of the silt simulation results (using an animation included as supplemental material available

online only) helped illuminate the cause of the discrepancies between the two solutions that persist during the simulation period from about day 205 to 405 at 100 cm depth (Figure 5-3c). On approximately day 205, the soil profile becomes dry, stalling the advancement of the concentration wave traveling vertically downward through the profile. At approximately the same time, a series of relatively high infiltration amounts were applied to the soil surface (Figure 5-2). The leading edge of the wetting front passes the 100 cm depth in VS2DT on about day 240, corresponding to the observed increase in concentration due to the wetting front pushing solute from higher in the profile down with it. In UZF-MT3DMS, however, pore space drainage due to decreased infiltration reduces the magnitude of this sharp wetting front above 100 cm, resulting in only a slight increase in concentration at 100 cm on about day 260. The sudden jump in concentration observed in both models on about day 330 corresponds to a relatively large wetting front moving through this depth, carrying the peak of the concentration wave with it. While small differences in the timing of concentration arrivals are evident, the overall magnitudes in both the silt and sand simulations suggest the models are in fact quite similar. For example, the total mass breakthrough at the 150 cm depth predicted by VS2DT and UZF-MT3DMS was 418.4 mg and 420.9 mg, respectively, a 0.6% discrepancy after two years. This demonstrates that although small differences in timing may be present, the two models predict nearly the same loading through the root zone, or below the 150 cm depth.

Results from the sand simulation with UZF-MT3DMS closely match predictions of VS2DT using Richards equation coupled with the advection-dispersion equation. Total mass breakthroughs at 150 cm depth also were checked for the sand simulation and again discrepancies between the two models were found to be small: VS2DT and UZF-MT3DMS

predicted 162.6 mg and 162.8 mg migrated past the 150 cm depth, respectively, a 0.1% discrepancy from each other.

5.4.3 Scenario 4: Nonlinear Equilibrium Sorption

Scenario 4 compares simulated results to analytical benchmarks with nonlinear equilibrium-controlled sorption. The Freundlich isotherm was used to simulate sorption in this problem. Because the shape of the concentration front remains constant with time, the analytical benchmark is provided for transformed depth coordinates (Figure 5-4a). Coordinate transformations were made using Equation 55 of Vanderborght et al. (2005). In order to make comparisons of the advancing front through time, results from UZF-MT3DMS and VS2DT simulations were compared at 20, 40, and 60 days (Figure 5-4b). R^2 values indicate that UZF-MT3DMS performs well under nonlinear transport conditions (Table 5-2). The R^2 values continue to improve with time, indicating that the shapes of the simulated concentration fronts have not yet reached the asymptotic analytical solution early in the simulation.

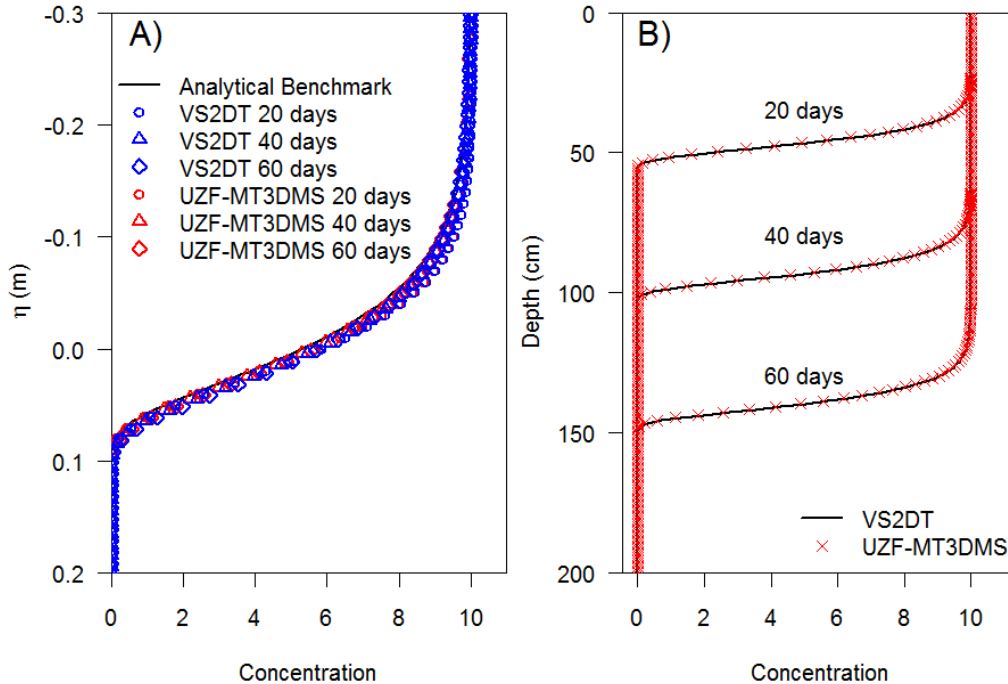


Figure 5-4. (A) Concentration-depth profile (using a transformed depth coordinate, η) for a nonlinearly sorbing solute, and (B) concentration 'fronts' moving through an unsaturated profile through time. The analytical benchmark of (A) published in Vanderborght et al. (2005).

5.4.4 Scenario 5: Nonequilibrium Sorption

Scenario 5 tests how well the modified MT3DMS model simulates linear non-equilibrium (rate-limited) controlled sorption by also comparing simulated results to a published analytical benchmark. A steady flow regime interrupted after 20 pore volumes (200 hours) was used. As described in Vanderborght et al. (2005), the stop-flow period was long enough to allow the dissolved and sorbed phases to equilibrate, after which flow was restarted.

Immediately prior to the stop flow period, dissolved and sorbed concentrations compare well with the analytical benchmarks based on R^2 values greater than 0.9 (Figure 5-5a; Table 5-2). During the stop flow period, dissolved concentrations increase such that when flow was restarted, a slight increase in the effluent concentration at 10 cm was observed. Peak concentrations in the UZF-MT3DMS breakthrough curve during the first 10 hours of the model

run (1 pore volume) were less than those predicted by the analytical benchmark (Figure 5-5b). This may be due in part to the extremely high jump in concentration (0 to 100,000 to 0) of the infiltrating fluid and associated numerical difficulties in advancing such a sharp front.

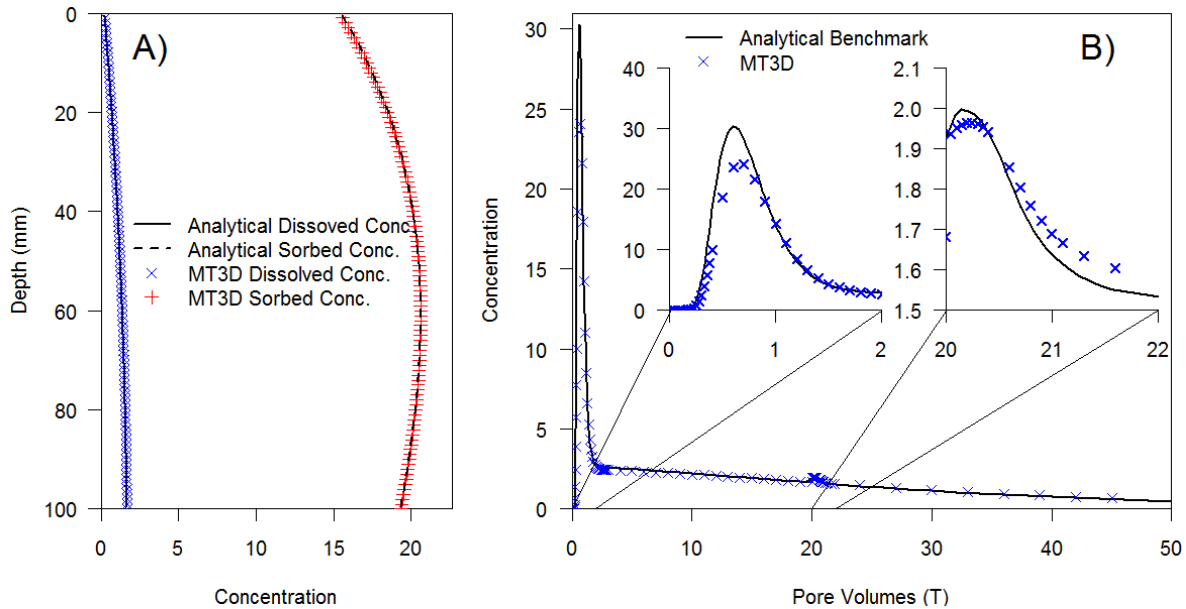


Figure 5-5. (A) Dissolved and sorbed concentrations in a 10 cm profile at 200 hr after a ‘pulse’ injection of a nonequilibrium sorbing solute. (B) Breakthrough concentrations at 10 cm with time depicted as pore volumes. Under the flow conditions listed in Table 5-1, one pore volume is equal to 10 hours. At 20 pore volumes flow was interrupted to allow the dissolved and sorbed concentration to equilibrate, after which flow was restarted. The published analytical benchmarks are from Vanderborght et al. (2005).

5.4.5 Scenario 6: Two-Dimensional Benchmark Simulation

Figure 5-6 shows the two-dimensional setup used in the UZF-MT3DMS and VS2DT models. In this problem, a 10 m wide by 5 m deep simulation domain with 0.25 m by 0.25 m grid cells was set up in both models, with results from VS2DT taken as the benchmark. Boundary conditions include a 1.625 m constant head on both sides of the domain, a specified flux of 0.1 m d^{-1} along the top of the simulation domain, and a no flow condition along the bottom boundary. Volumetric water content in the unsaturated zone was initially set to just

above residual ($\theta = 0.105$). A concentration of 1 mg L^{-1} was applied over 2.5 m (the middle 10 columns) of the surface of the domain at the beginning of the modeled period coinciding with the formation of the infiltrating wave that reached the water table during day eight of the simulation. This set of conditions was chosen primarily to investigate how well UZF-MT3DMS-predicted concentrations correspond to the VS2DT solution as the water table rises into the unsaturated zone.

Slight differences in the simulated water table elevations can be seen where it dips into a lower layer and is likely the result of the Newton solver in UZF-MT3DMS using upstream weighting to calculate the inter-cell conductance terms. Thus, the observed differences in the saturated zone concentration are likely due, at least in part, to the slight differences between the flow solutions as the water table mounds. Figure 5-6 shows close agreement between the two solutions in the unsaturated zone while R^2 statistics (Table 5-2) indicate an excellent fit ($R^2 = 0.999$) between UZF-MT3DMS and VS2DT.

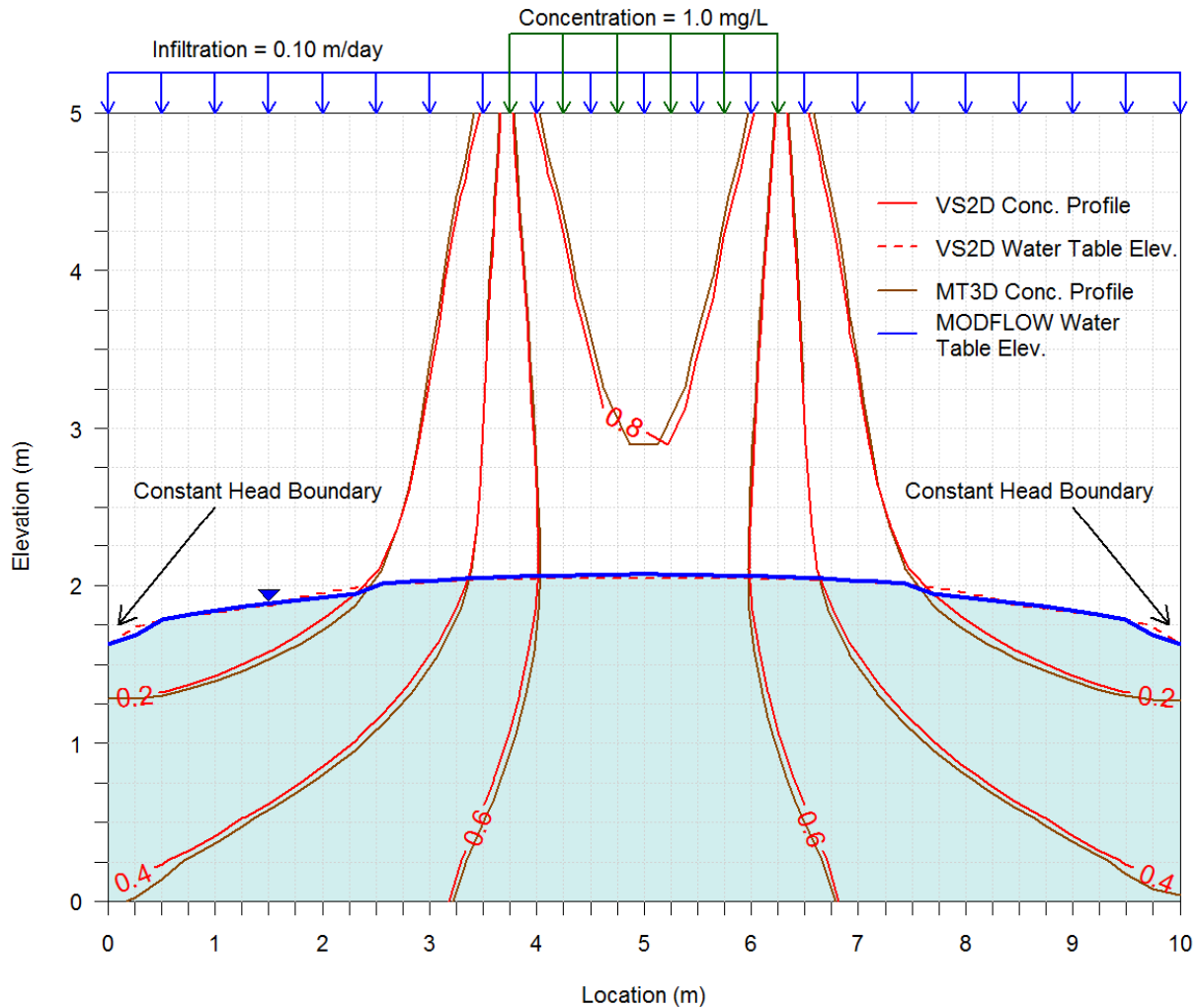


Figure 5-6. A 2-dimensional benchmark problem was established using results from the U.S. Geological Survey’s VS2DT model after 60 days. Comparisons in the unsaturated zone are very close with some differences appearing in the saturated zone and may be a result of slight differences in the location of the water table as mass begins to move laterally.

5.4.6 Scenario 7: Three-Dimensional Benchmark Simulation

The final UZF-MT3DMS benchmark (scenario 7) was designed to test the modified model in three dimensions and perform a preliminary investigation of the amount of time savings possible with UZF-MT3DMS at larger scales. A horizontal grid discretization of 100 m by 100 m and assorted vertical discretizations (described in more detail below) were used. The model domain stretches 8,000 m by 4,000 m by 15 m and is shown in Figure 5-7. Results from UZF-

MT3DMS were compared to 3 Richards-based models, including HYDRUS, SUTRA and CATHY/TRAN3D. The model domain has a 0.001 m slope along the 4,000 m side of the model domain. In addition, a constant head boundary was applied to the ‘uphill’ side and set equal to an elevation of 42 m. A constant head of 32 m was applied to the ‘downhill’ side of the model and no-flow boundaries were applied to the other two sides as well as to the bottom of the domain (Figure 5-7). Aquifer properties are homogeneous throughout the model domain and provided in Table 5-1. Infiltration rates varied on a monthly stress periods basis (see Table 5-1, scenario 7). ET was not simulated. A hypothetical spill was situated on a 2 km (rows 31 through 50) by 1 km (columns 21 through 31) section in the middle of the model.

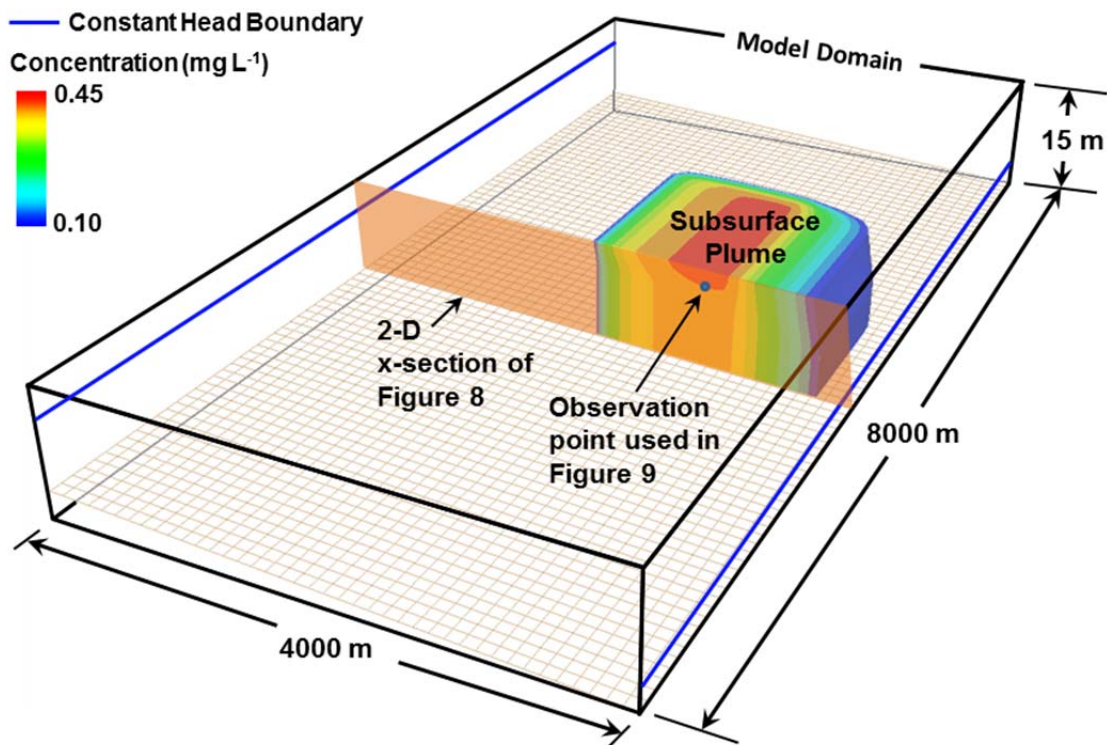


Figure 5-7. Perspective plot of 3-dimensional model showing location of cross section provided in Figure 5-8 (not to scale) and observation point of Figure 5-9.

Results from the simulations of the four models are displayed in a cross-section plot after 2 years (Figure 5-8) and several time series plots for a point 3m below ground surface (Figure 5-9). A limited number of contours are displayed on the cross-section to help reduce clutter. Minor differences between all four simulations are evident. SUTRA and CATHY/TRAN3D compare well at the 0.095 isoconcentration level while UZF-MT3DMS closely matches results

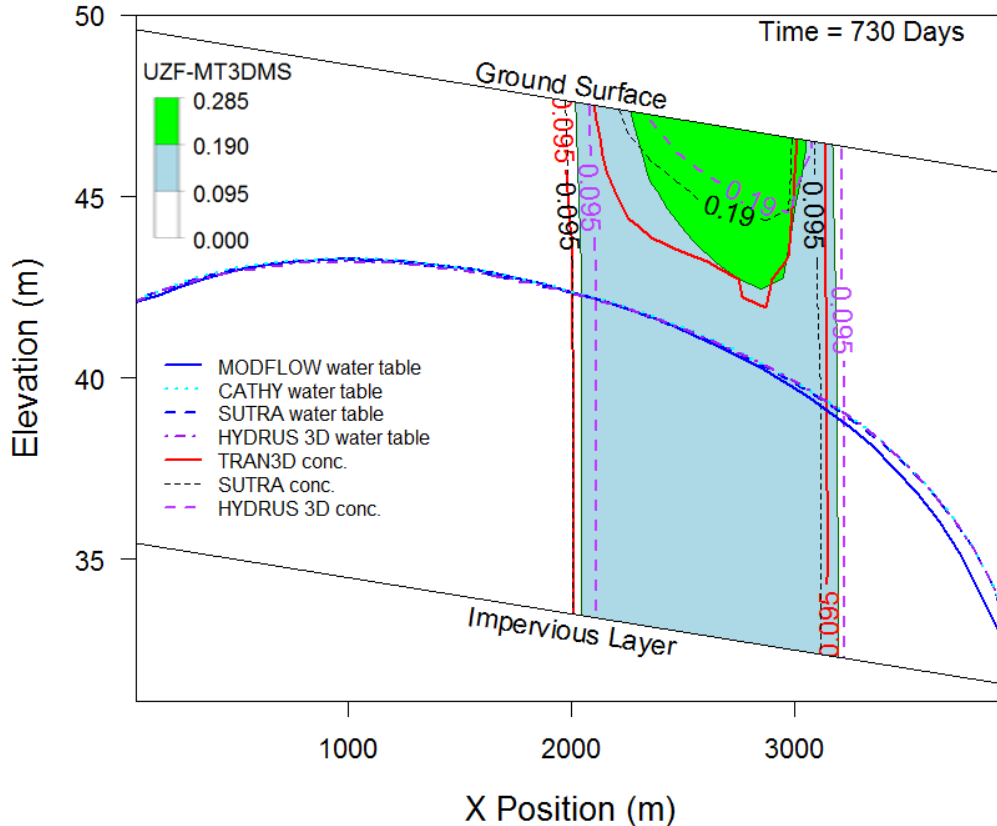


Figure 5-8. Cross sections comparing simulated extents of select isoconcentration contours after 730 days. UZF-MT3DMS concentrations are depicted by the color-filled contours while HYDRUS, TRAN3D, and SUTRA contours are shown by the lines described in the legend.

from HYDRUS. A larger degree of discrepancy is observed at the 0.190 isoconcentration level, with UZF-MT3DMS matching TRAN3D results the closest. Inter-model R^2 comparisons ranged between 0.924 (HYDRUS-SUTRA) and 0.992 (TRAN3D-SUTRA). Differences between the 0.095 and 0.190 isoconcentration lines could be the result of a number of factors, including 1)

different solution techniques (i.e., finite-difference vs. finite-element), 2) use of different governing equations (i.e., groundwater flow equation vs. Richards equation), 3) alternative approaches to the solution of longitudinal and transverse dispersivity, 4) an artifact of the interpolation technique used to plot the results, and 5) a difference in the number and position of the nodes where flow and transport fields were calculated. With these reasons in view, the UZF-MT3DMS solution appears to be corroborated by HYDRUS, SUTRA and CATHY/TRAN3D.

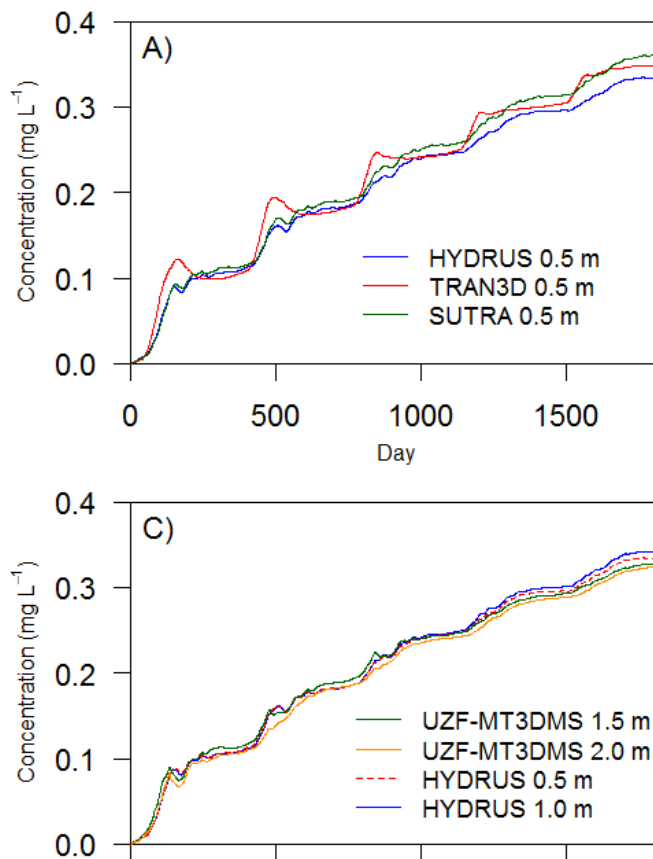


Figure 5-9. Concentration time series comparison for a point 3 m below the ground surface (Figure 5-7) were made between (A) three models that solve Richards equation using 0.5 m vertical discretization, and (B) two coarse UZF-MT3DMS vertical discretization schemes and two alternative vertical discretizations of HYDRUS.

Significantly shorter model runtimes were observed when running the UZF-MT3DMS simulation (Table 5-3). For both the 0.5 and 1.0 m vertical discretizations, HYDRUS was the second fastest simulation and took roughly 3 times as long to finish the simulation. Even greater time savings were found by coarsening the vertical discretization in UZF-MT3DMS to 1.5 m and 2.0 m (UZF-MT3DMS ran in less than one quarter of the time and nearly one-tenth of the time as HYDRUS, respectively) without significantly altering the solution (Figure 5-9b). A comparison of model results at an observation point located 3m below the surface (Figure 5-7) revealed a greater degree of variability between the Richards-based models (Figure 5-9a, where R^2 ranged between 0.966-981) than between the four alternative discretizations of UZF-MT3DMS ($R^2 > 0.979$ for all comparisons). Furthermore, the UZF-MT3DMS simulation using 1.5 m and 2.0 m vertical discretizations compared very well with the 0.5 m ($R^2 = 0.996$ and 0.991 , respectively) and 1.0 m ($R^2 = 0.993$ and 0.985 , respectively) HYDRUS simulations (Figure 5-9b). Attempts were not made to coarsen Richards equation-based solutions beyond 1m due to concern about the solution accuracy (Downer and Ogden, 2004, Simunek, personal communication, 2012; Vogel and Ippisch, 2008). In the event of more complex boundary conditions, such as the daily precipitation and evapotranspiration stresses used in scenarios 2 and 3 (Figure 5-2), the 1 m discretization for the three Richards equation-based models would likely need to be reduced.

It is important to recognize that although UZF-MT3DMS may be faster for this application, the selected models used to compare with would outperform UZF-MT3DMS in other situations. For example, UZF-MT3DMS cannot accommodate heterogeneity or two- and three-dimensional flow in the unsaturated zone. Thus, in settings with perched water tables or a need for highly resolved site-scale investigations, modelers would likely want to select a model

other than UZF-MT3DMS. Furthermore, model runtime differences should be viewed in light of the differences in governing equations, numerical solutions (i.e. finite difference vs. finite element approaches), and levels of discretization.

5.5 CONCLUSIONS

Several example problems have demonstrated that recent modifications made to MT3DMS extend its simulation capabilities to the unsaturated zone. By using the computationally efficient kinematic-wave approximation for unsaturated flow in the UZF1 package, the benefits of the UZF-MT3DMS coupling are manifold. First, existing MODFLOW models supporting MT3DMS transport models need only invoke the UZF1 package to extend their study domains to the unsaturated zone, alleviating the need to switch modeling venue. Given the wide-spread use of MODFLOW and MT3DMS, this option supports the natural evolution of model development. That is, UZF-MT3DMS facilitates extension of calibrated and tested saturated-zone models to also include the unsaturated zone as site-related concerns and questions grow ever-more complex. Second, users seeking to simulate unsaturated-zone flow can access the full suite of MT3DMS reaction capabilities depending on the complexities at their respective sites. Third, as demonstrated in scenario 7, the model is effective and efficient as a numerical tool for larger scale problems (i.e. km²). Should regional-scale models include large tracts of coarse sand and gravel material that often pose numerical difficulties for solutions involving Richards equation at discretizations typical of regional-scale problems (Van Dam and Feddes, 2000), UZF-MT3DMS immediately stands out as an attractive option for problems involving coarse-grained material. The flexibility afforded by the modular approach to MT3DMS allows users to code additional transport modules as understanding of the chemistry and biology in the unsaturated zone is enhanced. Potential users of UZF-MT3DMS will need to

weigh the accuracy-for-efficiency tradeoff for their specific applications. This work, however, has demonstrated that the UZF-MT3DMS model provides reasonably accurate solutions of variably saturated flow and transport. That is, results from UZF-MT3DMS match well with results from the numerical solution of Richards equation based flow solutions coupled with the advection-dispersion equation, showing that sacrifices in accuracy are small. On the other hand, potential for significant time savings was found while running the 3D benchmarks. Time savings are critical during automated calibration procedures when the number of estimable parameters in regional-scale simulation studies is high.

Table 5-3. Model runtimes for MODFLOW/MT3DMS and CATHY/TRAN3D are calculated as the sum of the flow and transport solutions. HYDRUS and SUTRA simultaneously solve flow and transport and are therefore reported as a single value.

Model Runtimes [†] (hh:mm:ss)								
Vertical Discretization	MF-UZF1	MT3DMS	Total	CATHY	TRAN3D	Total	HYDRUS	SUTRA
0.5 m	0:18:38	0:17:50	0:26:28	1:17:51	0:33:43	1:51:34	1:36:47	> 2:00:00
1.0 m	0:09:38	0:08:41	0:18:19	0:33:56	0:29:15	1:03:11	0:52:20	> 2:00:00
1.5 m	0:06:04	0:05:40	0:11:44					
‡2.0 m	0:02:42	0:02:51	0:05:33					

[†]Model runtimes based on 1 forward run of each model on a Xeon X5650 @ 2.67GHz.

[‡]Discretization in the unsaturated zone is equal to 2 m, and is >2 m in the saturated zone

6 SIMULATING SALT TRANSPORT IN THE LOWER ARKANSAS RIVER VALLEY WITH UZF-MT3DMS

6.1 INTRODUCTION

Dissolved salt concentrations (hereafter, “salt” is assumed to be equivalent to total dissolved solids) in the surface and groundwater of Colorado’s LARV have been at disturbingly high levels for a long period of time. Nearly 50 years ago, Odell et al. (1964) documented an increase in the concentration of river flow from 500 mg L⁻¹ near Pueblo to more than 4,000 mg L⁻¹ at the Colorado-Kansas state line, a trend that continues today (Miller et al., 2010). Although current water management practices may be able to continue without further exacerbating the salinity levels in the Arkansas River, average annual economic losses due to waterlogging and salinization associated with these practices are an estimated US\$4.3 million per year (Houk et al., 2006). Furthermore, dissolved selenium (Se) and uranium (U) levels, which are strongly correlated with salinity, exceed Colorado Department of Public Health and Environment (CDPHE) standards (Gates et al., 2009). Finally, a status-quo approach does little to address the long-term need for restored or improved crop production on waterlogged and salinized land in support of forecasted population growth.

High groundwater salinity concentrations within the LARV may well be “in a state of long-term dynamic equilibrium” (Konikow and Person, 1985). To demonstrate this, Konikow and Person (1985) plot groundwater salinity concentrations extending back to 1895 for a region below the Fort Lyon Canal [northeast of the city of La Junta (Figure 6-1)] in Figure 13 of their report. Analyses of salinity concentrations between sampling periods revealed no statistically significant differences. Nearly three decades later, observed groundwater concentrations persist

within the range observed by Konikow and Person (1985). For example, time series of observed groundwater salinity concentrations collected in CSU monitoring wells located within the Konikow and Person (1985) study area remain roughly equal to those observed over the last century [e.g., Figure 4d (well 70) in Burkhalter and Gates (2005) and in the following results presented herein].

A similar dataset for soil water salinity, one that extends back to the turn of the 20th century, has not been found in the literature for the LARV. However, Morway and Gates (2012) provide an assessment of the extent and severity of soil water salinity in the LARV extending back to 1999. As with the observed groundwater concentrations, soil water salinity concentrations have remained at or above threshold levels for crop yield reduction throughout much of the LARV.

The high concentrations in the soil root-zone salt are sustained by two sources. River flows that enter the LARV from Pueblo Reservoir, albeit with dilute salt concentrations, are diverted downstream into irrigation canals and distributed to cultivated fields. More than 100 years of intense irrigation in the semi-arid LARV have led to evaporative concentration of these salt-laden flows, thereby salinizing farm fields throughout much of the region. Moreover, recharge resulting from inefficient irrigation practices, canal seepage from unlined earthen delivery canals, and inadequate drainage facilities has created shallow groundwater tables throughout much of the LARV. Once saline shallow groundwater tables are in place, the upward movement of salts transported by capillary upflow (hereafter referred to as ‘upflux’) further exacerbates soil salinization. The magnitude of salt upflux depends on a number of additional factors, including soil properties, crop root distribution, and irrigation practices.

As root zone salt concentrations rise, some dissolved solutes will begin to precipitate out of solution. In the LARV, precipitated salts are predominantly in the form of gypsum and calcite and are likely present over much of the Valley. The amount of mass already in solid-phase storage may have important implications for alternative management interventions that would significantly alter flow conditions in the Arkansas River Valley. Noting the long-term dynamic equilibrium of salt loads in the LARV, significant shifts in water management practices would perturb the system and disrupt this equilibrium (Konikow and Bredehoeft, 1974a; Konikow and Bredehoeft, 1974b). For example, under alternative management practices described in Section 4.6, shifts in relative ET losses (Figure 4-11) would alter soil water contents. With more or less soil water present, long-term salt precipitation and dissolution patterns would be subject to perturbation.

Another source of salt in the LARV is dissolution from shale layers (Pierre Shale, Niobrara Shale, Carlisle Shale, and Graneros Shale) that underlie and outcrop both inside and outside the irrigated lands of the LARV. As oxygenated precipitation and irrigation water comes in contact with shale and weathered shale located throughout the LARV, salts within the shale material dissolve, and may further exacerbate groundwater concentrations (Wallender and Tanji, 2012). The relative magnitude of this source of salt remains uncertain and is not a focus of this report. Salt loads carried in the Arkansas River, as described in Miller et al. (2010) and expanded upon in Section 6.4.2.3 below, remain approximately uniform along the river during all but the wetter years, supporting the theory that a dynamic equilibrium has been achieved. Years showing an increase in salt load along the river are suggestive of short term perturbations within the long-term “dynamic” equilibrium.

Neither chemical precipitation nor dissolution of salts (including weathering of shale) is directly addressed in the conceptual and numerical models developed and documented here. Instead, a conservative salt transport model is employed as an important *first step* for informing the need for and the possible later use of a reactive transport model. The extent to which the numerical model simulations are unable to match observations (i.e., groundwater salinity concentrations, soil water salinity concentrations, and subsurface salt return loads to the river), may suggest the relative importance of these chemical reaction processes in determining the fate and transport of dissolved salt in the LARV.

6.2 LITERATURE REVIEW ON SALT TRANSPORT UNDER IRRIGATED CONDITIONS

The literature is replete with examples of numerical models equipping decision makers with valuable insights on groundwater system responses to proposed interventions to lower salinity in irrigated areas. For example, Singh (2010) used the SWASALT (Simulation of Water and SALT) finite difference model, an extension of the finite-difference code SWATRE (Feddes et al., 1978; Belmans et al., 1983), which solves the 1D Richards equation in the flow domain and the advection-dispersion equation for the salt transport problem, to explore the effects of various irrigation strategies [e.g., surface water alone (0.4 dS m^{-1}), groundwater alone (10 dS m^{-1}), a blended mixture of surface water and groundwater, and finally alternating applications of surface water and groundwater] and crop rotation combinations on ET efficiency, soil water storage, and soil water salinity. The model accounts for diminished ET due to excessive soil water salinity, drought, or waterlogging. Results demonstrated that groundwater with a concentration of 10 dS m^{-1} can be used safely for irrigation over long periods under certain crop rotations (e.g. mustard-millet rotation) provided it is blended with less saline canal water. In a

similar study, Mandare et al. (2008) apply the finite-different model Soil-Water-Atmosphere-Plant (SWAP) (van Dam et al., 1997) to three agricultural field sites located in northwest India where waterlogging and salinization are prevalent. Investigated scenarios include changes in applied irrigation depths, mixing of poorer quality groundwater with higher quality (but scarce) canal water, and combinations of these. Results compare the effect of various blends of surface water (good quality) and groundwater (poorer quality) on crop yields and soil water salinity. Chemical reactions were not considered.

Facing increased water demand in an irrigated basin located in arid Northwest China, Jiang et al. (2011) used SWAP to study the long-term impacts of “sufficient” versus deficit irrigation with saline water to better understand the onset of soil salinization. Simulated model results were calibrated against observations of soil water content, soil water EC, and leaf-area index (LAI) collected from a randomized split-plot design with three levels of irrigation applications and three levels of irrigation water salinity. After calibration, models were run forward in time and results demonstrate that increases in salt concentrations in the soil water accompanied decreased irrigation applications with increased salinity (saltier irrigation water). The researchers also concluded that severe deficit irrigation decreased the depth at which maximum salt accumulation occurred. The impact of deficit irrigation and accompanying soil salinization on wheat yields was evaluated in separate work (Jiang et al., 2012), wherein irrigation water salinity of 3 dS m^{-1} was found not to reduce wheat yield by any statistically significant amount. Jhorar et al. (2009) used the distributed irrigation water management model FRAME, itself a combination of two models, Simulation of Water management in Arid REgions (SIWARE) , which handles canal and on-farm management (Sijtsma et al., 1995), and the bucket-type model Standard Groundwater Model Package (SGMP) for simulating regional

(4,800 km²) groundwater flow (Boonstra and de Ridder, 1990), to investigate the impact of four alternative water management scenarios on ET (used as a measure of crop yield) and D_{wt} (used as a measure of waterlogging risk). SIWARE attempts to maintain a soil water balance by first calculating ET demand and then distributing surface and groundwater irrigation supplies to meet this demand. SIWARE requires user-specified soil water retention parameters (e.g., water content at field capacity, θ_{fc} ; water content at wilting point, θ_{wp}) to operate. SGMP simulates saturated groundwater flow and provides SIWARE with calculated values of D_{wt} . The two models are loosely-coupled, with data exchanges occurring at the end of each time step. Reduced ET due to osmotic stress associated with soil water salinity is accounted for. Here again, the scenarios included different groundwater and surface water mixing ratios. Decreased use of irrigation water, which often raises soil water salinity due to decreased leaching, did not result in appreciable gains in soil salinity due to leaching by natural rainfall. Jorenush and Sepaskhah (2003) used the Transient State Analytical Model (TSAM) to solve 1D transient flow and salt transport to evaluate capillary rise and salinization of soil profiles across a range of D_{wt} and groundwater salt concentrations in both irrigated and non-irrigated settings. Model results were compared to observations from a micro-lysimeter (Sepaskhah and Karimi-Goghary, 2003). To obtain a good fit between simulated and observed values, the TSAM model was modified so that a variable root depth and non-uniform root water uptake pattern could be simulated. With these enhancements, simulated soil water salinity profiles fit well for a variety of D_{wt} values (0.3–1.20 m) and irrigation water salinity levels (0.5-13.0 dS m⁻¹). Xu et al. (2008) compare observations of EC from soil columns planted with wheat to predicted results from the finite-different model Soil Water and Salt Transport Model (SWSTM) (Xu et al., 2005) and found good agreement between simulated and observed values. The 1D model simulates water and salt

movement through the unsaturated zone using Richards equation and the advection-dispersion equation for flow and solute transport, respectively. Water and salt uptake occurs in the presence of vertically distributed root mass within the root zone. Scenarios investigating the impact of different D_{wt} values were run and verify higher root zone soil water salinities under shallower water tables. The 1D SWSTM model was then applied to a number of locations in a catchment-scale problem in Northern China (Chen et al., 2011).

In the Murray Basin of southern Australia, the 1D physically-based, distributed-parameter WATER Vegetation Energy and Solutes WAVES model (Dawes and Short, 1993) was used for simulating the energy, water, carbon (plant growth), and solute balances and was compared to lysimeter results (Zhang et al., 1999). The impact of a saline groundwater table on leaf area index (LAI), ET rates, and amount of upflux to plant water supply was evaluated. Although a detailed description of the impact of groundwater salinity on key system dynamics [i.e., LAI (as an indicator of crop yield), reduction of ET, etc.] is offered, and confidence is expressed in the ability to design appropriate irrigation management schemes to ensure long-term sustainability of Lucerne, the study is restricted to a plot-scale (1.2×1.45 m) evaluation.

Schoups and Hopmans (2002) present a 1D analytical model for simulating flow and salt transport through the unsaturated zone that assumes a time-invariant leaching fraction and neglects hydrodynamic dispersion. Two important calculated outputs of their model include salt flux at a selected depth accounting for upward flow and transport and average root zone salt concentration. The analytical solution revealed that the average root zone salt concentration and predicted salt fluxes were similar when using depth-varying soil water profiles or equivalent average uniform soil water content. Use of an equivalent average soil water content enables rapid solution of travel times through the unsaturated zone thereby fulfilling its intended

application: to use local-scale 1D representation of transport processes for predicting long-term impacts of salinization.

Although helpful for demonstrating the effects of certain management practices at the field-scale, the *cumulative* impact over much larger scales is harder to predict due to the computational challenge that arises when simulating the previously-described detail over broad areas. To address this concern, Schoups et al. (2006) investigate the impacts of three model simplifications on the prediction of long-term soil water salinity and transport dynamics in the unsaturated zone. To overcome computational challenges, the investigators pursue a complex, 1D baseline simulation and compare results from alternative models that include simplifications and extend their findings to larger-scale (field to regional) models. Using the 1D UNSATCHEM model (Šimunek et al., 1996), the authors quantify average root-zone salinity and cumulative annual drainage salt load (i.e., salt load across the bottom of the root-zone) over a 10 year period for baseline simulations that include daily water stresses, 1 cm vertical discretization, and complex salt chemistry for a variety of water table depths, leaching fractions, soil gypsum content, groundwater salinities, with and without soil chemical reaction simulated. Next, various modeling simplifications, including (1) resolving averaging boundary conditions into an annual stress (i.e., daily stresses were averaged for an equivalent annual stress), (2) increasing vertical discretization from 1 cm to 15 cm, and (3) simplifying the complex salt chemistry simulated in the baseline models, were made and simulated results were compared to baseline simulations. Prediction of root-zone soil water salinity by time averaging the boundary conditions resulted in differences typically less than 20% for the 12 investigated scenarios, which include gradations of the three aforementioned simplifications [Table 4 in Schoups et al. (2006)]. Decreasing the vertical resolution of the model did not appreciably impact predicted results. Salt chemistry that

accounts for cation-exchange and gypsum dissolution-precipitation but that simplifies the complex salt chemistry outlined in Table 1 of the paper also resulted in adequate simulation of chemistry dynamics in the root zone. Large differences in predicted average root-zone soil water salinity and annual drainage salt load resulted if cation-exchange and gypsum dissolution-precipitation were not simulated. The authors conclude that in many cases, daily time step models with fine grid discretization (1 cm) and complex salt chemistry can be replaced by models with annually-averaged boundary conditions, relatively coarse vertical discretization, and simplified chemical reactions that include cation exchange and gypsum dissolution-precipitation only. The differences in predicted root-zone soil water salinity and drainage salt load resulting from these simplifications are likely small compared to the uncertainty in model predictions associated with parameter uncertainty.

Shah et al. (2011) present a framework for evaluating root-zone soil water salinity dynamics that does not rely on physically-based distributed-parameter models. Instead, their conceptual model assumes a homogenous root zone of a given thickness, a constant porosity, and a known D_{wt} , while also considering the impact of salt on the water balance [considering salt's impact on the water balance is what separates this work from that of Vervoort and van der Zee (2008)], to evaluate salt accumulation in the root-zone. Fluxes through the root zone and the associated impacts on salinity are evaluated analytically for 1D profiles with varying characteristics. In this way, a rapid assessment of root zone salt accumulation can be made, thereby avoiding the computational expense of numerical approaches. Results show that although the upward transport of salts into the root-zone is larger if the upward water flow rate is larger, the wetter root-zone that results (due to the transpiration limiting presence of salt) becomes more prone to leaching from irrigation and precipitation. Thus, long-term root zone

soil water salinity in the presence of a shallow water table is driven by non-linear relationships with capillary upflow, not solely on “monotonic” relationships with hydraulic conductivity, groundwater table depth, or climate boundary conditions.

A 400,000 ha swath of irrigated land along the west side of the San Joaquin Valley of California suffers from waterlogging and salinization. Installation of sub-surface drainage for lowering saline shallow water tables and reducing salinity is prohibited since no economically or environmentally feasible method for disposal of saline drain water exists (Hanson et al., 2008). Thus, better irrigation management may be the only means by which to combat these problems since current practices are not sustainable (Schoups et al., 2005b). Hanson et al. (2008) used HYDRUS-2D (Šimůnek et al., 1999) simulations to investigate the use of drip irrigation to adequately leach salt from soils. Among the scenarios investigated, larger but less frequent irrigation events using drip systems resulted in quicker salt mitigation than did smaller more frequent irrigation applications. Further south, in the Santa Clara River basin east of Los Angeles, elevated chloride concentrations resulting from increased discharge from water treatment facilities has placed parts of the river, including an agricultural area in a subbasin of the study area, on California’s list of impaired waters due to chloride. An integrated groundwater and surface water model capable of simulating both flow and transport was developed using the physically-based, distributed parameter finite-difference MODflow Hydrologic Modeling System MODHMS (HydroGeoLogic, 2000; Panday and Huyakorn, 2008). Although no alternative management interventions were specific to agricultural practices (focus was instead placed on enhanced treatment of recycled water and locations of effluent outfall), the impact of increased use of water laden with chloride on agriculture was considered (Panday et al., 2009).

Howitt et al. (2010) discuss a simulation model named the Statewide Agricultural Production Model. Developed specifically for California, it simulates agricultural production, water use, and the economics associated with each to evaluate the costs and benefits of various policies and environmental changes. An application of the model that incorporates water quality was made on the west side of the San Joaquin Valley. Current soil salinity is quite high in this region and the spatial extent of lands severely impacted by soil salinization is forecast to increase by 12 to 15 percent. The model projects that the associated revenue reduction from crop productivity losses due to increases in salinity will be on the order of tens of millions of dollars.

Using a generic framework, Vico and Porporato (2011) assess the feasibility of different irrigation schemes (i.e., surface, sprinkler, and “micro-irrigation”) by assessing the sustainability, productivity, and profitability associated with each approach but do not explicitly account for the mal-effects associated with salinization. They reference Hillel (2000) in pointing out that efforts to conserve water may be negated by the need to flush the soil of salt with large leaching applications, making water conservation unsustainable over the long term.

Concerned that models like HYDRUS (Vogel et al., 1996) and MIKE-SHE (Bathurst, 1986) over-simplify land-surface processes, Xu and Shao (2002) couple the Atmosphere and Land Surface Interaction Scheme ALSIS (Irannejad and Shao, 1998), which solves the 1D Richards equation for simulating unsaturated-zone flow, to MODFLOW, claiming a more robust handling of vegetation type, vegetation height, and leaf-area index to better describe the soil hydrological and thermal processes of the unsaturated zone. Xu and Shao (2002) develop a companion salt transport code for ALSIS and apply the coupled system to the salt-affected Wakool region of Australia. The authors corroborate previous work demonstrating that irrigation with fresh water is an effective salt reducing measure in the root zone, that irrigation

with saline groundwater should be avoided if possible, and finally, that the spatial distribution of salt mass in the root zone is correlated with the spatial distribution of D_{wt} .

Clearly, a large and diverse suite of modeling tools exists for simulating shallow saline groundwater flow and salinity, soil salinization, and salinity impacts on crop production. Many of these modeling tools, equipped with nuances intended to accurately simulate various components of the physical system they purport to represent, cannot be applied at regional-scales. A number of papers cite the limitations of such application of physically-based solute transport models, from data deficiencies (Hajhamad and Almasri, 2009; Basile et al., 2012) to lengthy simulation times (Suweis et al., 2010) and go on to recommend an alternative lumped-parameter approach, of which there are many. However, because lumped-parameter models may not accurately predict system-wide responses to altered stresses, they are not pursued. The following reviews highlight the usefulness of regional-scale, physically-based, distributed parameter models.

Gates and Grismer (1989) developed a regional-scale finite difference groundwater flow and salt transport model that simulates water table behavior in an intensely-irrigated portion of the Western San Joaquin Valley (WSJV), California. Economic loss resulting from the buildup of salts in the root zone of agricultural fields plagues the WSJV as it does the LARV. The developed model accounts for many of the flow and salt transport processes common to areas experiencing the negative economic impacts of waterlogging, salinization, salt loading, and non-beneficial consumptive use. An important goal of the research was to provide a tool capable of determining the "economically optimal irrigation and drainage strategies for long-term regional management" (Gates and Grismer, 1989). To this end, researchers found that an irrigation efficiency of 78% and a drainage efficiency of 91% produced the optimum balance between the

economic benefit resulting from increased crop yield with the associated costs of infrastructure improvements capable of supporting the conditions needed to achieve higher yields. The research was carried out in a stochastic context that allowed for the calculation of confidence bands on select model output (e.g. the aforementioned efficiencies achieved an economic benefit of \$162/ha·yr (\pm \$11/ha·yr at the 95% confidence level).

Flow models developed for the LARV (Gates et al., 2002; Burkhalter and Gates, 2005; Burkhalter and Gates, 2006) and summarized in Chapter 5 provided flow terms for a finite-difference model using the popular Mass Transport in 3 Dimensions for Multiple Species (MT3DMS) (Zheng and Wang, 1999a) model. Gates et al. (2002) documents a steady-state salt transport model that neglected hydrodynamic dispersion and chemical reactions. A transient salt transport model formulation followed (Burkhalter and Gates, 2005) that relied on the same assumptions as in the steady-state simulation but used a customized unsaturated-zone module to estimate salt concentration of the soil water in the unsaturated zone using the mass-balance described in Gates and Grismer (1989). Once baseline salt concentrations over the entire regional-scale study area were established through calibration and testing of the MT3DMS model (Burkhalter and Gates, 2005), Burkhalter and Gates (2006) compare the relative impacts of “potential solution alternatives” for mitigating crop yield losses due to high water tables and crop root-zone salt concentrations. Of the 38 investigated solutions, including recharge reductions achieved through improved irrigation efficiency, reduced seepage from earthen delivery canals, new or rehabilitated subsurface drainage facilities, increased groundwater pumping (to draw down the water tables), or combinations of these, a roughly 950 mg L⁻¹ reduction in soil water salinity in cropped areas was demonstrated, resulting in a 10% increase in crop yield over the cultivated areas within the study region.

This chapter explores the potential for simulating groundwater salinity concentrations, soil water salinity concentrations, and subsurface return loads of salts to streams using regional-scale physically-based, distributed-parameter models similar to Gates and Grismer (1989) and Burkhalter and Gates (2005; 2006). The models include both the saturated and unsaturated zone and expand the spatial extent of the analysis documented in Burkhalter and Gates (2005) through the addition of a salt transport model in the DSR. The models documented in this effort do not address chemical reactions (including precipitation, dissolution, adsorption, desorption, and complex geochemical parent-daughter chain reactions). Instead, they focus on unsaturated-zone flow and groundwater surface water exchange, assuming that advection and diffusion dominate the transport and distribution of salts over the regional scale. To the extent that the models are unable to reproduce field observations, researchers will be better informed on where model improvements and enhancements, including simulation of chemical reactions, should be focused.

To accomplish this goal, two regional-scale ($\sim 10^4 - 10^5$ ha) solute transport models using a two-layer numerical grid with 250 x 250 m cells, corresponding cell-for-cell with the flow model discussed in the previous chapter, are developed. The transport models use cell-by-cell flow terms calculated by MODFLOW (Niswonger et al., 2011) and its Unsaturated-Zone Flow (UZF1) (Niswonger et al., 2006) package. This modeling effort attempts to find middle-ground; a moderate level of complexity is retained to capture major mechanisms of salt transport over regional scales and to make full use of available field data, yet processes are neglected that require extended data and require the lengthy model calibration and simulation runtimes that often stall these types of investigations.

Finally, as was demonstrated in Chapter 5, evaluation of alternative management interventions is greatly assisted through the use of simulation models. In most regional-scale

applications, simulation models may be the only viable means of evaluating a wide range of interventions in combination (Singh, 2010). However, while models are ideal for providing quantitative measures of the relative impact of particular interventions on predicted model output, many examples of which are provided above, this exercise is not pursued for the salt transport models presented herein. In this effort, models are only used to quantify baseline conditions over a historic period. Future investigations will examine the impacts of alternative water management interventions aimed at improved water quality and agricultural production.

6.3 STUDY AREAS FOR SALT TRANSPORT MODELING

The salt transport models described in this chapter were developed and applied to the same two study areas of the LARV described in Chapters 1, 3, and 5. Figure 6-1 shows the locations of the two study areas along with the location of groundwater monitoring wells and surface water monitoring sites. Surface water measurements of temperature-corrected (each reading normalized to 25° C) electrical conductivity (EC) were made routinely at a total of about 163 sites in the USR (Gates et al., 2002) and at approximately 100 sites in the DSR. Of these, approximately 12 and 6 sites in the USR and DSR, respectively, are located in the river. The remaining monitoring sites are in canals, drains, and natural tributaries in the region. River EC readings collected by CSU show that the average EC of the river rises from 0.98 dS m⁻¹ to 2.02 dS m⁻¹ between the Manzanola, CO and Las Animas, CO monitoring sites. A similar 1 dS m⁻¹ increase in river EC is observed between the Lamar and Holly, CO monitoring sites, where the average EC increases from 2.69 dS m⁻¹ to 3.67 dS m⁻¹.

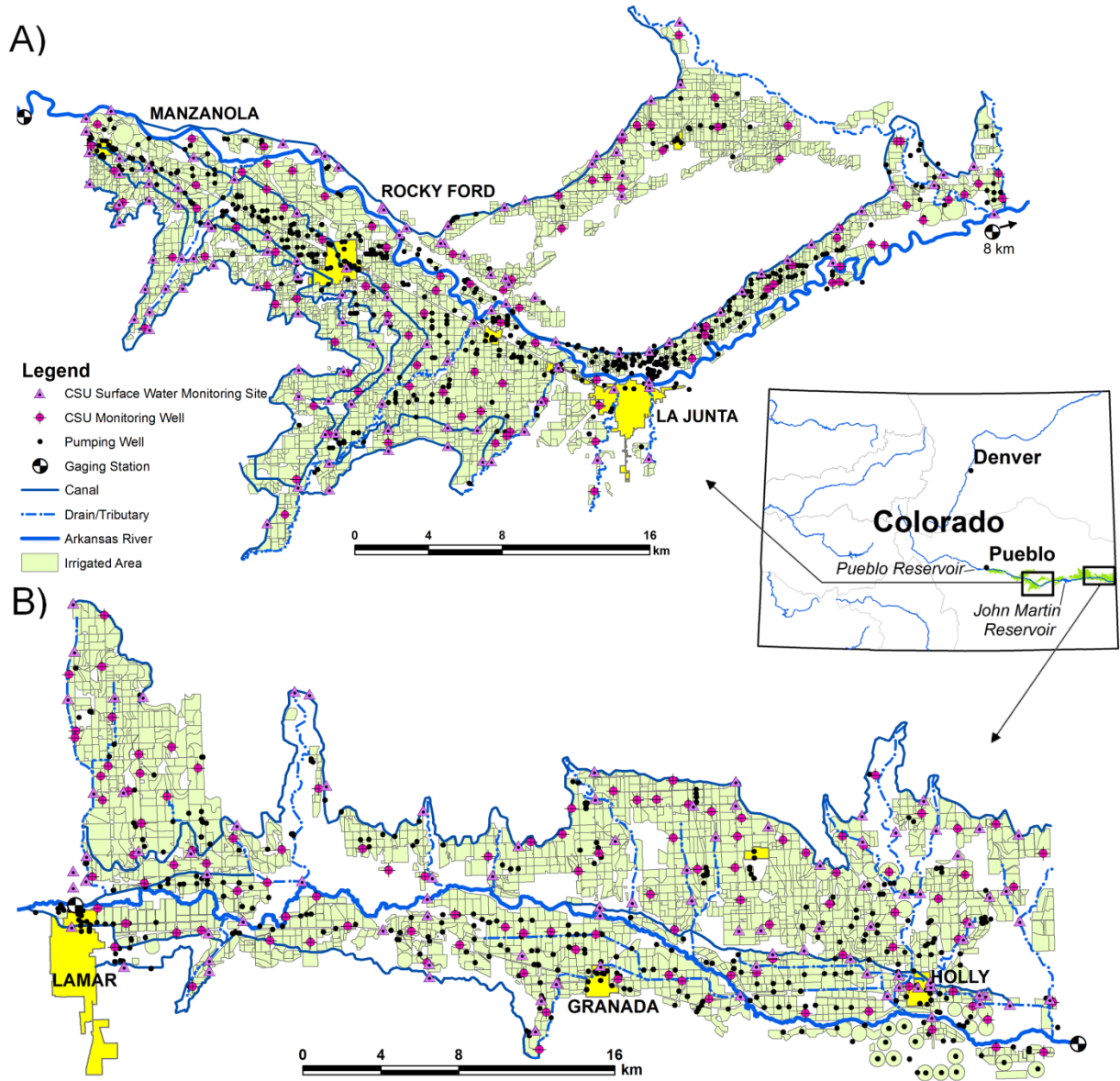


Figure 6-1. Map of (A) the USR and (B) the DSR showing surface water monitoring points (triangles) as well as groundwater monitoring well locations.

6.4 UZF-MT3DMS MODEL CONSTRUCTION AND COMPOSITION

6.4.1 Numerical Salt Transport Models

The two numerical salt transport models are built using UZF-MT3DMS, a modified version of the Mass Transport in 3-Dimensions for Multiple Species (MT3DMS) software (Zheng and Wang, 1999a) that interfaces with the unsaturated-zone flow (UZF1) module (Niswonger et al., 2006) of MODFLOW, described in detail in Morway et al. (2012) (Chapter 4).

Model extents correspond one-to-one (i.e., same number of active grid cells and grid-cell size) with the upstream study region (USR) and downstream study region (DSR) (Figure 6-1) flow models discussed in Chapter 5. Moreover, model stress periods and time steps were tailored to match exactly those of the flow models; one week stress periods with only one time step per stress period for the periods 1999-2007 in the USR and 2002-2007 in the DSR.

A single governing equation may be used to describe dissolved salt transport in the saturated and unsaturated portions of the alluvial aquifer,

$$\frac{\partial(\theta C^k)}{\partial t} = \frac{\partial}{\partial x_i} \left(\theta D_{ij} \frac{\partial C^k}{\partial x_j} \right) - \frac{\partial}{\partial x_i} (\theta v_i C^k) + q_s C_s^k + \sum_{n=1}^N R_n \quad (\text{Eq. 6-1})$$

where θ is the water content, C^k is the dissolved concentration of species k , t is time, $x_{i,j}$ is the distance along the respective Cartesian coordinate axis, D_{ij} is the hydrodynamic dispersion coefficient tensor, v_i is the linear pore water velocity, q_s is the fluid source (positive) or sink (negative) flux, C_s^k is the concentration of the source or sink flux of species k , and $\sum_{n=1}^N R_n$ is the chemical sink/source term that describes the rate of change in dissolved salt mass for a modeled species due to N chemical reactions.

Like the MODFLOW-UZF model described in Chapter 5, UZF-MT3DMS is a modular code that allows for different ‘packages’ to be activated depending on the selected set of simulated transport processes. Equipped with the cell-by-cell flow terms calculated by the calibrated flow models, subsurface salt transport is simulated for advection and dispersion processes only; reaction processes represented by the term $\sum_{n=1}^N R_n$ in Equation 6-1 are neglected.

As a result, chemical weathering of salts from shale (e.g. oxidation of pyrite to mobilize sulfate), dissolution-precipitation of gypsum and calcite, cation exchange, and adsorption are not simulated. Due to the extremely low permeability of shale, these deposits were not represented in the flow model by assuming that flow between the alluvium and underlying shale was negligible. This simplification manifests in the transport model in that no flow terms between the alluvium and shale deposits were calculated for subsequent use by the transport model.

The accuracy of the salt transport solution is most likely impacted by the omission of dissolution and precipitation of salts (i.e., gypsum and calcite) from their solid-phase states. Without this process, the model is unable to accurately simulate the loss or gain of salts from solid-phase storage within the model domain. Thus, this simplification may preclude the model’s ability to capture short-term ‘dynamic’ swings in salt loads within the long-term equilibrium. Implications of this simplification will be important in evaluating model results.

In saturated grid cells, the water content is set equal to the porosity ($\theta = \phi$). In the unsaturated zone, UZF1 solves for θ as described in Chapter 4 and in Niswonger et al. (2006). Vertical fluxes as well as water contents calculated by UZF1 are passed to UZF-MT3DMS via the same linker file historically used to pass only saturated flow terms.

Assumptions inherent in the UZF1 package include one-dimensional downward-only flow calculations. Owing to the numerical approach of UZF1 for partitioning infiltration into ET, changes in unsaturated-zone soil water storage, and downward-only flux, the diffusive term in Richards equation is neglected. Two simplifications result: the wetting front is always sharp, and upflux from the groundwater table is accounted-for through the removal of water from the saturated-zone based on D_{wt} .

The UZF1 package offers a middle ground between solutions of Richards equation (which rarely is employed in larger-than-local-scale applications) and “bucket”-type models that rely on lumped-parameters. Due to the regional-scale considered in this model application, a solution of Richards equation is not practical. First, numerical solutions in coarse grained material, where sharp wetting fronts develop, can be very problematic (Ross, 1990; Van Dam and Feddes, 2000). Both of the modeled regions host significant tracts of land with coarse-grained material. Moreover, available field data are inadequate to support parameterization of a Richards equation-based model. Thus, the level of detail required by Richards equation solutions of the unsaturated zone is avoided while at the same time seeking a physically-based approach that is absent in lumped-parameter models loosely-coupled to a detailed groundwater model.

Solute transport models that rely on a solution to Richards equation route dissolved solids upward into the soil profile in response to negative pressure gradients. Upward moving dissolved salts will be sorbed or precipitated out of solution as the water in which they are dissolved is taken up by plant roots or converted to water vapor. The depth at which the salt is deposited and subsequently accumulates is of great importance for simulating effects on crop yield. However, accurate simulation of salt deposition from upflux depends on a number of

additional factors, including (1) soil type, (2) groundwater table depth, (3) wetness of the root zone, and (4) vertical profile of the crop-root distribution, each of which is difficult to accurately simulate across regional scales with grid cells that encompass substantial intra-grid spatial heterogeneity. For the UZF-MT3DMS models applied to the LARV, this process is approximated using the volume-averaged approach described in Morway et al. (2012). For example, simulated ET, whether from the saturated zone or unsaturated zone, has a concentrating effect on the volume-averaged soil salt solution. Conversely, infiltrating irrigation water from surface water supplies with lower concentrations will dilute volume-averaged soil salt concentrations.

Due to the wide range of groundwater table conditions that may exist within the upper layer of grid cells in the models, interpretation of model results requires caution. Calculated salt concentrations are averaged over the entire upper layer and cannot be interpreted as being representative of only the root zone, or of only the unsaturated zone (Figure 6-2). Thus, discussion of model results needs to be couched in terms of overall averages and are assumed adequate for relative comparisons between various areas in the model domain, or between regions (i.e., USR vs. DSR), but not for comparisons between saturated and unsaturated zones. This simplification, which facilitated adoption of the UZF1 flow terms in MT3DMS with relative ease, increases model structural noise. Doherty and Welter (2010) define structural noise as the component of model-to-measurement misfit resulting from the “imperfect nature of a numerical model as a simulator of reality.” One approach for correcting this limitation would be to increase the vertical resolution of the numerical grid. For example, splitting layer 1 into two or more layers would focus, or limit, the vertical range over which the water table is volume-averaged. In such an approach, it is more likely that the simulated concentration of layer 1

would be more reflective of an unsaturated-only concentration and not unduly influenced by the volume-averaging approach.

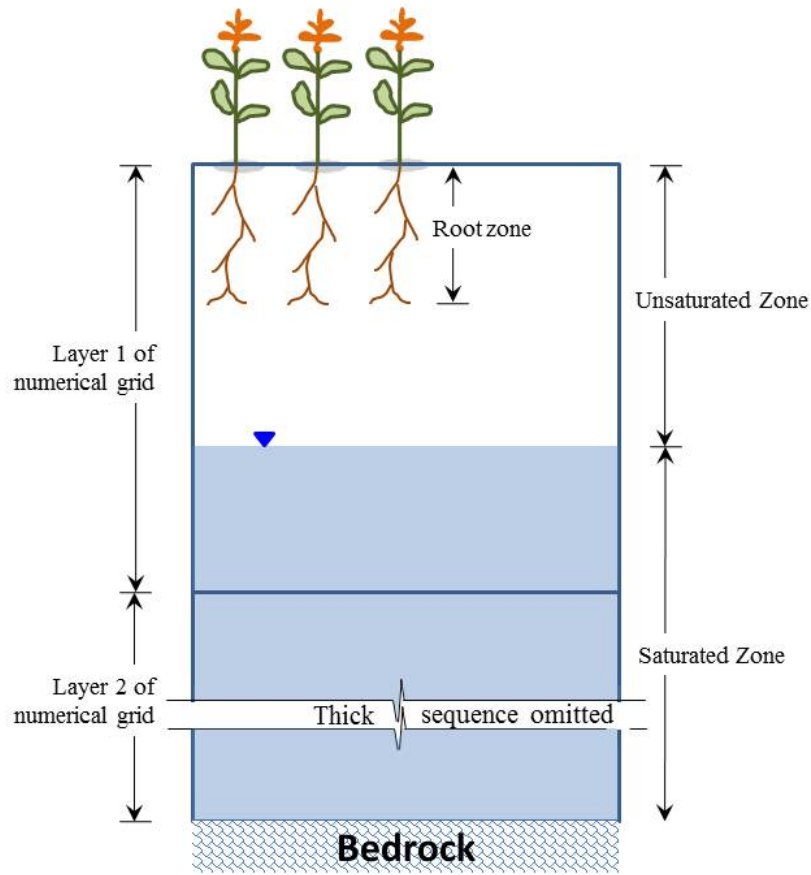


Figure 6-2. The numerical model vertical discretization with the ground surface, water table, unsaturated zone, root zone, and bedrock shown.

Attempts to reduce the structural noise associated with the vertical grid resolution through further vertical refinement may be offset by an increase in the structural noise associated with the horizontal grid resolution. That is, as vertical refinement is made, so too should horizontal refinement. Otherwise, the applicability of conditions calculated for a cell, with a horizontal area encompassing more than 6 ha in the present study, is challenged as the cell

thickness is reduced. Variability in land surface topography, for example, could be an order of magnitude (or more) greater than the total thickness of a thin cell. In addition, significant land classification and crop heterogeneity overlie nearly all of the layer 1 grid cells. Structural noise tradeoffs will invariably accompany grid refinement along any single dimension.

The regional-scale transport analyses described herein are further challenged by the heterogeneous land classification overlying each model grid cell. Only a small fraction of the top layer grid cells are overlain entirely by a single field. Modeled flow processes are driven by assorted stresses that are themselves averaged for multiple crop types that may overly any individual grid cell. For example, applied water depth, potential ET, extinction depth, and extinction water content (Niswonger et al., 2006) for a grid cell frequently is averaged for two or more crop types overlying that cell. As a result, only a single value of groundwater head, groundwater ET (GWET), and infiltration, among other quantities, will be calculated for each cell. In so doing, single values of soil water content and soil salt concentration are calculated over a relatively large spatial extent. The effect that such structural noise (Doherty and Welter, 2010) has on the overall analysis performed herein is uncertain. For now, it is simply acknowledged as a significant model limitation that precludes summary of model results for individual farms and fields. Model results are instead helpful for describing the severity and variability of salinization across regional scales and for later use in making relative comparisons of improved management conditions.

6.4.2 Salinity Observation Database

6.4.2.1 Groundwater Salinity

Model calibration is guided by a large number of field observations. The observation database includes approximately 4,800 discrete observations of EC and associated estimates of

salt (total dissolved solids) concentration from roughly 90 groundwater monitoring sites in the USR (Figure 6-1A). In the DSR, there are approximately 6,300 discrete observations of EC with estimated salt concentration from an additional 90 groundwater monitoring sites (Figure 6-1B).

6.4.2.2 Soil Water Salinity

Another dataset guiding model calibration is documented in Morway and Gates (2012) wherein the analysis of over 122,000 ground-survey points for soil water salinity is explained in detail. Surveyed values of electromagnetic (EM) induction sensor readings were converted to an equivalent electrical conductivity of a soil paste extract (EC_e) through the use of region-specific equations described in Wittler et al. (2006). Values collected on each of the surveyed fields for each survey event (carried out in the early and middle portions of the irrigation seasons) were averaged to obtain an estimate of the electrical conductivity of an equivalent soil paste extract. Normal inverse Gaussian probability distributions were fit to the frequency histograms of all \overline{EC}_e values collected in each region (Figure 3-3 in Chapter 3). The statistics of the resulting probability distributions over each region served as calibration targets for the simulated layer 1 concentrations after appropriate unit conversions. Figure 6-3 shows the disaggregated seasonal frequency histograms of \overline{EC}_e [not shown in Morway and Gates (2012)]. Interestingly, no statistically significant differences were found among the seasonal means of \overline{EC}_e for which surveys were made, despite extremely dry hydrologic conditions in the study regions in 2002 and

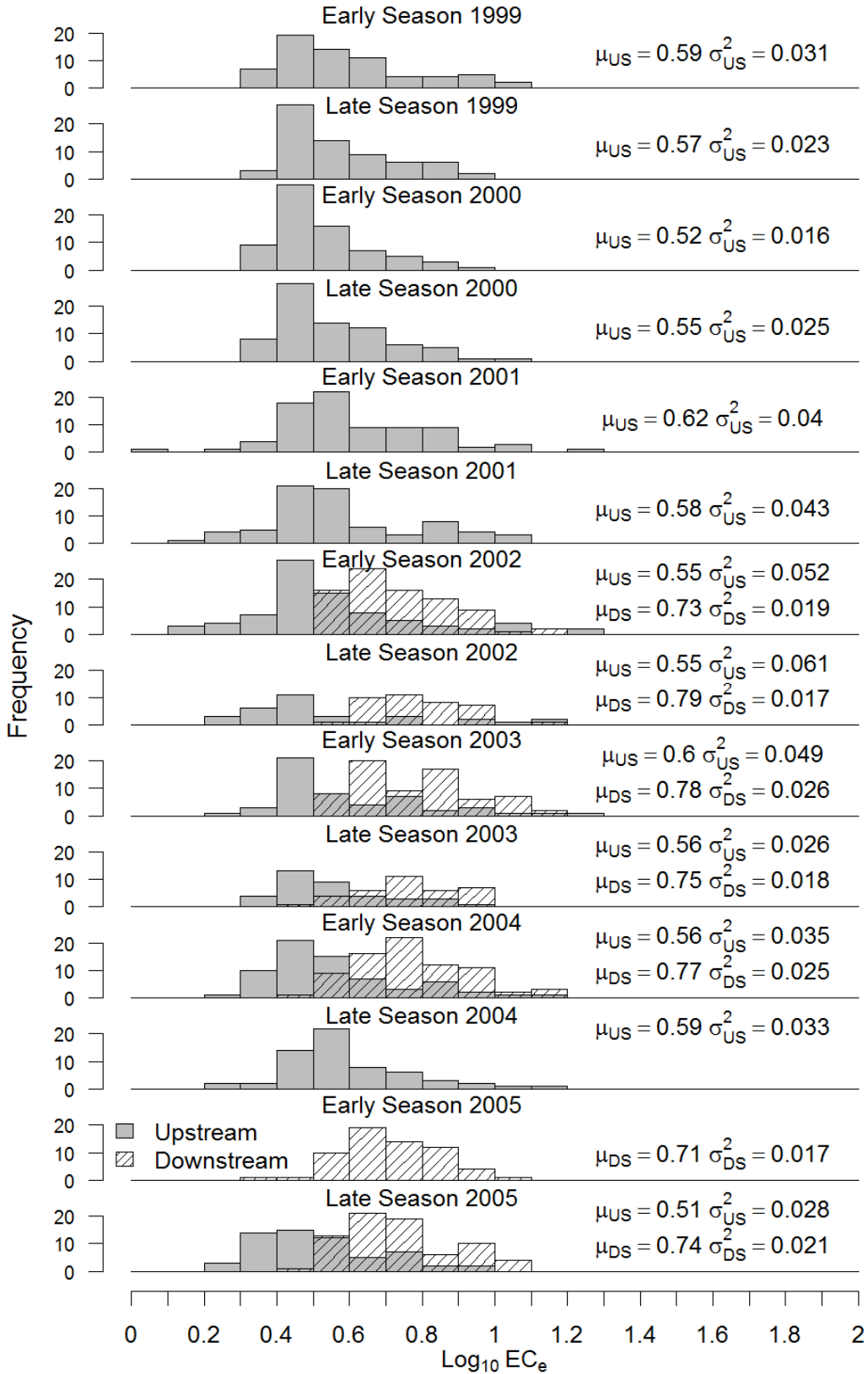


Figure 6-3. Frequency histograms of \overline{EC}_e in surveyed fields over the USR (solid) and DSR (cross-hatched) for each season surveyed.

2003. These data suggest that reduced irrigation strategies may take several years, perhaps decades, before intended reductions of soil water salinity manifest.

6.4.2.3 Salt Return Load to the River

Increasing concentrations in the Arkansas River in the downstream direction are suggestive that the LARV, and not just the upper Arkansas River basin (above Pueblo Reservoir), is a source of salt to the river system. However, in light of the steadily decreasing average annual stream flows in the downstream direction (Figure 12 in Miller et al., 2010), higher concentrations also would be expected due to the concentrating effects of evapotranspiration. Expanding upon the salt mass balance analysis by Miller et al. (2010) to also include salt loads in canals running parallel with the Arkansas River, annual salt loads passing through four north-south transects in the LARV (Figure 6-4) appear to increase in the

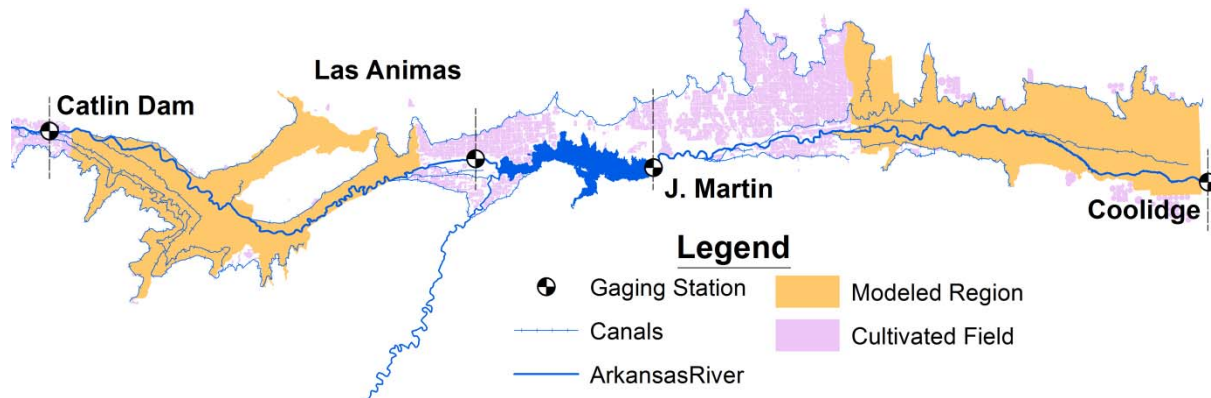


Figure 6-4. Dashed lines show transect locations for calculated salt load totals presented in the river and canals. Transect locations correspond to four USGS gages continuously collecting (every 15 min) flow and EC observations: (1) the Arkansas River at Catlin Dam, (2) Las Animas, (3) Below John Martin Reservoir, and (4) Coolidge, KS. Note that the Purgatoire River enters John Martin Reservoir from the south from outside the irrigated area.

direction during hydrologically wet and average years. During hydrologically dry years (with some short-term perturbations within the long-term dynamic equilibrium noted), however, in-

stream salt loads seem to not change appreciably in the downstream direction. This expanded analysis is described in this section.

Determination of hydrologically wet, average, and dry years was based on the total annual stream discharge as recorded by the gage located on the Arkansas River at Cañon City. Not only does the Cañon City gage host one of the oldest continuous record sets in the Arkansas River basin, but is located upstream of Pueblo reservoir and does not reflect the influence of reservoir operations on annual discharge, allowing it to serve as a rough indicator of the total water exiting the upper Arkansas River basin and entering the LARV. Figure 6-5 places the total

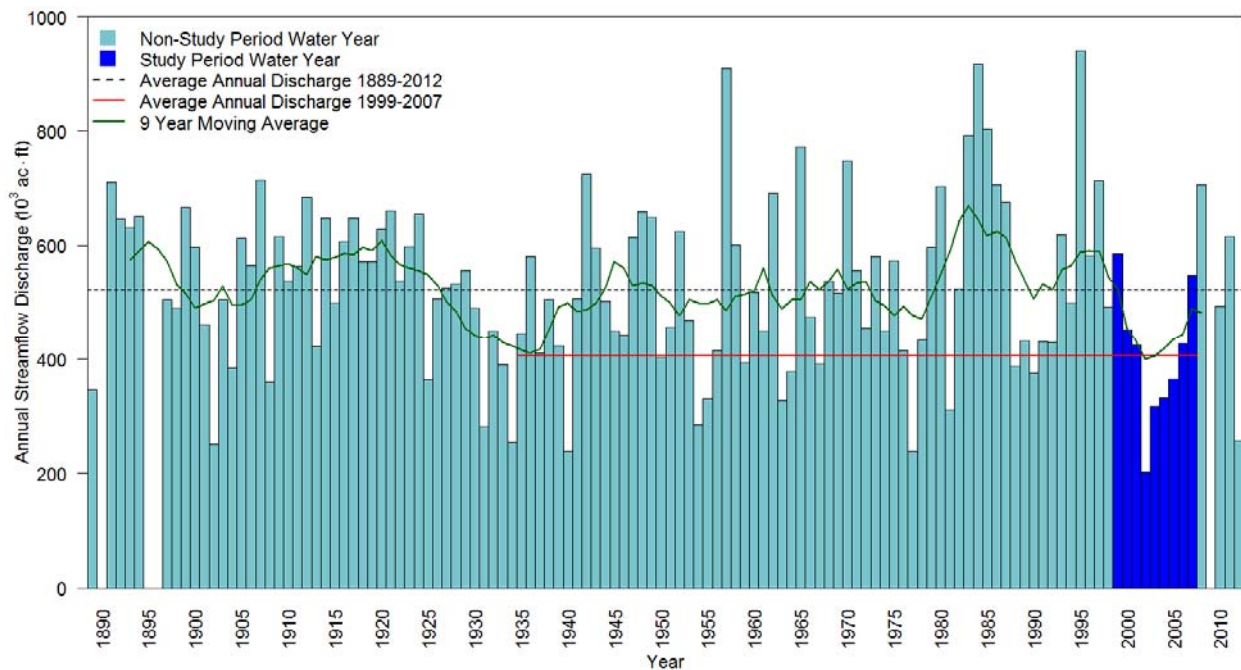


Figure 6-5. Total annual discharge as measured by the Cañon City gage on the Arkansas River. Blue bars highlight the water years coinciding with the study period.

water entering the LARV during the period of this study, 1999–2007, within the context of the complete record. The only nine-year period that was drier than the study period extended

between 1998–2006. Not even the “dust-bowl” period during the 1930’s was as dry as the study period, although it came very close (Figure 6-5). Within the nine year study period, the years 1999 and 2007 were the two wettest years. Furthermore, 1999 and 2007 are the only two years with a total annual stream discharge at the Cañon City gage above the 1889 – 2012 mean (dashed green line in Figure 6-5) and therefore are considered as being “wet” years in the discussion that follows. 2000, 2001, and 2006 are the next three wettest years of the study period, with total annual discharge above the study period mean (solid red line in Figure 6-5) but below the long-term mean. These three years are considered to be “average” in the discussion that follows. Finally, the remaining years of the study period, 2002–2005, are considered “dry” in the discussion below due to their respective total annual discharge falling below the study period mean and well below the long-term mean of total annual discharge.

6.4.2.3.1 EC-TDS Relationships

Water samples collected from surface water monitoring sites were randomly collected during field visits and sent to Ward Laboratories in Lincoln, Nebraska or to the Soil and Water Laboratory at Colorado State University for analysis of TDS. In-situ measurements of EC were paired with their lab-analyzed TDS value, plotted (Figure 6-6), and fit with both linear and non-linear regression models using the R statistical software (R Development Core Team, 2011). In either case, the coefficient of determination, r^2 , was high and statistically significant at significance level $\alpha=0.05$. Adhering to the principle of parsimony, the linear model was selected for use in converting all EC measurements to TDS. Regression equations specific to each region as well as to the surface and groundwater systems were developed and are reported in Figure 6-6.

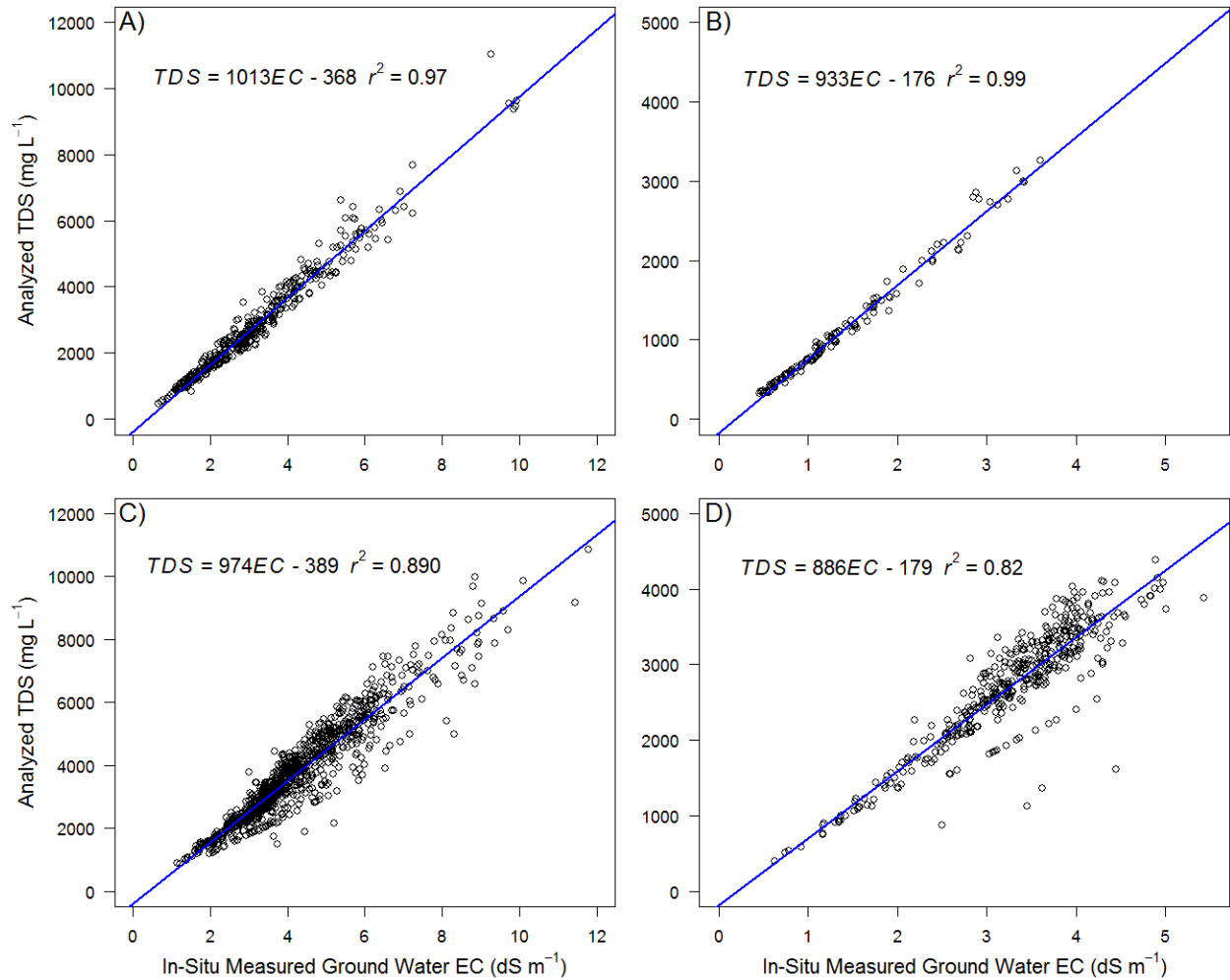


Figure 6-6. Fitted linear relationships between EC and TDS for (A) groundwater in the USR, (B) surface water in the USR, (C) groundwater in the DSR, and (D) surface water in the DSR.

6.4.2.3.2 LARV Salt Balance Model

Measured TDS concentrations in the Arkansas River increase, on average, 8-fold from where the river enters the LARV out of Pueblo Reservoir to where it crosses the Colorado-Kansas border. This increase is due in part to the low flows at the state line (less dilution) as well as an increase in the TDS accompanying groundwater return. The increase in the salt *load* carried in the river is less than that of its concentration counterpart. Miller et al. (2010) demonstrates this by contrasting salt concentration and load increases among the various USGS

gages located in the LARV that collect continuous measurements of both flow and EC. Using average salt load at each of these river gages between 2000 and 2006, Miller et al. (2010) report a decrease in salt load between the Avondale and Catlin Dam gages, as well as between the Catlin Dam and Las Animas gages. Because much of the load is likely bypassing these gages via the canal network present in the valley, further analysis is needed to get a better estimate of the change in in-stream salt load in the downstream direction.

The north-south transects divide, approximately, the lands between the Catlin Dam and Coolidge, KS, gages into thirds. Conveniently, the upper and lower thirds completely contain the two study areas. Thus, changes in the salt load in the surface water flows between the Catlin Dam and Las Animas gages, and between the Below John Martin and Coolidge, KS, gages provide insight into the total release and accumulation of salt storage from the study areas within the irrigated valley. Changes in salt storage within the surface water network are considered negligible during the one year periods of analysis.

The Catlin Dam transect intersects the Rocky Ford Highline, Otero, and Catlin Canals, requiring an estimation of the loads being transmitted in the canals at each of these locations. That is, the total salt load passing through the north-south transect located at the Catlin Dam is the sum of the individual loads in the Arkansas River, Rocky Ford Highline, Otero, and Catlin Canals flowing through this transect. The next two north-south transects, referred to as the Las Animas and Below John Martin north-south cross-sections, intersect both the Arkansas River and Fort Lyon Canal. Thus, the loads flowing past these north-south transects are the sum of the loads in these two surface water features. Similarly, the Coolidge, KS, north-south transect intersects both the Arkansas River and the Frontier Canal, requiring that the load in both of these water bodies be calculated to obtain the total load crossing the Colorado-Kansas border.

Fortunately, the diverted amount into each of these canals is recorded. By applying a spatial weight adjustment, where weights are calculated as the cultivated land area downstream of the transect location divided by the total land area commanded by the canal, is applied in order to estimate the flow rate in the canal through the transects described above. For example, under the Rocky Ford Highline, it is estimated that 70% of the command area is located east of the Catlin Dam stream gage, resulting in a 0.70 correction to the diverted amounts flowing past the Catlin Dam north-south transect. No corrections were applied to the Otero and Catlin Canal diverted amounts. Corrections of 0.78 and 0.57 were applied to the Fort Lyon Canal diversion corresponding to the Las Animas and Below John Martin transects, respectively. Although the Fort Lyon Canal is operated on a rotational schedule, the calculated loads represent annual totals. Also, the Fort Lyon Canal correction factors take into account the fact that irrigation water shares associated with cultivated fields in the downstream half of the canal are half the size as those found in the upstream half. No correction was necessary for the Frontier Ditch. A correction for salinity is also necessary as most of the canals (except the Catlin Canal and Frontier Ditch) divert water from a location between the gages that continuously monitor EC. The approach for applying this correction is described in Section 6.5.2.2 (“Applied Irrigation Salt Concentrations”). Furthermore, Section 6.4.2.3.1 describes the development of the TDS-EC relationship used to convert EC to salt concentrations for use in calculating salt load.

After applying corrections, average daily flow and concentration for each stream (i.e., Arkansas River, Fort Lyon Canal, etc.) were multiplied together and summed to obtain total annual salt load across all four transects for each year between 1999 and 2007. Figure 6-7 highlights differences in salt loads along the LARV for each year of the study period.

Between 1999 and 2001, when river flows were average to high (relative to the study period average) and ample irrigation water was available, significant net import of salt loads from the irrigated valley appears to have occurred. That is, the amount of mass crossing a downstream north-south transect generally was greater than the adjacent upstream transect, though not always. In 2000, for example, a net decrease in estimated salt load is indicated between the Catlin Dam and Las Animas transects (as well as in 2001), and between the Below John Martin and Coolidge, KS, transects. Considering that the 1999-2001 period followed a wet six year period (1993-1998), high water tables resulting from high recharge from excess irrigation and canal seepage sustain steeper gradients driving salt-laden groundwater back to the Arkansas River, likely contributing to the general increase in salt load in the downstream direction. Furthermore, in hydrologically wetter years like 1999, increased rainfall on shale outcrops adjacent (on the north and south) to the irrigated valley increases dissolution of salts from the weathered shales which are subsequently imported back to the valley through ungaged tributaries. In addition, the higher water tables and soil water contents resulting from the relative abundance of water leads to the dissolution of previously precipitated gypsum and calcite as solubility thresholds are crossed. Finally, because of the ample irrigation water supply, an increase in leaching of salts from the unsaturated to the saturated zones further contributes to elevated return loads back to the river.

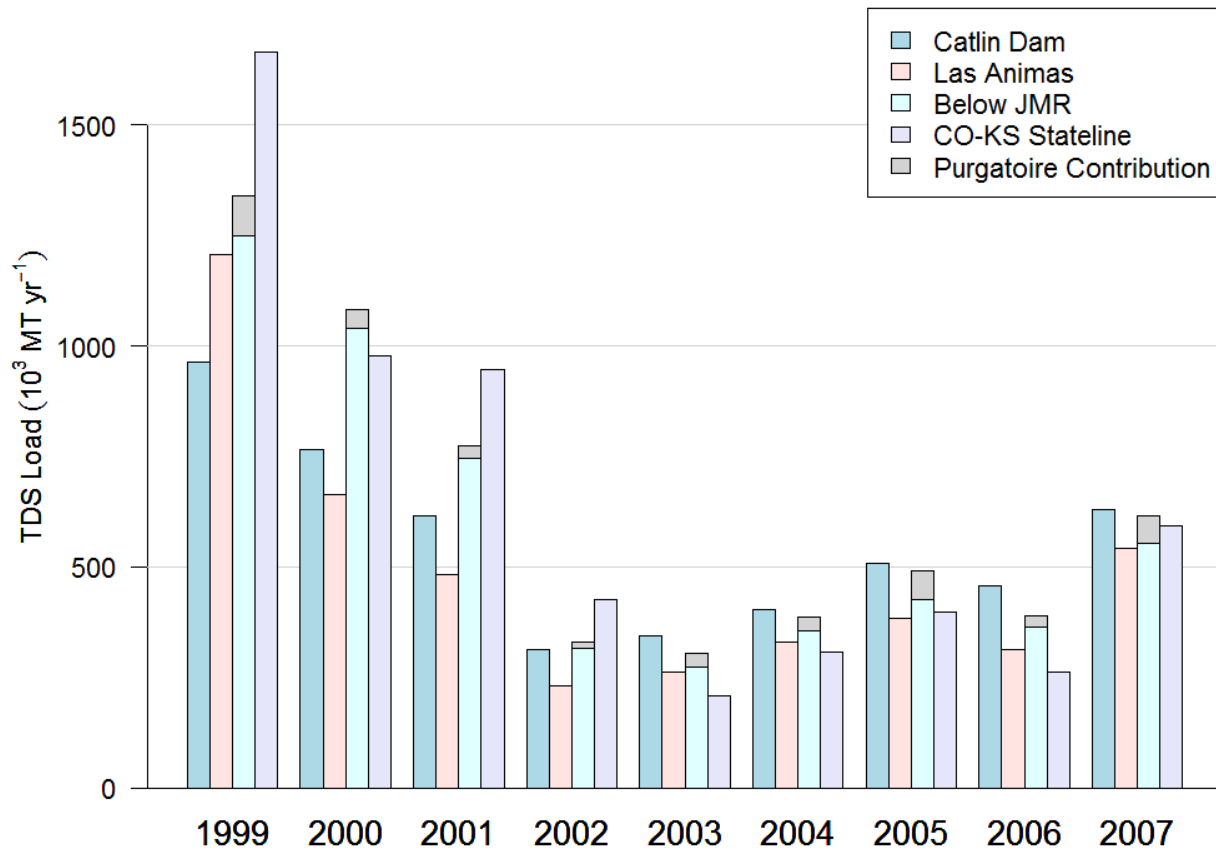


Figure 6-7. Salt load in the river and canals across four transects in the LARV located near the two study regions. Estimated contribution of salt load entering the LARV from the Purgatoire River also is shown.

An average EC for the Purgatoire River gage near Las Animas was calculated based on a now discontinued EC record that extends between water year (WY) 1990 and 1996. The average EC during this time frame was 3.2 dS m^{-1} . Converting this EC to TDS and multiplying by the flows in the Purgatoire River for the period October 1, 1998 to September 30, 2007, provides an estimate of the Purgatoire's contribution to the salt load at the Arkansas River gage Below John Martin. Because this represents a source of salt load derived from processes occurring outside the LARV, Figure 6-7 was amended to reflect this distinction.

The increasing salt load in the downstream direction evident between 1999 and 2001 is notably absent during the years that follow (2002-2007). Were estimates of the uncertainty for

each transect and year available, these between transect differences may prove statistically insignificant. Results indicate a decrease salt load between the Catlin Dam and Coolidge, KS transects for the years 2003 to 2007. These results indicate that during multi-year hydrologically dry spells, the LARV downstream of the Catlin Dam gage may be accumulating salts (perhaps via precipitation of gypsum and calcite salts) from the river system. Analysis of additional years that extend beyond the period presented here will help substantiate (or counter) these findings.

6.4.2.3.3 Calculation of Salt Return Load Targets

Salt load returning to the Arkansas River from a variety of sources is estimated for use in mass balance calculations of the component of salt return load associated with groundwater return loads during the modeled periods. The salt loads entering and exiting the USR in the Arkansas River are estimated from continuously gaged flows and EC at the Catlin Dam and Las Animas gages. Gaged tributary flows (with accompanying EC measurements) include Timpas and Horse Creeks and the gaged flows and periodic EC measurements available for the Holbrook, Rocky Ford, Fort Lyon Storage, Fort Lyon, and Las Animas Consolidated canals. In addition, a number of non-gaged sources for which flow rates were estimated also were considered, including tailwater returns from irrigation under each of the canals. Differentiation between tailwater originating from irrigation using canal water versus pumped groundwater is made using records of diverted and pumped amounts. In general, the EC of pumped groundwater is higher than that of canal water. Thus, despite the fact that the magnitude of groundwater irrigation is comparatively small relative to irrigation with canal water, salt load from groundwater irrigation tailwater is important to account for due to its higher salt concentration. Storage changes described in the previous chapter supported calculation of this component of the salt budget. The EC used for calculation of changes in salt mass stored in the river is taken as an average of the EC measured at the Catlin Dam and Las Animas gages.

In the DSR, estimates of the return salt load entering the river segment within the modeled area includes that entering the model domain in the river at the Lamar, CO stream gage, as well as through the two gaged tributaries on Big Sandy and Wild Horse Creeks. As in the USR, various other surface water return flows were estimated, including the EC associated with these flows and storage changes, to estimate a return salt load attributable to groundwater return flow.

In the USR, estimates of salt return load are associated with each of the flow components shown in Figure 6-8. That is, for each of the estimated return sources (or diversions) of flow, an estimate of the associated EC is made so that the total salt load leaving and returning to the river, including estimates of the salt mass storage change, can be differenced yielding an estimate of the unaccounted-for return load.

The following quantities were used to calculate total salt load in the Arkansas River: 1) calculated river loads into and out of the study regions, 2) estimates of canal loads entering and exiting each region at the gaged locations, 3) estimates of mass storage changes based on measured stage changes and surveyed cross-sections, 4) estimates of loads returning to the Arkansas River through gaged tributaries, and finally 5) estimates of irrigation tail-water return loads through open ditches. Precipitation runoff from natural areas was assumed to carry negligible return salt loads. The salt load mass balance is described by

$$L_{UR_k} = L_{IR_k} - L_{OR_k} + \sum_{l=1}^{N_T} L_{T_{kl}} - \sum_{m=1}^{N_C} L_{C_{km}} + \Delta S_{R_k} \quad (\text{Eq. 6-2})$$

where L_{UR_k} is the total unaccounted-for return salt load [$M T^{-1}$] to the river during the k th week and can be either a net gain (+) or loss (-); L_{IR_k} and L_{OR_k} are the k th salt loads [$M T^{-1}$] entering

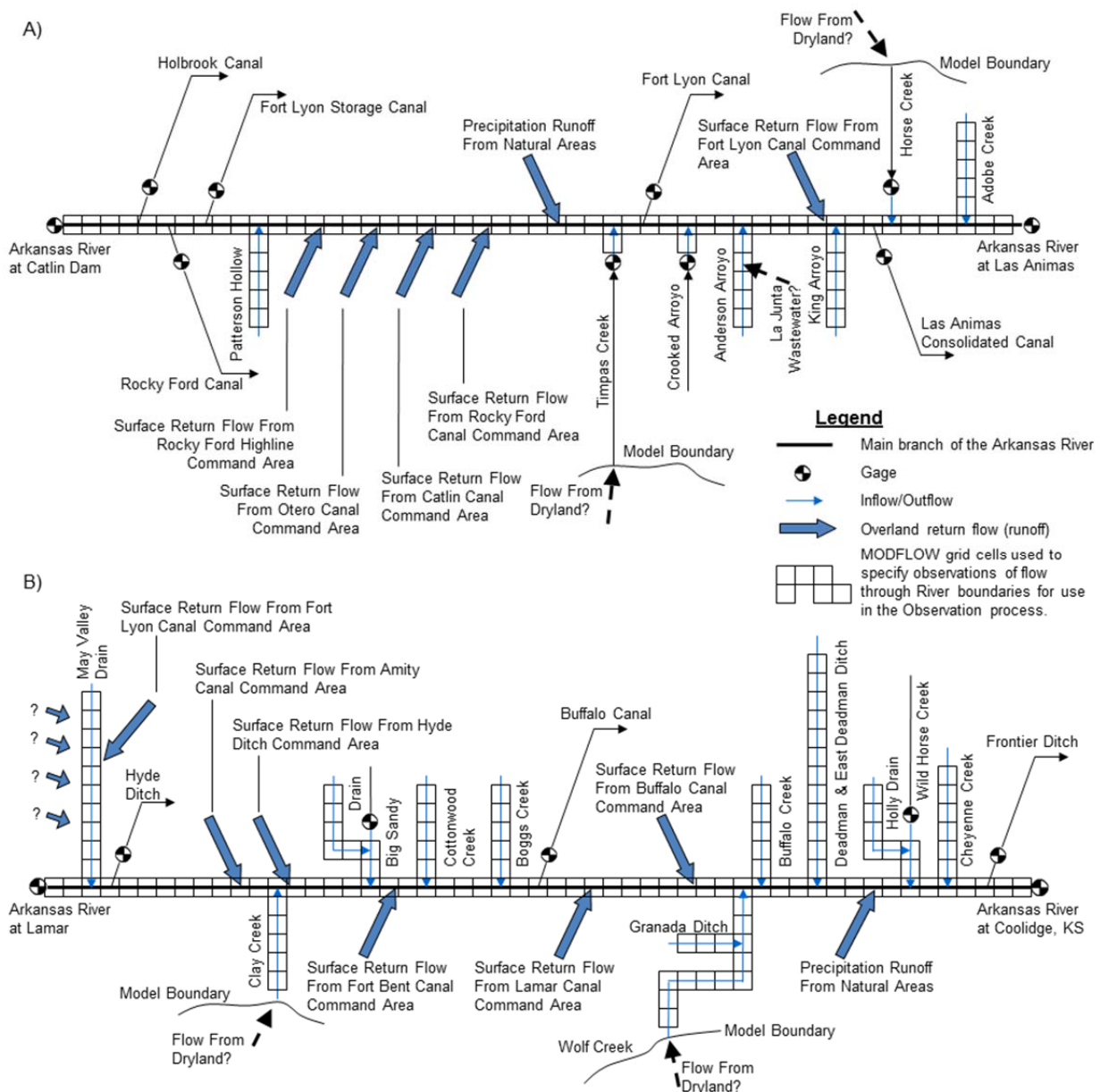


Figure 6-8. Schematics of surface water features for (A) the USR and (B) the DSR for use in calculating groundwater return loads. Surface water return flows originating from irrigation tail-water are further partitioned into surface water and groundwater returns to account for significant differences in their respective salt concentrations.

and exiting (as measured by gaging stations) at the upstream and downstream ends of the river reach, respectively; $L_{T_{kl}}$ is the k th salt load [$M T^{-1}$] measured in the l th gaged tributary along the river reach; N_T is the number of gaged tributaries along the river reach; $L_{C_{km}}$ is the k th salt load [$M T^{-1}$] measured in the m th gaged canal that diverts from the river along the reach; N_C is the number of gaged canals along the river reach; and ΔS_{R_k} is the k th rate of change in the salt mass stored [$M T^{-1}$] in the Arkansas River associated with measured changes in river stage. Because L_{UR_k} includes unmeasured tributary salt load and other surface return salt loads, in addition to groundwater return loads back to the river and tributaries, then $L_{GW_k} \leq L_{UR_k}$. Values of L_{UR_k} computed with Equation 6-2 are reduced by estimates of unmeasured surface loads to obtain values of L_{GW_k} for use in model calibration.

While some of the unaccounted-for return salt load may be attributable to sources entering the valley through tributary and groundwater inflow originating in lands adjacent to the Arkansas River Valley, the majority of unaccounted-for return load is assumed to be associated with alluvial groundwater return flow. Therefore, the calculated value of unaccounted-for return load is taken as an observation of alluvial groundwater return salt load and is targeted by the automated parameter estimation algorithm used for model calibration.

Weekly observations of accretion and depletion of total salt load in the river are used to constrain the automated parameter estimation. As was the case with estimation of groundwater return flow to the river, a notable assumption was made to enable this calculation. Surface water inflows occurring in the many ephemeral channels crossing the northern and southern boundaries of the model were assumed to carry negligible salt return loads. In the event of significant rainfall on lands adjacent to the modeled area that generates intermittent salt-laden streamflow,

this assumption would be violated. Any simulated misfit between calibrated model-simulated values of return salt loads and values estimated by mass balance may be due in part to such errors.

6.5 AUTOMATED SALT TRANSPORT MODEL CALIBRATION PROCEDURES

The solute transport models for the USR and DSR are calibrated using the generalized automated parameter estimation software, PEST (Doherty, 2002). PEST minimizes the residuals between simulated model output and field observations described in the ‘Observation Database’ section above. All three observation dataset types – groundwater salinity, groundwater return salt loads, and soil water salinity – are assimilated into the objective function minimized by PEST:

$$S(\mathbf{b}) = \sum_{j=1}^{N_s} \omega_{s_j} [s_j - s'_j(\mathbf{b})]^2 + \sum_{k=1}^{N_L} \omega_{L_k} [L_{GW_k} - L'_{GW_k}(\mathbf{b})]^2 + \sum_{i=1}^{N_C} \omega_{C_i} [C_i - C'_i(\mathbf{b})]^2 \quad (\text{Eq. 6-3})$$

where S is the value of the objective function, \mathbf{b} is a vector containing values of each of the parameters being estimated, N_s is the number of groundwater salinity observations, N_L is the number of groundwater return salt load observations, N_C is the number of points at which to compare between the simulated and observed soil water salinity cumulative distribution functions (CDF), s_j is the j th observed groundwater salinity [M L^{-3}] being matched by the regression, $s'_j(\mathbf{b})$ is the simulated groundwater salinity [M L^{-3}] that corresponds to the j th observed groundwater salinity (a function of \mathbf{b}), L_{GW_k} is the k th groundwater return salt load [M T^{-1}] estimated by the mass balance procedure, $L'_{GW_k}(\mathbf{b})$ is the simulated groundwater return salt load [M T^{-1}] that corresponds to the k th observed return load, C_i is the i th point along the CDF generated from the pooled distribution of TDS estimated from observed $\overline{\text{EC}}_e$ [-], $C'_i(\mathbf{b})$ is the i th

simulated point along the CDF corresponding to the pooled distribution of simulated TDS concentrations from layer 1 for all 99% cropped cells [-], ω_{s_j} is the weight for the j th groundwater salinity observation, ω_{L_k} is the weight for the k th groundwater return salt load observation, and ω_{C_i} is the weight for the i th point along the CDF generated from the pooled distribution of estimated TDS [-].

6.5.1 Calibration Objective Function Weights

Unlike the flow modeling calibration procedure, wherein weights were based on estimates of observed variability within field-scale studies performed within the modeled regional boundaries, selection of weights used in Equation 6-4 followed a less formal (except for groundwater return salt loads), but equally valid derivation. Within-group weights were either uniform (i.e., all groundwater salinity concentration observations were assigned the same weight) or, in the case of return salt load, reflect the weighting scheme described in Section 4.4.1.4.

The weights ω_{s_j} and ω_{C_i} were set equal for all j and i , respectively. Furthermore, ω_{s_j} and ω_{C_i} were adjusted such that the first and third summands on the right-hand side of Equation 6-3 contributed equally to the objective function, each of which were approximately equal to the contribution from the second summand on the right-hand side of Equation 6-3. In this way, the weighted residuals from each observation group contribute equally to the objective function; no one observation or observation group “drowns-out” another within the total objective function. This is a significantly different weighting approach than was adopted in the flow model calibration. Whereas mathematical formulations for assigning weights were described in the flow calibration, a philosophy leaning more heavily on ‘common sense’ is adopted here. Approaches leaning more heavily on formal mathematical formulations for deriving weights

recognize imperfections in the observations (i.e., measurement noise) and therefore derive weights which reflect sources of uncertainty. However, this approach fails to account for model structural noise arising out of grid discretization schemes and which can be much greater than measurement noise (Doherty and Welter, 2010). In other words, common sense has theoretical underpinnings and is a sound alternative to mathematically more rigid approaches (Doherty, personal communication, 2012).

6.5.2 Adjusted Salt Transport Model Parameters, (b)

Four model parameters were varied during calibration of the salt transport models, including initial salt concentration, concentration of applied irrigation water, aquifer porosity, and aquifer dispersivity. In this application, however, the flow and salt transport models for each region were calibrated separately. This approach likely limits the ability of the salt transport calibration to achieve as good a fit as possible. By divorcing the flow and salt transport models during the calibration process, the full potential of the information contained in the historical salt concentration and salt loading datasets goes unrealized. For example, to achieve better fits with regard to the return salt loads, it may prove advantageous to adjust parameters in the flow model rather than in the salt transport model. Because the flow model is fixed at the outset of the calibration of the salt transport model, calibrated parameters of the salt transport model could take on values that compensate in part for inadequacies of the flow model rather than “realistic” values. In all but applied salt concentration, a set of pilot points (Doherty, 2003) was used to estimate the spatial distribution of the estimated parameters (Figure 6-9). At each pilot point location, estimated parameter values could vary between the model layers. For example, there was no requirement that the initial salt concentration of model grid layer 1 equal that of layer 2.

Moreover, Tikonov regularization (Doherty, 2003), a method for instilling expert knowledge into the calibration process, was not required or used in the parameter estimation process.

6.5.2.1 Initial Salt Concentrations

Figure 6-9 shows the spatial distribution of pilot points where values of initial salt concentration were estimated. Utilities distributed with the PEST suite of software subsequently were used to krigé the estimated pilot point values into spatial arrays for insertion into the corresponding model input file. Estimated values of initial salt concentration (mg L^{-1}) were afforded considerable range; values at any given pilot point could vary as low as 500 mg L^{-1} to as high as $30,000 \text{ mg L}^{-1}$. Because the automated parameter estimation routine targeted observations of groundwater salinity collected very close to the beginning of the respective simulations, estimated pilot point values were reflective of concentrations observed near the beginning of the simulated period. Observations of groundwater salinity, measured as EC (dS m^{-1}) and converted to TDS concentration (mg L^{-1}), are directly comparable to simulated model output. Simulated concentrations in layer 2 are from predominately saturated cells. Therefore, the volume-averaging approach described in Section 5.3 is not expected to bias the simulated-to-observed comparison.

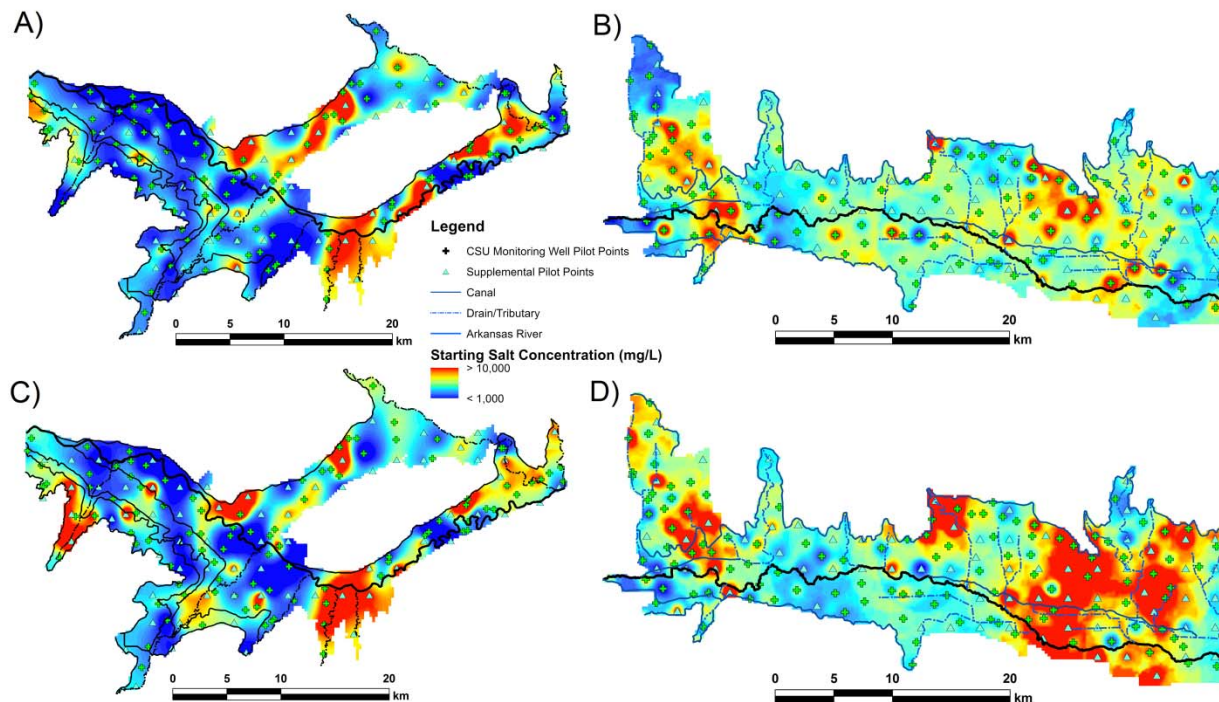


Figure 6-9. Estimated initial salt concentration arrays for layer 1 of the (A) USR and (B) DSR and for layer 2 of the (C) USR and (D) DSR. Pilot points coincide with CSU groundwater monitoring well locations and were supplemented by additional pilot points where their density was deemed sparse.

6.5.2.2 Applied Irrigation Salt Concentrations

Two steps were followed to generate salt concentrations of the applied irrigation water. First, it was necessary to convert observations of surface water salinity from their field-sampled EC units to the concentration units used in the numerical model, mg L^{-1} . Second, whenever the groundwater monitoring well network was sampled for D_{wt} and EC, surface water measurements of EC also were gathered (Figure 6-10 shows surface water monitoring points pertinent to this discussion, readers are referred to Figure 6-1 for a complete viewing of all surface water monitoring points in the USR and DSR, respectively). Measurements of EC for each canal were compared to the continuous record of EC at the nearest upstream Arkansas River gage. For example, in the USR, measurements of EC taken from the Fort Lyon and Rocky Ford canal sampling points were compared to time series of EC recorded at the Catlin Dam gage on the

Arkansas River (Figure 6-11A; Figure 6-11C). A similar analysis was conducted in the DSR; for example, measurements of EC from sampling points in the Amity and Buffalo canals (Figure 6-10B) were compared to the EC time series recorded at the gage below John Martin Reservoir (Figure 6-12A, Figure 6-12C). Next, the residuals between the discrete observations and the continuously monitored time series were plotted (Figure 6-11B, Figure 6-11D, Figure 6-12B, and Figure 6-12D). Visual inspection Figure 6-11B and Figure 6-11D indicate that the residuals follow normal distributions in the USR. In the DSR, residuals exhibit right-tailed distributions (Figure 6-12B and Figure 6-12D). Due to significantly longer distances between the sampling points and the nearest upstream river gage in the DSR and the presence of more intermediate surface water exchanges with other tributaries, more spread in the residuals (Figure 6-12B and Figure 6-12D versus Figure 6-11B and Figure 6-11D) would be expected. In addition to the Fort Lyon and Rocky Ford canals, measurement from the Catlin and Holbrook canals also were compared to the Catlin gage continuous record. Residuals in both canals display approximately Gaussian distributions.

Measurements of EC in both the Rocky Ford Highline and Otero canals were compared to the continuous record collected at the Avondale gage in the river. Whereas the residuals for the Rocky Ford Highline canal were distinctly Gaussian, residuals for the Otero Canal sampling points revealed a right-tailed distribution similar to what is shown in Figure 6-11D. All of the

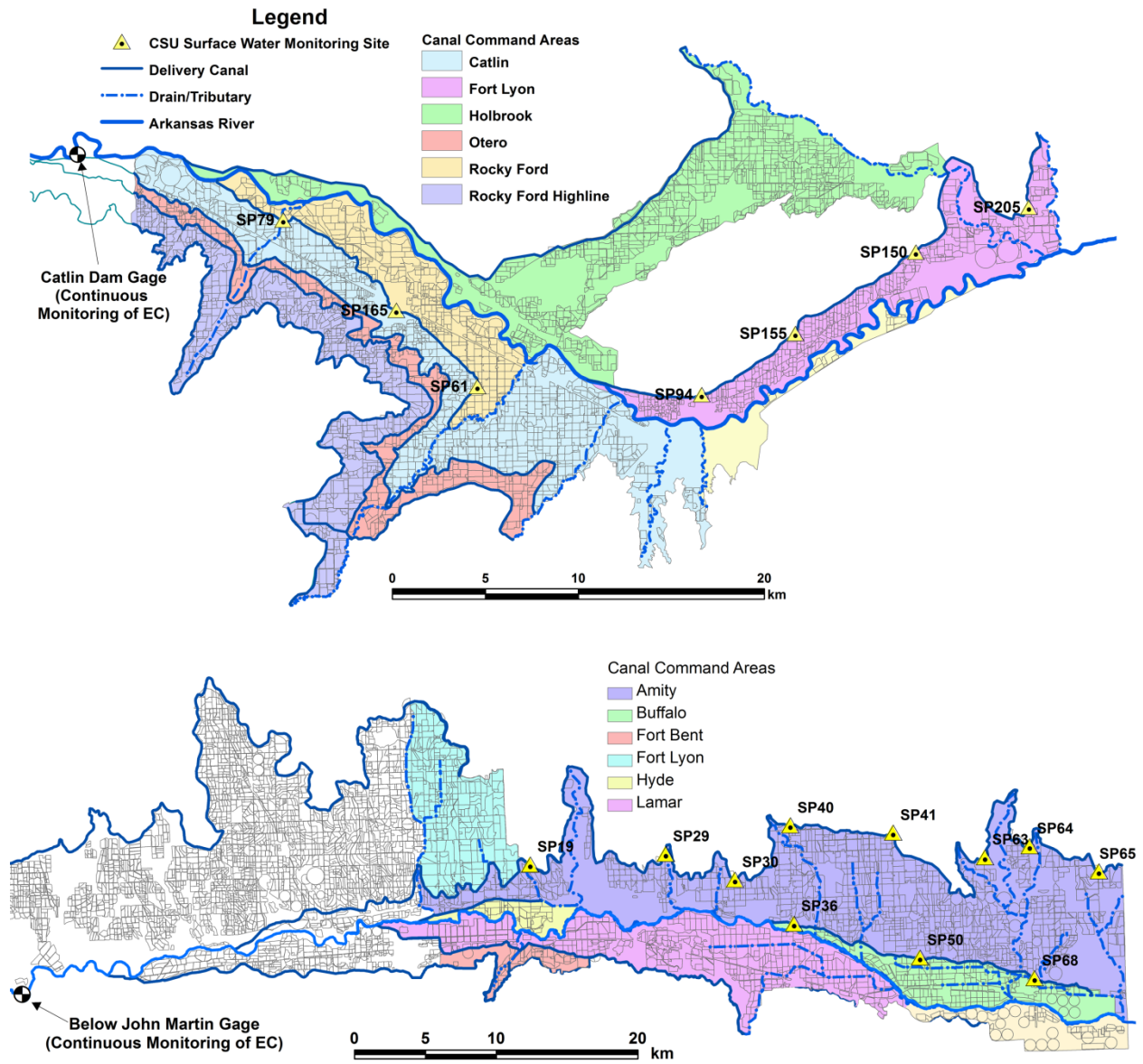


Figure 6-10. Command areas, or fields operated under specific canals, in the two model regions are highlighted. Yellow triangles depict the spacing of CSU surface water monitoring points along two canals within each region. Data collected at these locations guided adjustment of the salt concentration of applied water.

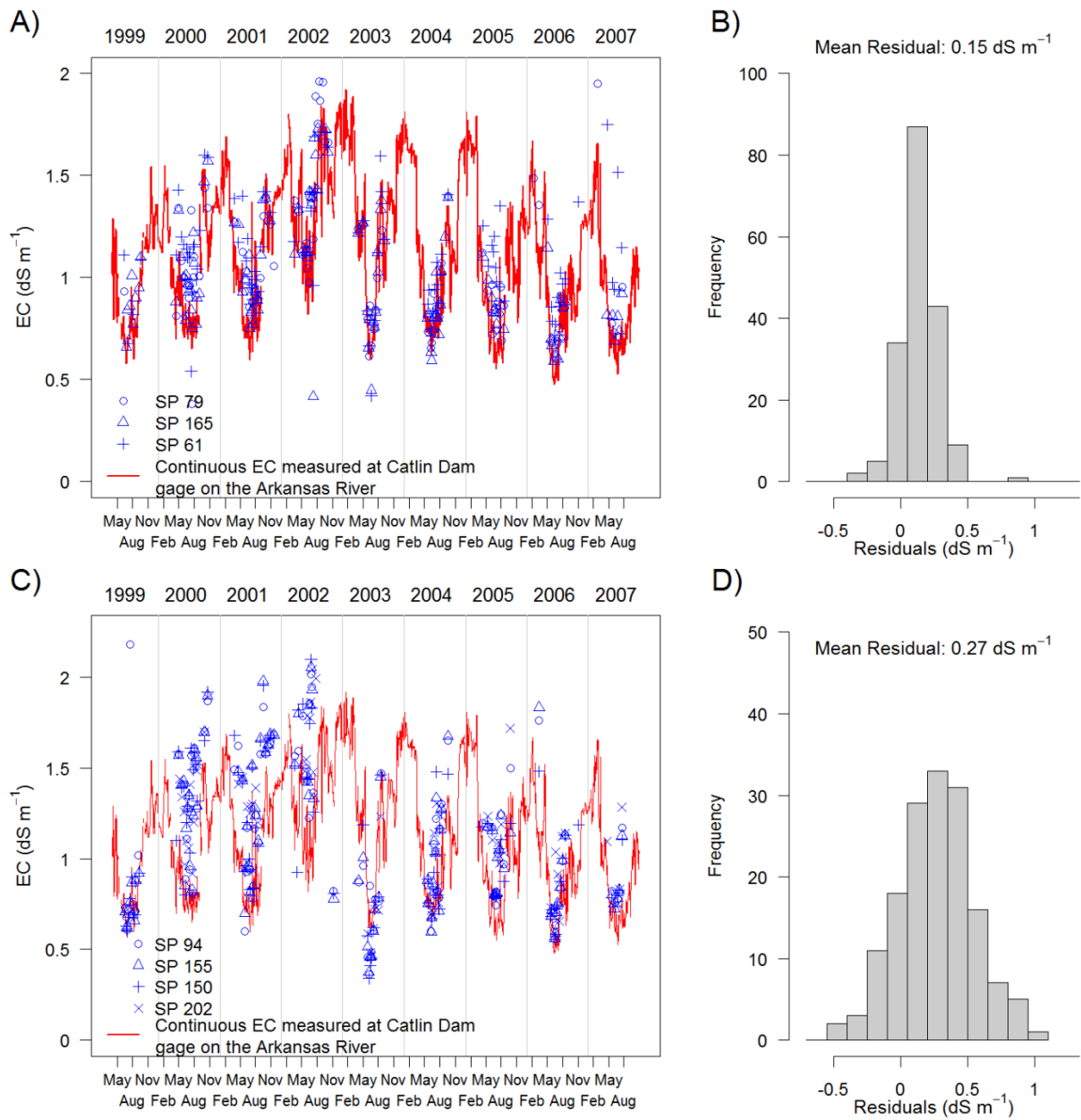


Figure 6-11. Time series plots comparing the continuously monitored EC at the gage located at Catlin Dam on the Arkansas River to the discrete measurements taken in the (A) Rocky Ford Canal and in the (C) Catlin Canal. To view the “SP” (surface point) locations, readers are referred to Figure 6-1A. The distribution of the residuals (difference between discrete measurements and simultaneous measurements at the continuously monitored gage location) calculated in (A) and (C) are shown in (B) and (D), respectively.

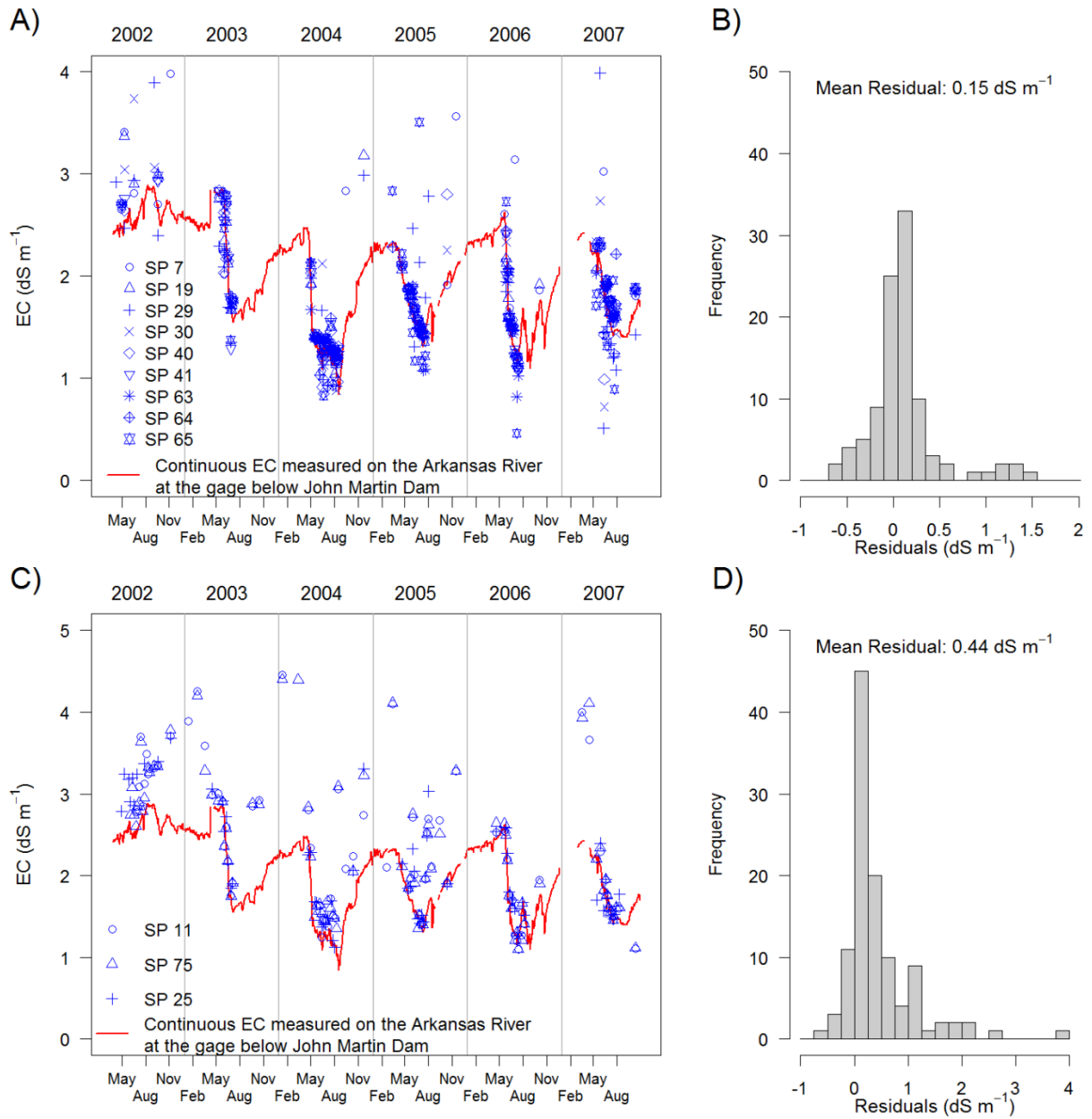


Figure 6-12. Time series plots comparing the continuously monitored EC at the gage on the Arkansas River located below John Martin Reservoir to the discrete measurements taken in the (A) Amity and in the (C) Buffalo Canals. To view the “SP” (surface point) locations, readers are referred to Figure 6-1B. The distribution of the residuals (difference between discrete measurements and simultaneous measurements at the continuously monitored gage location) calculated in (A) and (C) are shown in (B) and (D), respectively.

surface water measurements from the DSR were compared to the continuous EC dataset collected at the gage below John Martin Reservoir, except for measurements taken in the Fort Lyon Canal, which were compared to the Catlin Dam gage. Here again, the computed residuals

Hyde, Fort Lyon, and Fort Bent canals all had roughly Gaussian distributions, each exhibiting slight right-tail skew. In summary, the assumption of Gaussian distributions of the residuals for each canal is warranted.

The parameter estimation routine included parameters controlling the weekly salt concentration of applied irrigation water. Before any adjustment of the applied salt concentration took place, however, an initial estimate of the salt concentration of the irrigation water in a particular canal was set equal to the average salt concentration for the current week observed at the nearest upstream gage on the Arkansas River (i.e. Avondale, Catlin Dam, below John Martin Reservoir) and adjusted by adding the mean residual between the CSU-observed EC for the canal and that of the nearest upstream river gage. To demonstrate, consider a week in mid-2004 in the USR in which the average salt concentration for the week at the Catlin Dam river gage was 0.65 dS m^{-1} (Figure 6-11A). The salt concentration of irrigation water applied to canals under the Rocky Ford would therefore be calculated as 0.65 dS m^{-1} plus an average residual of 0.15 dS m^{-1} (Figure 6-11B). An initial estimate for salt concentration of 0.80 dS m^{-1} would then be applied to the cells under the Rocky Ford Canal receiving irrigation water. Because rain water and irrigation inputs are pooled, the applied salt concentration was adjusted to account for rainwater dilution. Similar calculations were performed for each canal in both study regions.

Canal-specific adjustments to the applied salt concentration associated with the irrigation water (mixed with rain water) were constrained by the observed variability in the residuals (i.e. Figure 6-11B, Figure 6-11D; Figure 6-12B, Figure 6-12D). In the USR, the standard deviation, σ , of the Rocky Ford Canal residuals (Figure 6-11B) is 0.15 dS m^{-1} , whereas the standard deviation for the Catlin Canal is 0.27 dS m^{-1} (Figure 6-11D). PEST was programmed to vary the

applied concentrations by $\pm 2\sigma$ (Table 6-1) of the calculated residual. Adjusted salt concentration values were not permitted to fall below 0, a physical impossibility. Revisiting the example above, the applied concentration under the Catlin Canal for the week in mid-2004 was free to range between $0.65 \text{ dS m}^{-1} \pm 2(0.27) \text{ dS m}^{-1}$, or between 0.11 and 1.19 dS m^{-1} .

Table 6-1. Summary of the observed salt concentration variability (1 standard deviation, σ) in each canal derived from comparisons to the continuous record from the nearest upstream river gage.

USR		DSR	
Canal	σ (dS m ⁻¹)	Canal	σ (dS m ⁻¹)
Catlin	0.27	Amity	0.15
Fort Lyon	0.28	Buffalo	0.44
Rocky Ford Highline	0.17	Fort Bent	0.49
Holbrook	0.30	Fort Lyon	0.20
Otero	0.54	Hyde	0.70
Rocky Ford	0.15	Lamar	0.64

In the end, model results were found to be insensitive to changes in applied salt concentration. Inspection of the perturbed applied salt concentration values for each canal at the end of a parameter estimation run revealed a strong tendency to be at the limit of their range. In other words, due to parameter insensitivity, the PEST algorithm attempted to make large adjustments to the applied concentrations but was restricted from doing so by a priori constraints based on expert knowledge. Therefore, subsequent parameter estimation runs fixed the applied concentrations at the weekly average concentration from the nearest upstream gage plus the average residual calculated for the simulation period.

6.5.2.3 Aquifer Porosity

Porosity is defined here as the “effective” porosity of the porous media system. Unlike initial salt concentration or applied salt concentration, it is related to parameter values estimated in the flow problem. Thus, estimation of the porosity fields apart from simultaneous adjustment of related parameters in the flow solution is handled with caution. For example, if the final estimated porosity value at a location was twice that of the estimated S_y , a measure of the drainable porosity and therefore related to the pore space inter-connectedness, a concern would immediately be raised.

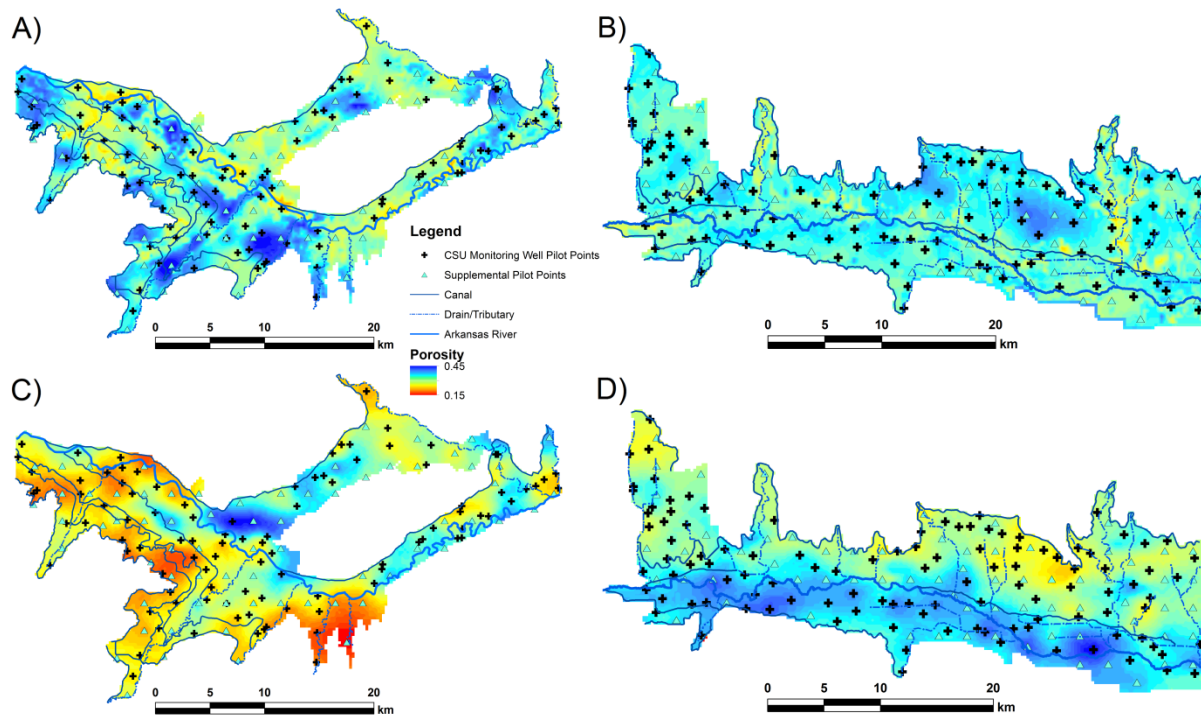


Figure 6-13. Estimated aquifer porosity values for layer 1 of (A) the USR and (B) the DSR and for layer 2 of (C) the USR and (D) the DSR. Blue corresponds to more porous areas.

The approach taken here was to adopt the S_y values obtained by calibration of the flow model as starting values for porosity. Perturbation of the porosity values was limited to between 50 and 150% of the initial values to limit the degree of discrepancy with the S_y values in an attempt to maintain a physically-realistic connection to the flow solution. Pilot points used to estimate the porosity arrays are shown in Figure 6-13.

6.5.2.4 Aquifer Dispersivity

The fourth and final dataset adjusted by the automated parameter estimation routine is aquifer dispersivity, which, in this application, refers only to the mechanical dispersion component; molecular diffusion is assumed negligible. As a mechanism, dispersion is generally well understood; it constitutes the spreading of mass from where it would be located and is derived from advection alone due to the heterogeneity of the porous media through which solute transport occurs (Domenico and Schwartz, 1998). A critical review of 59 field experiments by Gelhar et al. (1992) found that longitudinal dispersivity (aligned with the direction of flow and distinct from transverse dispersivity, which is aligned perpendicular to the flow field) increased indefinitely with increasing transport distance. However, not all of the experiments were classified as ‘reliable’. Of those that were, the scale of the study ranged from approximately 10 to 300 m and had a corresponding longitudinal dispersivity of less than 1 m to as much as 5 m. Among the ‘low reliability’ studies, ranges of longitudinal dispersivity were significantly greater, reportedly between 10^1 and 10^3 m for numerical grid scales between 10^1 and 10^5 m.

In the present study, initial estimates of dispersivity were set equal to 250 m corresponding to the grid spacing and uniformly were applied to both layers in both modeled regions. A distributed set of pilot points as well as the final estimated dispersivity values are shown in Figure 6-14.

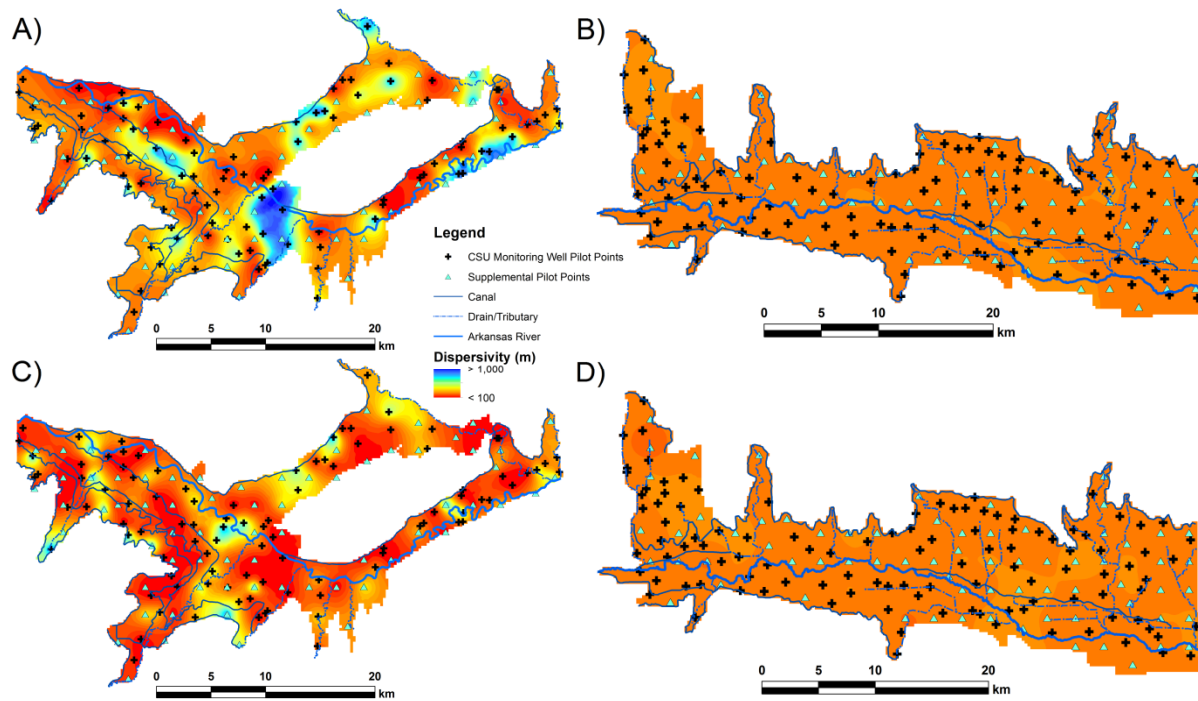


Figure 6-14. Estimated dispersivity values for layer 1 of (A) the USR and (B) the DSR and for layer 2 of (C) the USR and (D) the DSR.

6.6 FINAL CALIBRATED PARAMETER VALUES

6.6.1 Calibrated Initial Salt Concentration Values

Figure 6-9 shows the final calibrated values of the initial salt concentration arrays for layers 1 and 2 in the USR and DSR. In both regions, correlation between the estimated salt concentration in layers 1 and 2 is 0.71 in the USR and 0.38 in the DSR. Figure 6-15 depicts the distribution of initial salt concentrations for each layer in both the USR and DSR. As expected, the spatial mean initial salt concentration in the USR is lower than that in the DSR. In both regions, the initial salt concentration in layer 2 is greater than in layer 1, and corresponds to the prevalence of saturated conditions throughout layer 2. That is, although not all layer 2 cells will be saturated, they will at a minimum contain the water table. Layer 1, on the other hand, may be partially saturated or completely unsaturated in cells where the simulated groundwater table falls below the bottom of the layer. In both models, the spatial standard deviation in initial salt

concentration is approximately 3,000 mg L⁻¹, except for in layer 1 of the DSR, where it is about 1,800 mg L⁻¹. This may be due in part to the fact that the water table is generally deeper in the DSR, thereby possibly limiting the sensitivity of model simulation to initial salt concentration in layer 1.

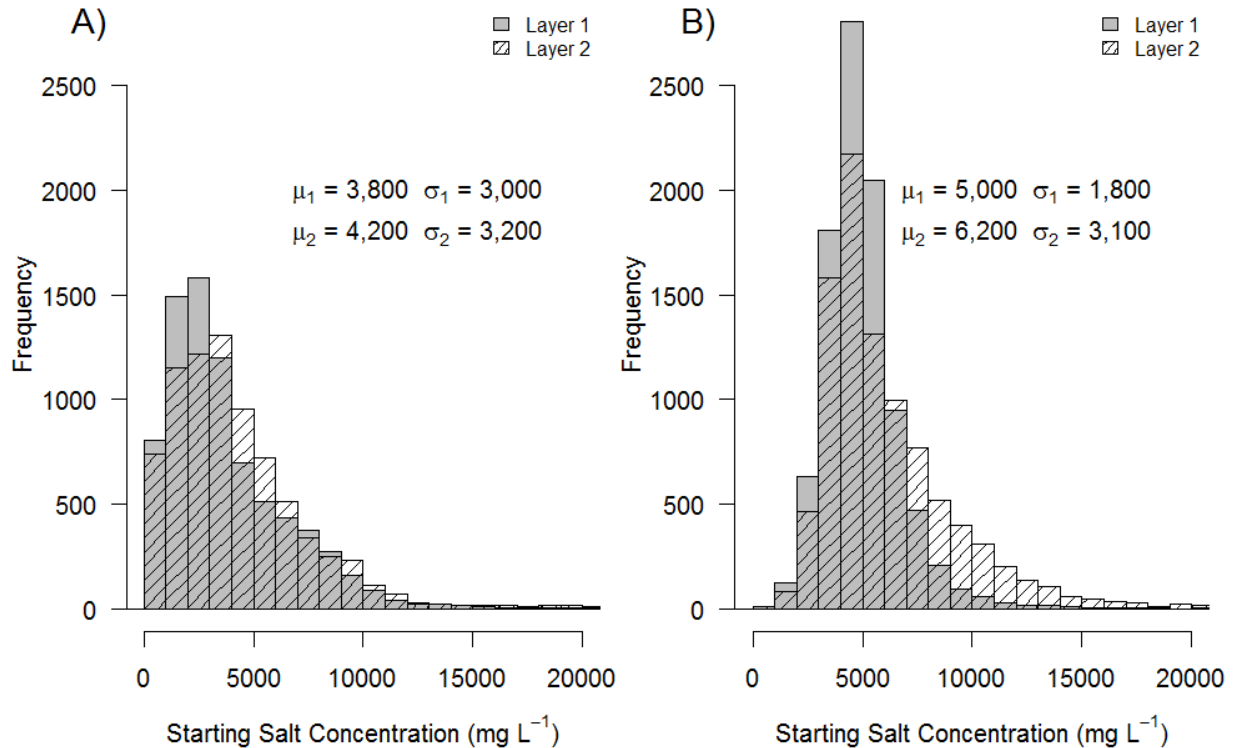


Figure 6-15. The distribution of the final estimated starting salt concentration arrays for both layers in (A) the USR and (B) the DSR.

6.6.2 Calibrated Aquifer Porosity Values

Distributions of the final estimated aquifer porosity values over the modeled regions are shown in Figure 6-16. A mean of 0.31 is observed in layer 1 of the USR and in both layers in the DSR. The lower porosity values in layer 2 of the USR were a result of the PEST optimization algorithm. Figure 6-17C shows that over nearly all of layer 2 in the USR, an adjustment factor value other than 1.0 was sought, indicating that the S_y array found during the

flow model calibration may have been significantly different had the flow model calibration been informed by observations related to the salt transport problem. Nevertheless, porosities in layer 2 of the USR salt transport model are clearly lower than those of layer 1, a non-intuitive result. There are a number of possible reasons for this result: 1) higher prevalence of fine-grained material in the deeper subsurface [see borehole information documented in Major et al. (1970)], 2) excessive salt precipitation resulting in lower porosities, 3) a compensatory response to an inadequately calibrated flow model, and 4) a lack of proper representation of precipitation and dissolution

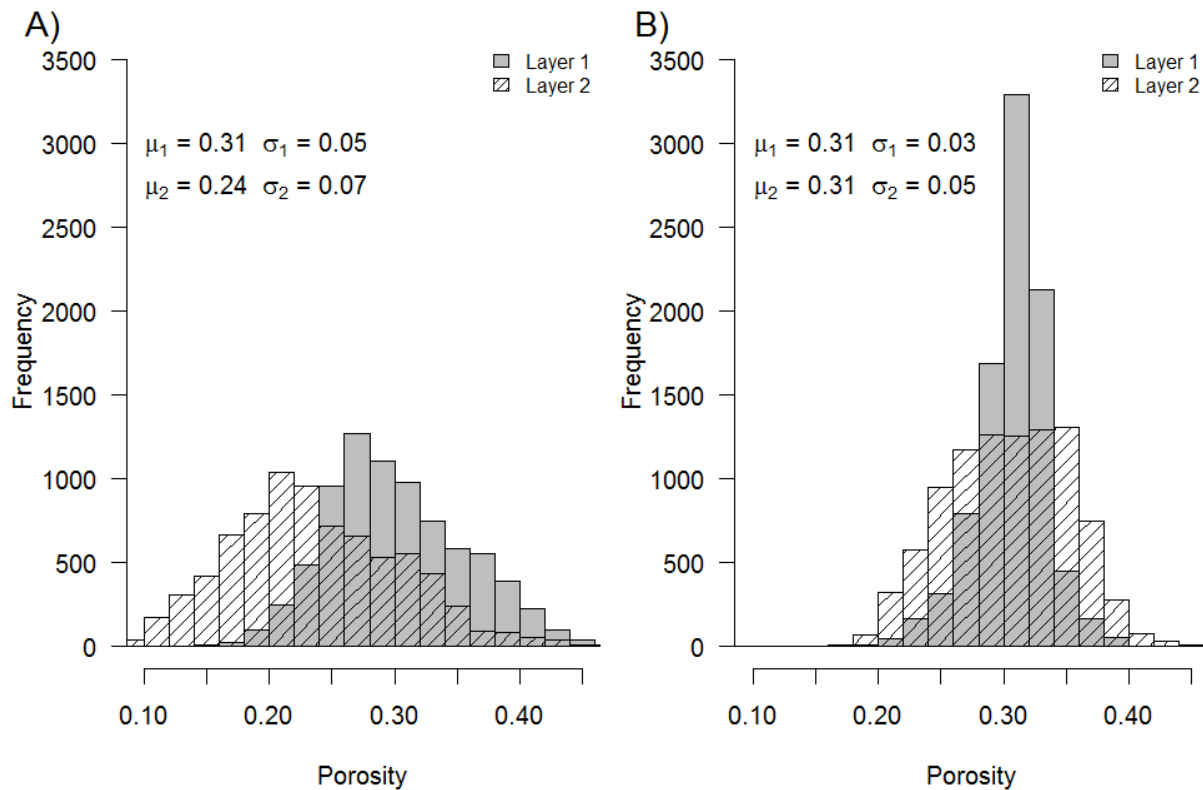


Figure 6-16. The distribution of the final estimated porosity arrays for both layers in (A) the USR and (B) the DSR.

reactions in the solute transport model. More spread in the porosity values is observed in the USR, where the standard deviations are 0.05 and 0.07 in layers 1 and 2, respectively. In the DSR, the standard deviations are 0.03 and 0.05 in layers 1 and 2, respectively.

Differences between aquifer porosity and S_y are expected; not all of the drainable pore space will effectively transmit dissolved solutes (Zheng and Wang, 1999a). Automated calibration departures from the starting estimates of porosity are plotted in Figure 6-17. Modification of an adjustment factor that modifies the porosity array was used for the following two reasons. First, adjustments to the flow model's S_y array were easily restricted to $\pm 25\%$.

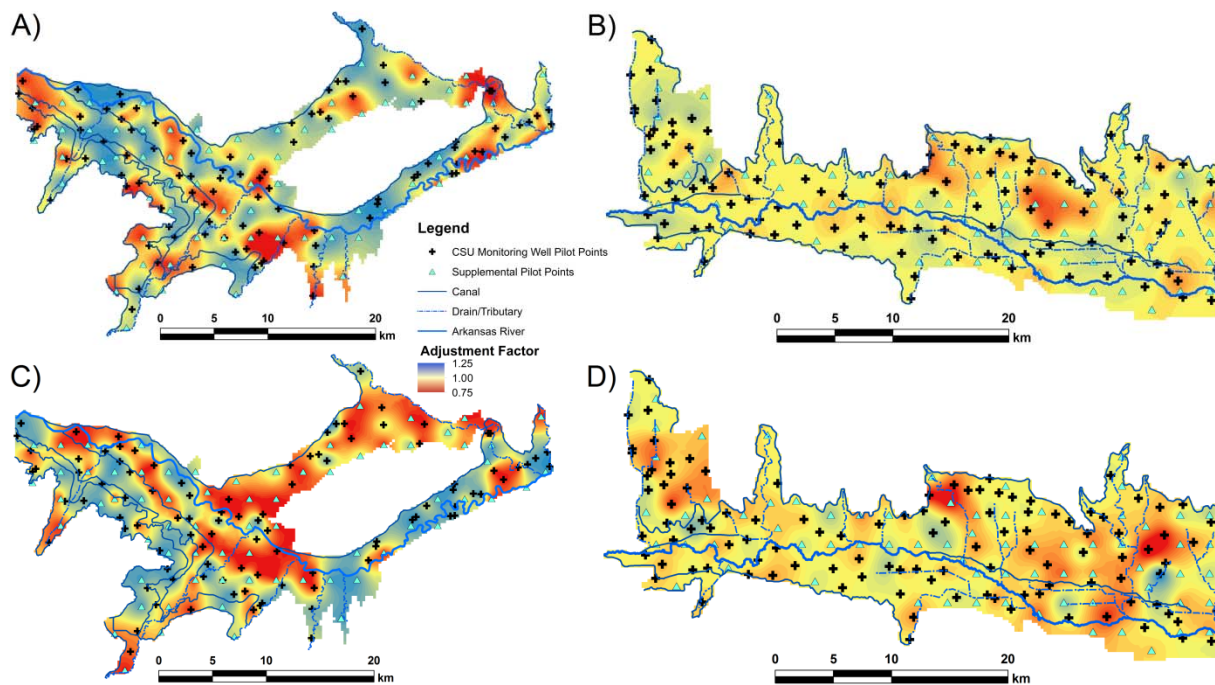


Figure 6-17. An adjustment factor, initially set equal to 1.0 over the modeled areas, was used to adjust the initial estimates of porosity values. The final estimated adjustment factor values ranged between approximately 0.75 and 1.25.

Second, the final result (Figure 6-17) highlights areas of departure from the flow model's calibrated S_y array and may be indicative of an inadequately calibrated S_y array in the flow model. Yellow and near-yellow colors displayed in Figure 6-17 indicate little or no adjustment

to porosity values. The extent of the adjustments is a bit greater in the USR where a preponderance of either reds or blues is observed. Reflecting on the final calibrated fit between simulated and calculated (“observed”) unaccounted-for return flow in the USR – discussed in Section 4.4 and used as a fixed flux in the salt transport models – the larger adjustments to porosity in the USR may be a compensatory response by the automated calibration algorithm applied to the salt transport model to overcome the fixed groundwater return fluxes.

6.6.3 Calibrated Aquifer Dispersivity Values

In the DSR, model results were found to be relatively insensitive to dispersivity values as evidenced by the fact that the final dispersivity arrays were relatively unchanged from their initial estimated values (Figure 6-14B and Figure 6-14D show are predominantly orange in color and indicate a dispersivity of roughly 250 m). In the USR, a greater sensitivity to dispersivity resulted in significant modification of the initial dispersivity values (see the final values displayed in Figure 6-14). The final estimated layer 1 and 2 mean dispersivity in the USR was 356 and 246 m, respectively, with standard deviations of 206 and 133 m in layers 1 and 2, respectively. An insensitivity to dispersivity values in the DSR kept the mean estimated dispersivity close to the initial values of 250 m with nearly no variability; standard deviations were 7 and 12 m in layers 1 and 2, respectively (Figure 6-18).

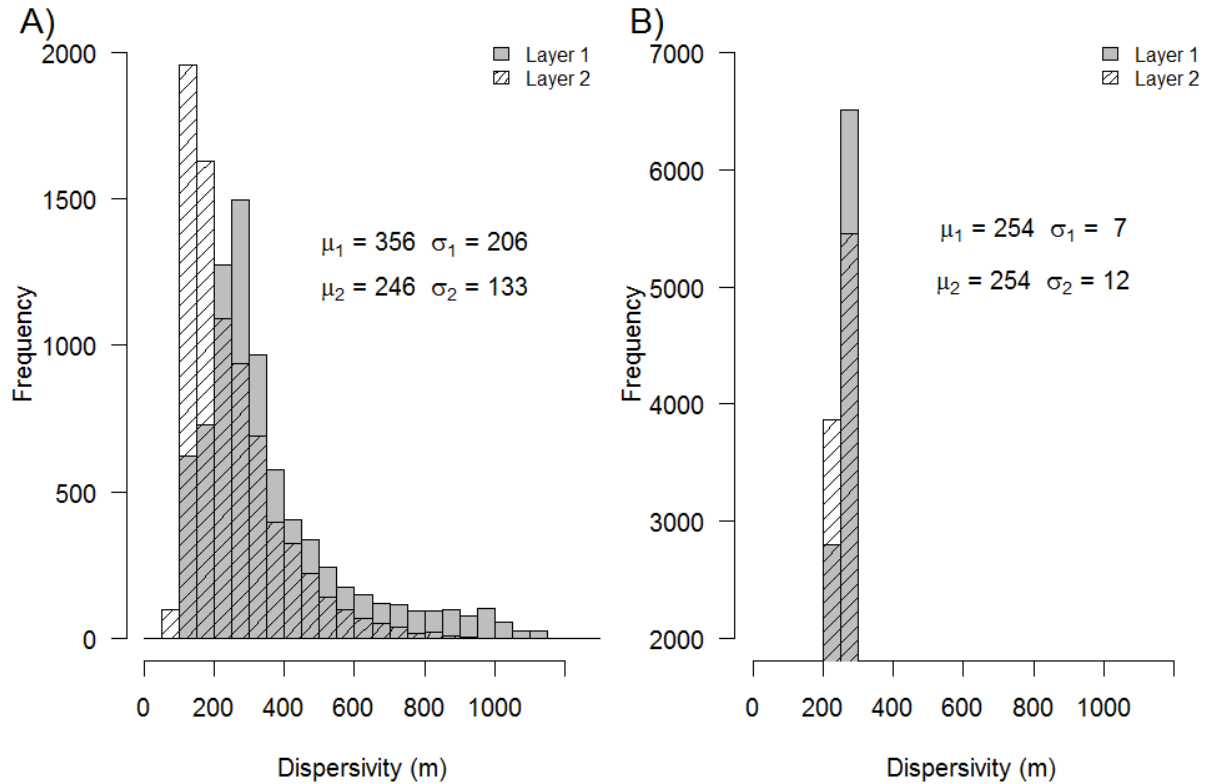


Figure 6-18. The distribution of the final estimated dispersivity arrays for both layers in (A) the USR and (B) the DSR.

A reasonable explanation for the differences in the final calibrated dispersivity values between the two regions is difficult to ascertain. Because the water table in the USR resides in layer 1 (much more so than in the DSR), and layer 1 is directly tied to two of the observation groups (groundwater salt return load and soil water salinity), greater model parameter sensitivity would be expected in the USR. The deeper water table in the DSR, where most of the groundwater flow will be occurring, may in effect inhibit the model parameters (e.g., layer dispersivity) influence on the total objective function. Also, these results may indicate that an insufficient suite of parameters are included in the automated parameter estimation routine, especially in the DSR. An overall insensitivity to dispersivity in the DSR suggests that including

salt precipitation and dissolution reactions in the conceptual model may result in a better calibrated salt transport model.

6.7 CALIBRATION AND TESTING PERFORMANCE MEASURES

The calibrated salt transport models are used to simulate baseline conditions only. Unlike in the previous chapter, these models are not used to run comparative scenario analyses. Instead, the ability to simulate conditions in the LARV using a conservative (i.e., non-reactive) transport approach, using the parameters described previously, is pursued. Observations from 1999-2007 and from 2002-2007 are used in the USR and DSR, respectively, to evaluate model performance.

6.7.1 Simulated Groundwater Salinity

The average groundwater salt concentration residuals, calculated as simulated values minus observed values, in the USR and DSR during the calibration period are 460 and 820 mg L⁻¹, respectively. Testing period residuals are 80 and 730 mg L⁻¹ in the USR and DSR, respectively (Figure 6-19). Consistent over-prediction of the groundwater salinity is likely related to the under-prediction of soil water salinity, discussed in Section 6.7.3 below. On the one hand, PEST will attempt to decrease the amount of salt in the system to resolve difference between simulated and observed groundwater salt concentrations. On the other hand, the automated parameter estimation algorithm also will attempt to add more salt to the simulation to correct under-simulation of soil water salt concentrations. Depending upon weighting scheme provided, PEST will minimize the observation group with the largest contribution to the total objective function. Chemical reactions (i.e., precipitation and dissolution), finer discretization of layer 1, and the ability to simulate the upward movement of salt (currently unavailable in MODFLOW-NWT and the UZF1 package) may resolve this discrepancy. Variability in the residuals is considerable, with standard deviations of 1,000 and 1,300 mg L⁻¹ for the USR and

DSR calibration period datasets, respectively. Residual standard deviation during the testing period increased to 1,300 and 1,600 mg L⁻¹ in the USR and DSR, respectively. The mean and standard deviation of the groundwater salinity observations were calculated for each well in the USR and DSR. The spatiotemporal coefficient of variation (CV) among the wells and over the simulated period in the USR and DSR is 0.72 and 0.86, respectively, indicating that the targeted values were highly variable.

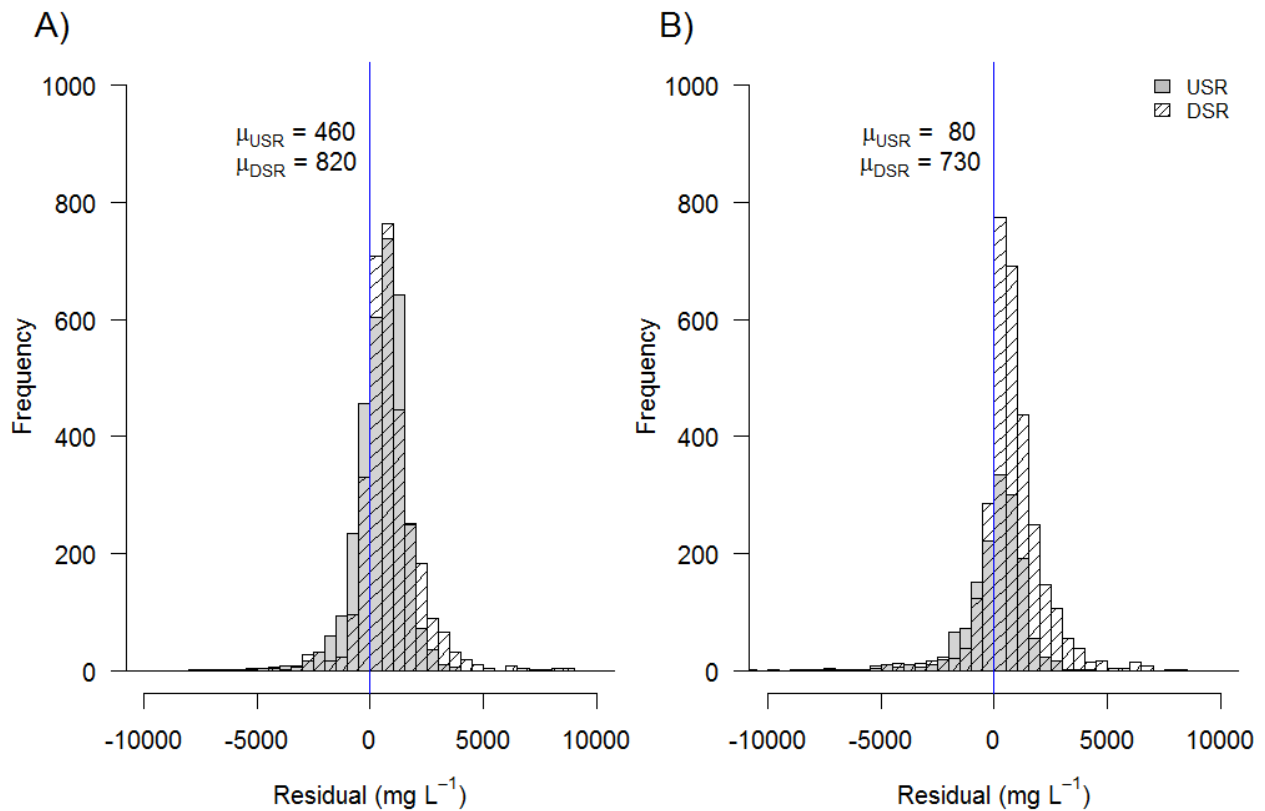


Figure 6-19. Groundwater salt concentration residuals for (A) the calibration and (B) the testing periods for both the USR and DSR.

Figure 6-20 shows example time series plots for four groundwater monitoring wells in each region. Fits of simulated to observed values range from good (well 344) to bad (well 80)

(Figure 6-20). Often, wells start with an acceptable fit (wells 356, 398), but then trend away from the observations. Inaccurate model input resulting from imprecise knowledge of historical cropping patterns (i.e., simulated irrigation applications deviate significantly from physical reality resulting in simulated water contents that are too high or too low and salt inputs that are too high or too low), model simplifications including the lack of chemical precipitation and dissolution reactions in the salt transport model, inaccurate data collected from monitoring wells, or combinations of these likely contribute to this type of misfit. The variability observed in wells 67 and 80 is considerable and may indicate the limitations of a coarsely-gridded regional-scale model to accurately simulate detailed field-scale processes. The trends in wells 344 and 356 were unexpected. Crop type in both of these fields remained fixed for the duration of the simulated period as pasture (344) and alfalfa (356) and maintained a large D_{wt} (approximately 5 m), likely due to their proximity to (within 250 m) quarter kilometer of the Amity Canal. However, because the Amity Canal was frequently water short and total canal seepage may have been less than during the preceding wet years, it is possible that groundwater salinity was dropping due to a combination of salt precipitation associated with a declining water table and correspondingly lower water contents and dilution from less saline groundwater flowing into the study region from the desert escarpment. However, there are no available observations from before the simulated period to corroborate this.

6.7.2 Simulated Return Salt Load

The average simulated groundwater return salt load to the Arkansas River in the USR region during the calibration period is 5,200 MT wk⁻¹, whereas the average observed return salt load is 4,400 MT wk⁻¹. Considerable variability is observed in the observation dataset; the temporal standard deviation over the calibration period is 6,400 MT wk⁻¹ and likely is due

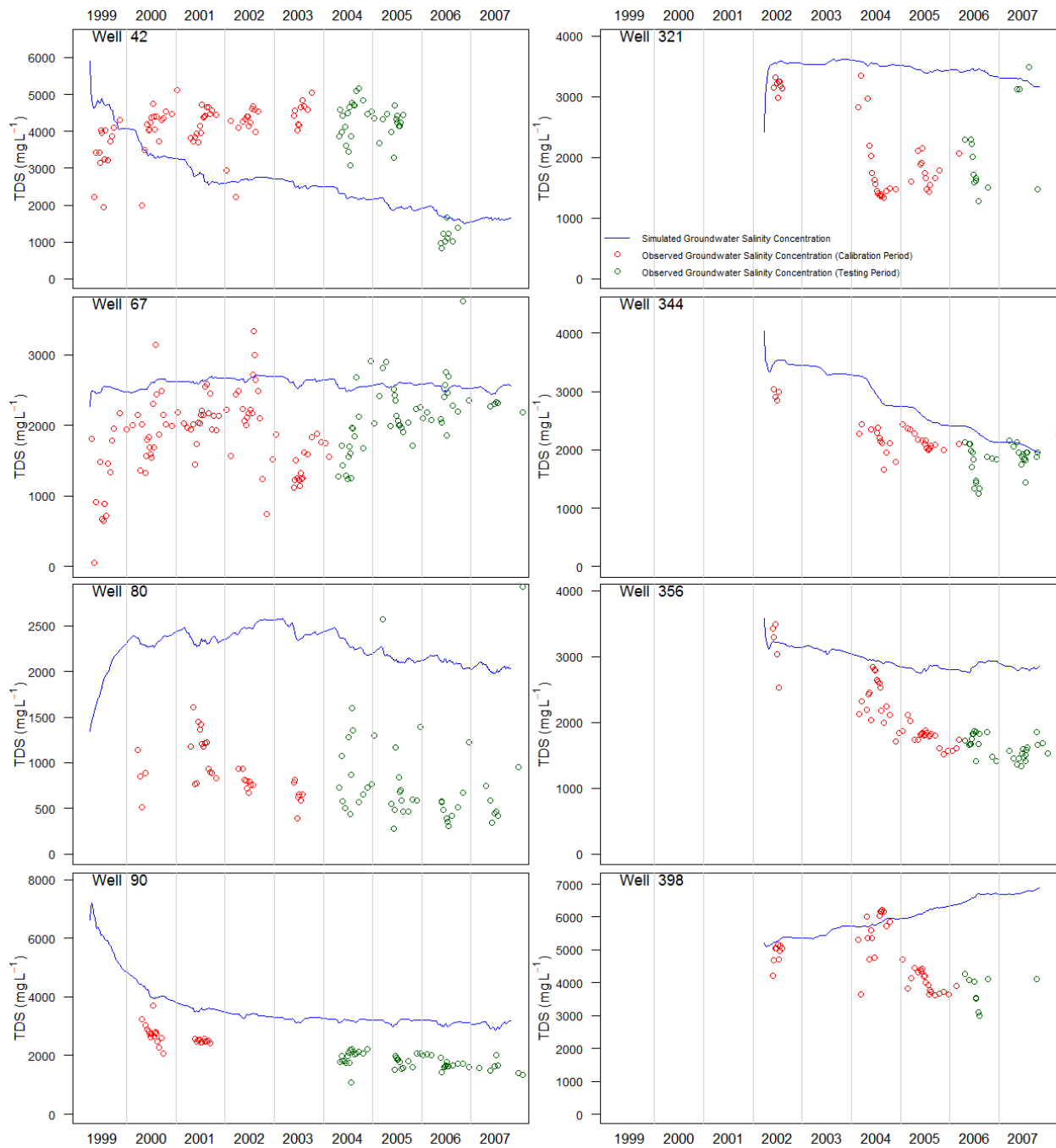


Figure 6-20. Model performance in predicted groundwater salt concentration in comparison to observed salt concentration in monitoring wells at four locations in the USR [wells 42, 67, 80, and 90 (Figure 4-1A)] and at four locations in the DSR [wells 321, 344, 356, and 398 (Figure 4-1B)]. The wells shown here correspond with those selected in Figure 4-5.

to the wet (1999-2001) and dry (2002-2003) stretches falling within this relatively brief span of time. The variability in the simulated return salt loads over the calibration period is approximately 2,100 MT wk⁻¹, less than a third of that in the observation dataset.

Statistics over the test period in the USR also demonstrate similar misfit between simulated and observed values. Mean return salt loads are 1,800 and 3,800 MT wk⁻¹ for the observed and simulated datasets, respectively. As with the calibration period, the standard deviation of the observed return salt loads was considerable at 5,800 MT wk⁻¹ due to negative values or loss of salt from the river to the underlying alluvial aquifer in the observation dataset. Simulated standard deviation during the testing period remained relatively unchanged from the calibration period at 1,400 MT wk⁻¹.

A similar situation is encountered during the DSR calibration period, the mean simulated calibration period return salt load, 5,800 MT wk⁻¹, is larger than the observed average of 4,200 MT wk⁻¹. Moreover, the standard deviation in the observed and simulated values, 2,800 MT wk⁻¹ and 1,500 MT wk⁻¹, respectively, follows a pattern similar to what was encountered in the USR. Whereas the simulated standard deviation was approximately one third of the observed in the USR, it was approximately one half in the DSR. The reduced variability in the DSR observation dataset likely is rooted in the absence of the 1999-2001 data; only the persistent dry conditions experienced from 2002 through 2005 are included in the observation dataset. The mean observed and simulated return salt loads during the testing period are 6,100 and 6,300 MT wk⁻¹, respectively. Standard deviation associated in the observed and simulated return salt load values for the test period is 3,400 and 1,800 MT wk⁻¹, respectively.

For reasons similar to those discussed in Section 4.4.3, misfit between simulated and calculated return salt loads is expected. First, the uncertainty associated with gaged flows and

especially with ungaged surface water return flows, as well as with their respective salt concentrations, downgrades the confidence in “observed” values of salt load. Second, the spatial and temporal discretization schemes adopted in the models fail to fully capture the heterogeneity found in nature and a number of physical processes that occur in study areas are neglected. Although inclusion of chemical reactions in the salt transport simulation would allow salt to precipitate out of solution and lower salt return loads back to the river, it is more likely that initial salt concentrations estimated by PEST place too much salt in the simulation that returns back to the river throughout the simulation period.

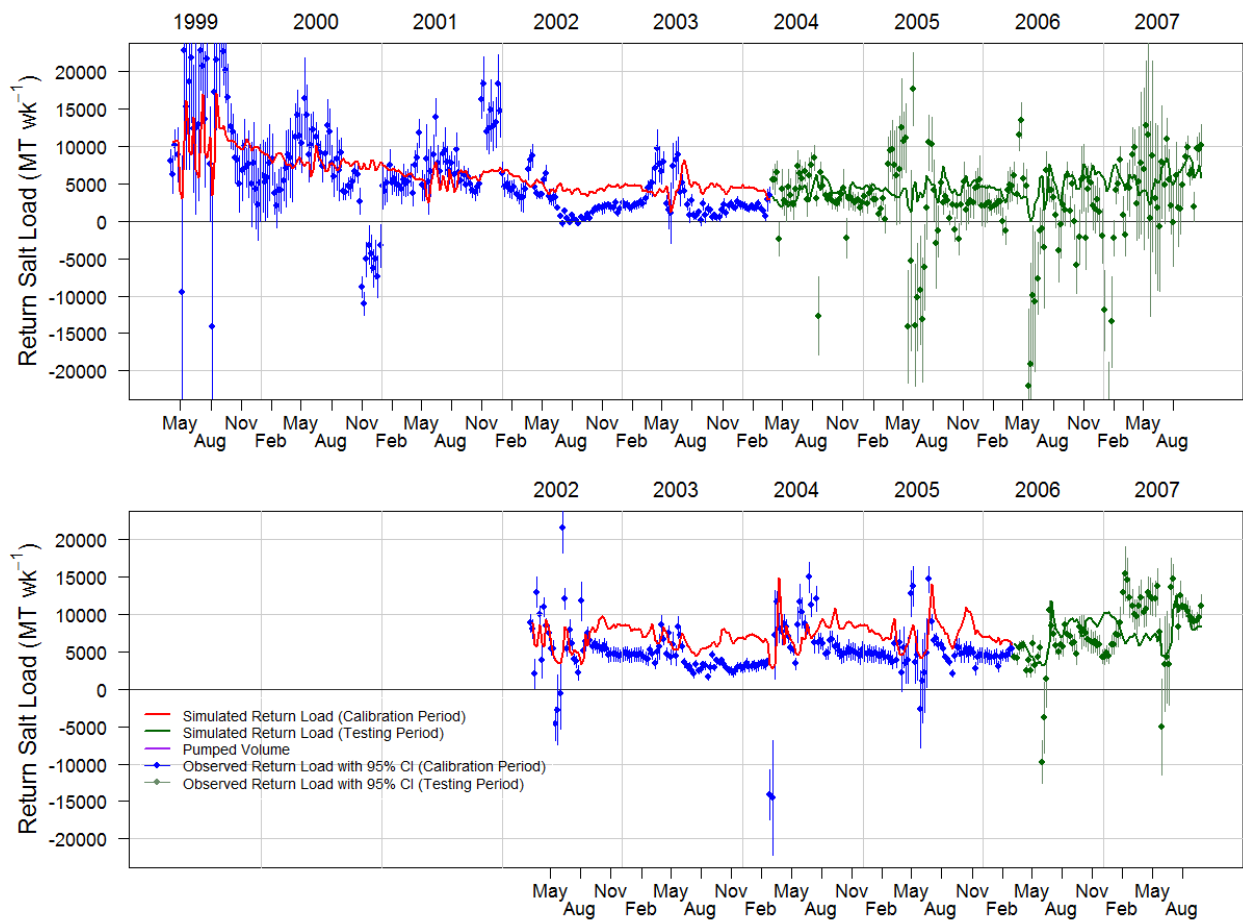


Figure 6-21. Groundwater return salt load to the Arkansas River in the (A) USR and (B) DSR.

As expected, a plot of the return salt load resembles the groundwater return flow plot for each region. Visual inspection of Figure 6-21 indicates that the limitations discussed in the flow models apply to the salt transport model as well. At times, the simulation appears to demonstrate the variability present in the observations (e.g., during the 1999 and 2003 irrigation season in the USR or during the 2002, 2004, and 2005 irrigation seasons in the DSR). However, the seasonal-scale periodicity present from 1999 through 2001 appears to be missing from the simulation in the USR.

6.7.3 Simulated Soil Water Salinity

Compiled soil water salinity survey results described in Morway and Gates (2012) serve as the target dataset for simulated soil water salinity. For the remainder of the discussion, the simulated layer 1 salt concentration (which encompasses both the vadose and saturated zones) is considered to roughly approximate the simulated soil water salinity. To ensure reasonable comparability, simulated and observed values were considered at only a select subset of numerical grid cells. First, the simulated salt concentrations were gathered only from those numerical grid cells with 99% crop coverage or greater. Through this restriction, difficulties associated with the interpretation of simulated salt concentrations associated with partially-cropped cells are eliminated. In addition to full crop cover, the simulated D_{wt} in a cell had to be greater than 1.5 m for it to be selected for comparing simulated salt concentrations to observed salt concentrations. Due to the volume-averaged approach adopted in UZF-MT3DMS (Morway et al., 2013), cells with a shallow water table would correspond to nearly-saturated conditions in layer 1, a state-of-affairs rarely encountered in the LARV while conducting soil salinity surveys. In both study regions, cells from across the modeled region fit the described criteria (Figure 6-22). Depending upon historical cropping patterns, cells often fit these two criteria in more than one growing season (e.g., a cell may have been cropped from 1999-2001 before being fallowed

in 2002) and therefore would contribute multiple predicted salt concentrations to the data displayed in Figure 6-23 and discussed next.



Figure 6-22. Location and frequency of cells in the USR and DSR used for generating a simulated layer 1 salinity distribution for comparison to the observed soil water salinity distribution.

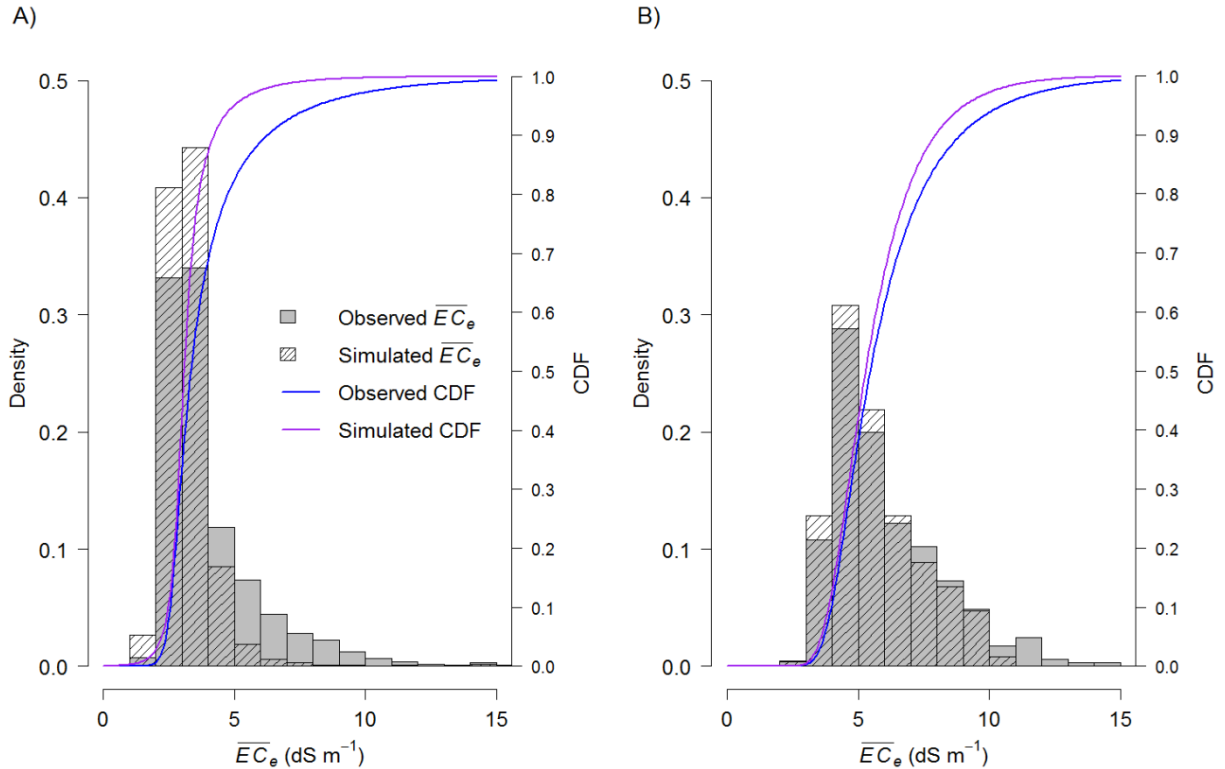


Figure 6-23. Comparison of frequency distributions and fitted cumulative distribution function (CDF) of observed soil water salinity and simulated layer 1 salinity expressed as EC (dS m^{-1}) in (A) the USR and (B) the DSR. CDFs of \overline{EC}_e are plotted to provide consistency with Figure 3-3, where observations of \overline{EC}_e first were reported and discussed.

Figure 6-23 shows the frequency histograms and corresponding CDFs for both the observed soil water salinity and simulated layer 1 salinity values in each study region. A post-processing routine was used to inform the automated parameter estimation software (PEST) of the difference between the CDFs as PEST searched for sets of parameter values to minimize the difference between the observed (blue) and simulated (purple) CDF curves, in addition to minimizing fits to other observations. Because no separate \overline{EC}_e -TDS regression relationship for soil water has been established for the LARV, the groundwater EC-TDS relationships shown in Figure 6-6A (USR) and Figure 6-6C (DSR) were used to convert predicted TDS values (mg L^{-1})

to an equivalent \overline{EC}_e . Finally, simulated \overline{EC}_e is interpreted as comparable to field-averaged observed values of \overline{EC}_e as reported in Morway and Gates (2012) (Chapter 3).

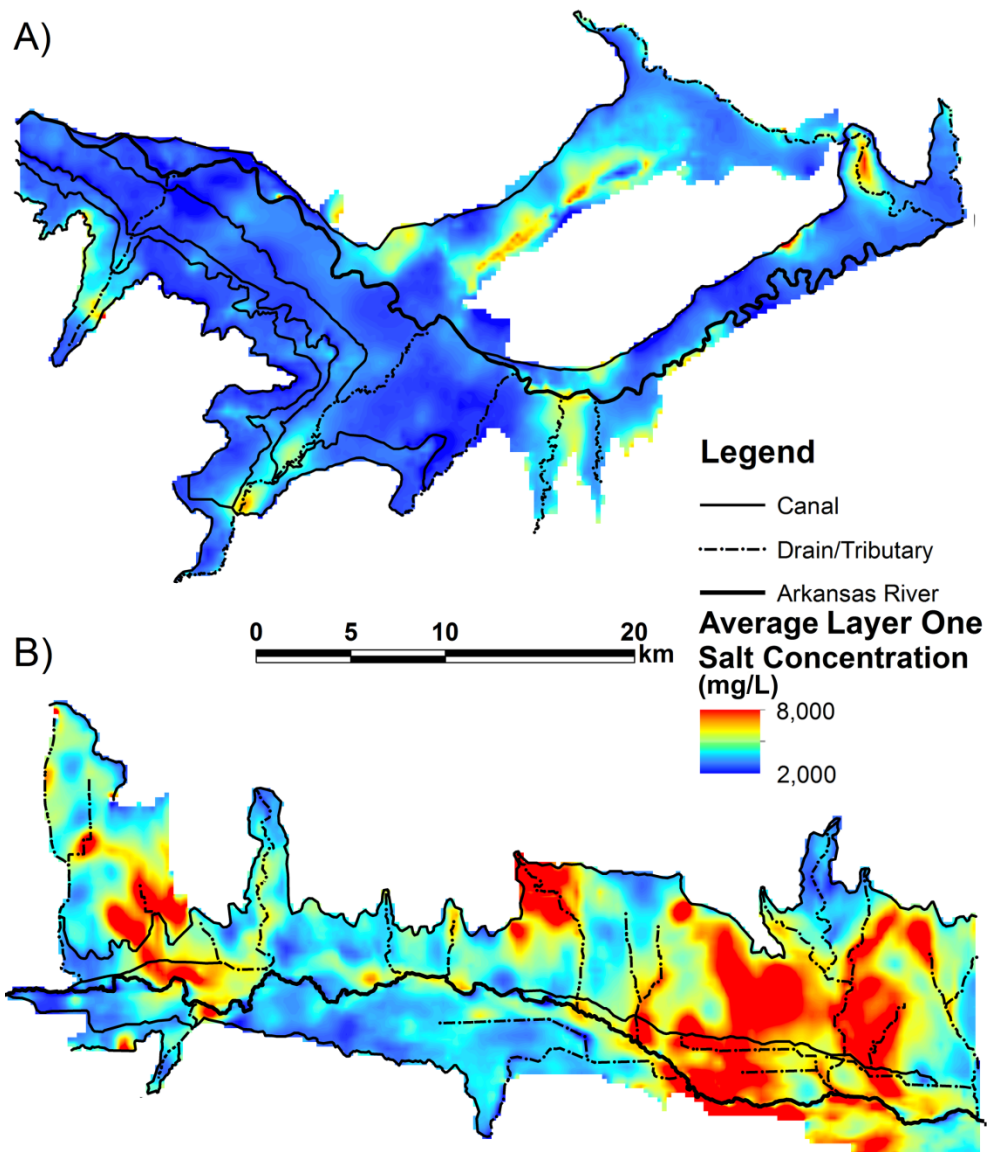


Figure 6-24. Average irrigation season dissolved salt concentration in layer 1 over the course of the simulated period for (A) the USR and (B) the DSR.

A relatively good fit was achieved in both study regions, especially in the DSR. In the USR, a significant proportion of the observed values fell between 2 and 5 dS m⁻¹, a characteristic that the parameter estimation was able to match fairly well. Above 5 dS m⁻¹, however, the model under-predicts soil water salinity, perhaps the result of neglecting the presence of precipitated salts (i.e., gypsum and calcite) in the unsaturated zone, which, had they been accounted for, would be available to re-enter the dissolved-phase and raise simulated concentrations. Due to a shallower water table which often resides in layer 1 in the USR, the volume average approach would result in higher simulated water contents. While higher water contents may tend to drive predicted salt concentrations down, they may instead facilitate greater dissolution of precipitated salts resulting in higher predicted concentrations. Conversely, in the DSR, where the water table is deeper and more commonly found in layer 2 and where chemical precipitation of soil salts may be more common, the volume-averaged approach may better approximate reality, explaining the good fit achieved in the DSR.

Although Figure 6-23 indicates the prevalence of higher soil water salt concentrations found in the DSR, Figure 6-24 reveals the stark contrast between the spatial distributions in the two regions. The predominantly blue hues in the USR are replaced by lighter shades of blue, yellows, and reds associated with higher salt concentrations in the DSR. In the DSR, where much more variability is observed, higher salt concentrations are simulated at various points throughout the region. Higher soil water concentrations in the DSR are no surprise due to the higher salt concentrations of the diverted irrigation water below John Martin Reservoir. Moreover, because surface water rights in the DSR are generally junior to those found in the USR, an increased reliance on pumped saline groundwater for irrigating crops sustains higher soil water concentrations in the DSR.

6.8 SIMULATION OF BASELINE SALINITY CONDITIONS

Using GIS spatial analysis routines, agricultural fields were intersected with the time-averaged simulated values layer 1 salt concentration for each irrigation season. Next, these average values were pooled according to their reported or remotely-sensed crop type, and are suggestive of the impact soil water salt concentrations have on LARV crop yields. Results for four of the predominant crop types grown in the LARV, alfalfa, corn, wheat, and sorghum, are provided in the four upper plots of Figure 6-25. The fifth plot shows results for ‘fruits and vegetables,’ including the various melons grown in the valley, onions, etc. For the most part, simulated salt concentrations remain steady through time for each of the selected crop categories, although a decline in the seasonal-average concentration for fruits and vegetables in the DSR is detected. The apparent decline in simulated values from 2002-2003 to 2004-2007 is likely not statistically significant due to the fact that very few fields fall under this classification. In the USR, average soil water salt concentrations hover around 3 dS m^{-1} for each of the displayed crop categories, or close to the threshold where crop yields begin to decline due to salinity. Concentrations in the DSR cropped fields are well in excess of threshold salinity values ($> 5 \text{ dS m}^{-1}$). Section 3.3.4 first described the meaning of the crop yield threshold band, above which the yields of the predominant crops grown in the LARV begin to decline in response to high soil water salinity.

Simulated layer 1 salinity concentrations (which are representative of soil water salinity concentrations) also were considered in relation to simulated D_{wt} . Simulated concentrations were estimated as equivalent \overline{EC}_e and paired with their corresponding simulated D_{wt} values. Figure 6-26 plots the simulated D_{wt} - \overline{EC}_e pairs with observed D_{wt} - \overline{EC}_e pairs described

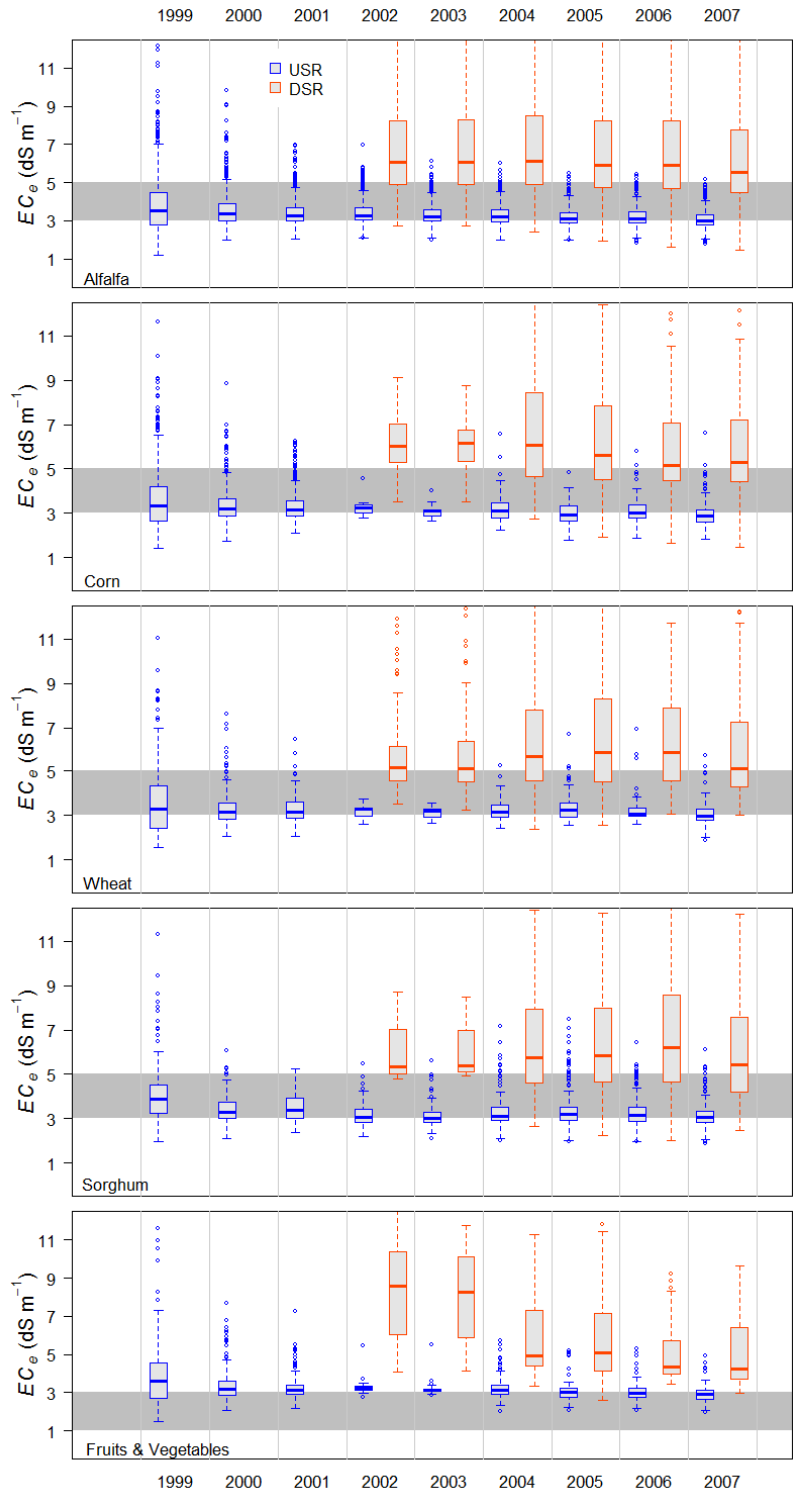


Figure 6-25. Temporal variability of the average simulated layer 1 dissolved salt concentration (expressed as EC_e) among the most common crops planted in the USR and DSR study regions. The 3-5 $dS\ m^{-1}$ zone of crop-yield reduction threshold is highlighted by the horizontal grey bar. Because the salt tolerance for fruits and vegetables is lower, a 1-3 $dS\ m^{-1}$ zone is shown in the bottom plot.

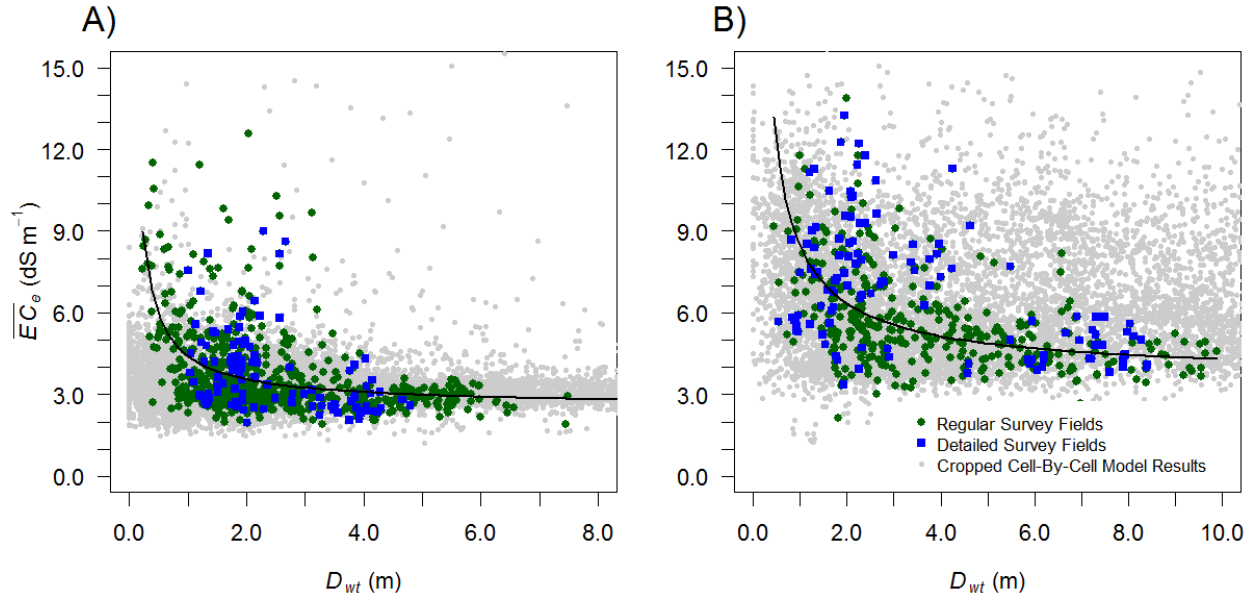


Figure 6-26. Simulated $D_{wt}\text{-}\overline{EC}_e$ versus observed $D_{wt}\text{-}\overline{EC}_e$ relationships for (A) the USA and (B) the DSR. Simulated $D_{wt}\text{-}\overline{EC}_e$ pairs are derived from average irrigation season values and include only those values from cells with > 99% crop coverage. Simulated \overline{EC}_e values are back-calculated from the concentration values simulated by UZF-MT3DMS.

in Morway and Gates (2012). It is important to recall that the simulated layer 1 salt concentration represents a volume average over the entire 5 m thickness of layer 1, whereas $D_{wt}\text{-}\overline{EC}_e$ pairs are based on soil water salinity for the upper 1.5 m. This volume averaging degrades the suitability of the comparison.

In both study regions, the lowest simulated layer 1 \overline{EC}_e values match well the lowest observed \overline{EC}_e values over the full range of D_{wt} . Also, just as there is more spread in the observed $D_{wt}\text{-}\overline{EC}_e$ pairs collected in the DSR versus the USA, there also is more spread in the simulated DSR $D_{wt}\text{-}\overline{EC}_e$ pairs in the DSR as compared to the USA. In the USA, where no $D_{wt}\text{-}\overline{EC}_e$ pairs exist for values of $D_{wt} > 3.5$ m and $\overline{EC}_e > 5$ dS m⁻¹, very few simulated $D_{wt}\text{-}\overline{EC}_e$ pairs fall in this range. In the DSR, a greater density of simulated $D_{wt}\text{-}\overline{EC}_e$ pairs appears to span between $3 \leq \overline{EC}_e \leq 12$ dS m⁻¹ for $D_{wt} < 3$ m than for $D_{wt} \geq 3$ m, a trend evident in the observed $D_{wt}\text{-}\overline{EC}_e$

pairs. However, there is a greater preponderance of simulated $D_{wt}-\overline{EC}_e$ pairs with $\overline{EC}_e \geq 6 \text{ dS m}^{-1}$ for $D_{wt} > 3 \text{ m}$ compared to the observed $D_{wt}-\overline{EC}_e$ pairs fitting the same criteria. These results suggest that the model is simulating excessively high \overline{EC}_e values due to over-predicting evaporative concentration (simulated water content is too low), underestimating salt leaching (not enough mass removal), and/or neglecting dissolved-phase solute to solid-phase precipitation of salt.

It appears that the selected method for generating initial groundwater salt concentrations, while facilitating a relatively good fit between the distribution of observed \overline{EC}_e and simulated \overline{EC}_e in layer 1 (Figure 6-23), hampers the model's ability to match the observed $D_{wt}-\overline{EC}_e$ relationship. Three alternative model refinements may help overcome this limitation. In the first approach, the relationship depicted in Figure 6-8 of Morway and Gates (2012) could have been used to generate initial soil water salt concentration for each cell. That is, using the average D_{wt} calculated for each model cell, an initial soil water salt concentration could be calculated and perturbed by a random residual derived from the observed variability.

In the second approach, the values over which layer 1 initial salt concentrations for each pilot point are permitted to range could be constrained based on the average D_{wt} at that pilot point location. Because there currently are no pilot point-specific constraints, other than the uniformly-applied constraint that concentration values range between 500 and 30,000 mg L^{-1} there is no mechanism for preserving the $D_{wt}-\overline{EC}_e$ relationships depicted in Figure 6-26.

Finally, rather than using the $D_{wt}-\overline{EC}_e$ relationship documented in Morway and Gates (2012) to generate initial salt concentrations in layer 1 of the model, it could have been used in the automated parameter estimation routine as a target relationship. By first quantifying the misfit between the simulated and observed $D_{wt}-\overline{EC}_e$ relationships and then including it in the

PEST objective function, PEST would aim to preserve the observed relationship depending on the weights assigned to the observation type. The value of this approach would be in monitoring the ability of PEST to improve the fit depicted in Figure 6-26 (i.e., the grey circle “cloud” would be more similar to the green circle and blue square “cloud”) while also preserving the frequency distribution shown in Figure 6-23. To the extent PEST is unable to preserve the distributions shown in Figure 6-23 and force the simulated $D_{wr}-\overline{EC}_e$ relationship to be more like the observed $D_{wr}-\overline{EC}_e$ relationship depicted in Figure 6-26, deficiencies in the conceptual model (i.e., neglect of reactions, etc.) will be further highlighted. However, it is not clear that this approach would work considering the volume-averaging approach inherent in the UZF-MT3DMS model. Due to the wide-ranging water table conditions found throughout layer 1, the pilot point approach offers greater flexibility for identifying an initial layer 1 salt concentration that achieves a good fit to the observed soil water salinity (Figure 6-23).

6.9 CONCLUSIONS

Two salt transport models, calibrated and tested with an extensive dataset are presented for use with the groundwater flow models described in Chapter 5 (Morway et al., 2013). Because the flow and salt transport models were calibrated separately, the information content within the salt concentration observations was not used to help constrain the flow solution. Since the flow solution was fixed at the outset of the salt transport parameter estimation routine, final parameter values may, in the end, reflect some compensation for inadequacies in the flow solution that would have been reduced had the salt transport solution informed the flow calibration.

Of the three targeted datasets, model fits to observations of return salt loads to the Arkansas River are poorest. This likely is caused, at least in part, by conceptual model errors.

Representation of the surface water network with the RIV package (Harbaugh, 2005) in MODFLOW rather than with the SFR2 package (Niswonger and Prudic, 2005) limits the robustness of the analysis. Conceptually, it would be more realistic to simulate groundwater/surface water solute exchange with a salt mass-routing surface water simulator rather than with a fixed boundary condition. Making this switch would facilitate calculation of total salt load entering and exiting the study regions, including both the Arkansas River and the canal flows crossing north-south transects located near the western and eastern model extents. Moreover, salt mass-routing capabilities would make it easier to incorporate “observations” of tributary salt loading in to the automated parameter estimation routine. For example, continuously-recorded flow rates in a number of the LARV tributaries (e.g., Timpas Creek, Horse Creek, Big Sandy, and Wild Horse Creek) along with periodic measurements of EC as recorded in the CSU LARV database make it possible to estimate the “observed” salt loads occurring in these tributaries, thereby refining spatially the sources of salt load back to the Arkansas River. Unfortunately, this analysis is not yet possible since MT3DMS currently is not equipped to simulate solute transport in open channels accounting for groundwater exchange. Were this model enhancement to become available, the simulation of salt loads for comparison to observations would be simplified (e.g., Figure 6-7 could be a target dataset). Rather than estimate various return load budget terms on the river (i.e., Equation 6-3), where the river is represented as a boundary rather than as an integrated component of the entire system, a far more simple approach would be to target the difference in salt load entering and exiting the study regions. Calculation of annual return salt loads revealed that in many of the simulated years of the study period, there was little to no increase in the annual return salt load. Thus, use of a conservative solute in the salt transport simulation seems to work well when considering annual

salt loads in all but the wettest years. If, on the other hand, seasonal (i.e., weekly to monthly) salt loading dynamics are suspected of straying significantly from the annual equilibrium observed during the hydrologically average to dry years, for example irrigation versus non-irrigation seasons dynamics, then chemical reactions that accommodate the build-up and release of salts from solid-phase storage and the oxidative dissolution of salts from shale may be necessary.

In addition, spatial refinement of the observations [i.e., estimation of return salt loads to the river between stream gages internal to the modeled domains (e.g., Rocky Ford gage in the USR or the Carlton gage in the DSR)] may benefit the analysis as well. Spatial refinement of the return salt loads would accommodate the spatially heterogeneous presence of salt-bearing shales. Here again, estimated parameter values, especially those impacted by the precipitation and dissolution of salts in and out of solid-phase storage, may be prone to taking on compensatory values due to the lack of spatial refinement in the salt return load observations.

Significant improvement in the simulation of salt return load would be nearly impossible without also re-calibrating the flow models using the information content contained in the salt concentration and salt load observations. While on the one hand a simultaneous calibration of the flow and salt transport model would help improve the return salt load fits, hard lessons learned during the flow model calibration exercise are not yet forgotten. Six calibration targets were used in the flow model calibration and proved very difficult to match simultaneously. Adding three (or more) targets would likely make the automated parameter estimation routine even more difficult to set up and would impose additional non-linearities on the gradient search algorithm in PEST.

Over much of the study regions, simulated groundwater salinity is high. It is not surprising, then, that return salt loads also are high. However, the fit achieved for the majority of monitoring wells in each region provides encouragement. Trends in saturated groundwater salt concentration fits achieved by PEST generally follow trends in the observed groundwater salinity time series. It is hard to imagine any model larger than a field-scale study capturing the variability present in the groundwater salinity time series for most of the monitoring wells. Few time series were found in the Arkansas River modeling literature demonstrating superior fits to those shown in Figure 6-20. There are some wells where the simulation clearly did a poor job of capturing observed trends [e.g., wells 80 and 321(Figure 6-20)]. How much of the misfit is attributable to a poor fit in the flow solution is unknown.

Achieving a closer match between simulated and observed groundwater salt concentrations in the mass transport modeling effort is further challenged by the fact that the actual irrigation history for each field is unknown. While this fact was acknowledged in Morway et al. (2013) in relation to simulated misfit in the flow model, the reality that this unknown dataset is at best only approximated by the flow models is good reason for lowering our expectations of what the salt transport model would be able to achieve on a well-by-well basis. For example, plots where the fit is reasonable [e.g., well 67 or well 344 (Figure 6-20)], suggest physical processes in the field in some years that are not accounted for by the models. Finally, given the considerable variability in the observed groundwater salt concentrations in many of the wells (e.g., well 67, well 80, well 321) it would be difficult for any model to capture such wide swings in concentrations, especially since some of the observed variability is due to measurement noise (i.e., poor instrument readings, poorly calibrated instruments, bad transcription of notebook values to databases, etc.).

A strength of the presented models are their ability to simulate soil water salinity, especially in the DSR. Baseline soil water salinity results suggest little temporal variability among the major crop types planted in the LARV, even during the extremely dry years of 2002 and 2003. However, while the model appears to fit well the observed distribution of \overline{EC}_e , it does not preserve the observed $D_{wr}-\overline{EC}_e$ relationships documented in Chapter 3 (Morway and Gates, 2012).

As was demonstrated in Chapter 3, insights gleaned from simulation models are helpful in ranking the efficacy of alternative management interventions. In most regional-scale applications, simulation models may be the only viable means of evaluating a wide range of interventions in combination (Singh, 2010). However, while models can be useful in providing quantitative measures of the relative impact of proposed interventions compared to a baseline simulation, decision makers also need to consider the impacts associated with social, legal, and other environmental concerns when weighing options.

The two salt transport models presented herein bear the hallmarks of model imperfections. Both models solve the advection-dispersion equation, with chemical reactions omitted. Undoubtedly, complex reactions occur in the field. However, a good understanding of conservative salt transport may help steer toward a better understanding of reactive transport processes. Cooper et al. (2008) suggest, with cautionary notes considered, that accurate simulation of reactions would be helpful, since fourteen successive soil-paste extractions using surrogate irrigation water on a pulverized soil sample from the LARV was unable to lower EC_e values below 4 dS m^{-1} . Neither of the described models are equipped to simulate high soil water concentrations sustained by dissolution of gypsum and calcite since reactions are not included in the models. Both physical and chemical considerations, like preferential flow pathways and

irrigation water chemistry, respectively, complicate the prediction of the efficacy of irrigation events aimed at leaching soil salts to improve crop growing conditions.

Ultimately, the adoption of alternative water management interventions aimed at improving crop growing conditions in the LARV will need to account for processes that may be much more significant under altered flow regimes. For example, lowering the groundwater table for reduced salt upflux and improved salt leaching conditions may not achieve the desired results if the dissolution of previously-precipitated salts (i.e., gypsum and calcite) sustains high soil water salt concentrations, as suggested by Cooper et al. (2008). In other words, disruption of current liquid-phase/solid-phase equilibria may offset the desired effects of altered management strategies. In addition to salt concentration gradients between dissolved and precipitated salts, alternative water management interventions should ensure that the chemistry of the interactions between the unsaturated-zone salts (e.g., gypsum, calcite) and the irrigation water do not preclude achievement of management objectives. Should these reactive processes become more pronounced under significantly altered flow regimes aimed at improving growing conditions, they should not be neglected in a numerical model used to predict system-wide improvements.

In summary, the omission of chemical reactions from the conceptual and numerical models unduly limited their ability to simulate return salt loads to the Arkansas River. While there appears to be no net accumulation of return salt loads to the Arkansas River between 2002 and 2007, there is an overall positive net return salt load (i.e., contribution of return salt load to the Arkansas River from the irrigated lands in the LARV) between 1999 and 2001. Affording the numerical models the flexibility necessary to simulate the accumulation and discharge of salt mass to and from storage and the oxidative dissolution of salts from shale and weathered shale

likely would result in a better return salt load calibration. Further, this modification would give added flexibility to the model for simulating soil water and groundwater concentrations. Where necessary, chemical reaction parameters could be adjusted to drive more or less salt into or out of solution resulting in higher or lower simulated concentrations to achieve better fits with observed values.

Activation of chemical reactions in the salt transport models would increase the data needs necessary to construct and calibrate the models, however. Currently, there are no known estimates of initial concentrations of precipitated salts in either the saturated and unsaturated zones. Obtaining estimates of initial solid-phase concentrations may prove difficult as discussed by Cooper et al. (2008), where after 14 saturated soil-paste extractions from a LARV soil sample, dissolved salt concentrations were not lowered below approximately 4 dS m⁻¹. Moreover, information useful for constraining parameters that control the partitioning between solid- and dissolved-phase salt concentrations has not been collected. Thus, there are important trade-offs to consider before activating the chemical reaction package in the UZF-MT3DMS model. While activation of the chemical reaction package may result in a “better” calibration, a scrutinizing evaluation of the parameters required by the chemical reaction package and adjusted by a PEST simulation that achieve the improved calibration should be performed. Additional data collection efforts may be necessary to gather estimated ranges of chemical reaction parameter values appropriate for the LARV.

7 BROAD CONCLUSIONS AND RECOMMENDATIONS

Each chapter offers a set of concluding remarks pertaining to the material presented therein. Presented here are some broad conclusions in consideration of the full research effort.

7.1 CONCLUSIONS

7.1.1 Conclusions for Objective 1: Quantify the Extent and Severity of Soil Water Salt Concentrations in the LARV

The ongoing productivity of irrigated agriculture in the LARV depends in part upon decisions that must be made in response to waterlogging and salinization. Chapter 3 details the extent and severity of high soil water salt concentrations in the LARV sustained by a saline water table in close proximity to ground surface. In both study regions, normalized inverse Gaussian probability distribution functions were fit to the soil water salt concentration survey results, revealing average concentrations, as measured by calibrated electromagnetic induction sensors, that are above yield-decline thresholds for crops grown in the LARV. In the USR, field-averaged soil water salt concentrations ranged from 3.4 to 4.6 dS m⁻¹ over the course of the study period. Field-averaged soil water salt concentrations were found to be even higher in the DSR; during the course of the survey period values ranged from 4.5 to as high as 8.0 dS m⁻¹. If the sample of surveyed fields is indicative of the full population of cultivated fields, then only 34% and 1% of cultivated fields in the USR and DSR, respectively, lie below the 3 dS m⁻¹ salt toxicity threshold where most crops grown in the LARV remain relatively unaffected by soil water salt concentrations. Approximately 46% and 40% of the cultivated lands in the USR and DSR, respectively, lie between the 3-5 dS m⁻¹ crop salt threshold range, above which crop yields begin to decline in response to reduced osmotic potential and toxicity. That leaves 20% and 59% of

the cultivated lands in the USR and DSR, respectively, with soil water salt concentrations above the brink of 5 dS m^{-1} . Ample opportunity exists for increasing crop yields through alternative improved water management interventions resulting in lower soil water salt concentrations.

7.1.2 Conclusions for Objectives 2 and 3: Develop Detailed Groundwater Flow Models for the LARV and Evaluate Alternative Management Interventions

Two models developed for the LARV study regions surpass previous groundwater flow modeling efforts in several ways. The new models are highlighted by their expansive domain of application (combined, the developed model domains span roughly half of the LARV); their use of a fully-integrated saturated and unsaturated flow solution that covers regional scales; their calibration using a significant number (six) of calibration targets using the latest automated parameter estimation techniques; and their use of highly-resolved estimates of precipitation, ET, and irrigation application patterns. Shallow water tables ($< 3 \text{ m}$) are found to persist over much of the modeled regions, between 25–70% of the USR and 35–40% of the DSR. Sustained high water tables make it difficult to leach salts from the crop root zone in cultivated areas and contribute to non-beneficial consumptive use originating from naturally-vegetated and fallow land. Potential for lowering the water table through alternative improved water management interventions is demonstrated. For example, compared to the baseline simulation, alternative management scenario C6 (Table 5-2), the most aggressive of the investigated scenarios, predicts an increase of 1.1 and 0.7 m in the average D_{wt} in the USR and DSR, respectively, by the end of the simulated periods. It is interesting to note that the USR simulation predicts more modest increases in D_{wt} compared to those earlier reported in Burkhalter and Gates (2006). Increases of 0.5, 0.8, and 0.9 m in the first, second, and third years (1999-2001) are predicted in scenario C6, whereas reductions of 0.9, 1.7, and 1.9 m are reported for a similar, but less aggressive, scenario

(50% recharge reduction and 90% seepage reduction) developed by Burkhalter and Gates (2006) for the same modeled extent. The management improvement under scenario C6, which specifies reductions in the amount of water applied to cultivated fields, corresponded to overall reductions in recharge of 63%, 77% and 79% in the first, second, and third years of the simulated period (Table 5-3). Thus, even with significantly greater recharge reduction and with 25% of the cultivated area fallowed, water table depth increases may not be as large as first reported (Burkhalter and Gates, 2006).

Comparison of DSR model results with those for the USR suggests that the two regions may respond with varied effect to alternative water management interventions. For example, implementing a lease-fallow option in the USR eventually brings about water savings in the form of reduced non-beneficial consumptive use. However, the USR simulation predicts that it would take three or more years for a net water savings to be realized under scenarios C2, C4, C5, and C6. There is no net water savings predicted in any of the lease-fallow scenarios in the DSR for the simulated period, suggesting that a water market type program may exacerbate non-beneficial consumptive use, at least in the short term, and should therefore be carefully evaluated for where and how it will be implemented. In both regions, the lease-fallow only option (F1) generated an additional 18,500 and 18,200 ac·ft of predicted non-beneficial consumptive over the USR and DSR study periods, respectively. Irrespective of the region (i.e., USR, DSR), results from alternative water management intervention scenarios that include a lease-fallow component suggest that a multi-year commitment to the strategy is necessary before water savings are realized, recognizing that in some of the alternative management scenarios substantial water salvage may never be realized. This is because the ET on the newly fallowed land converts from beneficial to non-beneficial consumption as the water table subsides in response to decreased

recharge. Non-beneficial consumptive use under fallowed land eventually will diminish, leading to an overall net water savings from all land over the region. Presently, the programs that facilitate temporary lease of water rights by fallowing ground, ensuring that ownership of the water remains in the LARV, may impose constraints that do not provide enough time for water savings to manifest. If water leases can occur at most three out of every 10 years, and it takes at least three consecutive years of consistent alternative water management practice for meaningful reductions in non-beneficial consumptive use (water savings) under naturally-vegetated and previously fallow land to overcome newly fallowed-land offsets (Figure 4-9B), then non-beneficial water-savings should not be touted as a collateral benefit of the program. In fact, if implemented ad-hoc, alternative water management interventions that include a lease-fallowing option may result in a net overall increase or small decrease in non-beneficial consumptive use.

Each of the investigated alternative water management scenarios resulted in predicted alterations in groundwater return flows to the Arkansas River. Under Colorado water law and the Arkansas River Compact (with Kansas), changes in river water management that alter historical groundwater return flow patterns are prohibited unless properly compensated. Every alternative water management scenario listed in Table 4-2 resulted in significant diminishment in groundwater return flow. Sections 4.7.5-4.7.8 quantify the impact that each intervention has on various predicted output (e.g., average D_{wt} , non-beneficial consumptive use, groundwater return flow, recharge rates, etc.), but water managers may have little choice but to abrogate them from consideration unless further analysis can demonstrate compensatory river management schemes that could serve to mimic historical return flows. It may be possible to alter reservoir storage and release operations such that historical groundwater return flow patterns are sufficiently

preserved. Section 7.2 offers additional factors complicating this approach that should be addressed with future research.

The choice of best alternative management intervention is further complicated by salt transport responses that may harm crop production and negate water-savings benefits. If irrigation applications are reduced to an extent that adequate leaching is no longer provided, then continued or exacerbated salt build up in the crop root zone may offset initial water savings benefits. Thus, salt transport simulations that accompany the alternative management interventions explored in Chapter 4 are needed to determine which interventions balance reduced irrigation with adequate leaching. Lower water tables that reduce upflux of salts may well drive an overall reduction in soil water salt concentration and restore crop yields.

7.1.3 Conclusions for Objective 4: Modify MT3DMS to Simulate Variably-Saturated Solute Transport Conditions

The UZF-MT3DMS groundwater solute transport model for variably-saturated conditions was developed and verified with benchmark models that tested solution accuracy under steady and unsteady flow regimes, chemically nonreactive and reactive conditions (including nonlinear sorption and nonequilibrium transport), and in 1-, 2-, and 3-dimensional settings. Mass balance checks verified that the model conserves mass. Finally, total model run-times were compared among UZF-MT3DMS, CATHY/TRAN3D, SUTRA, and Hydrus3D in the 3D benchmark model (described in Section 5.4.6). UZF-MT3DMS runtimes were less than a third of the next fastest model, Hydrus3D, for similarly dimensioned problems. Because the UZF1 package does not require that the unsaturated zone be discretized, UZF-MT3DMS and its MODFLOW counterpart were coarsened, and changes in the predicted results were monitored. Not only did model results remain relatively unchanged (Figure 5-9), but the UZF-MT3DMS model runtimes

were cut to roughly one fifth of original total runtime (Table 5-3). Thus, UZF-MT3DMS is both a viable simulator of saturated and unsaturated-zone subsurface solute transport and offers significant model runtime savings in applications where thousands of model runs may be required, such as in automated parameter estimation routines, especially over regional scales. Its application to salt transport in the LARV presents a unique opportunity for testing it in a real-world setting.

7.1.4 Conclusions for Objective 5: Develop and Apply Advection-Dispersion Salt

Transport Models for the LARV

Water quantity concerns embody one side of the difficulties facing LARV water purveyors; water quality issues constitute the other side. By the time the Arkansas River exits Colorado, TDS concentration increases roughly six-to-eight-fold from the entrance to the LARV in Pueblo. Because the Arkansas River has a documented history of being among the most saline rivers in the United States (Miles, 1977) and because a status quo approach in river management fails to improve river water quality, computer models are needed as tools for investigating alternative improved management options (in fact, Chapter 4 demonstrates this). However, as with the flow model investigations detailed in Chapter 4, well-calibrated baseline simulations are required before prospective interventions can be evaluated. Chapter 6 describes baseline salt transport simulations for the USR and DSR in satisfaction of the fifth objective.

The developed salt transport models simulate conservative salt transport with advection and dispersion only; they do not simulate sorption, desorption, redox reactions, chemical precipitation, or dissolution. The models were calibrated with observations of groundwater salt concentrations, soil water salt concentrations (Chapter 3), and calculated estimates of groundwater return salt loads. Of these three calibration targets, soil water salt concentrations

were simulated best by the USR and DSR salt transport models. Predicted groundwater salt concentrations match observations in some areas, but exhibit significant misfit in others. On average, groundwater salt concentrations were over-predicted in both study regions. Due in part to this result, the USR and DSR simulations over-predict return salt loads to the Arkansas River.

Two possibilities exist for reconfiguring the salt transport models to achieve a better baseline calibration. First, increased vertical discretization may help alleviate difficulties associated with the volume-average approach taken in UZF-MT3DMS. However, refining the vertical discretization without also refining the horizontal discretization may be accompanied by the adverse trade-offs discussed in Section 6.5.1. That is, model predictions from a vertically-refined but horizontally-coarse grid may be undermined by model “structural noise” (Doherty and Welter, 2010).

Including reactive transport processes in the baseline simulation is a second option available to modelers to improve model performance. More specifically, inclusion of chemical precipitation and dissolution reactions in the simulation likely will alleviate some of the misfit that results from competing components of the total calibration objective function. Because soil water salt concentrations are under-predicted in both study regions but both groundwater salt concentrations and return salt loads are over-predicted, mechanisms that allow for aqueous to solid-phase (and vice versa) storage buildup and release likely would result in higher predicted total salt mass in the unsaturated zone. If, in some years, additional mass associated with infiltrating irrigation water is stored in the unsaturated zone, the salt concentration of recharge water might actually be less and contribute to dilution of groundwater salt concentrations. Lower predicted return salt loads would accompany lower predicted groundwater salt concentrations and improve overall model performance. Conversely, during the wet years of the

simulation, previously precipitated salts will dissolve back into solution and raise groundwater and soil water salt concentrations and contribute to higher salt return loads. Inclusion of oxidative dissolution of salts from shale and weathered shale might further enhance model representation of the spatial and temporal patterns of salt concentration.

Additional limitations accompany the current salt transport model configurations. UZF1, and by extension, UZF-MT3DMS, currently has no mechanism for supporting preferential flow in the unsaturated zone. Also, as was described in Chapter 6, UZF1 simulates downward-only flow. It does not consider negative pressure gradients simulated in Richards equation formulations and therefore cannot explicitly simulate the capillary fringe. However, UZF1 simulates ET occurring from the saturated-zone using the empirical function implemented in the original ET Package released with MODFLOW-88 (McDonald and Harbaugh, 1988). Water removed from the saturated-zone in this manner is not routed through the unsaturated zone. Rather, it is simulated as a sink term and is removed from the saturated zone. The predicted groundwater heads account for the groundwater removed in this manner. Thus, MODFLOW-NWT provides modelers with an estimate of the total amount of water removed from the saturated zone via upflux, but does not attempt to predict how high in the unsaturated-zone profile the liquid water is transmitted before it is converted to a vapor, is taken up by plant roots, stored, or both. Accordingly, there remains some additional model enhancements if upward liquid fluxes need to be explicitly routed. Tools like Hydrus3D may be a better option if upflux is to be a focus of future analyses, since it solves the Richards equation. However, models like Hydrus3D that solve the full 3-dimensional Richards equation come with steep data requirements for characterizing the unsaturated zone. In addition, 3-dimensional Richards equation models

often struggle in coarse-grained materials where wetting fronts are sharp, as discussed in Section 5.2.

7.1.5 Further Reflections on the Situation in the LARV

Unless crop production is restored, the pressure to move water out of the LARV for economic benefit along Colorado's Front Range will continue to mount. Demand for water in Colorado, and indeed across the American West, continues to climb in response to population growth. Conversely, climate variability, regardless of whether it is anthropogenically-driven or natural (Pederson et al., 2013), portends a water supply that will continue to go through periods of sustained drought. In light of Upper Arkansas River River Basin tree-ring chronologies which are highly correlated with total annual runoff, droughts more extreme than those recorded over the last 100 years (corresponding approximately to the available gaged record set) have been observed (Woodhouse et al., 2011) and serve as an important warning for water managers of what likely lies ahead.

Brief analyses of temperature records collected from the weather station at the CSU Arkansas Valley Research Center near Rocky Ford and spanning more than a century (Figure 7-1) reveal an increasing number of days each year with temperatures above 32.2° C (90.0° F), which serves as a barometer of long-term crop water demand trends in the LARV. Moreover, the increase in hot days [$> 32.2^{\circ}\text{C}$ (90.0° F)] is accompanied by an extended growing season. The first and last days with a temperature in excess of 32.2° C (90.0° F) is tending to occur earlier and later, respectively, with each passing year [red and blue time series with best fit lines shown in black are statically significant ($p\text{-value} < 0.01$)]. Over the course of the 20th century, the window of time over which the 32.2° C (90.0° F) temperature threshold was exceeded for the first and last time extended by 28 days, or nearly a month.

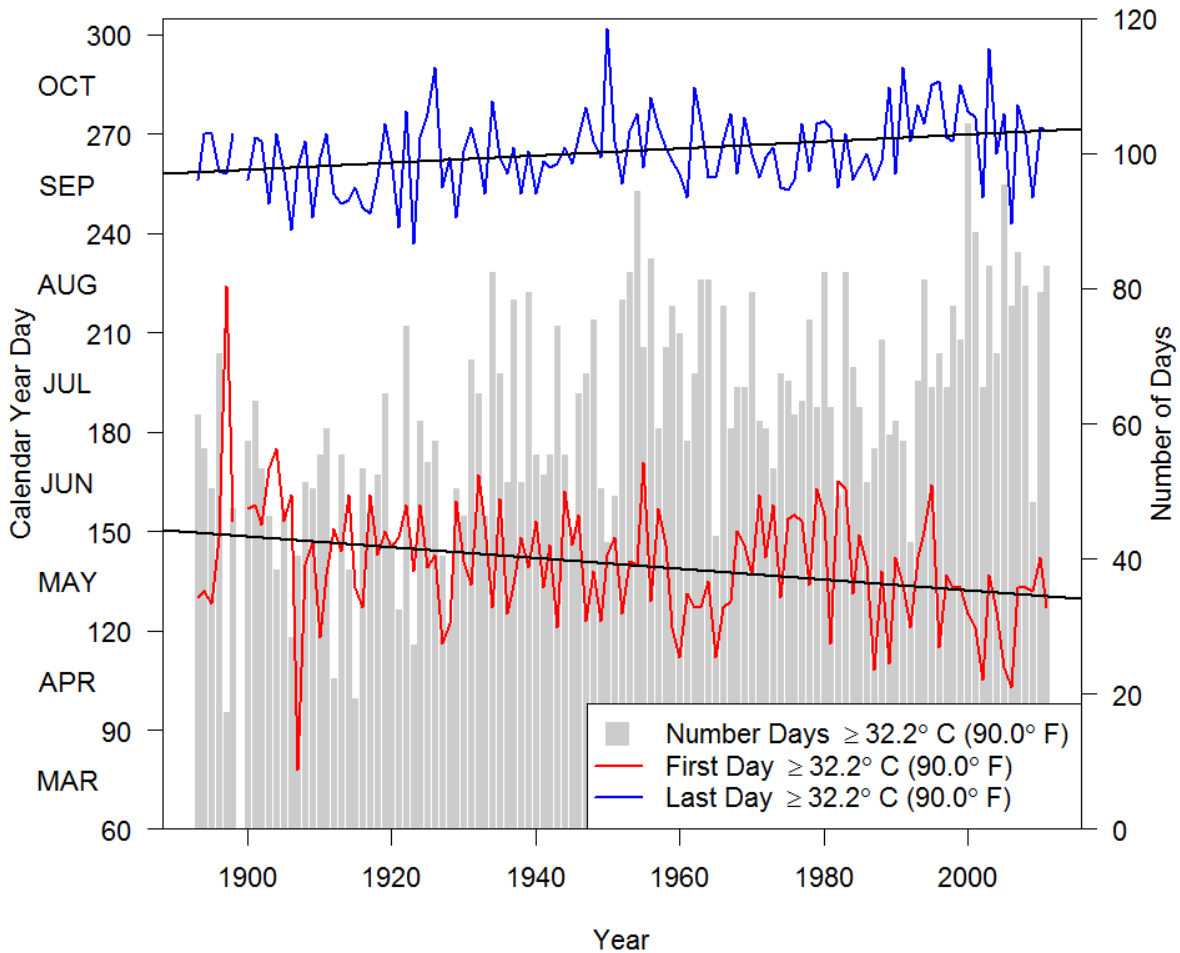


Figure 7-1. Grey bars qualitatively depict an upward trend in the total number of days with temperature exceeding 32.2 °C (90 °F) each year (gray bars correspond to the right y-axis). The first and last days of each growing season with a maximum temperature above 32.2 °C (90 °F) is trending earlier and later, respectively. Figure built with an R script described in Pederson et al. (2010).

The increasing temperatures in the LARV also have been accompanied by an apparent recent decrease in the amount of water flowing out of the upper watershed. Using the same dataset used to generate Figure 6-5, Figure 7-2 shows the annual hydrograph at the Cañon City gage (the Cañon City gage was selected since it lies upstream of Pueblo Reservoir and therefore does not reflect reservoir operations). Clearly, mean daily flow rates in the Upper Arkansas River Basin, not far from where the river discharges to the Lower Arkansas River Basin, have decreased during the spring runoff season. In addition, a 10-day forward shift in the average

peak runoff apparently has occurred. There also appears to be more peakedness in the post-1999 runoff hydrograph. Taken together, these factors are suggestive of a growing imbalance

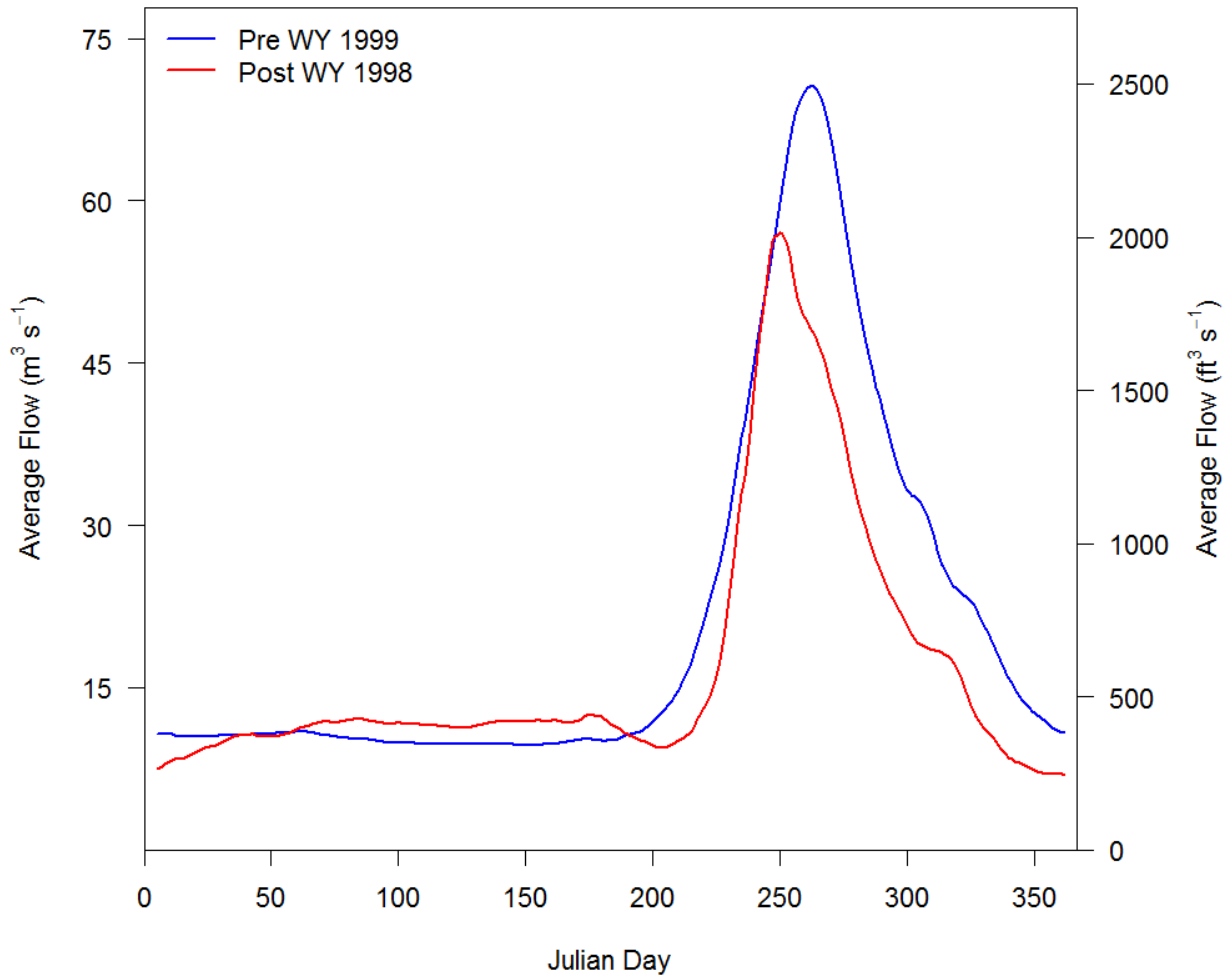


Figure 7-2. Mean daily flow rates for the Cañon City gage are calculated using the data collected before the study period began in the USR (blue line) and after the start of the study period (red line). Julian Day 1 in this plot corresponds to the start of the “water year,” or October 1st.

between water supply and demand in the LARV. However, some of the diminished supply may be offset by rainfall contributing runoff to Arkansas River tributaries in the LARV. It is likely that the increased imbalance will intensify the pressure placed on water managers to satisfy

competing demands. If, in the end, institutional rule changes that lead to meaningful water savings and improved water quality prove too time consuming, while the value of the water is driven higher by both increased demand and diminished supply, large amounts of agricultural water may leave the LARV long before alternative management interventions can be pursued.

Ensuring the sustainability of irrigated agriculture in the LARV is a function of many factors, including the lowering of high water tables through improved irrigation efficiency and rehabilitated infrastructure (i.e., canal lining) that contribute to waterlogging, non-beneficial consumptive use, steeper gradients driving groundwater of diminished quality back to the river, and salt-laden upflux to the root zone (which limits opportunity for leaching salt out of the crop root zone). Computer simulations of the alluvial aquifer in the LARV have demonstrated that carefully chosen management alternatives can increase D_{wt} and lead to improved growing conditions. By improving crop growing conditions and reducing water waste (i.e., irrigation tailwater, deep percolation, and non-beneficial consumptive use), agricultural production and the rural culture that it supports can be revitalized. Further, water savings realized under select management alternatives may help to satiate escalating urban water demand that historically has been addressed through procurement of the LARV's senior water rights.

For decades, the problems facing irrigated agriculture in the LARV have been characterized and carefully simulated, and potential solution strategies have been evaluated. Insights gleaned from the current effort in the LARV extend to other semi-arid irrigated regions as well. In a large river basin for which a detailed, physically-based, regional-scale model has been developed for a selected portion of the basin, solution strategies may not extend to the un-simulated portions of the basin. In the LARV, for example, alternative water management strategies that include a lease-fallow component lead to eventual water savings (reduced non-

beneficial consumptive use) in the USSR, but only worsened non-beneficial consumptive use in the DSR. Because the consumptive use occurring from previously cultivated (but now fallowed) fields switches from beneficial to non-beneficial, the hoped-for water savings may never be realized. Hence, studies that attempt to quantify the potential for water-savings through reduced non-beneficial consumptive use derived from shallow groundwater upflux under uncultivated lands should simulate conditions over multiple years in order to ascertain whether the initial increases in non-beneficial consumptive use continue to off-set water savings in perpetuity, or if water savings from pre-existing uncultivated lands eventually outpace non-beneficial consumptive use under newly-fallowed lands.

To combat high water tables, more efficient irrigation techniques like sprinkler and drip irrigation can replace flood and furrow irrigation. If these measures are adopted, then sealing or lining of delivery canals also should be adopted. As water tables decline in response to reduced irrigation recharge, increased gradients between the aquifer and the stage in the canal may induce additional seepage.

In irrigation regions where a solute transport simulation forms an important component of the analysis, simultaneous calibration of both the flow and transport simulation should be pursued. The information content of various salt concentration observations, or of salt loading observations, whether in a surface water channel or returning to a surface water feature, may help guide the estimation of the hydraulic properties of the aquifer.

Finally, in salinized regions dominated by calciferous and gypsiferous deposits, physically-based solute transport models should be designed to simulate chemical precipitation and dissolution processes. Because solid-phase salt storage in the unsaturated zone can be significant, it may be difficult to achieve a satisfactorily calibrated model if this mechanism is

ignored. Many modeling efforts attempt to keep the simulation as simple as possible, as was the case for the salt transport models described in Chapter 6. Results of this study demonstrate that this level of simplification may undermine the model's ability to adequately capture transients in groundwater and soil water salt concentrations as well as return salt load dynamics back to the river system.

7.2 SUGGESTED SYSTEM MONITORING ENHANCEMENTS

Oreskes and Belitz (2001) summarize the importance of a sound conceptual model, which is informed by the data that are available: "Conceptualization is probably the most thorny issue in modeling. It is the foundation of any model, and everyone knows that a faulty foundation will produce a faulty structure...Yet what to do about it remains a problem." In its original context, their statement preceded a discussion of model uncertainty; however, it also highlights the importance of good quality data which are important to forming a sound conceptual model. The following are some perceived areas where data underpinning the LARV numerical models may be improved or expanded upon, leading to improvement of the LARV groundwater flow and salt transport models.

The conceptual models upon which the MODFLOW and UZF-MT3DMS models described in Chapters 4 and 6 are built assume that the LARV crop histories are confidently known. Many of the datasets prepared for and used in the flow models (e.g., applied amounts, potential ET, extinction depth) are linked to the crop history dataset. In all but 2003, this information was collected from local Farm Service Agency records and in some cases was incomplete and/or incongruent with delineated acreage recorded in GIS coverages of farm fields; but, because it was the best information available, it therefore was adopted for generating the input datasets listed above.

Starting in 2003, GIS algorithms were developed to process satellite imagery for estimating valley-wide cropping patterns every five years. When results from the algorithm were compared to ground-truthed crop types, they were found to be 86% accurate (Ina Bernard, personal communication, 2003). Because the satellite imagery used by the algorithm is freely available from the U.S. Geological Survey and is of good quality dating back to 1985 [satellite image collection started in 1974, but resolution and reliability prior to 1985 is questionable (Susan Buto, personal communication, 2013)], it may be possible to assemble more accurate crop histories for a much longer period than is currently available. Unfortunately, cloud cover at the moment the image is collected interferes with the accuracy of the GIS algorithm and therefore requires user oversight.

Groundwater entering the irrigated portion of the LARV from the neighboring escarpment [i.e., from lands to the north and south of the upper-most (highest contour) irrigation canals] is not directly simulated in either the USR or DSR models. Because of the considerable distances over which this process would occur, it may represent an important component of the LARV groundwater budget and play a non-trivial role in the amount of groundwater that returns to the Arkansas River (i.e., explain some of the misfit in Figure 4-6). It may prove difficult to quantify the magnitude and timing of historical groundwater return flow patterns in a groundwater model of the alluvial aquifer without also estimating this potentially non-trivial source of groundwater entering the LARV. Observations of groundwater levels on the escarpment, adjacent to the modeled regions, may provide some indication of groundwater gradients into, or possibly out of, the LARV. Supplementing the CSU groundwater database with observations from outside the LARV (e.g., USGS groundwater monitoring network) could provide a quick assessment of broader regional gradients.

A number of sources contributing to the misfit observed in Figure 4-6 are discussed in more detail in Section 4.5.3. They include large and varying surface water diversions, significant well pumping, and ungaged tributary inflow, and cast doubt on the accuracy of the calculated groundwater return flow observations. Elimination of at least some of the uncertainty associated with these observations may be possible by measuring flow rates in ungaged tributaries and drains near their confluence with the Arkansas River. However, discrete measurements may not sufficiently address this data deficiency for long simulated periods.

7.3 SUGGESTED SYSTEM MODEL ENHANCEMENTS

Even if actual crop histories discussed above were known, it cannot be reasonably expected of the models described in Chapter 4 to represent farmer irrigation practices that drive baseline groundwater return flows with great accuracy. As was described in Section 4.3.3.2, the flow models attempt to capture regional irrigation practices but do not simulate the actual spatial and temporal patterns of historical irrigations. This may be one reason why predicted groundwater return flows vary significantly from observed unaccounted-for return flows (Figure 4-6). While the models did a great job in simulating groundwater table elevation and other head-dependent processes (e.g., total ET), simulated groundwater returns are among the weaker aspects of the flow models and may signal a potential model liability, depending on their intended use. Generation of a few alternative irrigation application input arrays and rerunning the MODFLOW-UZF models might help illuminate the sensitivity of the groundwater return flow solution to this particular dataset.

Two options are available for potentially improving model fit to the calculated observations of groundwater return flow. The first includes additional stream gaging of ungaged tributaries described at the end of the previous section. But because of perceived inadequacies

with this approach over long time periods, a second, more natural solution to the problem may be to replace the RIV package (Harbaugh, 2005) with one of the MODFLOW surface water routing packages (Niswonger and Prudic, 2005; Hughes et al., 2012). In these packages, streamflow is routed through the surface water network and is amended or deducted based on all sources and sinks specified by the user (i.e., precipitation, evaporation) or by the model (i.e., computed groundwater and surface water exchange). In this formulation, observations of flow as recorded by stream gages can be compared directly to simulated equivalents.

Unlike MODFLOW's RIV package (Harbaugh, 2005), the Streamflow Routing (SFR2) (Niswonger and Prudic, 2005) or Surface Water Routing (SWR1) (Hughes et al., 2012) packages preserve flow-stage relationships. Thus, as groundwater accrues in the Arkansas River, or any channel simulated by either of these packages, the simulated stage increases and the calculated groundwater and surface water exchange is adjusted based on the updated gradient between the stream and aquifer. In the RIV package, the user can vary the specified stage on a stress period-by-stress period basis, but it remains fixed during the simulation and will not adjust based on model-calculated accretions and depletions in the channel.

Ideally, the physically-based flow and salt transport models described herein should be replaced by a comparable model that encompasses all of the irrigated lands in the LARV. Because the flow models developed for the USR and DSR predict varied responses under the alternative water management interventions considered, it remains unknown how the non-modeled lands in the LARV (Pueblo County and significant portions of Bent and Prowers Counties) might respond to the identified interventions.

7.3.1 Expanding the Groundwater Flow Models

A number of anticipated benefits would accompany a physically-based model of the entire LARV irrigated lands. First, such a model would lend itself to direct integration with the

MODSIM river management models that have been developed for the LARV (Triana et al., 2009a; Triana et al., 2009b). The integration of physically-based groundwater models with river management models is an area of emerging research (Valerio et al., 2010; Condon and Maxwell, 2013). Due to the long history of data monitoring in the LARV, a MODSIM-MODFLOW simulation would be particularly well supported by data (e.g., instream flow, diversions, reservoir storage, groundwater pumping, groundwater levels, groundwater, soil water, and streamflow concentrations, precipitation, ET, etc.). In addition, an integrated MODSIM-MODFLOW model of the LARV would usurp the need for the Artificial Neural Network that is used to estimate groundwater-stream interaction in the currently un-modeled regions of the LARV and instead could be used to explore optimized water management with direct consideration of both quantity and quality of groundwater and river flow along the entire LARV. Also, such a model could be used to post-audit the ANN-model of the LARV (Triana et al., 2009a; Triana et al., 2009b) for those areas where a MODFLOW model was not developed. A MODSIM-MODFLOW integration would replace relatively simple representations of groundwater and surface water exchange in MODSIM with spatio-temporal estimates calculated by MODFLOW, thereby enabling improved assessment of impacts on water diversions and stateline flows. This development would be critical for evaluating whether proposed water management interventions can prevent injury to Colorado water rights and comply with the Arkansas River Compact by not materially depleting return flows to the Arkansas River. Again, because the investigated alternative water management interventions capable of achieving meaningful reductions in the water table, a necessary step for improving growing conditions and reducing non-beneficial consumption, significantly altered groundwater return flows (Figure

4-12), research efforts should begin to assess whether altered reservoir operations are a viable option.

An integrated hydrologic-administrative tool like a MODSIM-MODFLOW simulation may be the only such tool that could address some of the issues that would be raised if water quantity and quality preserving management measures are one day pursued. For example, conflicts may arise should water storage in Pueblo and John Martin Reservoirs be inadequate for honoring time delayed river flow augmentation commitments. Due to the long transit times (decade-scale) associated with irrigation recharge originating from cultivated fields near the northern and southern extents of the modeled regions (See Figure 7-1 in Bailey, 2012), stored water may simply be unavailable under persistent drought conditions.

The following recommended analyses could accompany the development of a MODSIM-MODFLOW model spanning the LARV. First, increased reservoir storage associated with the non-consumptive portion of the leased water will expand the surface area that will accompany increased reservoir stage. Thus, lease-fallow alternatives exacerbate evaporative losses occurring from the surface of the reservoir and as a result increase non-beneficial consumptive use occurring from the LARV. MODFLOW's lake (LAK) package (Merritt and Konikow, 2000) is a well-suited tool for quantifying the additional evaporative losses resulting from expanded surface areas. Second, head dependent groundwater and surface water exchanges may be impacted by increased reservoir storage. In other words, altered reservoir operations in support of preserving historical river flows may itself alter historical groundwater return flow in the vicinity of the reservoirs. Here again, the LAK package could quantify losses to the groundwater system and the resulting impact on groundwater returns as the reservoir is drawn down.

7.3.2 Expanding the Salt Transport Models

Expansion of the salt transport models in both time and space (to correspond with the recommended expanded flow model of the entire LARV), would offer a number of key benefits. First, a lengthened simulated period would allow an evaluation of the time required for a new dynamic equilibrium to be reached under altered water management.

A simulation of improved water alternatives in the upper reaches of the LARV could be examined to discover how the impacts might propagate downstream. For example, alternative water management strategies implemented above John Martin Reservoir that reduce return salt loads may deliver irrigation water of improved quality to downstream users. As with the unanticipated increase in net non-beneficial consumptive use that initially accompanied the conversion of cultivated land to fallow ground in the F1 and C1-C6 scenarios (Table 4-2), this approach may uncover unanticipated water quality effects of upstream management alterations on downstream water users that extend beyond expected alterations to groundwater return flows. Alternatively, it may reveal some deleterious impacts on river water quality. If, for example, storage in Pueblo Reservoir is increased to retain the non-consumed component of the leased water, increased evaporation from the now expanded reservoir surface area may not only increase non-beneficial consumptive use, as described above, but it may evapo-concentrate stored water.

To help sort out water quality issues impacted by alternative water management, a new version of MT3DMS that includes stream and lake transport capabilities currently is being developed by the USGS and may present a convenient modeling venue for pursuing such an analysis of water quality. Two new modules, tentatively named the Streamflow Transport (SFT) and Lake Transport (LKT) packages, interface directly with the groundwater transport solution for solving surface water transport problems influenced by interaction with groundwater.

Clearly, a number of complex issues, some of which elude this list, still need to be evaluated both qualitatively, and quantitatively, before storage and release from reservoirs can be considered a viable option for mimicking historical groundwater return flows. Nevertheless, there remains a current and growing imbalance between water supply and demand that will require more advanced tools to address all of the competing LARV needs and constraints.

REFERENCES

- Abbott, P.O., 1985. Description of Water-Systems Operations in the Arkansas River Basin, Colorado. U.S. Geological Survey. Water Resources Investigation Report 85-4092: 67p.
- Acquaah, G., 2005. Principles of crop production : theory, techniques, and technology. Pearson Prentice Hall, Upper Saddle River, N.J. .:
- Allen, R.G., Jensen, M.E., Wright, J.L., Burman, R.D., 1989. Operational estimates of reference evapotranspiration. *Agronomy Journal*, 81(4): 650-662.
- Allen, R.G., Pereira, L.S., Raes, D., Smith, M., 1998. Crop evapotranspiration : guidelines for computing crop water requirements. FAO irrigation and drainage paper 56. Irrigation and Drainage Paper 56, Food and Agriculture Organization of the United Nations, Rome, xxvi, 300 pp.
- ASCE-EWRI, 2005. The ASCE standardized reference evapotranspiration equation. Technical Committee report to the Environmental and Water Resources Institute of the American Society of Civil Engineers from the Task Committee on Standardization of Reference Evapotranspiration. ASCE-EWRI, 1801 Alexander Bell Drive, Reston, VA 20191-4400, 173 pp.
- ASTM Standard D 5981-96, 1996. Standard guide for calibrating a ground water flow model application, West Conshohocken, PA.
- Bailey, R.T., 2012. Regional selenium cycling in an irrigated agricultural groundwater system: conceptualization, modeling, and mitigation, Ph.D. thesis, Department of Civil and Environmental Engineering, Colorado State University, Fort Collins, CO.

- Bailey, R.T., Gates, T.K., Halvorson, A.D., 2013a. Simulating variably-saturated reactive transport of selenium and nitrogen in agricultural groundwater systems. *Journal of Contaminant Hydrology*.
- Bailey, R.T., Hunter, W.J., Gates, T.K., 2012. The influence of nitrate on selenium in irrigated agricultural groundwater systems. *Journal of Environmental Quality*, 41(3): 783-792.
- Bailey, R.T., Morway, E.D., Niswonger, R.G., Gates, T.K., 2013b. Modeling variably-saturated multi-species reactive groundwater transport with MODFLOW-UZF and RT3D. *Ground Water*, 51(5): 752-761.
- Barlow, P.M., Harbaugh, A.W., 2006. USGS directions in MODFLOW development. *Ground Water*, 44(6): 771-774.
- Basile, A., Buttafuoco, G., Mele, G., Tedeschi, A., 2012. Complementary techniques to assess physical properties of a fine soil irrigated with saline water. *Environmental Earth Sciences*: 1-11.
- Bastiaanssen, W., Molden, D., Makin, I., 2000. Remote sensing for irrigated agriculture: examples from research and possible applications. *Agricultural Water Management*, 46(2): 137-155.
- Bathurst, J.C., 1986. Physically-based distributed modelling of an upland catchment using the Système Hydrologique Européen. *Journal of Hydrology*, 87(1): 79-102.
- Bekesi, G., McConchie, J., 1999. Groundwater recharge modelling using the Monte Carlo technique, Manawatu region, New Zealand. *Journal of Hydrology*, 224(3-4): 137-148.
- Belmans, C., Wesseling, J., Feddes, R., 1983. Simulation model of the water balance of a cropped soil: SWATRE. *Journal of Hydrology*, 63(3): 271-286.

- Bittinger, M., Stringham, G., 1963. A study of phreatophyte growth in the lower Arkansas River Valley of Colorado, Colorado Agricultural Experiment Station, CER63MWB-GES6.
- Bixio, A.C., Orlandini, S., Paniconi, C., Putti, M., 2000. Physically-based distributed model for coupled surface runoff and subsurface flow simulation at the catchment scale, Computational Methods in Water Resources, Computational Methods in Water Resources, vol. 2, Computational Methods, Surface Water Systems and Hydrology, edited by L. R. Bentley et al., pp. 1115 – 1122, alkema, Rotterdam, Netherlands.
- Boonstra, J., de Ridder, N.A., 1990. Numerical modelling of groundwater basins, 2nd ed. Publication 29, International Institute for Land Reclamation and Improvement, Wageningen, The Netherlands, 226 p.
- Boyle, D.P., Gupta, H.V., Sorooshian, S., 2000. Toward improved calibration of hydrologic models: Combining the strengths of manual and automatic methods. Water Resour. Res, 36(12): 3663-3674.
- Bredehoeft, J., 2005. The conceptualization model problem—surprise. Hydrogeology Journal, 13(1): 37-46.
- Brendle, D.L., 2002. Evaluation of possible alternatives to lower the high water table of St. Charles Mesa, Pueblo County, Colorado, U.S. Geological Survey. Water-Resources Investigations Report 01-4190. Denver, Colo.
- Brooks, R.H., Corey, A.T., 1964. Hydraulic properties of porous media, Hydrology Papers No. 3. Colorado State University, Fort Collins, Colo.
- Brooks, R.H., Corey, A.T., 1966. Properties of porous media affecting fluid flow. Journal of Irrigation and Drainage Engineering, 101: 85-92.

- Burkhalter, J.P., 2005. Defining and engineering solutions for agroecological impacts of salinity and waterlogging in an irrigated river valley, Ph.D. thesis, Department of Civil and Environmental Engineering, Colorado State University, Fort Collins, CO.
- Burkhalter, J.P., Gates, T.K., 2005. Agroecological impacts from salinization and waterlogging in an irrigated river valley. *Journal of Irrigation and Drainage Engineering*, 131(2): 197-209.
- Burkhalter, J.P., Gates, T.K., 2006. Evaluating regional solutions to salinization and waterlogging in an Irrigated River Valley. *Journal of Irrigation and Drainage Engineering*, 132(1): 21-30.
- Cain, D., 1985. Quality of the Arkansas River and irrigation-return flows in the lower Arkansas River Valley, Colorado.
- Camporese, M., Paniconi, C., Putti, M., Orlandini, S., 2010. Surface-subsurface flow modeling with path-based runoff routing, boundary condition-based coupling, and assimilation of multisource observation data. *Water Resour. Res.*, 46.
- Carpenter, R.A., 1983. Natural systems for development: what planners need to know. Macmillan, New York.
- Carrera, J., Alcolea, A., Medina, A., Hidalgo, J., Slooten, L.J., 2005. Inverse problem in hydrogeology. *Hydrogeology Journal*, 13(1): 206-222.
- Carrera, J., Neuman, S.P., 1986. Estimation of aquifer parameters under transient and steady state conditions: 2. Uniqueness, stability, and solution algorithms. *Water Resources Research*, 22(2): 211-227.
- Cassel, F., Goorahoo, D., Zoldoske, D., Adhikari, D., 2008. Mapping soil salinity using ground-based electromagnetic induction. In: Metternicht, G., Zinck, J. (Eds.), *Remote Sensing of*

- Soil Salinization: Impact on Land Management. CRC Press, Taylor & Francis, Boca Raton, FL, pp. 199 pgs.
- Chang, S., 1992. Systems analysis. *Water Environment Research*, 64(4): 297-301.
- Charbeneau, R.J., 1984. Kinematic models for soil moisture and solute transport. *Water Resources Research*, 20(6): 699-706.
- Chen, X., Xu, L., Sun, Z., Yu, J., Jiang, J., 2011. Hydro-salinity balance and mobilization in oasis irrigation areas at two different scales. *Environmental Earth Sciences*, 62(1): 161-169.
- Chiew, F., Stewardson, M., McMahon, T., 1993. Comparison of six rainfall-runoff modelling approaches. *Journal of Hydrology*, 147(1-4): 1-36.
- Chilakapati, A., Yabusaki, S., Szecsody, J., MacEvoy, W., 2000. Groundwater flow, multicomponent transport and biogeochemistry: development and application of a coupled process model. *Journal of Contaminant Hydrology*, 43(3-4): 303-325.
- Cole, S.E., Sharma, D., Schreieder, W.A., 1994. A modern, refined application of a ground water flow model to the Arkansas River Basin. In: Warner, J.W., Van Der Heijde, P. (Eds.), *Proceeding of the 1994 Groundwater Modeling Conference*. Colorado School of Mines, Fort Collins, CO.
- Colorado Climate Center, 2007. CoAgMet data access, Available online at: <http://ccc.atmos.colostate.edu/~coagmet/index.php>.
- Colorado Revised Statutes, 1949. Arkansas River Compact, Sections 37-69-101 - 37-69-106. Colorado General Assembly.

- Condon, L., Maxwell, R., 2013. Implementation of a linear optimization water allocation algorithm into a fully integrated physical hydrology model. *Advances in Water Resources*, 60: 135-147.
- Cooper, C.A., 2006. Salt chemistry effects on salinity assessment and soil solution modeling in the Arkansas River basin, Colorado, Colorado State University, Fort Collins, CO.
- Cooper, C.A., Davis, J.G., Cardon, G.E., 2008. Influence of laboratory methods on calcareous saline soils for EC measurement and leaching. *Communications in Soil Science and Plant Analysis*, 39(3-4): 329-343.
- Corwin, D., Lesch, S., 2003. Application of soil electrical conductivity to precision agriculture: theory, principles, and guidelines. *Agronomy Journal*, 95(3): 455-471.
- Corwin, D.L., 1996. GIS applications of deterministic solute transport models for regional-scale assessment of non-point source pollutants in the vadose zone. In: Corwin, D. L., and Loague, K. (eds). *Applications of GIS to the modeling of non-point source pollutants in the vadose zone*. p. 69-100. SSSA Spec. Publ. 48. SSSA, Madison, WI.
- D'Agnese, F.A., Faunt, C.C., Hill, M.C., Turner, K.A., 1999. Death valley regional ground-water flow model calibration using optimal parameter estimation methods and geoscientific information systems. *Advances in Water Resources*, 22(8): 777-790.
- D'Agnese, F.A., Faunt, C.C., Turner, A.K., Hill, M.C., 1997. Hydrogeologic evaluation and numerical simulation of the Death Valley Regional ground-water flow system, Nevada and California. *US Geological Survey Water Resources*, 96: 4300.
- D'Agnese, F.A., O'Brien, G.M., Faunt, C.C., Belcher, W.R., San Juan, C., 2002. A three-dimensional numerical model of predevelopment conditions in the Death Valley regional

- ground-water flow system, Nevada and California, U.S. Geological Survey Water-Resources Investigations Report 02-4102.
- Dages, C., Voltz, M., Ackerer, P., 2008. Parameterization and evaluation of a three-dimensional modelling approach to water table recharge from seepage losses in a ditch. *Journal of Hydrology*, 348(3-4): 350-362.
- Darton, N.H., 1906. Geology and underground waters of the Arkansas Valley in eastern Colorado. U.S. Geological Survey, Professional Paper 52, 90 p.
- Dawes, W.R., Short, D., 1993. The efficient numerical solution of differential equations for coupled water and solute dynamics: The WAVES model. CSIRO Division of Water Resources, Technical Memorandum, 93/18.
- Doherty, J., 2002. Manual for PEST, 5th edition, Brisbane, Australia: Watermark Numerical Computing. Downloadable from www.sspa.com/pest.
- Doherty, J., 2003. Ground water model calibration using pilot points and regularization. *Ground Water*, 41(2): 170-177.
- Doherty, J., Welter, D., 2010. A short exploration of structural noise. *Water Resources Research*, 46(5): W05525, doi:10.1029/2009WR008377.
- Domenico, P.A., Schwartz, F.W., 1998. Physical and chemical hydrogeology. Wiley New York.
- Donnelly, J.P., 2005. Assessing irrigation-induced selenium and iron in the lower Arkansas River Valley in Colorado, M.S. Thesis, Dept. of Civil and Environmental Engineering, Colorado State University, Fort Collins, CO.
- Downer, C.W., Ogden, F.L., 2004. Appropriate vertical discretization of Richards' equation for two dimensional watershed scale modelling. *Hydrological Processes*, 18(1): 1-22.

- Earman, S., Dettinger, M., 2011. Potential impacts of climate change on groundwater resources-a global review. *Journal of Water and Climate Change*, 2(4): 213-229.
- Eldeiry, A., 2006. Spatial modeling of soil salinity using remote sensing, GIS, and field data, Ph.D. thesis, Department of Civil and Environmental Engineering, Colorado State University, Fort Collins, CO.
- Eldeiry, A.A., Garcia, L.A., 2008. Detecting soil salinity in alfalfa fields using spatial modeling and remote sensing. *Soil Science Society of America Journal*, 72(1): 201.
- Elhaddad, A., 2007. Use of remote sensing to estimate soil salinity and evapotranspiration in agricultural fields, Ph.D. thesis, Department of Civil and Environmental Engineering, Colorado State University, Fort Collins, CO.
- Elhaddad, A., Garcia, L., 2008. Surface energy balance-based model for estimating evapotranspiration taking into account spatial variability in weather. *Journal of Irrigation and Drainage Engineering*, 134: 681.
- Evans, R.O., Fausey, N.R., 1999. Effects of Inadequate Drainage on Crop Growth and Yield. *Agricultural Drainage*, 38: 13-54.
- FAO, 2009. Food and Agriculture Organization of the United Nations Statistical Databases <<http://apps.fao.org/>>
- Faunt, C.C., Blainey, J.B., Hill, M.C., D'Agnese, F.A., O'Brien, G.A., 2004. Transient numerical model of ground-water flow. Evaluation of the Death Valley regional ground-water flow system (DVRFS), Nevada and California, U.S. Geological Survey Scientific Investigations Report 2004-5205.

- Fazal, M.A., Imaizumi, M., Ishida, S., Kawachi, T., Tsuchihara, T., 2005. Estimating groundwater recharge using the SMAR conceptual model calibrated by genetic algorithm. *Journal of Hydrology*, 303(1-4): 56-78.
- Feddes, R.A., Kowalik, P.J., Zaradny, H., 1978. Simulation of field water use and crop yield. *Simulation Nomograph*. PUDOC, Wageningen, The Netherlands. p. 189.
- Fienen, M.N., Clemo, T., Kitanidis, P.K., 2008. An interactive Bayesian geostatistical inverse protocol for hydraulic tomography. *Water Resources Research*, 44 W00B01.
- Foley, J., DeFries, R., Asner, G., Barford, C., Bonan, G., Carpenter, S., Chapin, F., Coe, M., Daily, G., Gibbs, H., 2005. Global consequences of land use. *Science*, 309(5734): 570-574.
- Ford, D., 2006. Tall, grande, or venti models? *Journal of Water Resources Planning and Management*, 132(1): 1-3.
- Freeze, R., Cherry, J., 1979. *Groundwater*. Prentice Hall, Englewood Cliffs, NJ.
- Freeze, R., Massmann, J., Smith, L., Sperling, T., James, B., 1990. Hydrogeological decision analysis: 1. A framework. *Ground Water*, 28(5): 738-766.
- Fullen, M.A., Catt, J.A., 2004. *Soil management: problems and solutions*. Arnold London, UK.
- Gambolati, G., Pini, G., Putti, M., Paniconi, C., Zannetti, P., 1994. Finite element modeling of the transport of reactive contaminants in variably saturated soils with LEA and non-LEA sorption. In *environmental modeling vol. II: Computer methods and software for simulating environmental pollution and its adverse effects*, chapter 7: 173-212, Computational Mechanics Publications, Southampton, UK.

- Garabedian, S.P., 1986. Application of a parameter-estimation technique to modeling the regional aquifer underlying the eastern Snake River Plain, Idaho, U.S. Geological Survey Water Resources Investigation Report 2278, 60 pg.
- Gates, T.K., Burkhalter, J.P., Labadie, J.W., Valliant, J.C., Broner, I., 2002. Monitoring and modeling flow and salt transport in a salinity-threatened irrigated valley. *Journal of Irrigation and Drainage Engineering*, 128(2): 87-99.
- Gates, T.K., Cody, B.M., Donnelly, J.P., Herting, A.H., Bailey, R.T., Mueller Price, J., 2009. Assessing selenium contamination in the irrigated stream-aquifer system of the Arkansas River, Colorado. *Journal of Environmental Quality*, 38(6): 2344.
- Gates, T.K., Garcia, L.A., Hemphill, R.A., Morway, E.D., Elhaddad, A., 2012. Irrigation practices, water consumption, and return flows in Colorado's Lower Arkansas River Valley: field and model investigations, Colorado Water Institute Completion Report No. 221, Colorado Agricultural Experiment Station. No. TR 12-10. Available at: <http://cwi.colostate.edu/publications/CR/221.pdf>.
- Gates, T.K., Garcia, L.A., Labadie, J.W., 2006. Toward optimal water management in Colorado's Lower Arkansas River Valley: monitoring and modeling to enhance agriculture and environment. Colorado Water Resources Research Institute Completion Report (205).
- Gates, T.K., Grismer, M.E., 1989. Irrigation and drainage strategies in salinity-affected regions. *Journal of Irrigation and Drainage Engineering*, 115(2): 255-284.
- Gates, T.K., Wets, R.J.B., Grismer, M.E., 1989. Stochastic approximation applied to optimal irrigation and drainage planning. *Journal of Irrigation and Drainage Engineering*, 115(3): 488-502.

- Gee, G.W., Bauder, J.W., 1986. Particle-size analysis. In: Klute, A. (Ed.), *Methods of soil analysis, Part 1*, 2nd edition Agron. Monogr. 9, American Society of Agronomy, Inc. (ASA) and Soil Science Society of America (SSSA), Madison, WI, 383-411.
- Gelhar, L.W., Welty, C., Rehfeldt, K.R., 1992. A critical review of data on field-scale dispersion in aquifers. *Water Resources Research*, 28(7): 1955-1974.
- Ghassemi, F., Jakeman, A., Nix, H., 1995. *Salinisation of land and water resources: Human causes, extent, management and case studies*. Univ. New South Wales Press, Ltd., Sydney, Australia.
- Gillham, D.J., 2004. *Data and modeling of irrigated fields with saline high water tables*, M.S. Thesis, Department of Civil and Environmental Engineering, Colorado State University, Fort Collins, CO.
- Goff, K., Lewis, M.E., Person, M.A., Konikow, L.F., 1998. Simulated effects of irrigation on salinity in the Arkansas River Valley in Colorado. *Ground Water*, 36(1): 76-86.
- Gorelick, S.M., 1983. A review of distributed parameter groundwater management modeling methods. *Water Resources Research*, 19(2): 305-319.
- Hajhamad, L., Almasri, M.N., 2009. Assessment of nitrate contamination of groundwater using lumped-parameter models. *Environmental Modelling & Software*, 24(9): 1073-1087.
- Hallberg, N.U., Niemann, J.D., Gates, T.K., 2008. *Analyzing the effects of high water tables on evapotranspiration from uncultivated land in Colorado's Lower Arkansas River Valley*, Hydrology Days 2008, Colorado State University, Fort Collins, CO.
- Hanson, B., Grattan, S.R., Fulton, A., 1999. *Agricultural salinity and drainage*. University of California Irrigation Program, University of California, Davis.

- Hanson, B., Hopmans, J.W., Šimůnek, J., 2008. Leaching with subsurface drip irrigation under saline, shallow groundwater conditions. *Vadose Zone Journal*, 7(2): 810-818.
- Harbaugh, A.W., 2005. MODFLOW-2005, The U.S. Geological Survey modular ground-water model--the Ground-Water Flow Process, U.S. Geological Survey Techniques and Methods 6-A16.
- Harman, C., Rao, P., Basu, N., McGrath, G., Kumar, P., Sivapalan, M., 2011. Climate, soil, and vegetation controls on the temporal variability of vadose zone transport. *Water Resources Research*, 47(1): W00J13.
- Healy, R.W., 1990. Simulation of solute transport in variably saturated porous media with supplemental information on modifications to the U.S. Geological Survey's computer program VS2D. U.S. Geological Survey. Water Resources Investigations Report No. 90-4025.
- Helsel, D.R., Hirsch, R.M., 1992. Statistical methods in water resources. Studies in Environmental Science 49. Elsevier Science Publishers, Amsterdam.
- Hendrickx, J., Raza, B., Sadig, Z., Chaudhry, M., Akram, M., 1992. Soil salinity assessment by electromagnetic induction of irrigated land. *Soil Science Society of America Journal*, 56(6): 1933.
- Heuvelmans, G., 2010. Development and credibility assessment of a metamodel relating water table depth to agricultural production. *Agricultural Water Management*, 97(11): 1731-1741.
- Hill, M.C., 1998. Methods and guidelines for effective model calibration, U.S. Geological Survey, Water-Resources Investigations Report 98-4005, 90 p.

- Hill, M.C., Poeter, E., Zheng, C., 2010. Foreword: Groundwater modeling and public policy. *Ground Water*, 48(5): 625-626.
- Hill, M.C., Tiedeman, C.R., 2007. *Effective groundwater model calibration*. John Wiley & Sons, Inc, Hoboken.
- Hillel, D., 2000. *Salinity management for sustainable irrigation - integrating science, environment, and economics*. Environmentally and socially sustainable development - rural development, Washington, DC: The World Bank
- Hoffman, G., Evans, R., Jensen, M., Martin, D., Elliot, R., 2007. *Design and operation of farm irrigation systems*. 2nd Edition. American Society of Agricultural and Biological Engineers, St. Joseph, MI 49085-9659, USA.
- Houk, E., Frasier, M., Schuck, E., 2006. The agricultural impacts of irrigation induced waterlogging and soil salinity in the Arkansas Basin. *Agricultural Water Management*, 85(1-2): 175-183.
- Houk, E.E., 2003. *Economic assessment of water management in agriculture: Managing salinity and waterlogging in the Arkansas River Basin and environmental water shortages in the Platte River Basin*, Ph.D thesis, Department of Agricultural and Resource Economics, Colorado State University, Fort Collins, CO.
- Howitt, R.E., D, M., Medellin-Azuara, J., Lund, J.R., 2010. *Economic modeling of agriculture and water in California using the statewide agricultural production model*, Department of Agricultural and Resource Economics, University of California - Davis, 25 p.
- Hsieh, P.A., Barber, M.E., Contor, B.A., Hossain, A., Johnson, G.S., Jones, J.L., Wylie, A.H., 2007. *Ground-water flow model for the Spokane Valley-Rathdrum Prairie Aquifer*,

- Spokane County, Washington, and Bonner and Kootenai Counties, Idaho. US Geological Survey, Scientific Investigations Report 07-5044.
- Huang, K., Mohanty, B.P., Leij, F.J., Van Genuchten, M.T., 1998. Solution of the nonlinear transport equation using modified Picard iteration. *Advances in Water Resources*, 21(3): 237-249.
- Hughes, J.D., Langevin, C.D., Chartier, K.L., White, J.T., 2012. Documentation of the surface-water routing (SWR1) process for modeling surface-water flow with the U.S. Geological Survey modular ground-water model (MODFLOW-2005): U.S. Geological Survey Techniques and Methods 6-A40. Book.
- Hukkinen, J., 1993. Institutional distortion of drainage modeling in Arkansas River Basin. *Journal of Irrigation and Drainage Engineering*, 119: 743.
- Hunt, R.J., Feinstein, D.T., Pint, C.D., Anderson, M.P., 2006. The importance of diverse data types to calibrate a watershed model of the Trout Lake Basin, Northern Wisconsin, USA. *Journal of Hydrology*, 321(1): 286-296.
- HydroGeoLogic, 2000. MODHMS: a comprehensive MODFLOW-based hydrologic modeling system, Version 1.1, Code documentation and user's guide, HydroGeoLogic Inc., Herndon, VA
- Irannejad, P., Shao, Y., 1998. Description and validation of the atmosphere–land–surface interaction scheme (ALSIS) with HAPEX and Cabauw data. *Global and Planetary Change*, 19(1): 87-114.
- Itenfisu, D., Elliott, R.L., Allen, R.G., Walter, I.A., 2003. Comparison of reference evapotranspiration calculations as part of the ASCE standardization effort. *Journal of Irrigation and Drainage Engineering-Asce*, 129(6): 440-448.

- Jhorar, R., Smit, A., Roest, C., 2009. Assessment of alternative water management options for irrigated agriculture. *Agricultural Water Management*, 96(6): 975-981.
- Jiang, J., Feng, S., Huo, Z., Zhao, Z., Jia, B., 2011. Application of the SWAP model to simulate water-salt transport under deficit irrigation with saline water. *Mathematical and Computer Modelling*, 54(3): 902-911.
- Jiang, J., Huo, Z., Feng, S., Zhang, C., 2012. Effect of irrigation amount and water salinity on water consumption and water productivity of spring wheat in Northwest China. *Field Crops Research*, 137: 78-88.
- Jorenush, M., Sepaskhah, A., 2003. Modelling capillary rise and soil salinity for shallow saline water table under irrigated and non-irrigated conditions. *Agricultural Water Management*, 61(2): 125-141.
- Kahlown, M.A., Ashraf, M., 2005. Effect of shallow groundwater table on crop water requirements and crop yields. *Agricultural Water Management*, 76(1): 24-35.
- Kahlown, M.A., Azam, M., 2002. Individual and combined effect of waterlogging and salinity on crop yields in the Indus basin. *Irrigation and drainage*, 51(4): 329-338.
- Katerji, N., Van Hoorn, J., Hamdy, A., Mastrorilli, M., 2000. Salt tolerance classification of crops according to soil salinity and to water stress day index. *Agricultural Water Management*, 43(1): 99-109.
- Keating, E.H., Robinson, B.A., Vesselinov, V.V., 2005. Development and application of numerical models to estimate fluxes through the regional aquifer beneath the Pajarito Plateau. *Vadose Zone Journal*, 4(3): 653.
- Keidser, A., Rosbjerg, D., 1991. A comparison of four inverse approaches to groundwater flow and transport parameter identification. *Water Resources Research*, 27(9).

- Kirchner, J.W., Feng, X., Neal, C., 2000. Fractal stream chemistry and its implications for contaminant transport in catchments. *Nature*, 403(6769): 524-527.
- Kitanidis, P., Vomvoris, E., 1983. A geostatistical approach to inverse modeling in groundwater modeling and one-dimensional simulations. *Water Resources Research*, 19(3): 677–690.
- Kitanidis, P.K., 1996. On the geostatistical approach to the inverse problem. *Advances in Water Resources*, 19(6): 333-342.
- Konikow, L.F., Bredehoeft, J.D., 1974a. Modeling flow and chemical quality changes in an irrigated stream-aquifer system. *Water Resources Research*, 10(3): 546-562.
- Konikow, L.F., Bredehoeft, J.D., 1974b. A water quality model to evaluate water management practices in an irrigated stream-aquifer system, *Proceedings of the 15th Annual Western Resources Conference*, University of Colorado, Boulder, Colorado: Merriman.
- Konikow, L.F., Person, M., 1985. Assessment of long-term salinity changes in an irrigated stream-aquifer system. *Water Resources Research*, 21(11): 1611-1624.
- Kotuby-Amacher, J., Koenig, R., Kitchen, B., 2000. Salinity and plant tolerance. Rep. AG-SO-03, Cooperative Extension, Utah State University, Logan, UT.
- Kumar, R., Singh, J., 2003. Regional water management modeling for decision support in irrigated agriculture. *Journal of Irrigation and Drainage Engineering*, 129: 432.
- Kutner, M.H., Nachtsheim, C.J., Neter, J., Li, W., 2004. *Applied linear statistical models*. 5th ed. . McGraw-Hill Irwin, New York, NY, 02 pp.
- Lal, R., 2004. *Soil degradation in the United States : extent, severity, and trends*. Lewis Publishers, Boca Raton, FL.
- Lal, R., Shukla, M., 2004. *Principles of soil physics*. Books in soils, plants, and the environment. M. Dekker, New York, viii, 716 pp.

- Lappala, E.G., Healy, R.W., Weeks, E.P., 1987. Documentation of computer program VS2D to solve the equations of fluid flow in variably saturated porous media. US Geological Survey. Water-Resources Investigation Report 83-4099.
- Leavesley, G.H., Lichty, R.W., Troutman, B.M., Saindon, L.G., 1983. Precipitation-runoff modeling system: User's Manual,. U.S. Geological Survey. Water-Resources Investigation Report 83-4238, 207 p.
- LeCain, G.D., Anna, L.O., Fahy, M.F., 1998. Results from geothermal logging, air and core-water chemistry sampling, air injection testing and tracer testing in the northern Ghost Dance Fault, Yucca Mountain, Nevada, November 1996 to August 1998, U.S. Geological Survey Water Resources Investigation Report 99-4210.
- Lefkoff, L.J., Gorelick, S.M., 1990. Simulating physical processes and economic behaviour in saline, irrigated agriculture: Model development. *Water Resources Research*, 26(7): 1359-1369.
- Ley, T.W., Straw, D.E., Hill, R.W., 2009. ASCE standardized penman monteith alfalfa reference ET and crop ET estimates for Arkansas River compact compliance in Colorado. ASCE, World Environmental and Water Resources Congress 2009.
- Lin, Y.C., Yeh, H.D., 2008. Identifying groundwater pumping source information using simulated annealing. *Hydrological Processes*, 21(16): 3010-3019.
- Longenbaugh, R.A., 1967. Mathematical simulation of a stream-aquifer system, Proc. 3rd Annual American Water Resources Conference, pp. 74-83.
- Maas, E.V., 1990. Crop salt tolerance. In: Tanji, K.K. (Ed.), *Agricultural salinity assessment and management*, ASCE Manuals and Reports on Engineering Practice No. 71, ASCE, New York, 262-304.

- Major, T.J., Hurr, R.T., Moore, J.E., 1970. Hydrogeologic data for the lower Arkansas River Valley, Colorado. Colorado Water Conservation Board Basic Data Release No. 21, U.S. Geological Survey, Denver.
- Mandare, A., Ambast, S., Tyagi, N., Singh, J., 2008. On-farm water management in saline groundwater area under scarce canal water supply condition in the Northwest India. *Agricultural Water Management*, 95(5): 516-526.
- Markstrom, S.L., Niswonger, R.G., Regan, R.S., Prudic, D.E., Barlow, P.M., 2008. GSFLOW-coupled ground-water and surface-water flow model based on the integration of the Precipitation-Runoff Modeling System (PRMS) and the Modular Ground-Water Flow Model (MODFLOW-2005). U.S. Geological Survey Techniques and Methods 6-D1, 240 p.
- Martin, C.A., 2013. Uncertainty in measuring seepage from earthen irrigation canals using the inflow-outflow method and in evaluating the effectiveness of polyacrylamide applications for seepage reduction, Colorado State University, Fort Collins, Colorado.
- Martin, P.H., LeBoeuf, E.J., Dobbins, J.P., Daniel, E.B., Abkowitz, M.D., 2005. Interfacing GIS with water resource models: A state-of-the-art review. *Journal of the American Water Resources Association*, 41(6): 1471-1487.
- McCullagh, P., Nelder, J.A., 1989. *Generalized linear models*, Second Edition. London: Chapman & Hall.
- McDonald, M.G., Harbaugh, A.W., 1988. A modular three-dimensional finite-difference ground-water flow model. .

- McGrath, G., Hinz, C., Sivapalan, M., 2008a. Modelling the impact of within storm variability of rainfall on the loading of solutes to preferential flow pathways. *European Journal of Soil Science*, 59(1): 24-33.
- McGrath, G.S., Hinz, C., Sivapalan, M., 2008b. Modeling the effect of rainfall intermittency on the variability of solute persistence at the soil surface. *Water Resources Research*, 44(9): W09432, doi:10.1029/2007WR006652.
- McMahon, T.G., Smith, M.G., 2011. The Arkansas Valley Super Ditch: A local response to 'buy and dry' in Colorado water markets. Available at: <http://ssrn.com/abstract=1922444>.
- Merritt, M.L., Konikow, L.F., 2000. Documentation of a computer program to simulate lake-aquifer interaction using the MODFLOW ground-water flow model and the MOC3D solute-transport model. U.S. Geological Survey. Water-Resources Investigations Report 00-4167, 146 p.
- Metternicht, G., Zinck, J., 2003. Remote sensing of soil salinity: potentials and constraints. *Remote Sensing of Environment*, 85(1): 1-20.
- Miles, D.L., 1977. Salinity in the Arkansas Valley of Colorado. Cooperative Extension Service, Colorado State Univ., Fort Collins, Colo.
- Miller, L., Watts, K., Ortiz, R., Ivahnenko, T., 2010. Occurrence and distribution of dissolved solids, selenium, and uranium in groundwater and surface water in the Arkansas River Basin from the headwaters to Coolidge, Kansas, 1970–2009, U.S. Geological Survey Scientific Investigations Report 2010-5069, 59 pgs.
- Milliken, G.A., Johnson, D.E., 1984. Analysis of messy data, volume I: designed experiments. Van Nostrand, Holland.

- Milliken, G.A., Johnson, D.E., 2002. Analysis of messy data, volume III: analysis of covariance. Chapman & Hall/CRC, New York.
- Molz, F., Boman, G., Young, S., Waldrop, W., 1994. Borehole flowmeters: Field application and data analysis. *Journal of Hydrology*, 163(3): 347-371.
- Moore, J., Wood, L., 1967. Data requirements and preliminary results of an analog-model evaluation—Arkansas River valley in eastern Colorado. *Ground Water*, 5(1): 20-23.
- Morway, E.D., Gates, T.K., 2012. Regional assessment of soil water salinity across an intensively irrigated river valley. *Journal of Irrigation and Drainage Engineering*, 138(5): 393-405.
- Morway, E.D., Gates, T.K., Niswonger, R.G., 2013. Appraising options to enhance shallow groundwater table and flow conditions over regional scales in an irrigated alluvial aquifer system. *Journal of Hydrology*.
- Morway, E.D., Niswonger, R.G., Langevin, C.D., Bailey, R.T., Healy, R.W., 2012. Modeling variably saturated subsurface solute transport with MODFLOW-UZF and MT3DMS. *Ground Water*, 51(2): 237-251.
- Mudgway, L.B., Nathan, R.J., McMahon, T.A., Malano, H.M., 1997. Estimating salt loads in high water table areas. I: Identifying processes. *Journal of Irrigation and Drainage Engineering*, 123(2): 79-90.
- Mueller Price, J., Gates, T.K., 2008. Assessing uncertainty in mass balance calculation of river nonpoint source loads. *Journal of Environmental Engineering*, 134(4): 247-258.
- Nielsen, D., Van Genuchten, M.T., Biggar, J., 1986. Water flow and solute transport processes in the unsaturated zone. *Water Resources Research*, 22(9S): 89S-108S.

- Niemann, J.D., Lehman, B.M., Gates, T.K., Hallberg, N.U., Elhaddad, A., 2011. Impact of shallow groundwater on evapotranspiration losses from uncultivated land in an irrigated river valley. *Journal of Irrigation and Drainage Engineering*, 137(8): 501-512.
- Niswonger, R., Panday, S., Ibaraki, M., 2011. MODFLOW-NWT, A Newton formulation for MODFLOW-2005, U.S. Geological Survey Techniques and Methods 6-A37, 44 p.
- Niswonger, R., Prudic, D., 2009. Comment on 'evaluating interactions between groundwater and vadose zone using the HYDRUS-Based flow package for MODFLOW' by Navin Kumar C. Twarakavi, Jirka Simunek, and Sophia Seo. in press.
- Niswonger, R., Prudic, D., Regan, R., 2006. Documentation of the unsaturated-zone flow (UZFI) package for modeling unsaturated flow between the land surface and the water table with MODFLOW-2005. US Department of the Interior, US Geological Survey Techniques and Methods 6-A19 62 p; Reston, VA.
- Niswonger, R.G., Prudic, D.E., 2004. Modeling variably saturated flow using kinematic waves in MODFLOW, *in* Hogan, J. F., Phillips, F. M., Scanlon, B. R., eds., *Groundwater Recharge in a Desert Environment: The Southwestern United States*: American Geophysical Union, Washington, D.C., Water Science and Application Series, v. 9, p. 101-112, 101-112 pp.
- Niswonger, R.G., Prudic, D.E., 2005. Documentation of the streamflow-routing (SFR2) package to include unsaturated flow beneath streams--A modification to SFR1. U.S. Geological Survey Techniques and Methods 6-A13, 48 p.
- NOAA, 2008. NCDC NEXRAD data inventory search, Available online at:
<http://www.ncdc.noaa.gov/nexradinv/>.

- Nosetto, M., Jobbágy, E., Jackson, R., Sznaider, G., 2009. Reciprocal influence of crops and shallow ground water in sandy landscapes of the Inland Pampas. *Field Crops Research*, 113(2): 138-148.
- Odell, J.W., Coffin, D.L., Langford, R.H., 1964. Mineral and water resources of Colorado, Report for use of U.S. Senate Committee on Interior and Insular Affairs, 88th Congress, 2nd Session, p. 249.
- Oreskes, N., Belitz, K., 2001. Philosophical issues in model assessment. In: Anderson, M.P., Bates, P.D. (Eds.), *Model validation: perspectives in hydrological sciences*, New York: John Wiley and Sons, pp. 23-41.
- Panday, S., Brown, N., Foreman, T., Bedekar, V., Kaur, J., Huyakorn, P.S., 2009. Simulating dynamic water supply systems in a fully integrated surface-subsurface flow and transport model. *Vadose Zone Journal*, 8(4): 858.
- Panday, S., Huyakorn, P.S., 2008. MODFLOW SURFACT: A state-of-the-art use of vadose zone flow and transport equations and numerical techniques for environmental evaluations. *Vadose Zone Journal*, 7(2): 610.
- Parkhurst, D.L., Christenson, S.C., Breit, G.N., 1996. Ground-water-quality assessment of the central Oklahoma Aquifer, Oklahoma : geochemical and geohydrologic investigations, U.S. Geological Survey, Water Supply Paper 2357-C, Denver, CO.
- Peak, W., 1977. Institutionalized inefficiency: The unfortunate structure of Colorado's water resource mangement system. *Journal of the American Water Resources Association*, 13(3): 551-562.

- Pederson, G.T., Betancourt, J.L., McCabe, G.J., 2013. Regional patterns and proximal causes of the recent snowpack decline in the Rocky Mountains, US. *Geophysical Research Letters*: 1-6.
- Pederson, G.T., Graumlich, L.J., Fagre, D.B., Kipfer, T., Muhlfield, C.C., 2010. A century of climate and ecosystem change in Western Montana: what do temperature trends portend? *Climatic Change*, 98(1-2): 133-154.
- Person, M., Konikow, L.F., 1986. Recalibration and predictive reliability of a solute-transport model of an irrigated stream-aquifer system. *Journal of Hydrology*, 87(1-2): 145-165.
- Poeter, E., Hill, M., 1997. Inverse models: A necessary next step in ground-water modeling. *Ground Water*, 35(2): 250-260.
- Poeter, E., Hill, M., Banta, E., Mehl, S., Christensen, S., 2005. UCODE_2005 and six other computer codes for universal sensitivity analysis, calibration, and uncertainty evaluation. *USGS Techniques and Methods Report TM 6-A11*.
- Poeter, E.P., 2007. Reader's forum. *Ground Water*, 45(4): 390-391.
- Postel, S., 1999. *Pillar of sand: Can the irrigation miracle last?* Norton, New York.
- R Development Core Team, 2011. *R: A language and environment for statistical computing*. R Foundation for Statistical Computing, Vienna, Austria. ISBN 3-900051-07-0, Available at: <http://www.R-project.org>.
- Rhoades, J.D., Chanduvi, F., Lesch, S.M., 1999. *Soil salinity assessment: Methods and interpretation of electrical conductivity measurements*, Irrigation and Drainage Paper No. 57. Food and Agriculture Organization United Nations, Rome.
- Richards, L.A., 1954. *Diagnosis and improvement of saline and alkali soils*. U.S. salinity laboratory staff agriculture handbook no. 60, USDA, Washington, D.C.

- Ronayne, M.J., Gorelick, S.M., Caers, J., 2008. Identifying discrete geologic structures that produce anomalous hydraulic response: An inverse modeling approach. *Water Resources Research*, 44(8).
- Ross, P., 1990. Efficient numerical methods for infiltration using Richards' equation. *Water Resour. Res.*, 26(2): 279-290.
- Rotter, R.C., 2006. Improving draining of agricultural lands in the lower Arkansas Valley, M.S. Thesis, Dept. of Civil and Environmental Engineering, Colorado State University, Fort Collins, CO.
- Sanford, W., 2002. Recharge and groundwater models: an overview. *Hydrogeology Journal*, 10(1): 110-120.
- Schaap, M.G., Leij, F.J., van Genuchten, M.T., 2001. ROSETTA: A computer program for estimating soil hydraulic parameters with hierarchical pedotransfer functions. *Journal of Hydrology*, 251(3-4): 163-176.
- Scheibe, T.D., Chien, Y.J., 2003. An evaluation of conditioning data for solute transport prediction. *Ground Water*, 41(2): 128-141.
- Schoups, G., Addams, C.L., Gorelick, S.M., 2005a. Multi-objective calibration of a surface water-groundwater flow model in an irrigated agricultural region: Yaqui Valley, Sonora, Mexico. *Hydrology and Earth System Sciences*, 9(5): 549-568.
- Schoups, G., Hopmans, J., Tanji, K., 2006. Evaluation of model complexity and space-time resolution on the prediction of long term soil salinity dynamics, western San Joaquin Valley, California. *Hydrological processes*, 20(13): 2647-2668.
- Schoups, G., Hopmans, J.W., 2002. Analytical model for vadose zone solute transport with root water and solute uptake. *Vadose Zone Journal*, 1(1): 158-171.

- Schoups, G., Hopmans, J.W., Young, C.A., Vrugt, J.A., Wallender, W.W., Tanji, K.K., Panday, S., 2005b. Sustainability of irrigated agriculture in the San Joaquin Valley, California. *Proceedings of the National Academy of Sciences of the United States of America*, 102(43): 15352.
- Sepaskhah, A., Karimi-Goghary, S., 2003. Growth and chemical composition of pistachio affected by salinities and depths of water table. *Communications in soil science and plant analysis*, 34(3-4): 343-355.
- Seyfried, M., Schwinning, S., Walvoord, M., Pockman, W., Newman, B., Jackson, R., Phillips, F., 2005. Ecohydrological control of deep drainage in arid and semiarid regions. *Ecology*, 86(2): 277-287.
- Shah, S.H.H., Vervoort, R.W., Suweis, S., Guswa, A.J., Rinaldo, A., van der Zee, S.E.A.T.M., 2011. Stochastic modeling of salt accumulation in the root zone due to capillary flux from brackish groundwater. *Water Resources Research*, 47(9).
- Shanafield, M., Pohll, G., Susfalk, R., 2010. Use of heat-based vertical fluxes to approximate total flux in simple channels. *Water Resources Research*, 46(3): W03508.
- Sherow, J.E., 1990. *Watering the valley: Development along the High Plains Arkansas River, 1870-1950*. University Press of Kansas.
- Sijtsma, B.R., Boels, D., Visser, T.N.M., Roest, C.W.J., Smit, M.F.R., 1995. SIWARE user's manual. Reuse Report 27. The Winand Staring Centre for Integrated Land, Soil and Water Research, now Alterra Green World Research, Wageningen, The Netherlands, 158 p.
- Silva, C., Martínez, V., Carvajal, M., 2008. Osmotic versus toxic effects of NaCl on pepper plants. *Biologia Plantarum*, 52(1): 72-79.

- Simunek, J., Bradford, S.A., 2008. Vadose Zone Modeling: Introduction and Importance. *Vadose Zone Journal*, 7(2): 581.
- Šimunek, J., Bradford, S.A., 2008a. Vadose zone modeling: Introduction and importance. *Vadose Zone Journal*, 7(2): 581.
- Šimunek, J., Jacques, D., van Genuchten, M.T., Mallants, D., 2006. Multicomponent geochemical transport modeling using the HYDRUS computer software packages. *Journal of American Water Resources Association*, 42: 1537-1547.
- Šimunek, J., Šejna, M., van Genuchten, M.T., 1999. The HYDRUS-2D software package for simulating two-dimensional movement of water, heat, and multiple solutes in variable saturated media. Version 2.0. 1539-1663, IGWMC-TPS-53. Int. Ground Water Modeling Center, Colorado School of Mines, Golden.
- Šimunek, J., Suarez, D., Šejna, M., 1996. The UNSATCHEM software package for simulating one-dimensional variably saturated water flow, heat transport, carbon dioxide production and transport, and multicomponent solute transport with major ion equilibrium and kinetic chemistry, U.S. Salinity Laboratory, Research Report No. 141.
- Šimunek, J., van Genuchten, M.T., Šejna, M., 2008b. Development and applications of the HYDRUS and STANMOD software packages and related codes. *Vadose Zone Journal*, 7(2): 587-600.
- Singh, A., 2010. Decision support for on-farm water management and long-term agricultural sustainability in a semi-arid region of India. *Journal of Hydrology*, 391(1): 63-76.
- Singh, G., Bundela, D., Sethi, M., Lal, K., Kamra, S., 2010. Remote sensing and geographic information system for appraisal of salt-affected soils in India. *Journal of Environmental Quality*, 39(1): 5-15.

- Singh, R., Kroes, J., van Dam, J., Feddes, R., 2006. Distributed ecohydrological modelling to evaluate the performance of irrigation system in Sirsa district, India: I. Current water management and its productivity. *Journal of Hydrology*, 329(3-4): 692-713.
- Singh, V., 2002. Is hydrology kinematic? *Hydrological Processes*, 16(3): 667-716.
- Smedema, L., Vlotman, W., Rycroft, D., 2004. *Modern land drainage: planning, design and management of agricultural drainage systems*. Taylor & Francis.
- Smith, R., Hebbert, R., 1983. Mathematical simulation of interdependent surface and subsurface hydrologic processes. *Water Resources Research*, 19(4): 987-1001.
- Struthers, I., Hinz, C., Sivapalan, M., 2006. A multiple wetting front gravitational infiltration and redistribution model for water balance applications. *Water Resources Research*, 42(6): W06406.
- Suarez, D., Simunek, J., 1997. UNSATCHEM: Unsaturated water and solute transport model with equilibrium and kinetic chemistry. *Soil Science Society of America Journal*, 61(6): 1633-1646.
- Susfalk, R., Sada, D., Martin, C.A., Young, M., Gates, T.K., Rosamond, C., Mihevc, T., Arrowood, T., Shanafield, M., Epstein, B., Fitzgerald, B., Lutz, A., Woodrow, J., Miller, G., Smith, D., 2008. Evaluation of linear anionic polyacrylamide (LA-PAM) application to water delivery canals for seepage Reduction, DHS Publication No. 41245, Available at: http://pam.dri.edu/docs/PAM_Field_Studies_041245.pdf
- Sutherland, P.L., Knapp, J.A., 1988. The impacts of limited water: A Colorado case study. *Journal of Soil and Water Conservation*, 43(4): 294.
- Suweis, S., Rinaldo, A., Van der Zee, S., Daly, E., Maritan, A., Porporato, A., 2010. Stochastic modeling of soil salinity. *Geophysical Research Letters*, 37(7).

- Tanji, K.K., Keyes, C.G., 2002. Water quality aspects of irrigation and drainage: Past history and future challenges for Civil Engineers. *Journal of Irrigation and Drainage Engineering*, 128(6): 332-340.
- Tanji, K.K., Kielen, N.C., 2002. Agricultural drainage water management in arid and semi-arid areas. Irrigation and Drainage Paper 61, Food and Agriculture Organization United Nations, Rome. FAO.
- Tiedeman, C.R., Hill, M.C., 2007. Model calibration and issues related to validation, sensitivity analysis, post-audit, uncertainty evaluation and assessment of prediction data needs, *In: Thangarajan, M (eds.), Groundwater: Resource Evaluation, Augmentation, Contamination, Restoration, Modeling and Management*. Springer, New York.
- Tilman, D., Cassman, K., Matson, P., Naylor, R., Polasky, S., 2002. Agricultural sustainability and intensive production practices. *Nature*, 418(6898): 671-677.
- Tilman, D., Fargione, J., Wolff, B., D'Antonio, C., Dobson, A., Howarth, R., Schindler, D., Schlesinger, W., Simberloff, D., Swackhamer, D., 2001. Forecasting agriculturally driven global environmental change. *Science*, 292(5515): 281.
- Triana, E., Labadie, J.W., Gates, T.K., 2009a. River GeoDSS for agro-environmental enhancement of Colorado's Lower Arkansas River Basin. I: Model development and calibration. *Journal of Water Resources Planning and Management*, In Press.
- Triana, E., Labadie, J.W., Gates, T.K., 2009b. River GeoDSS for agro-environmental enhancement of Colorado's Lower Arkansas River Basin. II: Evaluation of strategies. *Journal of Water Resources Planning and Management*, In Press.

- Triana, E., Labadie, J.W., Gates, T.K., Anderson, C.W., 2010. Neural network approach to stream-aquifer modeling for improved river basin management. *Journal of Hydrology*, 391(3): 235-247.
- Tsai, F., Sun, N., Yen, W., 2003b. A combinatorial optimization scheme for parameter structure identification in ground water modeling. *Ground Water*, 41(2): 156-169.
- Tsai, F., Yeh, W., 2004. Characterization and identification of aquifer heterogeneity with generalized parameterization and Bayesian estimation. *Water Resources Research*, 40(10): W10102.
- Tsai, F.T.C., Sun, N.Z., Yeh, W.W.G., 2003a. Global-local optimization for parameter structure identification in three-dimensional groundwater modeling. *Water Resources Research*, 39(2): 1043.
- Tung, C., Tan, C., 2005. An optimal procedure for identifying parameter structure and application to a confined aquifer. *Environmental Geology*, 47(8): 1062-1071.
- Tung, C.P., Chou, C.A., 2004. Pattern classification using tabu search to identify the spatial distribution of groundwater pumping. *Hydrogeology Journal*, 12(5): 488-496.
- Twarakavi, N.K.C., Simunek, J., Seo, S., 2008. Evaluating interactions between groundwater and vadose zone using the HYDRUS-based flow package for MODFLOW. *Vadose Zone Journal*, 7(2): 757-768.
- U.S. Supreme Court, 1995. *Kansas v. Colorado*, Case 514 U.S. 673.
- Umali, D.L., 1993. Irrigation-induced salinity : a growing problem for development and the environment. Technical Paper No. 215, World Bank, Washington, DC.
- United Nations, 2004. *World population prospects: The 2002 revision*. UN Department of Economic and Social Affairs, Population Division, New York.

- USGS, 2008. Water resources of the United States - 2008 annual data report: Explanation of stage- and water-discharge records, Available online at:
<http://wdr.water.usgs.gov/current/documentation.html#stage>.
- Valerio, A., Rajaram, H., Zagona, E., 2010. Incorporating groundwater-surface water interaction into river management models. *Ground Water*, 48(5): 661-673.
- Van Dam, J.C., Feddes, R.A., 2000. Numerical simulation of infiltration, evaporation and shallow groundwater levels with the Richards equation. *Journal of Hydrology*, 233(1-4): 72-85.
- van Dam, J.C., Huygen, J., Wesseling, J.G., Feddes, R.A., Kabat, P., Walsum, P.E.V., Groenendijk, P., van Diepen, C.A., 1997. Theory of SWAP version 2.0; simulation of water flow, solute transport and plant growth in the soil-water-atmosphere-plant environment, Report 71, Subdep. Water Resources, Wageningen University, Technical document 45, Alterra Green World Research, Wageningen.
- van Schilfgaarde, J., 1984. Drainage design for salinity control. *Soil salinity under irrigation: Processes and management*, 1984, Springer-Verlag, Berlin, 190-197.
- Vanclooster, M., Boesten, J., Tiktak, A., Jarvis, N., Kroes, J., Muñoz-Carpena, R., Clothier, R., Green, S., 2005. On the use of unsaturated flow and transport models in nutrient and pesticide management. In: Feddes, R., De Rooij, G., and Van Dam, J. (eds), pp. 331-361, Kluwer Academic Publishers, 6(0): 331-361.
- Vanderborght, J., Kasteel, R., Herbst, M., Javaux, M., Thiery, D., Vanclooster, M., Mouvet, C., Vereecken, H., 2005. A set of analytical benchmarks to test numerical models of flow and transport in soils. *Vadose Zone Journal*, 4(1): 206.

- Ventura, F., Spano, D., Duce, P., Snyder, R.L., 1999. An evaluation of common evapotranspiration equations. *Irrigation Science*, 18(4): 163-170.
- Vervoort, R.W., van der Zee, S.E.A.T.M., 2008. Simulating the effect of capillary flux on the soil water balance in a stochastic ecohydrological framework. *Water Resources Research*, 44(8).
- Vico, G., Porporato, A., 2011. From rainfed agriculture to stress-avoidance irrigation: II. Sustainability, crop yield, and profitability. *Advances in Water Resources*, 34(2): 272-281.
- Voegeli, P.T., 1965. Geology and ground-water resources of Prowers County, Colorado. US Geological Survey, Water-supply paper 1772, Washington.
- Vogel, H.J., Ippisch, O., 2008. Estimation of a critical spatial discretization limit for solving Richards equation at large scales. *Vadose Zone Journal*, 7(1): 112-114.
- Vogel, T., Huang, K., Zhang, R., van Genuchten, M.T., 1996. The HYDRUS code for simulating one-dimensional water flow, solute transport, and heat movement in variably-saturated porous media, Research Report 140. U.S. Salinity Laboratory, USA.
- Voss, C.I., 1984. Finite-element simulation model for saturated-unsaturated fluid density-dependent groundwater flow with energy transport or chemically-reactive single-species solute transport (SUTRA). U.S. Geological Survey. Water-Resources Investigations Report 84-4369, 409 p.
- Voss, C.I., Provost, A.M., 2002. SUTRA: A model for saturated-unsaturated, variable-density ground-water flow with solute or energy transport. US Geological Survey, Water-Resources Investigations Report 02-4231.

- Vrugt, J.A., Stauffer, P.H., Wöhling, T., Robinson, B.A., Vesselinov, V.V., 2008. Inverse modeling of subsurface flow and transport properties: A review with recent advances in self-adaptive global optimization, sequential data assimilation, and parallel computing. *Vadose Zone Journal*, 7(2): 843-864.
- Wallender, W.W., Tanji, K.K., 2012. *Agricultural salinity assessment and management*. 2nd Ed., ASCE, Reston, VA.
- Weir, G.J., 1989. The direct inverse problem in aquifers. *Water Resources Research*, 25(4).
- Weist, W.G., 1965. *Geology and occurrence of ground water in Otero County and the southern part of Crowley County, Colorado, U.S. Geological Survey, Denver.*
- Wesseling, J.G., 1974. Crop growth in wet soils. In: van Schilfgaard, J. (Ed.), *Drainage for Agriculture*. ASA, Madison, WI pp. 7-37.
- White, M., Oostrom, M., Lenhard, R., 1995. Modeling fluid flow and transport in variably saturated porous media with the STOMP simulator. 1. Nonvolatile three-phase model description. *Advances in Water Resources*, 18(6): 353-364.
- Wilson, W.W., 1965. *Pumping tests in Colorado. Ground water series circular; no. 11. U.S. Geological Survey, Denver, CO., 361 pp.*
- Wittler, J.M., 2005. *Calibration of electromagnetic sensors for regional salinity assessment in an irrigated river valley*, M.S. thesis, Colorado State Univ., Fort Collins, Colo.
- Wittler, J.M., Cardon, G.E., Gates, T.K., Cooper, C.A., Sutherland, P.L., 2006. Calibration of electromagnetic induction for regional assessment of soil water salinity in an irrigated valley. *Journal of Irrigation and Drainage Engineering*, 132(5): 436-444.

- Woodhouse, C.A., Pederson, G.T., Gray, S.T., 2011. An 1800-yr record of decadal-scale hydroclimatic variability in the upper Arkansas River basin from bristlecone pine. *Quaternary Research*, 75(3): 483-490.
- Wu, S.C., Tan, Y.C., Chen, C.H., Lin, S.T., Ke, K.Y., 2008. A two-dimensional inverse model to identify transmissivity in an anisotropic aquifer. *Hydrological Processes*.
- Xu, L., Yang, J., Zhang, Q., Niu, H., 2008. Modelling water and salt transport in a soil–water–plant system under different groundwater tables. *Water and Environment Journal*, 22(4): 265-273.
- Xu, L.G., Yang, J.S., Zhang, Q., Liu, G.M., 2005. Salt-water transport in unsaturated soils under crop planting: Dynamics and numerical simulation. *Pedosphere*, 15(5): 634-640.
- Xu, P., Shao, Y., 2002. A salt-transport model within a land-surface scheme for studies of salinisation in irrigated areas. *Environmental Modelling & Software*, 17(1): 39-49.
- Xu, T., Sonnenthal, E., Spycher, N., Pruess, K., 2003. TOUGHREACT: A new code of the TOUGH family for non-isothermal multiphase reactive geochemical transport in variably saturated geologic media, Earth Sciences Division, Lawrence Berkeley National Laboratory, University of California, Berkeley, CA 94720.
- Xu, X., Huang, G., Qu, Z., Pereira, L.S., 2010. Assessing the groundwater dynamics and impacts of water saving in the Hetao Irrigation District, Yellow River basin. *Agricultural Water Management*, 98(2): 301-313.
- Yeh, T.C.J., Liu, S., 2000. Hydraulic tomography: Development of a new aquifer test method. *Water Resources Research*, 36(8): 2095-2105.
- Yeh, W., Yoon, Y., 1981. Aquifer parameter identification with optimum dimension in parameterization. *Water Resources Res.*, 17(3): 664-672.

- Zhang, L., Dawes, W., Slavich, P., Meyer, W., Thorburn, P., Smith, D., Walker, G., 1999. Growth and ground water uptake responses of Lucerne to changes in groundwater levels and salinity: lysimeter, isotope and modelling studies. *Agricultural Water Management*, 39(2): 265-282.
- Zheng, C., 2009. Recent developments and future directions for MT3DMS and related transport codes. *Ground Water*, 47(5): 620-625.
- Zheng, C., Bennett, G.D., 2002. *Applied contaminant transport modeling*. 2nd edition. John Wiley, Hoboken, NJ, 621 pp.
- Zheng, C., Hill, M.C., Hsieh, P.A., 2001. MODFLOW-2000, the U.S. Geological Survey modular ground-water model: User guide to the LMT6 package, the linkage with MT3DMS for multi-species mass transport modeling, US Geological Survey. Open-File Report 01-82.
- Zheng, C., Wang, P., 1996. Parameter structure identification using tabu search and simulated annealing. *Advances in Water Resources*, 19(4): 215-224.
- Zheng, C., Wang, P., 1999a. MT3DMS: A modular three-dimensional multispecies transport model for simulation of advection, dispersion, and chemical reactions of contaminants in groundwater systems; Documentation and user's guide, Contract Report SERDP-99-1. Vicksburg, MS. U. S. Army Engineer Research and Development Center.
- Zheng, C., Wang, P.P., 1999b. An integrated global and local optimization approach for remediation system design. *Water Resources Research*, 35(1): 137-148.
- Zimmerman, D.A., de Marsily, G., Gotway, C.A., Marietta, M.G., Axness, C.L., Beauheim, R.L., Bras, R.L., Carrera, J., Dagan, G., Davies, P.B., 1998. A comparison of seven

geostatistically based inverse approaches to estimate transmissivities for modeling
advective transport by groundwater flow. *Water Resources Research*, 34(6): 1373-1413.